Impact of noise (auto)correlation on power system dynamic performance

Muhammad Adeen

17209004

A thesis submitted to University College Dublin
in fulfilment of the requirements for the degree of

Doctor of Philosophy

College of Engineering and Architecture
School of Electrical & Electronic Engineering
Head of School: Prof. John T. Sheridan

Supervisor: Prof. Federico Milano

June 2022

I hereby certify that the submitted work is my own work, was completed while registered as a candidate for the degree stated on the Title Page, and I have not obtained a degree elsewhere on the basis of the research presented in this submitted work.

Acknowledgements

This thesis is a product of my hard work during past 4 years under the supervision of Prof. Federico Milano at University College Dublin. I am grateful to Prof. Federico for providing me with the opportunity to work as a PhD student and to the Science Foundation Ireland for the financial support under project Advanced Modelling for Power System Analysis and Simulation (AMPSAS), Investigator Programme Award, Grant No. SFI/15/IA/3074.

Working closely with Prof. Federico I have succeeded at polishing my skills in power system modelling, scripting and simulations. His knowledge, expertise, and experience in power systems and other related fields have been a valuable contribution and key factor towards the completion of my PhD. Without his support, motivation, constant feedback, and continuous push for more work, I would not have been able to produce this document.

I would also like to thank all of my colleagues at the AMPSAS for sharing their experience and knowledge in power systems. I have learned a lot while working with all of the group members.

Finally, I would like to thank my family, especially my parents. Without the support of my parents I would not have been able to make it to the PhD. My mom has supported me a lot with education at my early childhood days. My father has always provided with the due diligence in the life changing decisions of my life. For instance the decision to pursue this PhD programme. Without the help and support of my parents I would not have completed this degree. Thanks to my brothers Haseeb and Humayun, whom are close to my heart. Especial thanks to my dearest friend Nikita for all the support and motivation during the ups and downs of the past 4 years.

Muhammad Adeen

Dublin, Jun 2022

Abstract

Non-deterministic loads and non-dispatchable renewable energy sources such as wind and photovoltaic are the major sources of random fluctuations and volatility in power systems. The techniques to account for the effects of random fluctuations on the transient behaviour of the power system have been developed and well-assessed in the literature. On the other hand, the analysis of impact of volatility on the power system short-term dynamic and transient behaviour has not been fully explored so far.

For power system dynamic studies, volatility can be modelled as a fast-varying time-continuous stochastic process. Stochastic processes are formulated as Stochastic Differential Equations (SDEs). SDEs are then conveniently introduced into existing power system dynamic models, i.e., deterministic nonlinear differential algebraic equations. Doing so produces nonlinear Stochastic Differential Algebraic Equations (SDAEs). SDAEs are the fundamental tool, utilised in this thesis, to study the dynamic behaviour of the power system subjected to volatility.

Stochastic processes can be identified through their distinct features, namely, drift, correlation, and diffusion. While the impact of the latter on the system dynamics has been studied widely, that is not the case for the other two. The drift term defines the variability of the process in time. Whereas the correlation is the measure of degree of similarity between two processes. Thus, the question on what is the impact of drift and correlation of the stochastic processes on the dynamic behaviour of the power system and how to quantify it remains unanswered.

This thesis aims at providing systematic and generalized methods based on data measurements to model correlation on stochastic processes and introduce them into power system dynamic studies. The thesis also provides a general technique to extract correlation from stochastic processes from the measurement data. The methods provided in this thesis are independent of dimensions, time-scales, drifts, and probability distributions of the processes. This allows for the inclusion of a wide range of sources of volatility into existing power system dynamic models, and the study of their impact on power system dynamics without the need for any simplifications or modifications to the original system.

Another topic considered in this thesis is the impact of the drift of the stochastic processes on the power system dynamic behaviour by means of nonlinear SDAEs through time- and frequency-domain analyses. The former involves the study of the impact of the

drift of the stochastic processes on the power system algebraic variables in normal grid operation. Whereas the latter consists in the study of the dynamic interactions between the drift of the stochastic processes and the electro-mechanical oscillatory modes of the power system.

The thesis also presents a direct method to assess the probability that a power system's physical limit is violated when modelling stochastic processes in normal grid operation. The accuracy and computational efficiency of the direct method is demonstrated using the dynamic model of the bench-mark real-world Irish system. Note that all the available direct methods rely on simplification, and linearization of the power system around an equilibrium point. Direct methods can only study the power system dynamic in stationary conditions and, hence, cannot provide any insights on the course of the individual trajectories simulated through time domain simulations. The detailed dynamic behaviour of the power system simulating stochastic processes, controller hard limits, saturations, and system nonlinearities can only be studied using the nonlinear models, which do not have a closed form solution. For this reason, the analyses conducted in the entire thesis, except for the direct method, rely on time domain simulations.

Several case studies utilising the real-world Irish system, are illustrated throughout the thesis to demonstrate the practical applications of the introduced methods and techniques to model and study the impact of correlated stochastic processes on the power system dynamic and transient security. As the modelling techniques presented in the thesis are general, based on measurement data, and easy to implement in software tools. They are expected to be readily adopted by the system operators to ensure the security and stability of the power system in the presence of stochastic processes.

Contents

List of Figures

List of Tables

List of Acronyms and Abbreviations

ACF	Autocorrelation Function
AGC	Automatic Generation Control
AVR	Automatic Voltage Regulator
AIITS	All-Island Irish Transmission System
AMPSAS	Advanced Modelling for Power System Analysis and Simulation
CDF	Cumulative Distribution Function
CoI	Center of Inertia
DAE	Differential-Algebraic Equation
FDR	Frequency Disturbance Recorder
KS	Kolmogorov-Smirnov
LE	Linear Estimation
MLE	Maximum Likelihood Estimation
MC	Monte Carlo Method
OU	Ornstein-Uhlenbeck
PDF	Probability Density Function
PMU	Phasor Measurement Unit
PSS	Power System Stabilizer
RCDF	Real-World Cumulative Density Function

RES	Renewable Energy Sources
SCADA	Supervisory Control And Data Acquisition
SDE	Stochastic Differential Equation
SDAE	Stochastic Differential Algebraic Equation
SEAI	Sustainable Energy Authority of Ireland
TDS	Time Domain Simulation
TG	Turbine Governor
TSO	Transmission System Operator
WPP	Wind Power Plant
WSCC	Western Systems Coordinating Council

Notation

This section states the notation adopted throughout the thesis.

Vectors and Matrices

a, A	scalar
$\boldsymbol{a}$, $\mathbf{a}$	vector
$\boldsymbol{A}$, $\mathbf{A}$	matrix
$\boldsymbol{A}^{\mathrm{T}}$	matrix transpose
$\boldsymbol{I}_n$	identity matrix of dimensions $n \times n$
$\mathbf{0}_{n,m}$	zero matrix of dimensions $n \times m$

Sets and Units

$\mathcal{C}^n$	n time continuously differentiable functions
$\mathbb{N}$	natural numbers
$\mathbb{R}$	real numbers

Parameters

α	autocorrelation coefficient
r	correlation coefficient
c	constant
h	time step size
μ	mean
σ	standard deviation

Variables and Functions

p	active power

q	reactive power
t	time
u	input signal
w	wind speed
x	state variable
y	algebraic variable
κ	uncorrelated stochastic variable
η	correlated stochastic variable
ξ	uncorrelated white noise
ζ	correlated white noise
v	voltage magnitude
θ	voltage phase angle
ω	rotor angular speed
δ	rotor angle
N	number of realizations

Superscripts and Subscripts

p	active power
q	reactive power
e	WPP
w	wind
agg	aggregated
g	synchronous generator
L	load consumption
0	initial condition

Chapter 1

Introduction

1.1 Motivation

Modern power systems are subjected to stochastic fluctuations due to the increasing penetration of converter-based Renewable Energy Sources (RES) such as wind and photovoltaic. Another significant source of noise are electrical loads, whose uncertainty and volatility has increased in recent years due to the electrification of transportation and heating systems. As a consequence, it has become quite challenging to model and study the dynamic behavior of the power system: in normal operation, to avoid violations of physical limits and technical constraints; and after a disturbance to avoid instability.

The increase of the penetration of RES is accompanied by a reduction of the conventional fossil-fuel driven synchronous generator-based power plants. This leads to the reduction of the total inertia available in the system, as well as the increase of *uncertainty* (slow variations) and *volatility* (fast variations). Moreover, converter-based RES, unlike conventional generation, is "non-synchronous", i.e., does not respond to grid power unbalances by varying its frequency. For this reason, the high penetration of RES makes frequency control a complex task as fewer synchronous generators are available to provide the system with inertia and power reserve. Consequently, such systems experience high frequency deviations [2], which, in turn, can lead to a higher risk of instability.

The analysis of the effect of uncertainty on the dynamic of the power system is conventionally performed via *probabilistic analysis*. This has been well established in literature. On the other hand, the effect of volatility on the dynamic behaviour of the power system is studied through time-continuous stochastic processes. Stochastic processes

are modelled using time-continuous Stochastic Differential Equations (SDEs) and are included into the set of nonlinear deterministic Differential-Algebraic Equations (DAEs) to formulate a set of nonlinear Stochastic Differential Algebraic Equations (SDAEs) [17,51,73]. The analysis of power system dynamic modelled as a set of SDAEs has gained interest in the literature in recent years.

Stochastic processes are identified by the following features: Probability Density Function (PDF), Autocorrelation Function (ACF), and correlation [25, 28, 31, 63, 82]. Most of the research available on the analyses of the dynamic behaviour of the power system modelled via nonlinear SDAEs focuses on stationary independent Gaussian distributed processes [51,59,71,75,80]. While in some cases stochastic processes are in effect local and independent, there exist processes that are intrinsically correlated. For example, in most locations, cloudy days tend to be more windy than clear-sky ones. Then the variations of the active and reactive power consumption of loads are coupled if the loads have a constant power factor. While the correlation of stochastic processes has been thoroughly discussed for unit-commitment and long-term power system operation problems, the impact of correlation among different stochastic processes on the short-term dynamics of power systems has not been discussed in the literature yet. Moreover, the literature is either incomplete or silent on the topic of the ACF of stochastic processes as well.

Thus, the existing literature does not provide methods to mathematically formulate correlated stochastic processes to be included into power system dynamic studies. Neither does it provide stability assessment tools to study the impact of short-term dynamics, i.e., the ACF, of the stochastic processes on the power system dynamic behaviour. This makes the subject of this thesis particularly relevant as this research is focused on formulating mathematical models for Gaussian and/or non-Gaussian correlated stochastic processes based on measurement data to be readily incorporated into existing power system dynamic models. Furthermore, it provides detailed discussion on the evaluation of the impact of the ACF of the stochastic processes on the power system dynamic, in normal operation, and stability, following a contingency.

1.2 Literature Review

In power system dynamic studies, uncertainty can be thought of as randomness and consists in continuous variations around a mean value. The short-term dynamics of load consumption [57, 63], and the faster time-continuous variations in the wind generation [28, 43] are all examples of volatility. On the other hand, uncertainty is the deviance with respect to a forecasted value.

A well-assessed technique that allows considering the effect of uncertainty in transient stability analysis is through a *probabilistic analysis*. Probabilistic analysis consists in initializing the set of deterministic DAEs that model the system using a random initial value, chosen with given PDFs [1, 8, 12]. In such an analysis the randomness is included at the initialization step, and the rest of the system is simulated in steady state. This makes the probabilistic analysis particularly suited to study the sensitivity of the model with respect to parameter uncertainty. In this thesis, however, only the impact of volatility on the power system transient is of concern.

In power system transient analysis, volatility is characterized as a time-continuous stochastic process, which is conveniently modelled as a SDE. A SDE consists of two terms: the *drift* and the *diffusion*. The diffusion term defines the amplitude of the stochastic process, i.e., its standard deviation in stationary conditions. The dynamic interaction between the drift and the diffusion terms defines the ACF of the process, i.e., how the process evolves in the long term. The impact of a stochastic process on the power system transient can be studied through SDEs, as well.

A fair number of works are available that study the impact of the diffusion term on the stability of power systems, e.g., [32, 48, 78]. These works utilise SDEs to study the impact of stochastic processes on the power system dynamics. The advantage of SDE modelling is that analytical solutions are formulated based on the theory of stability of SDEs. The drawback of these analytical solutions is that they require strong linearization [48, 78] and/or high simplification [32, 72] of the power system dynamic models. The stability assessment techniques presented in the works, in this paragraph, focus on stationary conditions, i.e., consider the probability distribution and standard deviation of the variables.

A technique that allows studying the dynamic behaviour of a power system subject to stochastic processes without the need of linearization or simplification of the models

is through the set of nonlinear SDAEs. Nonlinear SDAEs are created when SDEs are incorporated into the deterministic DAEs [17, 51, 73]. A considerable amount of literature has been dedicated to the evaluation of the probability distribution of transient stability of power system modelled as a set of SDAEs [59, 71, 75, 80]. These references focus on the diffusion term, i.e., PDF of stochastic processes. However, the ACF of the stochastic disturbance and its impact on short-term dynamics of the power system is not considered. An exception is [30], where the authors exploit the property of the ACF to initialize the set of SDAEs that model the system.

The power system dynamic modelled as a set of SDAEs in the aforementioned studies considers independent stochastic processes. Some of these processes may be local and independent, while others are intrinsically correlated. For example, geographically close wind sites show similar variations in the wind speeds [24]. Consequently, the power production of the WPPs also shows a degree of correlation that depends on their location and proximity to each other. Similarly, the correlation in the behavior of the consumers is reflected on the energy consumption at consumer's end.

The correlation on the wind speeds, and load power consumption should be carefully considered when modelling such processes in power system dynamic studies [31, 65, 66]. It is well known, for example, that inaccurate estimations of the power production of aggregated WPPs highly affect the results of the unit-commitment and, in turn, the market clearing price [15]. On the other hand, the correlation on load active and reactive power consumption modelled as SDEs worsens the impact of contingencies [31].

The use of correlation in probabilistic analysis has gained increasing interest in recent years. For example, the effect of spatio-temporal correlation between wind speeds; and between power generation and load power consumption, on the system limits; and the security-constrained unit commitment problem is evaluated in [39, 42, 56]. In [68] the authors exploit the property of correlated load consumption to improve load forecast accuracy. Despite the availability of abundant literature on the topic of correlation in power system uncertainty analysis, the question of what is the impact of correlation of stochastic processes on the short-dynamic behaviour and stability analysis of the power system still remains unanswered. Reference [31], which is an exception to this rule, outlines the formulation of correlation on two-dimensional stochastic processes only. Hence, the

question of how to formulate correlation on multi-dimensional stochastic processes remains unanswered.

The aforementioned studies rely on numerical integration schemes because SDAEs are nonlinear and have high dimensions for large power systems. The use of numerical schemes for their integration is thus unavoidable. The stochastic terms require a significant extra computational burden to solve the integration [76]. Moreover, SDAEs must be studied with a Monte Carlo Method (MC). The MC requires the system of SDAEs to be simulated several hundreds or even thousands of times, to properly estimate the statistical properties, such as probability distribution and variance, of the system variables. Consequently, the MC poses a large computational burden for the simulation of SDAE, which is directly proportional to the size of the system.

The MC is the best available technique when studying the short-term dynamics of power systems modelled as SDAEs. However, it is often required to study the impact of stochastic processes on the estimation of the probability that physical limits such as voltage insulation ratings of a substation, the thermal limits of the lines/transformers, are violated in normal operation. Several techniques are available in the literature that provide the statistical properties, in stationary conditions, of the *state variables*, e.g., [72] and [30]. These methods are based on the properties of the Fokker-Planck equation and the solution of the Lyapunov equation. Other relevant works that provide direct methods to estimate the stability probability of the power systems subject to stochastic disturbances are [32, 48, 78]. However, direct methods that allow the evaluation of the variances of power system algebraic variables are unavailable.

This thesis focuses on filling the gaps mentioned in this section. With this aim, the thesis provides techniques to: (i) formulate correlated stochastic processes based on measurement data; (ii) incorporate such processes into existing power system dynamic models and study their impact; (iii) study the impact of ACF of the noise on the power system dynamics; and (iv) evaluate the variances of the power system algebraic variables.

1.3 Thesis Overview

1.3.1 Contributions

The focus in this thesis is on the modelling and incorporation of correlated stochastic processes into existing power system dynamic models for the study of the power system dynamic performance. The main contributions of the thesis are expressed as follows:

- A general data-driven method to set up correlated processes with arbitrary: time-scales; ACFs; PDFs; and dimensions using multi-dimensional correlated SDEs.
- A systematic and generalized approach to include various sources of correlated processes in power system dynamic models for the dynamic security and transient stability assessment of power systems.
- The analysis on the impact of ACF and correlation of the processes on the short-term dynamic behavior and transient stability of the power systems.
- A direct method to evaluate the variances of the power system algebraic variables.

The models presented in this thesis enable Transmission System Operators (TSOs) to quantify the effect of correlation among stochastic disturbances on the dynamic security and transient stability of the power system. It is important to note that the proposed models allow TSOs to setup correlated stochastic processes based on measurement data with arbitrary ACFs, PDFs and time-scales. These models can be applied to systems of any order and complexity without the need for any simplifications or assumptions in the original model.

* * *

The simulation results illustrated in this thesis are obtained using the Python-based power system analysis software tool Dome [50]. These include TDSs, and results obtained via the direct method. In addition, the methods and models presented in this thesis are implemented in Dome, during the course of this thesis.

1.3.2 Organization

The remainder of the thesis is organized as follows.

Chapter 2 provides a detailed discussion on the modelling of correlated stochastic processes for power system dynamic studies. With this regard, the statistical properties of the stochastic processes required for their modelling are presented in Section 2.2. The stationary stochastic processes are modelled as independent SDEs in Section 2.3. Section 2.4 provides a discussion on the modelling of the relevant features of SDEs, i.e., ACF and PDF. A set of multi-dimensional correlated SDEs to model correlated processes with arbitrary: time-scales; ACFs; and PDFs are introduced in Section 2.5.1. Section 2.5.2 describes a generalized procedure to calculate correlation from multi-dimensional correlated stochastic processes. Section 2.6 provides details on setting up SDEs based on measurement data. Section 2.7 presents methods to formulate and simulate Gaussian and non-Gaussian correlated stochastic processes of arbitrary dimensions. Finally, Section 2.8 provides relevant remarks and conclusions.

In Chapter 3, power system dynamic models are introduced. Chapter 3 utilises the methods introduced in Chapter 2 to model the sources of stochastic disturbances in the power system. With this aim, at first, the power system modelled as a set of deterministic DAEs is introduced in Section 3.2. Then, a non-deterministic dynamic model of power system modelled as independent SDAEs is presented in Section 3.3. A systematic and general approach to model the dynamic behaviour of the power system in the presence of correlated stochastic disturbances is then introduced in Section 3.4. Moreover, the sources of stochastic disturbances such as non-deterministic load consumption, and stochastic wind speeds are modelled via correlated SDAEs in Section 3.5. A technique to formulate aggregated wind speed process using correlated winds is provided in Section 3.6. Finally, Section 4.6 provides a summary of the models presented in Chapter 3.

Chapter 4 illustrates the calculations of the variations of the algebraic variables of power systems modelled as a set of nonlinear SDAEs. With this regard, a linearized method (Linear Estimation) based on the solution of Lyaponov equation is also presented. At first, the impact of the conventional MC on the computational complexity and burden is discussed in Section 4.2. Then, the impact of setting up correlated SDAEs with different PDFs based on measurement data on the dynamic behaviour of the power system is discussed in Section 4.3. Then, in Section 4.4, the Linear Estimation (LE) is introduced. The case study, by utilising the dynamic model of the real-world 1479-bus All-Island Irish Transmission System (AIITS), demonstrates that the LE has high accuracy, and

significantly reduced computational time as compared to the MC. Finally, conclusions are drawn in Section 4.6.

Chapter 5 analyses the interactions between the most relevant feature of the stochastic process, i.e., ACF, and the dynamic behaviour of the power system. This is done by analysing the impact of ACF of the stochastic processes on power system dynamics in both time- and frequency-domain, in Sections 5.2 and 5.3, respectively. The impact of ACF on the short-term dynamics of the stochastic process itself in time- and frequency-domain is studied in Sections 5.2.1 and 5.3.1, respectively. Section 5.2.2 studies the impact of the ACF of the stochastic processes on the variances of the relevant power system quantities in normal grid operation, and the transient stability of the power system after a contingency. While, the dynamic interaction between the ACF of the stochastic processes and the electro-mechanical oscillatory modes of the power systems is discussed in Section 5.3.2. The case studies presented in Chapter 5 utilise the well-known two-area system and the dynamic model of the real-world 1479-bus AIITS. Finally, Section 5.4 draws relevant conclusions.

In Chapter 6, the impact of correlation of stochastic disturbances on the dynamic behaviour and transient stability of the power system is analysed. The models of sources of stochastic disturbances presented in Chapter 3 are utilised throughout the case studies presented in Chapter 6. First, the chapter illustrates the construction of correlation matrix based on measurement data in Section 6.2, using the procedures provided in Chapter 2. Correlation scenarios for the dynamic simulations are defined in Section 6.3. The impact of correlation modelled on stochastic active and reactive power consumption, and wind speeds on the variances of power system algebraic variables is illustrated in Sections 6.4 and 6.5, respectively. In Section 6.6, a case study is presented, where several power system dynamic models are utilised to study the impact of correlated stochastic disturbances on the stability of the power system modelled as a set of SDAEs. In particular, the impact of correlated stochastic loads on the voltage and rotor angle stability of the two-area system is studied in Section 6.6.1. Whereas, the impact of correlated wind speeds on the voltage stability of the two-area system is analysed in Section 6.6.2. In Section 6.6.3, the dynamic model of the real-world 1479-bus AIITS modelled as correlated SDAEs including all sources of disturbances, introduced in Chapter 3, is studied. Finaly, conclusions are drawn in Section 6.7.

Finally, Chapter 7 summarizes the most relevant conclusions and suggests directions for future work.

1.3.3 Publications

Journal papers

(Published)

1. **M. Adeen** and F. Milano, Modelling of Correlated Stochastic Processes for the Transient Stability Analysis of Power Systems, in IEEE Transactions on Power Systems, vol. 36, no. 5, pp. 4445-4456, Sept. 2021. DOI: 10.1109/TPWRS.2021.3066453.

2. **M. Adeen** and F. Milano, On the Impact of Auto-Correlation of Stochastic Processes on the Transient Behavior of Power Systems, in IEEE Transactions on Power Systems, vol. 36, no. 5, pp. 4832-4835, Sept. 2021. DOI: 10.1109/TPWRS.2021.3068038.

3. **M. Adeen** and F. Milano, Stochastic Aggregated Dynamic Model of Wind Generation with Correlated Wind Speeds, Elsevier, Electric Power Systems Research, accepted in Mar 2022, in press. **This paper has been accepted for presentation at 22nd Power Systems Computation Conference, Porto, Portugal - June 27 - July 1, 2022**.

4. F. Milano, M. Liu, M. A. A. Murad, G. Jónsdóttir, G. Tzounas, **M. Adeen**, Á. Ortega, I. Dassios, An overview on Advanced Modelling for Power System Analysis and Simulation, IET Smart Grid, accepted in April 2022, in press.

(Submitted)

5. F. Bizzarri, Davide del Giudice, **M. Adeen**, S. Grillo, D. Linaro, A. Brambilla, F. Milano, On the Calculation of the Variance of Algebraic Variables in Power System Dynamic Models with Stochastic Processes, IEEE Power Engineering Letters, submitted Mar. 2022.

Book Chapters

6. G. M. Jónsdóttir, **M. Adeen**, R. Zárate-Miñano, F. Milano, Chapter 4: Modelling Power Systems with Stochastic Processes, in Advances in Power System Modelling, Control and Stability Analysis, 2^{nd} edition, editor F. Milano, to be printed by Sep 2022.

Conference Papers

Related

7. **M. Adeen**, G. M. Jónsdóttir and F. Milano, Statistical Correlation between Wind Penetration and Grid Frequency Variations in the Irish Network, 2019 IEEE International Conference on Environment and Electrical Engineering and 2019 IEEE Industrial and Commercial Power Systems Europe (EEEIC / ICPS Europe), 2019, pp. 1-6. DOI: 10.1109/EEEIC.2019.8783475.

8. **M. Adeen** and F. Milano, On the Dynamic Coupling of the Autocorrelation of Stochastic Processes and the Standard Deviation of the Trajectories of Power System Variables, 2021 IEEE Power Energy Society General Meeting (PESGM), 2021, pp. 1-5. DOI: 10.1109/PESGM46819.2021.9637935.

9. **M. Adeen**, F. Milano, On the Impact of Probability Distributions of Stochastic Processes on Power System Dynamics, IEEE PES General Meeting, Denver, CO, 17-21 July 2022.

Not Related

10. F. Ebrahimzadeh, **M. Adeen** and F. Milano, On the Impact of Topology on Power System Transient and Frequency Stability, 2019 IEEE International Conference on Environment and Electrical Engineering and 2019 IEEE Industrial and Commercial Power Systems Europe (EEEIC / ICPS Europe), 2019, pp. 1-5. DOI: 10.1109/EEEIC.2019.8783880.

Chapter 2

Stationary Stochastic Processes

2.1 Introduction

Stochastic processes occur in power systems due to several reasons. For example, physical phenomena occurring in nature such as wind speeds, which affect the power production of wind power plants, and solar irradiation, which affect the power output of photo-voltaic. Moreover, load power consumption is also not fully deterministic and can be characterized as a stochastic process [63]. The aforementioned sources cause stochastic disturbances in the power system variables, which have a non-negligible effect on the dynamics of the power system. These disturbances are modelled as Stochastic Differential Equations (SDEs).

A number of works are available in the literature on power systems that deal with the modelling of stochastic processes in power system dynamic studies through SDEs [17, 32, 48, 51, 73, 78]. The models presented in these studies can formulate independent stochastic processes only. However, as mentioned in Chapter 1 stochastic processes do exhibit correlation. The correlation on the stochastic processes can modify power system's transient behaviour [3, 29].

The correlation among the stochastic processes can be conveniently modelled using correlated SDEs. Correlated SDEs, in power systems, were first introduced in [29]. The model in [29] can only formulate two-dimensional stochastic processes. Whereas, in this chapter the main goal is to present a method to formulate multi-dimensional correlated SDEs. This is one of the main contributions of the thesis as well.

The remainder of the chapter is organized as follows. Section 2.2 provides a brief overview of the stationary stochastic processes. Stochastic processes are modelled as

a set of independent SDEs in Section 2.3. Section 2.4 outlines the features of SDEs. Correlated stochastic processes are modelled as a set of correlated SDEs in Section 2.5. A data driven technique to set up correlation matrix is presented in Section 2.5.2. A method based on measurement data to set up SDEs is discussed in Section 2.6. A few examples of Gaussian and non-Gaussian correlated stationary stochastic processes generated using correlated SDEs are illustrated in Section 2.7. Finally, conclusions are drawn in Section 2.8.

2.2 Stationary Stochastic Process

A continuous-time real-valued random process $\{X(t),\, t \in \mathbb{R}\}$ is wide sense **stationary** if its statistical properties are independent of time. In other words, the mean, and the variance of $X(t)$ do not vary over time. Let us assume that $X(t_1)$ and $X(t_2)$ are instances of $X(t)$ at t_1 and t_2, respectively, where $t_1 \neq t_2, \forall t_1, t_2 \in \mathbb{R}$, the mean and variance of $X(t_1)$ and $X(t_2)$ are:

$$\begin{aligned} \mathrm{E}[X(t_1)] &= \mathrm{E}[X(t_2)]\,, \\ \mathrm{E}\big[\big(X(t_1) - \mathrm{E}[X(t_1)]\big)^2\big] &= \mathrm{E}\big[\big(X(t_2) - \mathrm{E}[X(t_2)]\big)^2\big]\,, \end{aligned}$$

where E is the *expectation* operator. The definitions above imply that the mean of $X(t)$, $\forall t \in \mathbb{R}$ is a constant:

$$\mathrm{E}[X(t)] = \mu_X\,,$$

and the variance of $X(t)$, $\forall t \in \mathbb{R}$ is finite:

$$\mathrm{E}\big[\big(X(t) - \mathrm{E}[X(t)]\big)^2\big] = \epsilon_X < \infty\,,$$

Another relevant property of the stationary stochastic process is that its Autocorrelation Function (ACF) is not a function of time rather a function of the time difference, i.e.,:

$$\mathrm{Cov}[X(t_1), X(t_2)] = R_X(t_1, t_2) = R_X(t_2 - t_1, 0) = R_X(\tau)\,, \tag{2.1}$$

where $\tau = t_2 - t_1$ is the time difference. This is discussed in detail later in Section 2.4.1 in this Chapter.

Stationary stochastic processes can be identified by their Probability Density Functions (PDFs). The distribution of all possibilities and likelihoods for all outcomes of a discrete random variable, say Y (discrete means Y has finite number of outcomes), can be defined using the PDF. The PDF of the outcome y ($\forall y \in \Omega$) of Y is an integrable function $f(y)$ with the following properties:

1. $f(y)$ is positive in the entire space Ω, i.e., $f(y) \geq 0$, $\forall y \in \Omega$.

2. $f(y) \leq 1$, $\forall y \in \Omega$, i.e., a probability cannot be greater than 1.

3. The integral of $f(y)$ over entire space Ω is:

$$\int_{\Omega} f(y)dy = 1\,, \tag{2.2}$$

4. Probability that $y \in [a, b]$, is calculated by integrating $f(y)$ over $[a, b]$:

$$\mathrm{P}[a \leq y \leq b] = \int_{a}^{b} f(y)dy\,, \tag{2.3}$$

Property (2.3) is useful for time-continuous random variables. Since uncountably infinite values can be assigned to a time-continuous random variable $X(t)$, $\mathrm{P}[X(t) = x]$ cannot be defined. Instead, the probability that x is contained in a very small interval of length ϵ around x, say $A = [x - \epsilon/2, x + \epsilon/2]$, i.e., $\mathrm{P}[X(t) = x, \forall x \in A]$ can be defined using Cumulative Distribution Function (CDF), where CDF ($F_X(x)$) is written as:

$$F(x) = \mathrm{P}[X(t) = x, \forall x \in A] = \int_{A} f(x)dx\,, \tag{2.4}$$

The PDF ($f(x)$) for a time-continuous random variable can be calculated by differentiating the CDF ($F(X)$), using fundamental theorem of calculus, as:

$$f(x) = \frac{dF(x)}{dx}\,, \tag{2.5}$$

A commonly used PDF type to define physical processes is the Normal or Gaussian PDF. A random variable X is said to be normally distributed, if its PDF is written as:

$$f_{\mathrm{N}}(x) = \frac{1}{\sigma\sqrt{2\pi}}\exp\left(-\frac{1}{2}\Big(\frac{x-\mu}{\sigma}\Big)^2\right), \tag{2.6}$$

where μ and σ are the mean and standard deviation, respectively. A random variable X following Gaussian PDF is often referred to as $X \sim N(\mu, \sigma)$. Gaussian PDF has a bell-shaped curve with all the outcomes normally distributed around its mean. Figure 2.1 shows an example of PDF and CDF of a Gaussian variable with zero mean and unit standard deviation.

The Gaussian PDF provides a good fit for many physical phenomena occurring in nature. Other non-Gaussian PDFs are also common in many applications. For example, in power systems, wind speeds are usually modelled with Weibull PDF. It is an asymmetric distribution that is heavily skewed on one side and has a long tail. This PDF type fits wind speed density because lower wind speeds are more common than the higher wind speeds. The Weibull PDF is given as:

$$f_{\mathrm{W}}(x) = \begin{cases} \frac{k}{\lambda}\left(\frac{x}{\lambda}\right)^{k-1} \exp\left[-\left(\frac{x}{\lambda}\right)^{k}\right] & \text{if } x \geq 0 \\ 0 & \text{if } x < 0 \end{cases}, \tag{2.7}$$

where k is a shape parameter and λ is a scale parameter. Figure 2.2 shows an example of the Weibull PDF and CDF.

In power system dynamic analysis, where the effect of uncertainty on the dynamic behaviour of power system in steady-state is of concern, a technique known as probabilistic analysis is utilised. This technique requires initializing the power system dynamic equations randomly using predefined PDFs. This type of analysis cannot capture the effect of volatility during the Time Domain Simulation (TDS), which is of primary interest in this

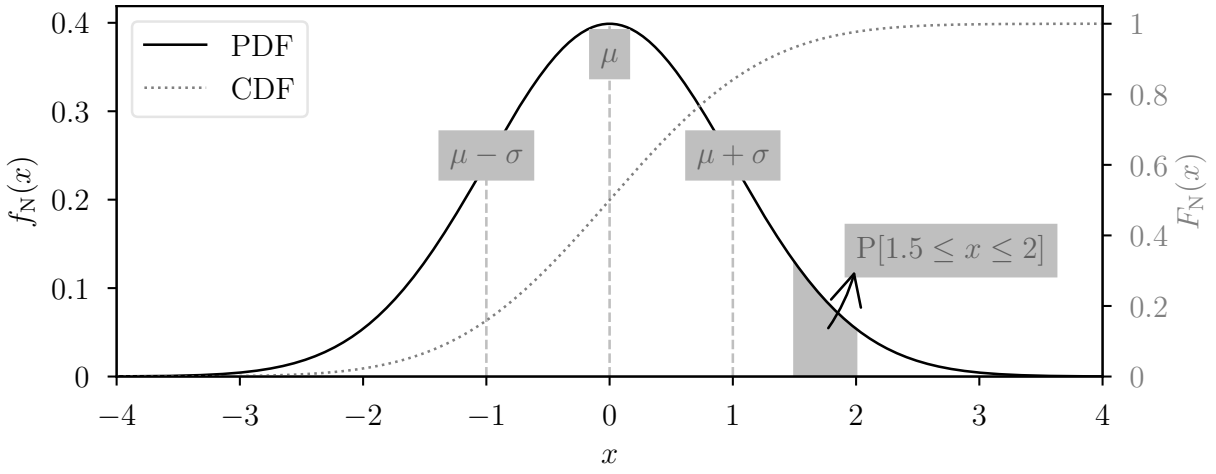

Figure 2.1: PDF and CDF of a Gaussian random variable $X \sim N(0, 1)$.

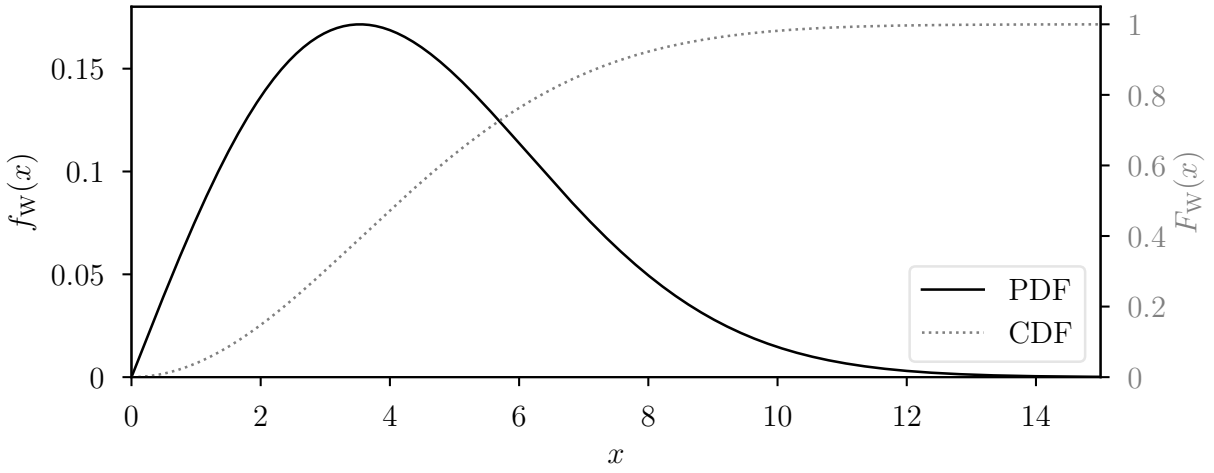

Figure 2.2: PDF and CDF of a random variable that follows Weibull distribution with scale = 5, and shape = 2.

thesis. For this reason, a power system dynamic analysis that includes volatility during the TDS requires modelling power system dynamic equations using stochastic processes. Stochastic processes can be modelled using SDEs, which are discussed here below.

2.3 Uncorrelated Stochastic Differential Equations (SDEs)

SDEs are a mathematical tool to model time-continuous stochastic processes. SDEs find their applications in economics, finance (stock markets), and physics (motion of particles). They are widely used in power systems to model physical processes such as wind speeds, solar irradiation, stochastic load consumption, and much more. A n-dimensional set of uncorrelated SDEs is written as:

$$\dot{\boldsymbol{\kappa}}(t) = \boldsymbol{a}(t, \boldsymbol{\kappa}(t)) + \boldsymbol{b}(t, \boldsymbol{\kappa}(t)) \circ \boldsymbol{\xi}(t)\,, \tag{2.8}$$

where $\boldsymbol{\kappa} \in \mathbb{R}^{n_\kappa}$ are uncorrelated stochastic processes; $\boldsymbol{a} \in \mathbb{R}^{n_\kappa}$ and $\boldsymbol{b} \in \mathbb{R}^{n_\xi}$ are continuous functions representing the *drift* and *diffusion* terms, respectively; $\circ$ is the Hadamard product, i.e. the element-wise product of two vectors; $\boldsymbol{\xi}(t) \in \mathbb{R}^{n_\xi}$ is a vector of uncorrelated *white noise*. Modelling the drift and diffusion terms in (2.8) independent of time produces stationary stochastic processes. Therefore, SDEs defining n uncorrelated stationary

stochastic processes are written as:

$$\dot{\boldsymbol{\kappa}}(t) = \boldsymbol{a}(\boldsymbol{\kappa}(t)) + \boldsymbol{b}(\boldsymbol{\kappa}(t)) \circ \boldsymbol{\xi}(t)\,, \tag{2.9}$$

In (2.9) $\xi(t)$ is a random process whose increments follow Gaussian PDF with zero mean. In mathematical terms, $\xi(t)$ is defined as the time derivative of the Wiener process, as follows:

$$\boldsymbol{\xi}(t)\,dt = d\boldsymbol{W}(t)\,, \tag{2.10}$$

where $\boldsymbol{W} \in \mathbb{R}^{n_w}$ is a vector of standard uncorrelated Wiener processes, whose elements, say $W_i(t)$, $i = 1, \ldots, n_w$, are fully independent and have the following properties:

1. $W_i(0) = 0$, with probability 1.
2. $W_i(t)$ is a continuous function of t.
3. $W_i(t)$ has unbounded variation in every interval.
4. The increments of $W_i(t)$ follow Gaussian PDF, i.e., $\forall t \geq 0$, $dW_i = W_i(t+h) - W_i(t) \sim \mathcal{N}(0, h)$.
5. $W_i(t)$ has independent increments, i.e., $\forall 0 \leq s < t$, $\mathrm{cov}[dW_i(t), dW_i(s)] = 0$.

A few examples of realizations of sample paths of $W_i(t)$ are shown in Figure 2.3. The sample paths of $W_i(t)$ cannot be differentiated in time, i.e., $\lim_{h\to 0}(W_i(t+h) - W_i(t))/h$ does not exist. Note that this property does not contradict the expression of the white noise given in (2.10), which is only a formal definition that allows to express SDE in differential form but has no practical application. The integration of (2.9) only involves $d\boldsymbol{W}$ and sufficiently small time steps h [34]. In other words, $\boldsymbol{\xi}$ *per se* is not needed in the calculations and is not computed explicitly. In fact, substituting (2.10) into (2.9) and integrating the result one obtains the common integral form of SDEs, which is the one actually implemented in numerical tools:

$$\boldsymbol{\kappa}(t) = \boldsymbol{\kappa}(0) + \int_t \boldsymbol{a}(\boldsymbol{\kappa}(\tau))\,d\tau + \int_W \boldsymbol{b}(\boldsymbol{\kappa}(\tau)) \circ d\boldsymbol{\kappa}(\tau)\,, \tag{2.11}$$

where $\boldsymbol{\kappa}(0)$ is the initial value of the process at time $t = 0$. Note that a SDE can either be initialized deterministically say $\boldsymbol{\kappa}(0) = \boldsymbol{0}$, or randomly where $\boldsymbol{\kappa}(0)$ can be chosen

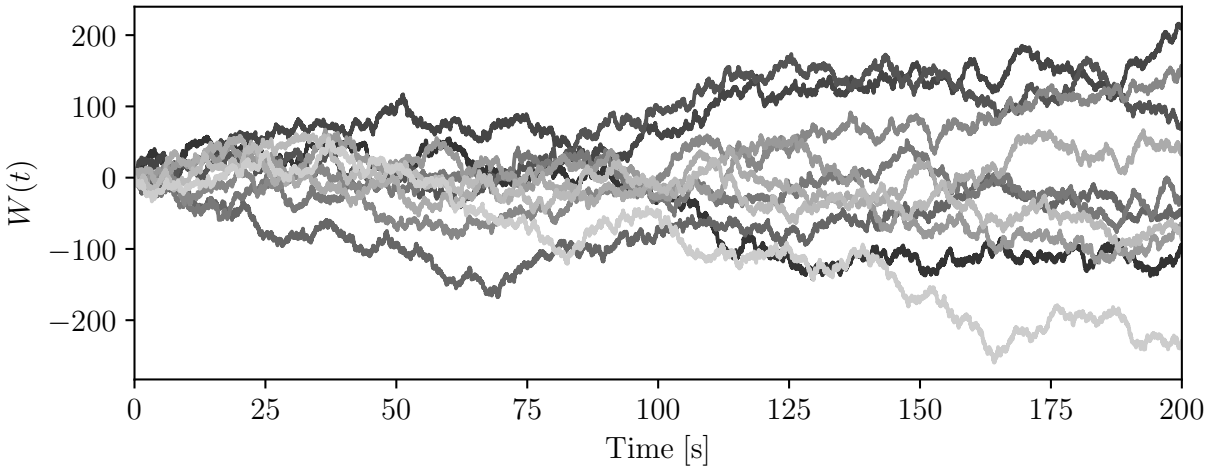

Figure 2.3: Realizations of ten sample paths of Wiener process $W(t)$.

from a given PDF. Note also that even though the Wiener process follows Gaussian PDF by definition, non-Gaussian PDFs can also be generated through SDEs by using proper definitions of the drift and diffusion terms.

Equation (2.9) is non-deterministic due to the presence of the integral with respect to the Wiener process. This integral is termed as stochastic integral and cannot be interpreted as the conventional Riemann-Stieltjes' integral due to the unbounded variations of the Wiener process. Several approaches have been proposed to interpret stochastic integrals, e.g., Itô and Stratonovich approach. The choice of the stochastic integral approach depends on the application of the SDE. Widely used interpretation of stochastic integral in the power systems is the Itô integration approach, which is adopted throughout this thesis as well.

The solution of (2.9) involves the integration of two terms, namely drift and diffusion. The integral involving the drift term is a deterministic integral and is solved as a conventional Riemann-Stieltjes' integral. Whereas, the integration of the diffusion term involves stochastic approach, e.g., Itô integral. Most SDEs cannot be solved analytically due to the complexity of the non-deterministic integral. However, it is possible to obtain information about the statistical properties, such as mean and variance, of the SDEs by solving the Fokker-Planck, forward or backward Kolmogorov equations. These are also generally solved numerically. The numerical methods available to solve SDEs are as follows. The drift term is integrated using conventional methods such as implicit trapezoidal method or the backward differentiation formulas [49]. The sample paths of the Wiener process are created using Euler-Maruyama, Milstein or Runge–Kutta

method. The Euler-Maruyama method is the most utilised to solve Itô SDEs by time discretization [35, 60].

2.4 Features of SDEs

2.4.1 Autocorrelation Function

Autocorrelation Function (ACF) of a stochastic process is the measure of correlation of the current values to the past values of the process. In other words, the ACF measures the linear dependence of the process to the delayed version of the same process over progressive time delays. The ACF can be expressed as a function of time delay τ, and is written as follows:

$$R_\kappa(\tau) = \frac{\mathrm{E}[(\kappa(t) - \mu_\kappa)(\kappa(t+\tau) - \mu_\kappa)]}{\sigma_\kappa^2}, \tag{2.12}$$

where R_κ is the ACF of the stochastic process κ; and μ_κ and σ_κ^2 are the mean and variance of κ, respectively.

The extensive data analysis of a variety of stochastic processes observed in power systems has revealed an ACF [9, 11, 28, 41, 44, 46, 63], where the nearby data points of the process are closely related, whereas the distant data points show a weak correlation. This gives rise to an ACF with higher correlation for smaller τ, and this correlation decreases monotonically as τ advances. The ACF of stationary stochastic process depends only on τ. Its dependence on τ can be approximated with a exponential function, and written as:

$$R_\kappa(\tau) = e^{-\alpha_\kappa \tau}, \tag{2.13}$$

where α_κ is the autocorrelation coefficient of process κ. According to (2.13) the higher the α_κ the faster the decay.

The desired ACF can be enforced in (2.9) through the drift term. The drift term defines the long term trend of the stationary stochastic process, i.e., the evolution of process in time. In (2.9), an exponentially decaying ACF can be obtained by defining the drift term via a first order linear differential equation. The drift term is written as:

$$a(\kappa(t)) = -\alpha_\kappa(\kappa(t) - \mu_\kappa)\,, \tag{2.14}$$

where α_κ and μ_κ are the autocorrelation coefficient and mean of the process κ, respectively.

2.4.2 Probability Density Function

Stationary stochastic processes are characterized by stationary PDFs. In other words, the data points of a stationary stochastic process obtained over two equal-length time intervals follow the PDFs with similar statistical properties. Stationary stochastic processes with the required ACFs and given PDFs can be created through SDEs using proper formulations of drift and diffusion terms in (2.9). The expressions for the drift and diffusion term in (2.9) can be obtained using either of the two methods, namely, Fokker-Planck equation [13, 81, 82] or memory less transformation [9, 28, 46, 83].

Both methods require that either the drift or diffusion term is defined first and then the expression for the other term to satisfy the required conditions is determined. The diffusion term through its dynamic interaction with the drift term is responsible for defining the PDF of the stationary stochastic process. Since, in this thesis we are interested in autocorrelated stationary stochastic processes, the expression for the drift term in (2.14) is used throughout the thesis. Based on the definition of the drift term in (2.14) the expression for the diffusion term to impose required PDF can be calculated using one of the two methods, mentioned above in this section.

Note that the procedure to evaluate the autocorrelation coefficient and the fitting PDF from measurement data is provided in detail later in Section 2.6. A few examples of stationary stochastic processes constructed using SDEs along with the expressions for drift and diffusion terms are illustrated later in Section 2.7.

2.5 Correlated SDEs

2.5.1 SDEs with Correlated Wiener Processes

This section presents a procedure to construct correlated SDEs from uncorrelated SDEs. This method was proposed in [3] and is one of the main contributions of the thesis. To construct correlated SDEs from uncorrelated SDEs, let us again consider (2.9). Defining $\boldsymbol{W}$ as a vector of independent Wiener processes makes (2.9) a set of uncorrelated SDEs. $\boldsymbol{W}$ is a vector of independent Wiener processes only if the cross-correlation between

the elements of $\boldsymbol{W}$ is zero. In this case the elements of the variance-covariance matrix $\mathbf{P} \in \mathbb{R}^{n \times n}$ of the increments $d\boldsymbol{W}$ are defined as follows:

$$P_{i,j} = \text{cov}[dW_i, dW_j] = \begin{cases} \sigma_{\text{i}}^2, & \text{if } i = j\,, \\ 0, & \text{if } i \neq j\,, \end{cases} \tag{2.15}$$

where dW_i (dW_j) represents the infinitesimal increment of the i-th (j-th) element of $\boldsymbol{W}$.

To correlate SDEs in (2.9), it is required to create a vector of correlated Wiener processes, say $\boldsymbol{V}$. This can be done by writing $\boldsymbol{V}$ in terms of $\boldsymbol{W}$ using a linear relationship. This relationship should correlate the Wiener processes without affecting their statistical properties, i.e., mean and variance. This is to ensure that the information stored in the form of PDFs of the individual processes remains unaltered.

The correlation between the elements of $\boldsymbol{V}$ can be assigned using the correlation matrix $\boldsymbol{R} \in \mathbb{R}^{n \times n}$ defined as:

$$\boldsymbol{R} = \begin{bmatrix} 1 & r_{1,2} & r_{1,3} & \dots & r_{1,n} \\ r_{2,1} & 1 & r_{2,3} & \dots & r_{2,n} \\ r_{3,1} & r_{3,2} & 1 & \dots & r_{3,n} \\ \vdots & \vdots & \vdots & \ddots & \vdots \\ r_{n,1} & r_{n,2} & r_{n,3} & \cdots & 1 \end{bmatrix},$$

where $r_{i,j}$ represents the correlation between dV_i and dV_j, whose value can be calculated using Pearon's correlation coefficient provided in Appendix B.2.1. The element $r_{i,j}$ considers both spatial and temporal correlations. The value of $r_{i,j}$ can either be a constant, i.e., in case of spatial correlation (since the distance between any two points remains fixed) or a function of time, i.e., temporal correlation. In case of temporal correlation $r_{i,j}$ becomes a time-continuous process.

The elements $r_{i,j}$ can be defined through a stochastic process, as follows:

$$\dot{r}_{i,j} = a(r_{i,j}) + b(r_{i,j})\xi\,, \tag{2.16}$$

Note that in the case of temporal correlation, the value of $r_{i,j}$ is updated in $\boldsymbol{R}$ at every time step of the TDS. This makes $\boldsymbol{R}$ a scalar matrix, i.e., $\mathbf{R}$, whose elements are updated at every time step.

The procedure to calculate the correlation between dV_i and dV_j through measurement data is thoroughly explained in the next subsection. The diagonal elements of $\mathbf{R}$ are always 1 since the correlation of a process with itself is 1 by definition. The elements of variance-covariance matrix $\mathbf{P} \in \mathbb{R}^{n \times n}$ of $d\boldsymbol{V}$ are written as:

$$\mathrm{P}_{i,j} = \mathrm{cov}[dV_i, dV_j] = \begin{cases} \sigma_i^2, & \text{if } i = j\,, \\ r_{i,j}\sigma_i\sigma_j, & \text{if } i \neq j\,, \end{cases} \tag{2.17}$$

The procedure to write $d\boldsymbol{V}$ in terms of $d\boldsymbol{W}$ is involved and is thoroughly explained in [16]. Here, we simply provide the final expression:

$$d\boldsymbol{V} = \mathbf{C}\, d\boldsymbol{W}\,, \tag{2.18}$$

where $\mathbf{C} \in \mathbb{R}^{n \times n}$ is chosen such that:

$$\mathbf{R} = \mathbf{C}\,\mathbf{C}^T\,, \tag{2.19}$$

A family of $\mathbf{C}$ matrices satisfies (2.19) but the best choice of $\mathbf{C}$ is a lower triangular matrix as it reduces memory requirements and the computational burden of numerical implementations. A lower triangular matrix is obtained by performing Cholesky-decomposition of $\mathbf{R}$. Cholesky-decomposition requires that the input matrix is positive semi-definite. This condition is generally satisfied for stochastic processes of power systems [3]. Note that correlating the elements of $d\boldsymbol{W}$ using (2.18) does not affect the individual PDFs of the elements of $d\boldsymbol{W}$. Note also that $\mathbf{R} = \mathbf{I}$ makes $d\boldsymbol{V} = d\boldsymbol{W}$, where $\mathbf{I}$ is the identity matrix. In other words, $\boldsymbol{V}$ becomes a vector of fully independent Wiener processes.

By substituting the definition of correlated Wiener processes in (2.9), correlated SDEs can be modelled as:

$$\begin{aligned} \dot{\boldsymbol{\eta}}(t) &= \boldsymbol{a}(\boldsymbol{\eta}(t)) + \boldsymbol{b}(\boldsymbol{\eta}(t)) \circ \boldsymbol{\zeta}(t)\,, \\ \boldsymbol{\zeta}(t) &= \mathbf{C}\,\boldsymbol{\xi}(t)\,, \end{aligned} \tag{2.20}$$

where $\boldsymbol{a}$, $\boldsymbol{b}$ and $\boldsymbol{\xi}$ have the same meaning as in (2.8) and (2.9); $\mathbf{C}$ satisfies (2.19); $\boldsymbol{\eta} \in \mathbb{R}^{n_\eta}$ is the vector of correlated stochastic processes; and $\boldsymbol{\zeta} \in \mathbb{R}^{n_\zeta}$ is the vector of correlated white noises.

Remarks

Even though the set of n-dimensional correlated SDEs in (2.20) is constructed utilising correlated Wiener processes, the PDFs of the processes resulting from the correlated SDEs do not change. Since, the PDF depends only on the drift a, and the diffusion b, see Sections 2.4 and 2.7. These terms a and b are not modified by the correlation of Wiener process. Note that (2.20) is valid for stochastic processes with different ACFs and PDFs, i.e., for $a_i(\eta_i) \neq a_j(\eta_j)$ and $b_i(\eta_i) \neq b_j(\eta_j)$. Also note that (2.20) can be used for arbitrary time-scales and arbitrary dimensions. This makes (2.20) able to model correlated stochastic processes with arbitrary ACFs, PDFs, time-scales, and dimensions.

The numerical algorithms available to generate random numbers only generate independent Wiener processes. Thus $\boldsymbol{\zeta}$ can be obtained only indirectly, i.e., through the calculation of $\mathbf{C}\,\boldsymbol{\xi}$. Note that $\mathbf{C} = \mathbf{I}$ for $\mathbf{R} = \mathbf{I}$, where $\mathbf{I}$ is the Identity matrix, causes (2.20) to generate uncorrelated stochastic processes. Since (2.20) can generate both uncorrelated and correlated stochastic processes, (2.20) will be used throughout the thesis to represent SDEs.

2.5.2 Setting Up Correlation Matrix

The correlation matrix $\mathbf{R}$ is the core mathematical object that allows defining the correlation between stochastic processes in (2.20). The elements $r_{i,j}$ of $\mathbf{R}$ are defined based on measurement data. The value of $r_{i,j}$ is obtained by calculating the correlation between the infinitesimal increments of the two stochastic processes. These increments are termed as *noise elements*. This section aims at the calculation of the correlation matrix through the calculation of the noise elements of a stochastic process from measurement data. This method was originally proposed in [6], and is one of the main contributions of the thesis.

Let us consider, an individual exponentially decaying autocorrelated stochastic process. This process is obtained by substituting the value of drift term a from (2.14) into (2.9), and is written as:

$$\dot{\kappa}_i = -\alpha_i(\kappa_i - \mu_i) + b_i(\kappa_i)\xi_i\,, \quad i = 1, \ldots, n, \tag{2.21}$$

where α_i and μ_i have the same meaning as in (2.14), and all remaining parameters and variables have the same meaning as in(2.9).

To extract the noise elements of the processes with arbitrary PDFs the analytical solution of (2.21) is considered. The solution of (2.21) can be established by multiplying it by $e^{\alpha t}$, and re-arranging as:

$$\alpha\kappa(t)e^{\alpha t}dt + e^{\alpha t}d\kappa(t) = e^{\alpha t}\big[\mu\alpha + b\left(\kappa(t)\right)\, dW(t)\big]\,. \tag{2.22}$$

Note that

$$d\left(e^{\alpha t}\,\kappa(t)\right) = \alpha\kappa(t)e^{\alpha t}dt + e^{\alpha t}dW(t)\,, \tag{2.23}$$

Substituting (2.23) into (2.22) and integrating, one obtains:

$$\kappa(t) = \kappa(0)e^{-\alpha t} + \int_0^t \mu\alpha e^{\alpha(s-t)}ds + \int_0^t b\left(\kappa(s)\right)e^{\alpha(s-t)}dW(s)\,, \tag{2.24}$$

where $\kappa(0)$ is the initial value of the process at $t = 0$. The first integral is the conventional Riemann-Stieltjes' integral, and integrates to $\mu\left(1-e^{-\alpha t}\right)$. The second integral is expressed as an Itô integral. Using Itô isometry [26, 54], the second integral integrates to a normal random variable with mean zero and variance given as:

$$E\left[\int_0^t b\left(\kappa(s)\right)e^{\alpha(s-t)}dW(s)\right]^2 = \frac{b^2\left(\kappa(t)\right)}{2\alpha}\left(1-e^{-2\alpha t}\right)\,, \tag{2.25}$$

Note that according to the definition given in (2.9), $b(\kappa)$ does not explicitly depend on t. Thus, the analytical solution of (2.21) is written as:

$$\kappa(t) = \kappa(0)\,e^{-\alpha t} + \mu\left(1-e^{-\alpha t}\right) \quad + b\big(\kappa(t)\big)\,\psi_\kappa(t)\,\sqrt{\frac{1-e^{-2\alpha t}}{2\alpha}}\,, \tag{2.26}$$

where $\psi_\kappa(t)$ is the random variable, which is distributed normally with zero mean and unit variance. $\psi_\kappa(t)$ can be extracted from (2.26) and written as:

$$\psi_\kappa(t) = \frac{\kappa(t) - \kappa(0)\,e^{-\alpha t} - \mu\left(1-e^{-\alpha t}\right)}{b\big(\kappa(t)\big)\,\sqrt{\frac{1-e^{-2\alpha t}}{2\alpha}}}\,, \tag{2.27}$$

Equation (2.27) is employed to estimate the noise element $\psi_\kappa(t)$ from the empirical data, provided the underlying process can be defined using (2.21).

The solution provided in (2.26) is valid for an arbitrary time interval $[0, t]$ and any initial condition. It can also be applied to an arbitrarily chosen time step Δt beginning

at t_{i-1} and ending at t_i. Let us assume equidistantly spaced time steps such that $\forall i \in \mathbb{Z}_+, t_i - t_{i-1} = \Delta t > 0$. To calculate the increment in the stochastic process at an arbitrarily chosen step size of Δt, we assume that the value of the process at the previous time step t_{i-1} serves as the initial condition for time step t_i. Therefore, the increment in the stochastic process for the step size Δt is calculated using (2.26) as:

$$d\kappa(t_i) = \kappa(t_{i-1})\, e^{-\alpha \Delta t} + \mu\,(1 - e^{-\alpha \Delta t}) \quad + b\big(\kappa(t_{i-1})\big)\, \psi_\kappa(t_i) \sqrt{\frac{1 - e^{-2\alpha \Delta t}}{2\alpha}}\,, \tag{2.28}$$

Similarly, the increment of $\psi(t_i)$ for the time step Δt is written as:

$$d\psi_\kappa(t_i) = \frac{\kappa(t_i) - \kappa(t_{i-1})\, e^{-\alpha \Delta t} - \mu\,(1 - e^{-\alpha \Delta t})}{b\big(\kappa(t_{i-1})\big)\, \sqrt{\frac{1 - e^{-2\alpha \Delta t}}{2\alpha}}}\,, \tag{2.29}$$

Note that since the term b is not modified in (2.29), and also that (2.29) was created using an autocorrelated ACF. This makes (2.29) valid for stochastic processes with arbitrary time-scales, dimensions, PDFs, and ACFs, i.e., autocorrelation coefficient. The application of (2.29) to extract $d\psi$ from stochastic processes with various time-scales, dimensions, PDFs, and ACFs, and the construction of correlation matrix based on measurement data is illustrated in Chapter 6.

2.5.3 Special Case of 2-dimensional Correlated SDEs

This section discusses a relevant special case of (2.20), namely a two-dimensional correlated stochastic process, which is helpful, for example, to model correlated active and reactive load power consumption. Assuming a correlation r between the infinitesimal increments of the two processes the correlation matrix $\mathbf{R}$ is written as:

$$\mathbf{R} = \begin{bmatrix} 1 & r \\ r & 1 \end{bmatrix},$$

Using (2.19) and Cholesky-decomposition, $\mathbf{C}$ is calculated as:

$$\mathbf{C} = \begin{bmatrix} 1 & 0 \\ r & \sqrt{1 - r^2} \end{bmatrix},$$

A 2-dimensional correlated SDE is constructed by inputting $\mathbf{C}$ in (2.20), and is written as:

$$\begin{aligned} \dot{\eta}_1(t) &= a_1(\eta_1(t)) + b_1(\eta_1(t))\,\xi_1(t)\,, \\ \dot{\eta}_2(t) &= a_2(\eta_2(t)) + b_2(\eta_2(t))\big(r\,\xi_1(t) + \sqrt{1-r^2}\,\xi_2(t)\big)\,, \end{aligned} \tag{2.30}$$

where r is the correlation between the two processes; and all the remaining parameters and variables have same meaning as in (2.9).

2.6 Setting Up SDEs

This section provides details on the set up of the SDE defined through either (2.9) or (2.20). As explained in Section 2.4 that a SDE in (2.9) or (2.20) contains two terms, namely the drift a and the diffusion b, that are responsible to model the behaviour of a process. This section deals with the evaluation of these terms based on the measurement data. Note that the procedure presented in this section is independent of the drift, i.e., ACF, and the diffusion, i.e., PDF, of the stochastic process. Hence, the procedure described in this section is general and can be applied to stationary stochastic processes with arbitrary ACFs, PDFs, and time-scales.

The first step is to set up the drift a of the SDE. This is done by calculating the ACF of the stochastic process using (2.12). As explained in Section 2.4.1, the ACFs of the stationary stochastic processes follow exponential functions with negative coefficient. This coefficient is calculated by fitting a exponentially decaying function to the ACF obtained from the measurement data. The coefficient obtained is the autocorrelation coefficient α, which is the fundamental element to set up the drift a of the SDE [28, 83].

The next step is to set up the diffusion b of the SDE. The diffusion term in interaction with the drift term is responsible for defining the PDF of the SDE. For this reason, it is necessary to identify the PDF that best fits the measurement data. The parameters of the best fitting PDF must be calculated based on measurement data as well. There are various statistical tests available that reveal the best fitting PDF. In this thesis, the Kolmogorov-Smirnov (KS) test is utilized. The KS test is a non-parametric test that measures the closeness of the probability distribution of the sampled measurement data to a given PDF. Whereas the parameters of the fitting PDF are obtained through the

Maximum Likelihood Estimation method. Once the fitting PDF and its parameters are known, the diffusion term can be set up using any of the methods introduced in Section 2.4.2. The methods described in this section have been utilized in various power system dynamic studies [6, 28].

2.7 Example Stochastic Processes

The SDE in (2.20) can be utilised to generate correlated stationary stochastic processes, which will follow any required ACF and PDF, through the proper implementation of the drift a and diffusion b terms. In this section, a few examples of Gaussian and non-Gaussian correlated stationary stochastic processes are discussed. These processes are utilised in power system dynamic simulations throughout the thesis. Examples of various PDF types are considered in this section. It is important to note that processes with any other PDFs can be utilised. All PDF types, in fact, can be created through the proper definition of a and b using the methods mentioned in Section 2.4.

2.7.1 Gaussian Processes

Modelling the diffusion term in (2.9) and/or (2.20) as a constant, creates a stochastic process that follows Gaussian PDF, and is known as OU process. The OU process is a continuous process with mean-reversion. That is, it drifts towards its mean with an exponential rate. This causes it to have a bounded variance unlike the Wiener process. These features make the OU process adequate to model the volatility of bounded physical quantities such as stochastic load dynamics [57, 58, 70] and short-term wind fluctuations [9, 11, 28, 44, 55]. The OU process is discussed in further details in Chapter 5.

Correlated Ornstein-Uhlenbeck Process

Correlated OU processs can be generated using (2.20) with the drift and diffusion terms given as:

$$\begin{aligned} a(\eta(t)) &= -\alpha(\eta(t) - \mu)\,, \\ b(\eta(t)) &= \sqrt{2\alpha}\sigma\,, \end{aligned} \tag{2.31}$$

where α is the autocorrelation coefficient of the process, and μ and σ are the mean and standard deviation of the process at the stationary condition, respectively.

Figure 2.4 illustrates the realizations of two-dimensional correlated OU processes for different values of r while keeping α, μ and σ constant. The PDFs of the OU processes in Figure 2.4 are shown in Figure 2.5. From Figure 2.5 it is evident that the processes η_1 and η_2 follow Gaussian PDFs, despite being generated for different values of r between them.

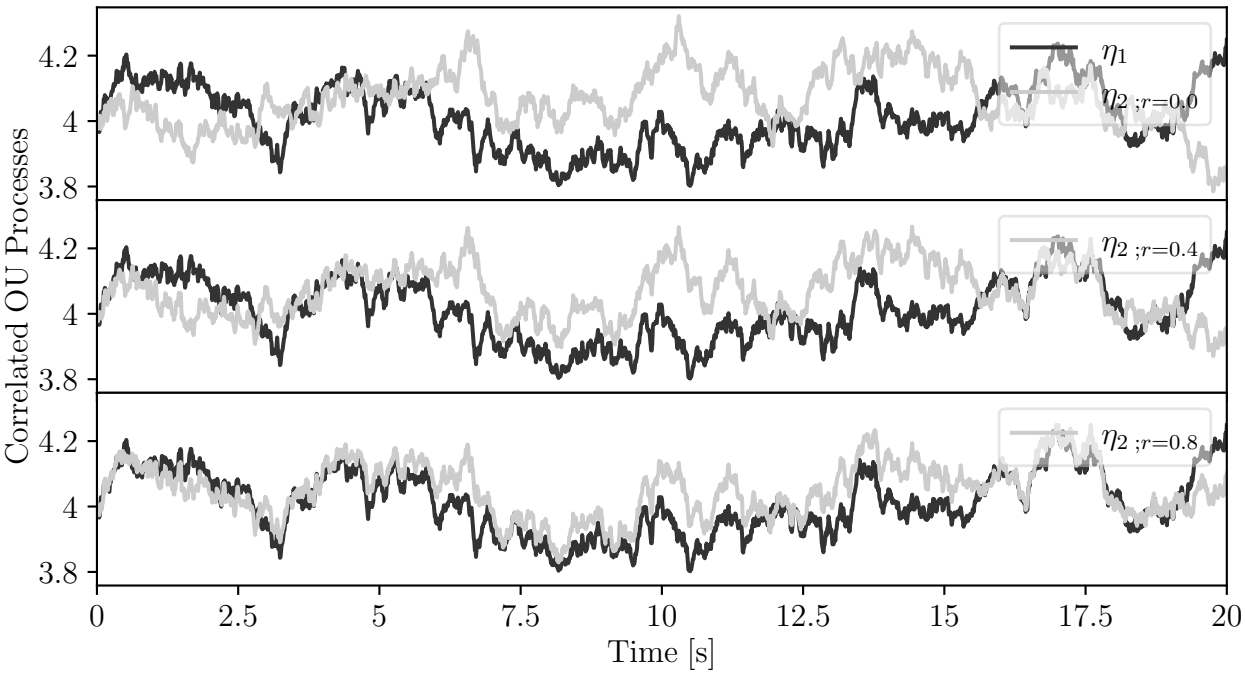

Figure 2.4: Realization of two-dimensional correlated OU process, η_1 and η_2, for different values of correlation r, and for $\alpha_1 = \alpha_2 = 1s^{-1}$, $\mu_1 = \mu_2 = 4$, and $\sigma_1 = \sigma_2 = 0.1$.

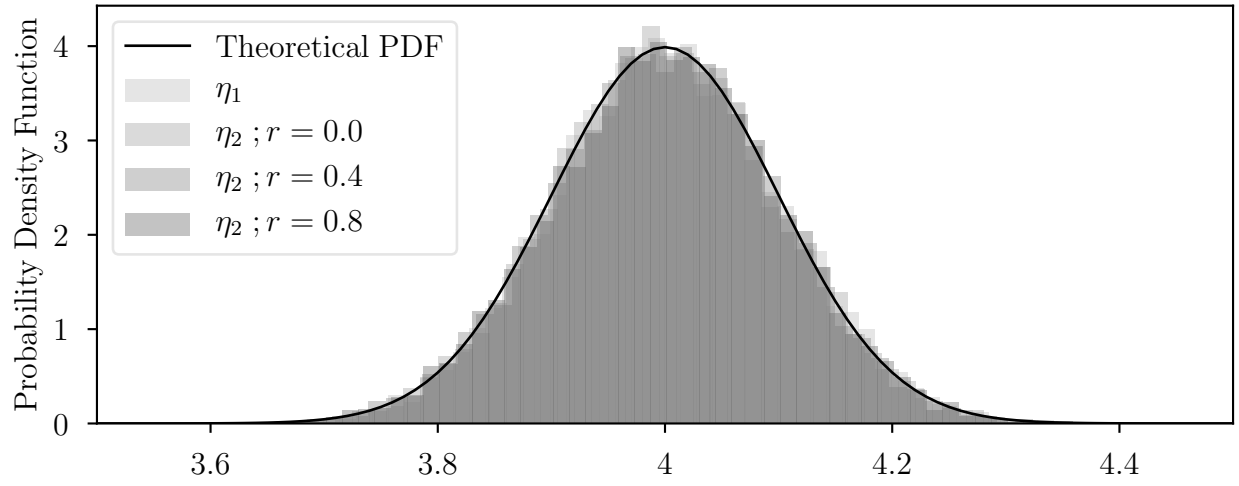

Figure 2.5: PDF of correlated OU processes in Figure 2.4.

2.7.2 Non-Gaussian Processes

Non-Gaussian processes occur in power systems in many forms. For example, in [63] the authors, through measurement data, show that the load consumption follows a Normal-Inverse Gaussian PDF with heavy tails. Non-Gaussian PDFs such as two-parameter Weibull PDF are used in the literature to model wind speeds. The fitting PDFs and their parameters depend upon the time-scale and location of the wind speeds [28]. In this subsection, a variety of correlated stochastic processes following different PDFs are presented.

2.7.2.1 Correlated Weibull Distributed Processes

N-dimensional correlated Weibull distributed processes that follow the PDF in (2.7) are generated using (2.20) [82] with the drift term as:

$$a(\eta) = -\alpha \left(\eta - \lambda\Gamma\left(1 + a^{-1}\right)\right) , \tag{2.32}$$

and the diffusion term as:

$$b(\eta) = \sqrt{b_1(\eta) b_2(\eta)} , \tag{2.33}$$

with

$$b_1(\eta) = 2\alpha\,\eta\, c_1 \frac{\lambda}{a} \left(c_2\right)^{-a} , \tag{2.34}$$

and

$$b_2(\eta) = a \exp\left(\left(c_2\right)^a\right) \Gamma\left(1 + c_1, \left(c_2\right)^a\right) - \Gamma\left(c_1\right) , \tag{2.35}$$

where $c_1 = 1/a$ and $c_2 = \eta/\lambda$; α is the autocorrelation coefficient; a is a shape parameter; λ is a scale parameter; $\Gamma(\cdot)$ is the Gamma function; and $\Gamma(\cdot,\cdot)$ is the Incomplete Gamma function.

Figure 2.6 illustrates the realizations of two-dimensional correlated Weibull distributed processes for different values of r while keeping shape and scale constant. The PDFs of the Weibull distributed processes presented in Figure 2.6 are shown in Figure 2.7. This figure shows that the processes η_1 and η_2 follow, in effect, a Weibull PDF and can be correlated with each other while preserving their PDFs and other statistical properties.

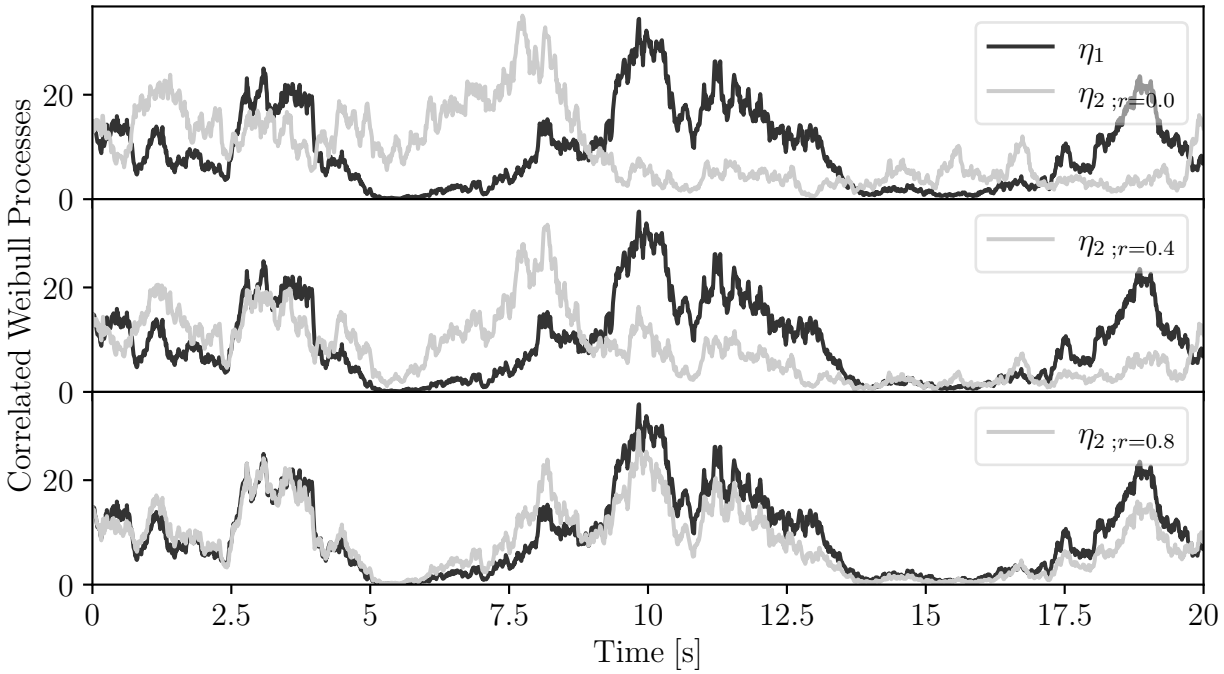

Figure 2.6: Realization of two-dimensional correlated Weibull distributed process, η_1 and η_2, for different values of the correlation r, and for $\alpha_1 = \alpha_2 = 0.5s^{-1}$; $\text{shape}_1 = \text{shape}_2 = 2$; and $\text{scale}_1 = \text{scale}_2 = 8$.

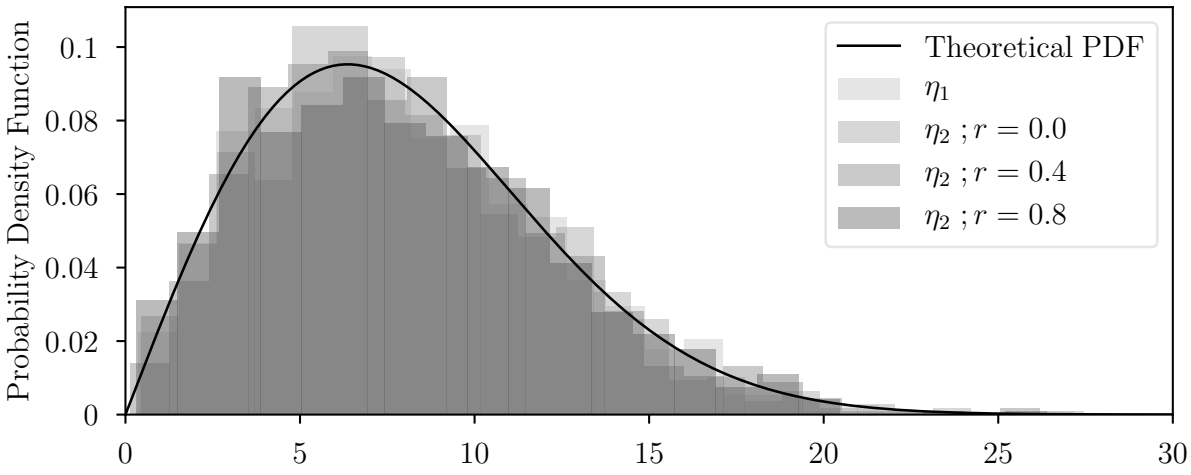

Figure 2.7: PDF of correlated Weibull distributed processes in Figure 2.6.

2.7.2.2 Correlated Three-parameter Beta Distributed Processes

The PDF of the three-parameter Beta distribution ($f_{\text{B}}(\eta)$) is

$$f_{\text{B}}(\eta) = \begin{cases} \dfrac{1}{\lambda\, B\,[a,b]} \left(\dfrac{\eta}{\lambda}\right)^{a-1} \left(\dfrac{\lambda-\eta}{\lambda}\right)^{b-1} & \text{if } \eta > 0 \\ 0 & \text{if } \eta \leq 0 \end{cases},$$

where $B[\cdot,\cdot]$ is the Beta function, a and b are shape parameters, and λ is a noncentrality parameter.

A multidimensional correlated three-parameter Beta distributed process can be created using (2.20) [82] with the drift and diffusion terms as follows:

$$\begin{aligned} a(\eta) &= -\alpha \left(\eta - \frac{a\,\lambda}{a+b}\right), \\ b(\eta) &= \sqrt{\frac{2\,\alpha\,(\lambda-\eta)\,\eta}{a+b}}, \end{aligned} \tag{2.36}$$

Two-dimensional correlated Beta distributed processes and their PDFs are shown in Figures 2.8 and 2.9, respectively. These Figures show that the correlation modelled on the stochastic processes does not modify their PDFs.

2.7.2.3 Correlated Two-parameter Gamma Distributed Processes

The PDF of the two-parameter Gamma distribution ($f_{\mathrm{G}}(\eta)$) is

$$f_{\mathrm{G}}(\eta) = \begin{cases} \dfrac{1}{\lambda^a\,\Gamma\,[a]}\;\eta^{a-1}\,\exp\left[-\dfrac{\eta}{\lambda}\right] & \text{if } x > 0 \\ 0 & \text{if } x \leq 0 \end{cases},$$

where $\Gamma[\cdot]$ is the Gamma function, a is a shape parameter, and λ is a scale parameter.

The drift and diffusion terms to generate correlated stochastic processes using (2.20) that follow two-parameter Gamma distribution are written as follows:

$$\begin{aligned} a(\eta) &= -\alpha\,(\eta - a\,\lambda), \\ b(\eta) &= \sqrt{2\,\alpha\,\lambda\,\eta}\,. \end{aligned} \tag{2.37}$$

Figure 2.10 illustrates the realizations of two-parameter Gamma distributed processes for different correlations while keeping shape and scale constant. The PDFs of the correlated stochastic processes, illustrated in Figure 2.10, are shown in Figure 2.11. Again the processes are correlated without their PDFs being modified.

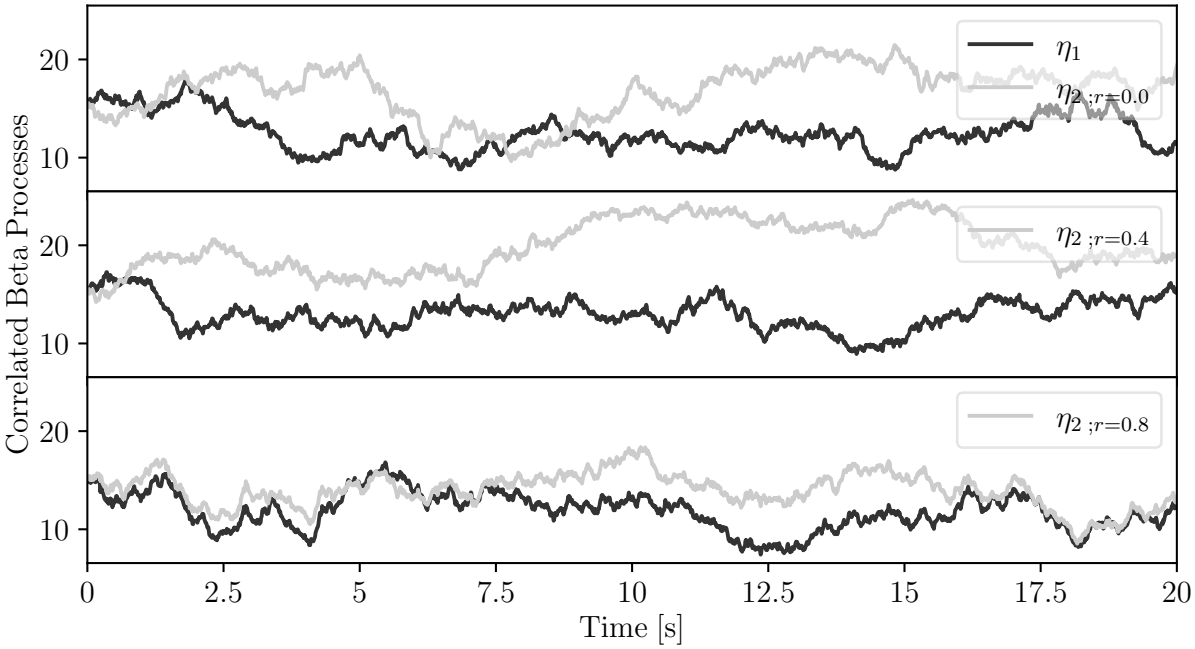

Figure 2.8: Realization of two-dimensional correlated Beta distributed process, η_1 and η_2, for different values of the correlation r, and for $\alpha_1 = \alpha_2 = 0.1s^{-1}$; $a_1 = a_2 = 2$; $b_1 = b_2 = 8$; and $\text{scale}_1 = \text{scale}_2 = 30$.

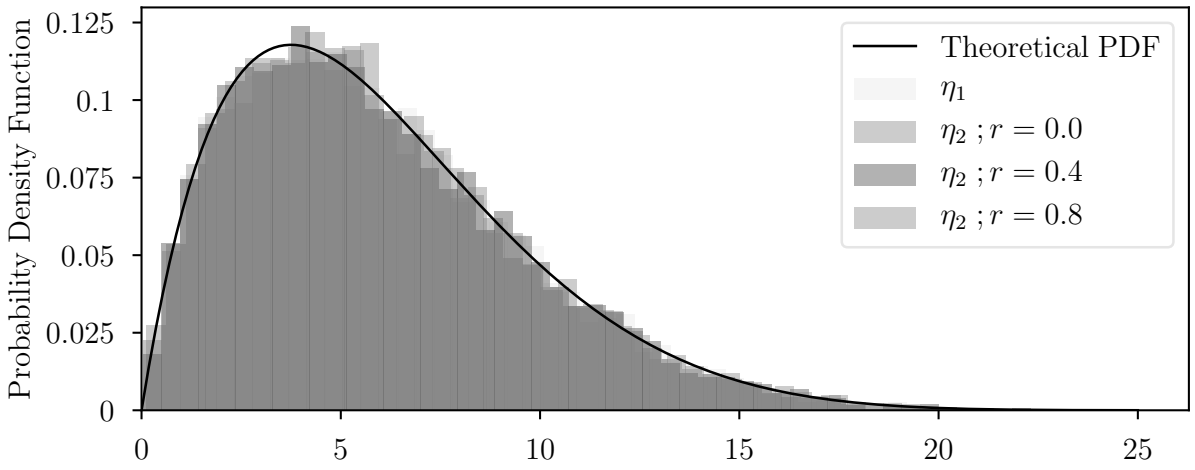

Figure 2.9: PDF of correlated Beta distributed processes in Figure 2.8.

2.8 Conclusions

This chapter introduces the stochastic processes modelled through SDEs. The relevant features, namely, drift and diffusion, of the stochastic processes are also discussed. A data-driven method to formulate correlated stochastic processes is presented as well. With this aim, two novel methods to: (i) model correlated stochastic processes using multidimensional SDEs; and (ii) construct correlation matrix, which is the fundamental

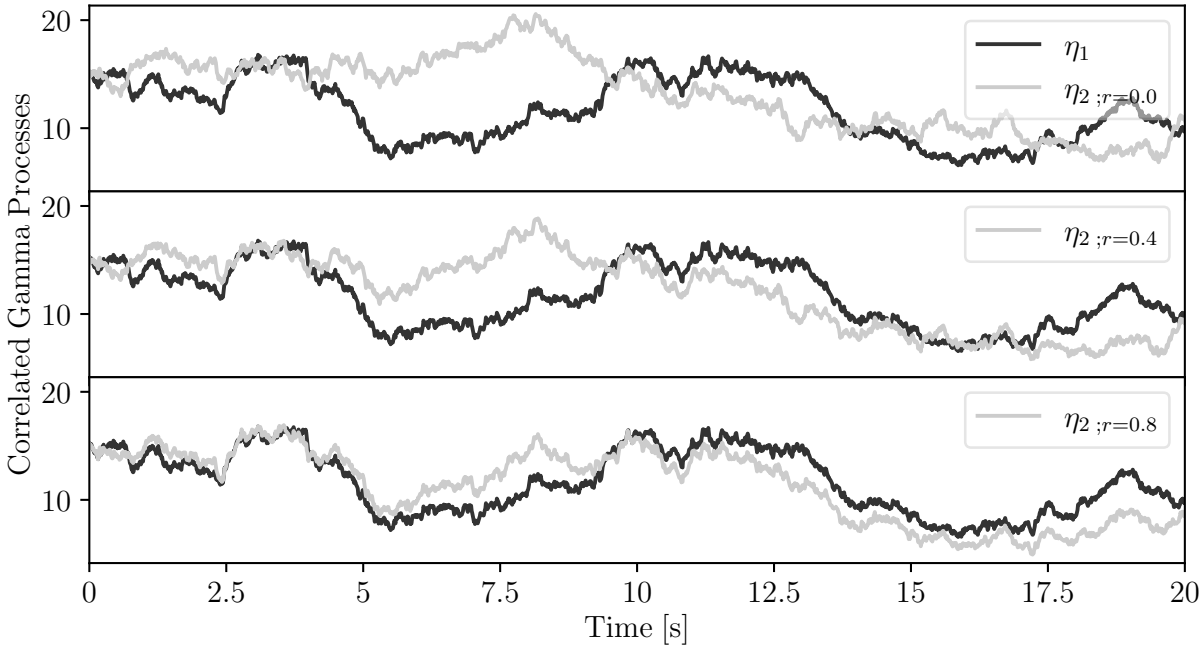

Figure 2.10: Realization of two-dimensional correlated Gamma distributed process, η_1 and η_2, for different values of the correlation r, and for $\alpha_1 = \alpha_2 = 0.1s^{-1}$; $\text{shape}_1 = \text{shape}_2 = 2.5$; and $\text{scale}_1 = \text{scale}_2 = 3.5$.

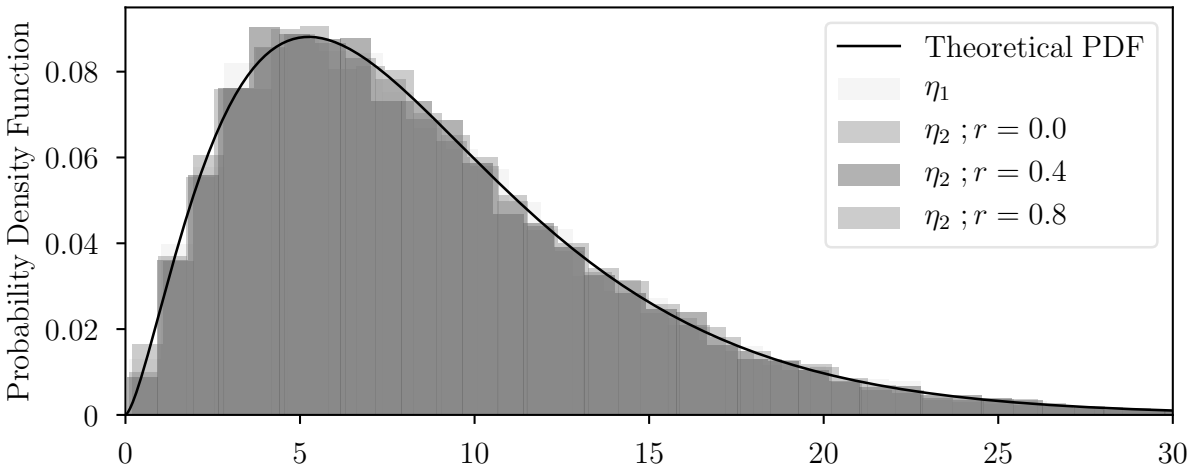

Figure 2.11: PDF of correlated Gamma distributed processes in Figure 2.10.

tool to set up correlated SDEs, based on measurement data are provided. The chapter also provides a discussion on the methods to set up SDEs based on the measurement data. Note that the methods provided in this chapter are independent of time-scales, PDFs, ACFs, and dimensions of the stochastic processes being modelled. Finally, a few examples to generate Gaussian and non-Gaussian correlated stochastic processes are also illustrated.

Chapter 3

Modelling Power Systems with Stochastic Processes

3.1 Introduction

The impact of stochastic disturbances on the dynamic response of power systems can be conveniently studied using Stochastic Differential Algebraic Equations (SDAEs). This has been thoroughly discussed in [17, 51, 73]. Reference [51] also presents a general approach to incorporate stochastic disturbances in power systems using SDAEs. A common assumption of the literature available on SDAE models for power systems is that stochastic disturbances are fully uncorrelated. However, this is not always the case, as introduced in Chapter 1, stochastic disturbances exhibit correlation, which has a worsening impact on the power system's dynamic. This is discussed later in detail in Chapter 6.

The correlation on the stochastic disturbances can be formulated as correlated Stochastic Differential Equations (SDEs) introduced in Chapter 2. Correlated SDEs can be incorporated into power system dynamic modelled as a set of DAEs. This gives rise to correlated SDAEs, which can be utilised to study the impact of the correlated stochastic disturbances on the dynamic behaviour of power systems. The main goal of this chapter is to provide a systematic and generalised approach to include correlated disturbances in existing power system dynamical models using correlated SDAEs. With this regard, this chapter also provides procedures to set up correlated disturbances on various sources of volatility, such as stochastic load power consumption, stochastic power flows, and penetration of Renewable Energy Sources (RES), i.e., production of Wind

Power Plants (WPPs), for the dynamic security and transient stability assessment of power systems.

Due to the granularity of wind sites, WPPs are typically connected to the grid in a tree-like topology as shown in Figure 3.1. This hierarchical structure leads to several levels at which wind production can be aggregated. It is crucial, however, that independently from the level at which WPPs are aggregated, the statistical properties of the power injected into the grid by the aggregated WPPs are similar to the ones obtained by simulating the detailed network. This chapter aims at providing a SDE-based model to properly set up an aggregated wind speed considering correlated wind speed fluctuations. The aggregated wind speed process is formulated such that when a aggregated WPP is driven by this process, the aggregated WPP reproduces accurately the statistical and dynamic behaviour of the original network, i.e., detailed representation of the network.

The models presented in this chapter enable the system operators to quantify the effect of correlation among stochastic disturbances on the dynamic security and transient stability of the power system. The proposed models can also be applied to systems of any order and complexity without the need for any simplifications or assumptions in the original model.

The remainder of the chapter is organised as follows. Section 3.2 provides a brief introduction to existing power system dynamic models. An overview of uncorrelated SDAEs is provided in Section 3.3. Whereas, correlated SDAEs are presented in Section 3.4. The methods to include correlated disturbances in the sources of volatility are

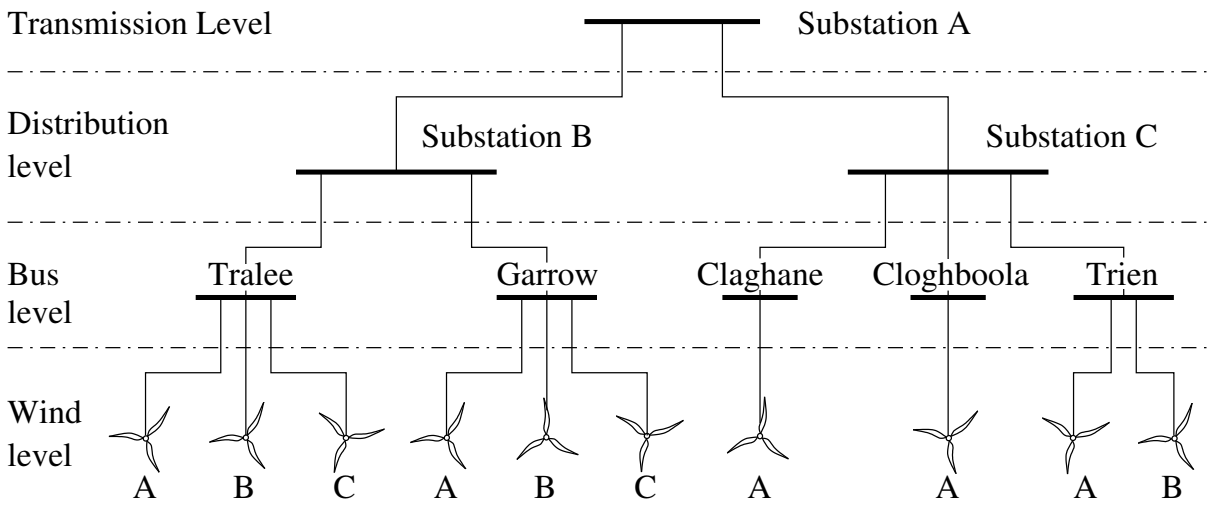

Figure 3.1: Typical tree of a power grid with inclusion of wind power generation.

provided in Section 3.5. Section 3.6 provides the model for aggregating correlated wind speeds. Finally, Section 3.7 draws conclusions.

3.2 Differential-Algebraic Equations

The transient behaviour of the power system is conventionally modelled using the following set of DAEs:

$$\begin{aligned} \dot{\boldsymbol{x}}(t) &= \boldsymbol{f}(\boldsymbol{x}(t), \boldsymbol{y}(t), \boldsymbol{u}(t)) \,, \\ \boldsymbol{0} &= \boldsymbol{g}(\boldsymbol{x}(t), \boldsymbol{y}(t), \boldsymbol{u}(t)) \,, \end{aligned} \tag{3.1}$$

where vectors $\boldsymbol{f} : \mathbb{R}^{n_x+n_y+n_u} \mapsto \mathbb{R}^{n_x}$ and $\boldsymbol{g} : \mathbb{R}^{n_x+n_y+n_u} \mapsto \mathbb{R}^{n_y}$ are the differential and algebraic equations, respectively; $\boldsymbol{x} \in \mathbb{R}^{n_x}$ represents the state variables, e.g., generator rotor angles; $\boldsymbol{y} \in \mathbb{R}^{n_y}$ are the algebraic variables, e.g., line flows; and $\boldsymbol{u} \in \mathbb{R}^{n_u}$ are the inputs, e.g., dispatch of generators.

Set of DAEs in (3.1) are deterministic equations but highly nonlinear. They can be used to study sensitivity of the model with respect to parameter through probabilistic analysis. However, they cannot consider the dynamic behaviour of a stochastic process during the Time Domain Simulation (TDS), which is the core interest of this thesis. Stochastic disturbances can be included in power system dynamic equations, i.e., DAEs, through SDAEs. This is discussed in the next section.

3.3 Uncorrelated Stochastic Differential Algebraic Equations

Stochastic disturbances are considered as perturbations on power system variables while modelling the transient behaviour of the power system. These stochastic perturbations can be modelled as SDEs, as in (2.9). SDEs are then incorporated into DAEs to formulate SDAEs. The dynamic behaviour of power systems subjected to stochastic disturbances is, thus, conveniently modelled as a set of nonlinear SDAEs, as follows [51]:

$$\begin{aligned} \dot{\boldsymbol{x}}(t) &= \boldsymbol{f}(\boldsymbol{x}(t), \boldsymbol{y}(t), \boldsymbol{\kappa}(t), \boldsymbol{u}(t)) \,, \\ \boldsymbol{0} &= \boldsymbol{g}(\boldsymbol{x}(t), \boldsymbol{y}(t), \boldsymbol{\kappa}(t), \boldsymbol{u}(t)) \,, \\ \dot{\boldsymbol{\kappa}}(t) &= \boldsymbol{a}(\boldsymbol{\kappa}(t)) + \boldsymbol{b}(\boldsymbol{\kappa}(t)) \circ \boldsymbol{\xi}(t) \,. \end{aligned} \tag{3.2}$$

where $\boldsymbol{\kappa} \in \mathbb{R}^{n_\kappa}$ are the uncorrelated stochastic processes; $\boldsymbol{a} \in \mathbb{R}^{n_\kappa}$ and $\boldsymbol{b} \in \mathbb{R}^{n_\xi}$ are the drift and diffusion terms, respectively; and $\boldsymbol{\xi} \in \mathbb{R}^{n_\xi}$ is the vector of independent white noises. All remaining variables have the same meaning as in (3.1). The functions $\boldsymbol{f}$ and $\boldsymbol{g}$ are modified to include $\boldsymbol{\kappa}(t)$.

SDAEs in (3.2) model uncorrelated stochastic disturbances. Thus, they cannot study the impact of correlated stochastic disturbances on the power system's dynamic behaviour. This can be done by modelling stochastic disturbances in the set of SDAEs in (3.2) via a set of correlated SDEs. This creates correlated SDAEs, which are proposed in the next section.

3.4 Correlated Stochastic Differential Algebraic Equations

A set of multi-dimensional correlated SDAEs is formulated as follows:

$$\begin{aligned} \dot{\boldsymbol{x}}(t) &= \boldsymbol{f}(\boldsymbol{x}(t), \boldsymbol{y}(t), \boldsymbol{\eta}(t), \boldsymbol{u}(t))\,, \\ \boldsymbol{0} &= \boldsymbol{g}(\boldsymbol{x}(t), \boldsymbol{y}(t), \boldsymbol{\eta}(t), \boldsymbol{u}(t))\,, \\ \dot{\boldsymbol{\eta}}(t) &= \boldsymbol{a}(\boldsymbol{\eta}(t)) + \boldsymbol{b}(\boldsymbol{\eta}(t)) \circ \boldsymbol{\zeta}(t)\,. \end{aligned} \tag{3.3}$$

where $\boldsymbol{\eta} \in \mathbb{R}^{n_\eta}$ are the correlated stochastic processes; $\boldsymbol{a} \in \mathbb{R}^{n_\eta}$ and $\boldsymbol{b} \in \mathbb{R}^{n_\zeta}$ are the drift and diffusion terms, respectively; and $\boldsymbol{\zeta} \in \mathbb{R}^{n_\zeta}$ is the vector of correlated white noises. The rest of the variables and functions have the same meaning as in (3.2). Note that the model in (3.3) was originally proposed in [3].

Remarks

SDAEs in (3.2) and (3.3) are highly nonlinear and non-deterministic. Such equations cannot be solved in closed form. Thus, numerical methods are employed for their integration. The functions $\boldsymbol{f}$, $\boldsymbol{g}$ and $\boldsymbol{a}$ in (3.2) and (3.3) are deterministic and are integrated using usual integration schemes. In this thesis, implicit trapezoidal integration scheme has been adopted for the integration of these functions. Whereas, integration of $\boldsymbol{b}$ in (3.2) and (3.3) is associated to the non-deterministic integral with respect to Wiener

process, as explained in Chapter 2. This integral is solved using Euler-Maruyama, in this thesis, as introduced in Chapter 2.

Equation (3.3) is a general way of modelling correlated stochastic disturbances into power system dynamics because in (3.3) the drift a and the diffusion b of the stochastic processes are not modified, and (3.3) also does not require any simplifications or modifications to the original system while modelling the detailed dynamic behaviour. The latter property allows for modelling of nonlinearities, controller hard limits and saturations.

Dynamic Analysis

Due to the complexity involved, and non-availability of the analytical solutions of nonlinear SDAEs, the impact of the stochastic processes on the dynamic behaviour of the power systems can only be assessed through TDSs. The TDS employs numerical integration schemes to simulate the trajectories of the power system variables. The trajectories of the power system variables are then analysed to assess any instabilities in the system. This allows for assessing the stability of the system for one particular scenario. However, in the case of stochastic processes multiple scenarios can be simulated.

To get a realistic estimate on the probability of instability, the system of SDAEs should be simulated multiple times to include all possible scenarios. This procedure is termed as the Monte Carlo Method (MC). The total number of trajectories simulated using the MC depends on the stationary conditions of the stochastic processes being simulated. This is discussed in detail later in Chapter 4. Each trajectory of the power system variables obtained through the MC is then analysed to account for any instabilities such as voltage collapse, loss of synchronism, etc. The probability of instability is calculated based on the number of unstable trajectories against the total simulated trajectories. In the entire thesis, the MC are simulated exploiting parallelism on an 80 core Intel(R) Xeon(R) CPU @ 2.20GHz.

3.5 Sources of Volatility

This section introduces the methods to model correlated disturbances on the sources of volatility for power system dynamic studies. These models were originally proposed in [3], and are presented here in the following Subsections.

3.5.1 Load Power Consumption

Stochastic load models are well-established in the literature [53]. The stochastic load model introduced in [51] considers the well-known voltage dependent load model and uses uncorrelated Ornstein-Uhlenbeck (OU) processes to define stochastic perturbations on active and reactive load power consumption. This is the starting point of the models presented in this thesis.

3.5.1.1 Correlation on Active and Reactive Power Consumption

Two-dimensional correlated SDEs in (2.30) are utilized to model correlated stochastic perturbations on active and reactive power consumption of stochastic loads. The proposed model is as follows:

$$\begin{aligned} p_{\mathrm{L}}(t) &= (p_{\mathrm{L}_0} + \eta_p(t))(v(t)/v_0)^{\gamma}\,, \\ q_{\mathrm{L}}(t) &= (q_{\mathrm{L}_0} + \eta_q(t))(v(t)/v_0)^{\gamma}\,, \\ \dot{\eta}_p(t) &= a_p(\eta_p(t)) + b_p(\eta_p(t))\,\xi_p(t)\,, \\ \dot{\eta}_q(t) &= a_q(\eta_q(t)) + b_q(\eta_q(t))(r_{p,q}\,\xi_p(t) + \sqrt{1 - r_{p,q}^2}\,\xi_q(t))\,, \end{aligned} \tag{3.4}$$

where p_{L_0} and q_{L_0} are the nominal values of active and reactive power consumption, respectively; $v(t)$ represents the magnitude of the bus voltage at the load bus; v_0 is the initial value of this voltage magnitude at time $t = 0$; and γ defines the voltage dependency of the load, i.e., $\gamma = 0$ is used for constant power load, and for constant impedance loads $\gamma = 2$ is used.

In (3.4) a, b, and ξ have the same meaning as in (2.30). Whereas $r_{p,q}$ is the linear correlation between the two stochastic processes associated with active and reactive load power consumption, i.e., η_p and η_q, respectively. Note that the correlation between the active and reactive power load consumption can be easily removed using $r_{p,q} = 0$.

3.5.1.2 Correlated Load Consumption

In practice, some level of spatial and temporal correlation exists between load power consumption at different load buses. This is true because consumer behaviour is correlated. The correlation between the load consumption at multiple load buses can be conveniently modelled using multidimensional correlated SDEs. Modifying (3.4) to include correlated stochastic disturbances on load consumption of n_l buses, gives:

$$\begin{aligned}
\boldsymbol{p}_{\mathrm{L}}(t) &= (\boldsymbol{p}_{\mathrm{L}_0} + \boldsymbol{\eta}_p(t)) \circ \boldsymbol{v}_p(t)\,, \\
\boldsymbol{q}_{\mathrm{L}}(t) &= (\boldsymbol{q}_{\mathrm{L}_0} + \boldsymbol{\eta}_q(t)) \circ \boldsymbol{v}_q(t)\,, \\
\dot{\boldsymbol{\eta}}_p(t) &= \boldsymbol{a}_p(\boldsymbol{\eta}_p(t)) + \boldsymbol{b}_p(\boldsymbol{\eta}_p(t)) \circ \boldsymbol{\zeta}_p(t)\,, \\
\dot{\boldsymbol{\eta}}_q(t) &= \boldsymbol{a}_q(\boldsymbol{\eta}_q(t)) + \boldsymbol{b}_q(\boldsymbol{\eta}_q(t)) \circ \boldsymbol{\zeta}_q(t)\,,
\end{aligned} \tag{3.5}$$

where vectors $\boldsymbol{p}_{\mathrm{L}} \in \mathbb{R}^{n_l}$ and $\boldsymbol{q}_{\mathrm{L}} \in \mathbb{R}^{n_l}$ represent the active and reactive power consumption at load buses, respectively; $\boldsymbol{p}_{\mathrm{L}_0} \in \mathbb{R}^{n_l}$ and $\boldsymbol{q}_{\mathrm{L}_0} \in \mathbb{R}^{n_l}$ are the initial active and reactive power consumption at load buses at time $t = 0$, respectively; and $\boldsymbol{v}_p \in \mathbb{R}^{n_l}$ and $\boldsymbol{v}_q \in \mathbb{R}^{n_l}$ are vectors, whose elements are calculated as:

$$v_{p,i}(t) = v_{q,i}(t) = (v_i(t)/v_{0,i})^{\gamma_i}\ , \quad i = 1, \ldots, n_l\,,$$

where parameter γ has the same meaning as in (3.4).

In (3.5) $\boldsymbol{a}_p$, $\boldsymbol{a}_q$, $\boldsymbol{b}_p$ and $\boldsymbol{b}_q$ are all n_l-dimensional vectors with same meanings as in (2.20); and $\boldsymbol{\zeta}_p \in \mathbb{R}^{n_l}$ and $\boldsymbol{\zeta}_q \in \mathbb{R}^{n_l}$ are the vectors of correlated white noises associated to the stochastic processes, i.e., $\boldsymbol{\eta}_p$ and $\boldsymbol{\eta}_q$, on load active and reactive power consumption, respectively, and are obtained using (2.18), as follows:

$$\begin{bmatrix} \boldsymbol{\zeta}_p(t) \\ \boldsymbol{\zeta}_q(t) \end{bmatrix} = \mathbf{C}\,\boldsymbol{\xi}(t)\,,$$

where $\boldsymbol{\xi} \in \mathbb{R}^{2n_l}$ are the independent white noises; $\mathbf{C}$ is a lower-triangular matrix of dimensions $2n_l \times 2n_l$, and is obtained as the Cholesky decomposition of the correlation

matrix $\mathbf{R}$ with the following structure:

$$\mathbf{R} = \begin{bmatrix} \mathbf{R}_{p,p} & \mathbf{R}_{p,q} \\ \mathbf{R}_{q,p} & \mathbf{R}_{q,q} \end{bmatrix}, \tag{3.6}$$

where $\mathbf{R}_{q,p} = \mathbf{R}_{p,q}^T$ and:

$$\mathbf{R}_{p,p} = \begin{bmatrix} 1 & r_{p_1,p_2} & \dots & r_{p_1,p_{n_l}} \\ r_{p_2,p_1} & 1 & \dots & r_{p_2,p_{n_l}} \\ \vdots & \vdots & \ddots & \vdots \\ r_{p_{n_l},p_1} & r_{p_{n_l},p_2} & \dots & 1 \end{bmatrix},$$

$$\mathbf{R}_{p,q} = \begin{bmatrix} r_{p_1,q_1} & r_{p_1,q_2} & \dots & r_{p_1,q_{n_l}} \\ r_{p_2,q_1} & r_{p_2,q_2} & \dots & r_{p_2,q_{n_l}} \\ \vdots & \vdots & \ddots & \vdots \\ r_{p_{n_l},q_1} & r_{p_{n_l},q_2} & \dots & r_{p_{n_l},q_{n_l}} \end{bmatrix},$$

$$\mathbf{R}_{q,q} = \begin{bmatrix} 1 & r_{q_1,q_2} & \dots & r_{q_1,q_{n_l}} \\ r_{q_2,q_1} & 1 & \dots & r_{q_2,q_{n_l}} \\ \vdots & \vdots & \ddots & \vdots \\ r_{q_{n_l},q_1} & r_{q_{n_l},q_2} & \dots & 1 \end{bmatrix},$$

3.5.2 Stochastic Power Flow Equations

To ensure a secure operation of the grid, it is required that generation and demand are balanced at all times. The power balance at i-th bus is given by the well-known power flow equations, which in polar form are written as:

$$\begin{aligned} 0 &= p_{\mathrm{G},i}(t) - p_{\mathrm{L},i}(t) \\ &\quad - \hat{v}_i(t) \sum_{j=1}^{n_\mathrm{B}} [\hat{v}_j(t) \mathrm{B}_{ij} \sin(\hat{\theta}_i(t) - \hat{\theta}_j(t)) \\ &\quad + \hat{v}_i(t) \mathrm{G}_{ij} \cos(\hat{\theta}_i(t) - \hat{\theta}_j(t))], \quad i = 1, \dots, n_\mathrm{B}, \\ 0 &= q_{\mathrm{G},i}(t) - q_{\mathrm{L},i}(t) \\ &\quad - \hat{v}_i(t) \sum_{j=1}^{n_\mathrm{B}} [\hat{v}_j \mathrm{G}_{ij} \sin(\hat{\theta}_i(t) - \hat{\theta}_j(t)) \\ &\quad - \hat{v}_j(t) \mathrm{B}_{ij} \cos(\hat{\theta}_i(t) - \hat{\theta}_j(t))], \quad i = 1, \dots, n_\mathrm{B}, \end{aligned} \tag{3.7}$$

where $p_{\mathrm{G},i}$ and $q_{\mathrm{G},i}$ represent the sum of the active power generations, and the sum of reactive power generations at the i-th bus, respectively. Similarly, $p_{\mathrm{L},i}$ and $q_{\mathrm{L},i}$ is the sum of the active power consumption, and the sum of the reactive power consumption at the i-th bus, respectively. n_{B} is the total number of buses of the grid. G_{ij} and B_{ij}, respectively, are the real and imaginary part of the (i, j) element of the system admittance matrix.

In [51], stochastic disturbances are included in the bus voltage phasors to account for effects of random phenomena not modelled in the set of DAEs for transient stability analysis, e.g., the effects of harmonics, nonlinearities, load unbalances, and electromagnetic transients, etc. In the same vein, the stochastic disturbances in (3.7) are included through the variables $\hat{v}_i$ and $\hat{\theta}_i$, which are the bus voltage magnitude and the voltage phase angle, respectively, and are obtained as n_{B}-dimensional correlated SDE as follows:

$$\begin{aligned}
\hat{\boldsymbol{v}}(t) &= \boldsymbol{v}(t) - \boldsymbol{\eta}_v(t)\,, \\
\hat{\boldsymbol{\theta}}(t) &= \boldsymbol{\theta}(t) - \boldsymbol{\eta}_\theta(t)\,, \\
\dot{\boldsymbol{\eta}}_v(t) &= \boldsymbol{a}_v(\boldsymbol{\eta}_v(t)) + \boldsymbol{b}_v(\boldsymbol{\eta}_v(t)) \circ \boldsymbol{\zeta}_v(t)\,, \\
\dot{\boldsymbol{\eta}}_\theta(t) &= \boldsymbol{a}_\theta(\boldsymbol{\eta}_\theta(t)) + \boldsymbol{b}_\theta(\boldsymbol{\eta}_\theta(t)) \circ \boldsymbol{\zeta}_\theta(t)\,,
\end{aligned} \tag{3.8}$$

where n_{B} is the number of buses in the network; $\boldsymbol{v} \in \mathbb{R}^{n_{\mathrm{B}}}$ is the vector of the noise-free components of the bus voltage magnitudes; $\boldsymbol{\theta} \in \mathbb{R}^{n_{\mathrm{B}}}$ represents the noise-free components of the bus voltage phase angles, at network buses; $\boldsymbol{a}_v$, $\boldsymbol{a}_\theta$, $\boldsymbol{b}_v$ and $\boldsymbol{b}_\theta$ are all n_{B}-dimensional vectors with same meanings as in (2.20); and $\boldsymbol{\zeta}_v \in \mathbb{R}^{n_{\mathrm{B}}}$ and $\boldsymbol{\zeta}_\theta \in \mathbb{R}^{n_{\mathrm{B}}}$ are the vectors of correlated white noises associated to the stochastic processes, i.e., $\boldsymbol{\eta}_v$ and $\boldsymbol{\eta}_\theta$, on bus voltage magnitudes and phase angles, respectively. The vectors $\boldsymbol{\zeta}_v$ and $\boldsymbol{\zeta}_\theta$ are calculated from the vector of independent white noises $\boldsymbol{\xi} \in \mathbb{R}^{2n_{\mathrm{B}}}$ using (2.18):

$$\begin{bmatrix} \boldsymbol{\zeta}_v(t) \\ \boldsymbol{\zeta}_\theta(t) \end{bmatrix} = \mathbf{C}\,\boldsymbol{\xi}(t)\,, \tag{3.9}$$

$\mathbf{C} \in \mathbb{R}^{2n_{\mathrm{B}} \times 2n_{\mathrm{B}}}$ in (3.9) is calculated from the correlation matrix $\mathbf{R} \in \mathbb{R}^{2n_{\mathrm{B}} \times 2n_{\mathrm{B}}}$, using (2.19). $\mathbf{R}$ contains the correlation values between the elements of $\boldsymbol{v}$ and $\boldsymbol{\theta}$. The structure

of $\mathbf{R}$ is similar to that of (3.6), namely:

$$\mathbf{R} = \begin{bmatrix} \mathbf{R}_{v,v} & \mathbf{R}_{v,\theta} \\ \mathbf{R}_{\theta,v} & \mathbf{R}_{\theta,\theta} \end{bmatrix}, \tag{3.10}$$

where $\mathbf{R}_{\theta,v} = \mathbf{R}_{v,\theta}^T$ and:

$$\mathbf{R}_{v,v} = \begin{bmatrix} 1 & r_{v_1,v_2} & \dots & r_{v_1,v_{n_\mathrm{B}}} \\ r_{v_2,v_1} & 1 & \dots & r_{v_2,v_{n_\mathrm{B}}} \\ \vdots & \vdots & \ddots & \vdots \\ r_{v_{n_\mathrm{B}},v_1} & r_{v_{n_\mathrm{B}},v_2} & \dots & 1 \end{bmatrix},$$

$$\mathbf{R}_{v,\theta} = \begin{bmatrix} r_{v_1,\theta_1} & r_{v_1,\theta_2} & \dots & r_{v_1,\theta_{n_\mathrm{B}}} \\ r_{v_2,\theta_1} & r_{v_2,\theta_2} & \dots & r_{v_2,\theta_{n_\mathrm{B}}} \\ \vdots & \vdots & \ddots & \vdots \\ r_{v_{n_\mathrm{B}},\theta_1} & r_{v_{n_\mathrm{B}},\theta_2} & \dots & r_{v_{n_\mathrm{B}},\theta_{n_\mathrm{B}}} \end{bmatrix},$$

$$\mathbf{R}_{\theta,\theta} = \begin{bmatrix} 1 & r_{\theta_1,\theta_2} & \dots & r_{\theta_1,\theta_{n_\mathrm{B}}} \\ r_{\theta_2,\theta_1} & 1 & \dots & r_{\theta_2,\theta_{n_\mathrm{B}}} \\ \vdots & \vdots & \ddots & \vdots \\ r_{\theta_{n_\mathrm{B}},\theta_1} & r_{\theta_{n_\mathrm{B}},\theta_2} & \dots & 1 \end{bmatrix},$$

3.5.3 Stochastic Wind Speeds

The electrical power generated from WPPs is a function of the wind speed, which is highly affected by weather conditions. In the time-scale of transient stability analysis, wind speed can be conveniently modelled as a stochastic process. This introduces volatility in the power system dynamic model. Due to the stochastic nature of the wind speed, it becomes incredibly important to study its effects on power system dynamics to ensure a secure and reliable operation. The uncorrelated volatility model of wind speed is the following:

$$\begin{aligned} w(t) &= w_0 + \eta_w(t)\,, \\ \dot{\eta}_w(t) &= a_w(\eta_w(t)) + b_w(\eta_w(t))\,\xi_w(t)\,, \end{aligned} \tag{3.11}$$

where w_0 is the average wind speed in a given period; and a_w, b_w, and ξ_w have the same meaning as in (2.9).

The spatial and temporal correlation between different wind turbines within a WPP, as well as among WPPs can be modelled as a set of correlated wind speeds. The model to correlate wind speeds through correlated SDEs is as follows:

$$\begin{aligned} \boldsymbol{w}(t) &= \boldsymbol{w}_0 + \boldsymbol{\eta}_w(t)\,, \\ \dot{\boldsymbol{\eta}}_w(t) &= \boldsymbol{a}_w(\boldsymbol{\eta}_w(t)) + \boldsymbol{b}_w(\boldsymbol{\eta}_w(t)) \circ \boldsymbol{\zeta}_w(t)\,, \end{aligned} \tag{3.12}$$

where $\boldsymbol{w}_0 \in \mathbb{R}^{n_\mathrm{W}}$ is the vector of uncorrelated wind speeds; and other variables and parameters have same meanings as in (2.20).

3.6 Aggregation of Correlated Wind Speeds

In recent years, the modelling of aggregated WPPs has become an important field of research [7, 14, 38, 40, 64, 69, 77, 79]. These works propose various techniques to model an aggregated WPP that reproduces the behaviour of the detailed network, i.e., generates similar amount of active power at a given wind speed as in the case of the detailed network. Some of the works cited above, e.g., [79] and [77], propose a way to calculate an equivalent wind speed that can be applied to the aggregated WPP to obtain the behaviour of the active power similar to that generated by the WPPs of the original network. However, these works model power system dynamics through deterministic DAEs. The drawback of this approach is that the randomness in wind speeds is included into the set of DAEs only in the initialization step. Then the wind speed is assumed to remain constant during the simulation. This approach does not allow the modelling of volatility on wind speeds.

This section presents a formula to calculate an equivalent wind speed process that is then applied to the aggregated WPP to generate the desired behaviour of the wind power production at the point of aggregation. This new wind speed process is hereinafter referred to as "aggregated wind speed process". The cluster of WPPs of a given region in a grid can be aggregated by using any of the methods presented in [7, 14, 38, 40, 64, 69, 77, 79]. The aggregated WPP is then driven by the aggregated wind speed process so that it generates active power at the point of aggregation, which has statistical properties similar to the one generated by the detailed network. This solution is thus convenient when one is interested in analysing the dynamic behaviour of the power network in the time scale of

transients, and in testing the performance of different controllers, and services provided by the WPPs in the presence of a cluster of WPPs.

The aggregated wind speed process is obtained as the average of the underlying wind speed processes. This method of averaging the underlying wind speeds has also been utilised in other works, e.g., [79] and [77]. However, these references consider neither wind speed dynamics nor correlated wind speeds. In this thesis, on the other hand, we are interested in the aggregation of the correlated wind speed processes modelled through correlated stochastic processes in the time scale of transients. The aggregated wind speed process is thus modelled as a stochastic process that is an average of the underlying individual wind speed processes in (3.12). The proposed aggregated wind speed model is built using (3.12) and (2.26), as follows:

$$w_{\text{agg}}(t) = \frac{1}{n}\sum_{i=1}^{n}\left[\mu_{w_i} + e^{-\alpha_{w_i}t}\big(w_i(0) - \mu_{w_i}\big) \quad + \psi_{w_i}\sum_{j=1}^{n}\big(\sigma_{w_j}c_{j,i}\big)\right]. \tag{3.13}$$

where $c_{i,j}$ is the i,j element of matrix $\mathbf{C}$, and σ_{w_j} is the standard deviation of the j-th wind speed process from (2.25).

3.7 Conclusions

This chapter provides discussion on the modelling of power system dynamic behaviour through deterministic DAEs. Then, modelling of stochastic disturbances into power system dynamic equations through SDAEs is introduced. A general approach to model power systems as a set of correlated SDAEs is, then, presented. A few examples to model correlated stochastic disturbances on sources of volatility are discussed. Finally, a model to aggregate correlated wind speeds is presented.

Chapter 4

Variances of Power System Algebraic Variables

4.1 Introduction

This chapter deals with the calculation of the variances of algebraic variables of power systems modelled as a set of Stochastic Differential Algebraic Equations (SDAEs). The variances of the algebraic variables are required to ensure that none of the system physical limits are violated in normal grid operation. With this aim, two methods namely, the conventional Monte Carlo Method (MC) and a direct method are utilised.

The conventional method, i.e., MC requires that the system of equations is simulated multiple times. With this regard, the chapter discusses the complexities involved and the computational burden of the MC. The chapter also illustrates the impact of setting up the stochastic processes with different Probability Density Functions (PDFs) fitting the measurement data on the variances of the algebraic variables of the power system with the help of the MC.

One of the byproducts of the MC is that the variances of the power system variables, in stationary conditions, are readily available. A relevant aspect of modeling power system as a set of SDAEs is that system nonlinearities and controller hard limits can be defined. Whereas this is not the case for the direct methods as they rely on linearization of the system. Available direct methods can only describe the system linearized around an equilibrium point and at stationary conditions, and, hence, cannot account for the

time-continuous variations, i.e., the drift term, of the stochastic processes, any system nonlinearities or hard limits.

As explained in Chapter 1, available direct methods provide statistical properties only of the state variables of the power system at stationary conditions. While, in this chapter the evaluation of the variances of the algebraic variables is the primary goal. The method presented in this chapter utilises the solution of a Lyapunov equation and requires the calculation of the state matrix of the system. This method is termed as the Linear Estimation (LE). The accuracy and the computational efficiency of the LE compared to the conventional MC has also been demonstrated.

The remainder of the chapter is organized as follows. Section 4.2 presents a discussion on the computational burden of the MC. Then, the impact of modelling stochastic processes with various PDFs on the variances of the power system variables and the probability of violation of system limits in case of a transient are discussed in Section 4.3. The LE is presented in Section 4.4. The case study presented in Section 4.5 utilises two power systems of different sizes to demonstrate the accuracy and computational efficiency of the LE. Finally, conclusions are drawn in Section 4.6.

4.2 Monte Carlo Method

The computational burden of the MC is proportional to the following: the complexity and size of the power system; the total simulated time; the time-step used for integration; and the number of trajectories simulated. The latter three aspects are discussed in this section.

The dynamic behaviour of the set of SDAEs is best studied through Time Domain Simulations (TDSs). A single trajectory of a stochastic process modeled as Stochastic Differential Equation (SDE) and simulated using TDS needs to be simulated for at least $t_f = 2/\alpha$ s, where α is the autocorrelation coefficient, to become stationary, i.e., reach a constant standard deviation ($\sigma(t) = \sigma$). This is demonstrated later in Chapter 5, where the processes with different α are simulated to show that they reach stationarity at different t_f. Hence, the smaller the value of α the higher the computational time of the MC. Similarly, the time-step utilised to integrate the SDAEs has a direct impact on the computational time of the MC. Note, however, that the integration step-size cannot

be increased too much because the integration of the Wiener process requires sufficiently small time steps, as explained in Chapter 2.

Another relevant aspect of the MC that has a greater impact on the computational time of the MC is the number of trajectories being simulated. The rationale behind this is explained as follows. Let us consider N to be the number of trajectories simulated in the MC. N is chosen based on a hit and trial method. The hit and trial method contains two steps. Step 1 simulates the process using the MC for a small N, and calculates $\sigma(N)$. The second step increases N by a small quantity and repeats step 1. Note that the hit and trial method relies on the fact that for an increase in N an increase in $\sigma(N)$ is observed. The steps are repeated until $\sigma(N)$ converges, i.e., $\sigma(N) = \sigma$, with a given tolerance.

To illustrate the hit and trial method, the 9-bus (Western Systems Coordinating Council) system is chosen. The 9-bus system contains 3 synchronous generators, 3 load devices, and is shown in Figure 4.1. The stochastic disturbances are introduced into load active and reactive power through (3.5). The stochastic processes are modeled through independent Ornstein-Uhlenbeck (OU) processes with the following parameters:

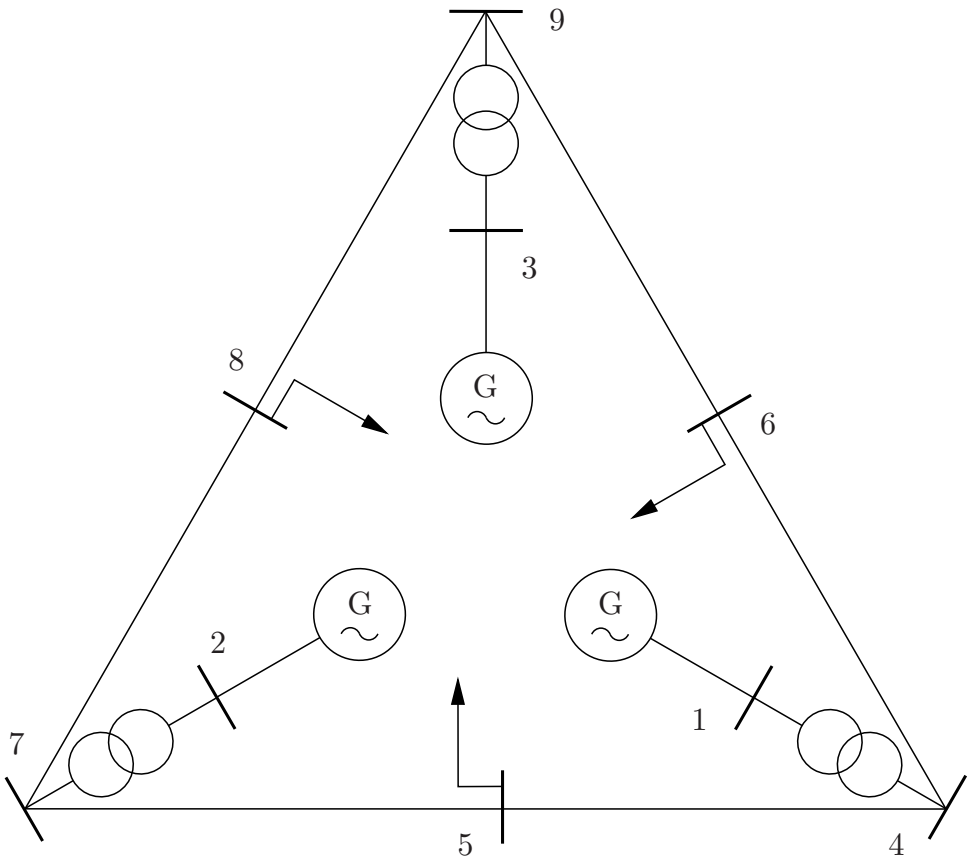

Figure 4.1: Single-line diagram of the 9-bus system.

the autocorrelation coefficients of η_p and η_q are $\alpha_p = \alpha_q = 0.1$ s^{-1}, respectively; and the standard deviations of η_p and η_q are $\sigma(\eta_p) = 0.5\%$ of p_{L_0} and $\sigma(\eta_q) = 0.5\%$ of q_{L_0}, respectively. The final simulation time for each realization is $t_f = 2/\alpha = 20$ s. The integration of the deterministic part of SDAEs is performed with a time step $\Delta t = 0.01$ s. The OU processes are integrated using a step size $h = 0.01$ s. Figures 4.2 to 4.5 show the profile of $\sigma(N)$ plotted against N obtained for various power system variables in the 9-bus system. These figures illustrate that $\sigma(N)$ converges for $N \to 1000$. Note that $N = 1000$ is used throughout the thesis for the MC.

So far in the thesis the stochastic processes $\boldsymbol{\eta}$ were initialized such that $\eta_i(t_0) = 0$. As explained in Chapter 2, η_i can be initialized to a random value chosen from the probability density function of the process. Doing so removes the need to simulate the process, when using MC, till $t_f = 2/\alpha$ s, as the process displays stationarity at $t_0 = 0$. Note that even though the process reaches stationarity at t_0, the dynamics of the SDAEs do not allow the power system variables to reach stationarity at t_0. This is demonstrated as follows.

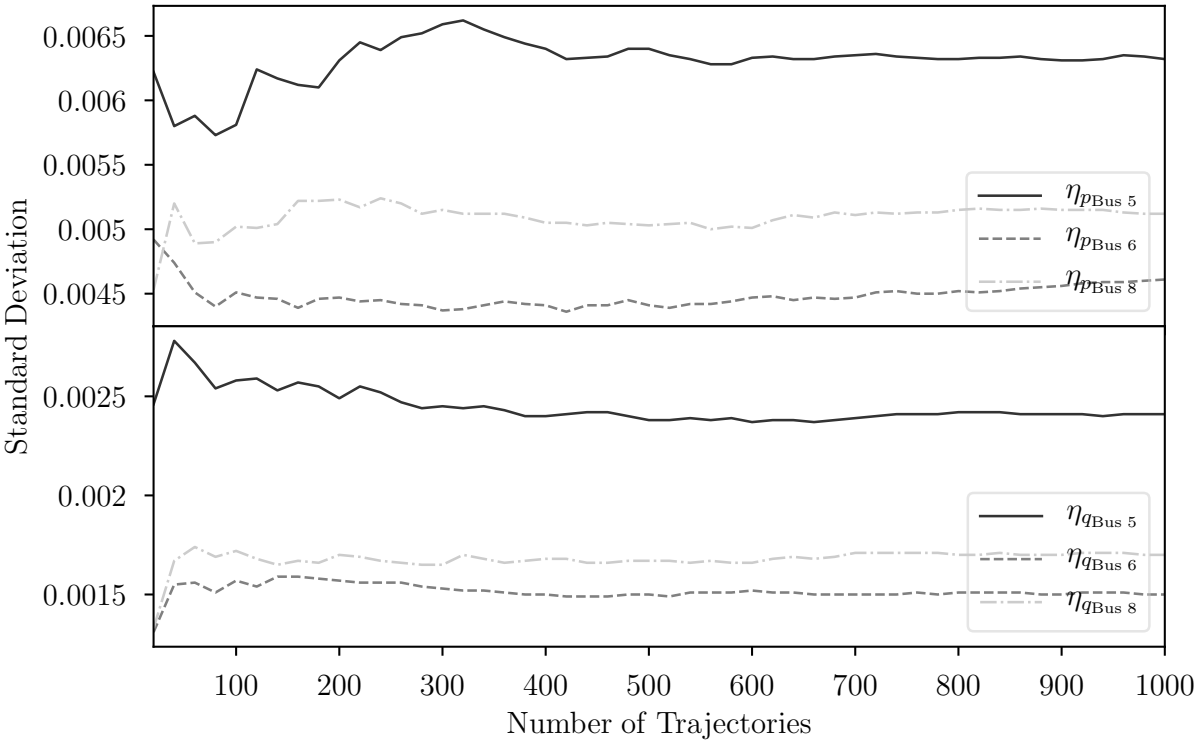

Figure 4.2: Standard deviation of load active η_p and reactive η_q power consumption in the 9-bus system.

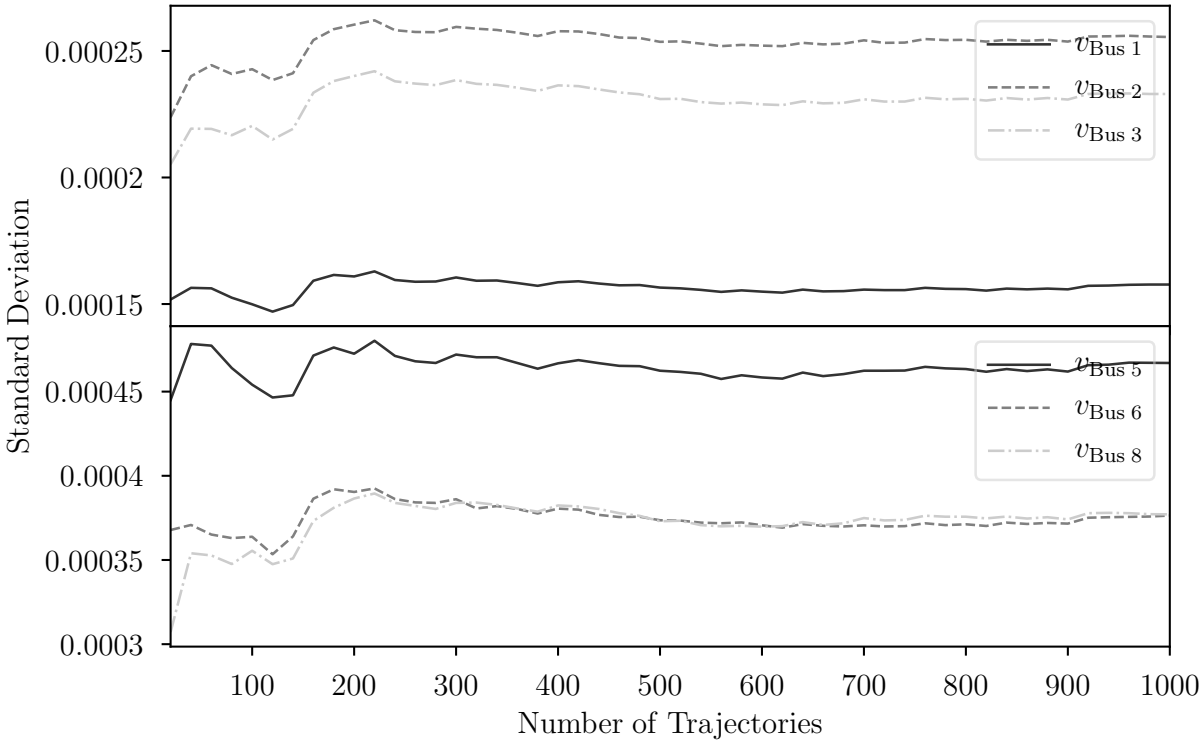

Figure 4.3: Standard deviation of bus voltage magnitudes v in the 9-bus system.

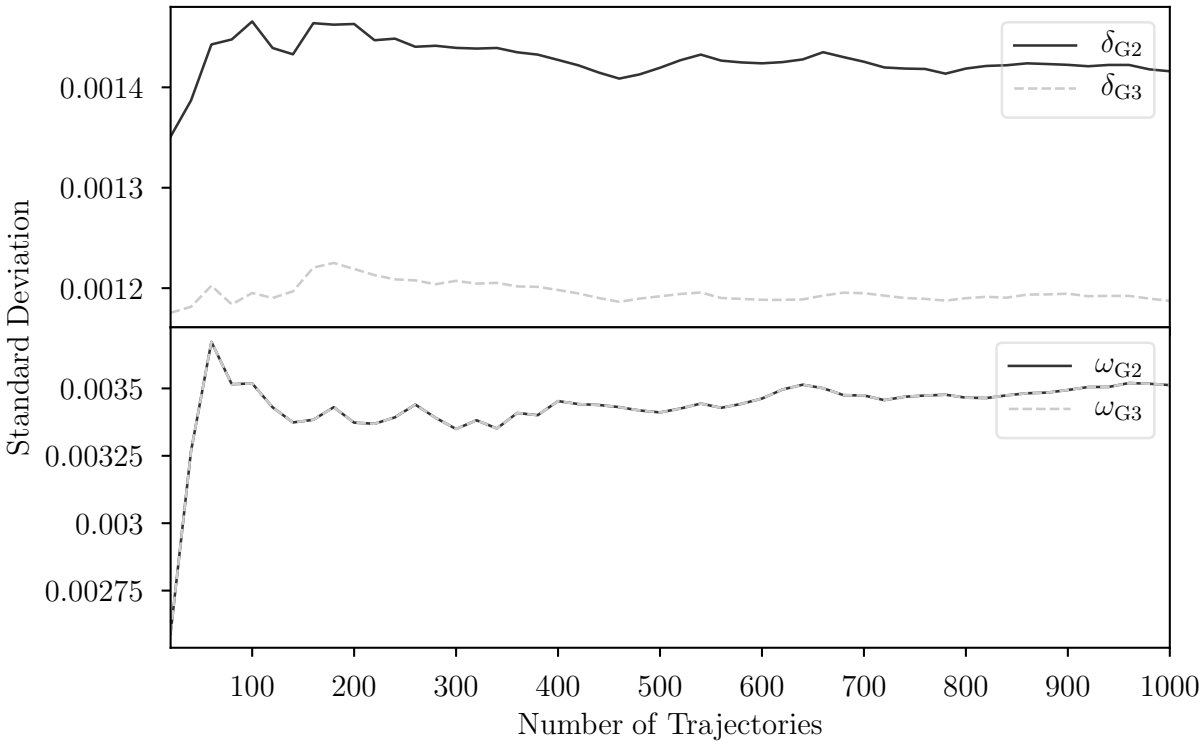

Figure 4.4: Standard deviation of rotor angle δ and rotor speed ω of the synchronous machines in the 9-bus system.

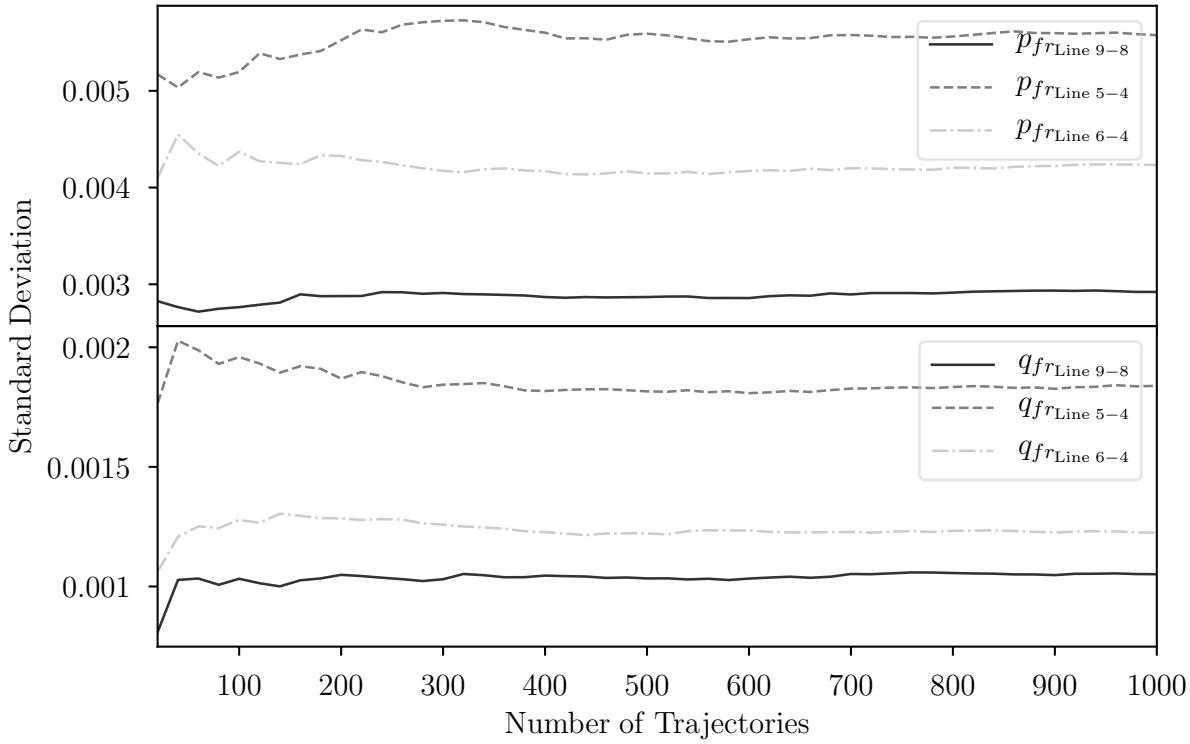

Figure 4.5: Standard deviation of active p_{fr} and reactive q_{fr} power injections at the sending-end buses in the 9-bus system.

The stochastic disturbances are introduced in the 9-bus system at load consumption at bus 5 through the OU process. The values of autocorrelation coefficient of the process is chosen as $\alpha_p = \alpha_q = 0.1$ s^{-1}. Whereas the values of σ are chosen from the following scenarios. Scenario S1 considers $\sigma(\eta_p) = 0.1\%$ of p_{L_0} and $\sigma(\eta_q) = 0.1\%$ of q_{L_0}; scenario S2 considers $\sigma(\eta_p) = 0.4\%$ of p_{L_0} and $\sigma(\eta_q) = 0.4\%$ of q_{L_0}; and scenario S3 considers $\sigma(\eta_p) = 0.8\%$ of p_{L_0} and $\sigma(\eta_q) = 0.8\%$ of q_{L_0}. The OU process is initialized such that $\eta(t_0) \sim \mathcal{N}(\mu, \sigma)$. The 1,000 trajectories of the stochastic process at load consumption at bus 5 of the 9-bus system are shown in Figure 4.6. This Figure illustrates that the OU process reaches stationarity at the start of the simulation, i.e., $t = 0$. However, this is not the case for the power system variables. The 1,000 trajectories of rotor speed ω of the synchronous machine G1 in the 9-bus system is illustrated in Figure 4.7. This Figure shows that the power system variables do not reach stationarity until $t_f = 2/\alpha$ s, even though the stochastic processes show stationarity at t_0.

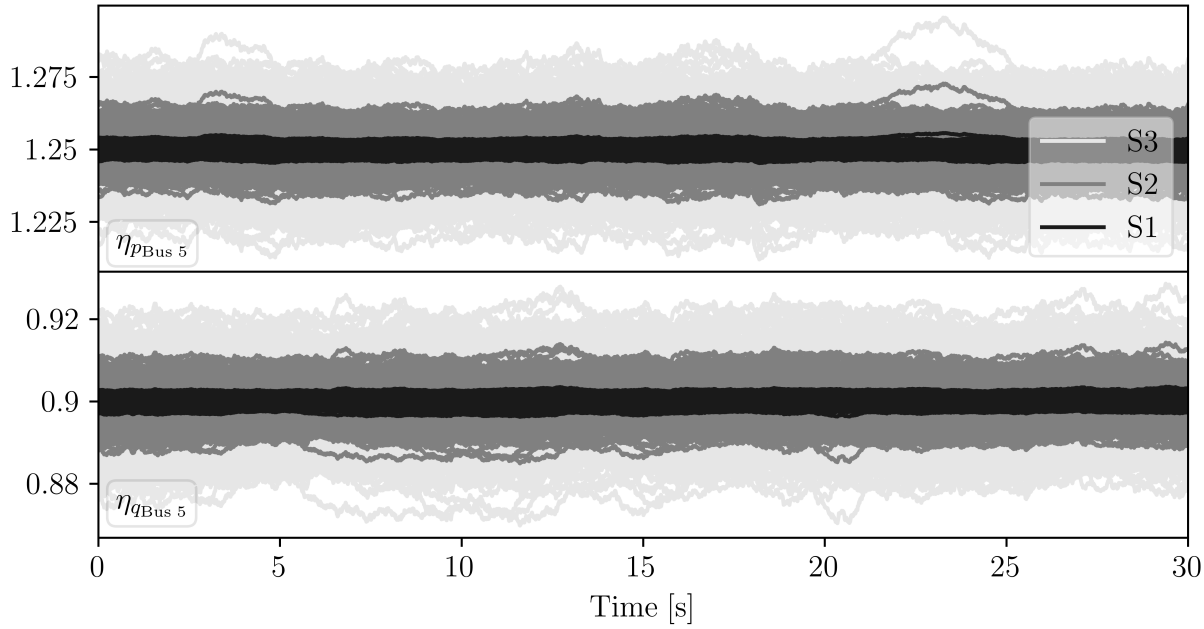

Figure 4.6: 1,000 trajectories of load active η_p and reactive η_q power consumption at bus 5 in the 9-bus system.

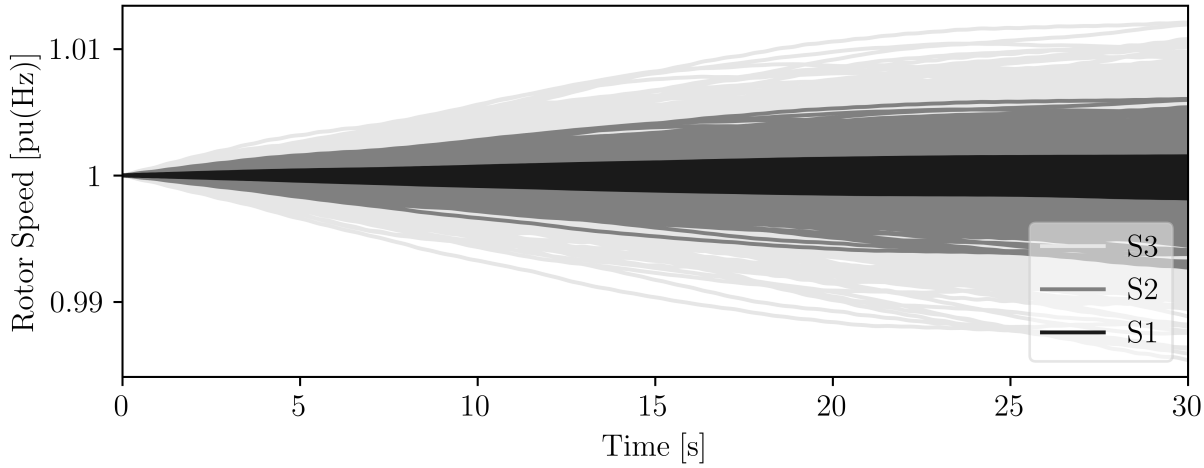

Figure 4.7: 1,000 trajectories of rotor speed ω of the synchronous machine G1 in the 9-bus system.

4.3 Probability Distributions of Stochastic Processes

The study presented in this section originates from the observation that when setting up stochastic processes based on the measurement data, it is often possible that various PDFs fit to the same data. Based on this observation the question such as what is the impact of the different PDFs on the variances of the quantities of the power system modelled as SDAEs, naturally arises. This section aims to provide an answer to this question.

With the help of the case study utilising the distribution network, this section demonstrates that setting up stochastic processes based on the actual PDF type and the parameters of the modelling PDF calculated from the measurement data leads to a more realistic estimate on the variances of the power system quantities and the probability of instability of the power system modelled as a set of SDAEs.

The procedures applied in this section are as follows. In Section 4.3.1, various PDFs and their respective parameters based on the measurement data required to set up SDAEs are calculated. Whereas the impact of setting up stochastic processes through different PDFs on the power system transient behaviour is quantified in Section 4.3.2.

4.3.1 Fitting Probability Density Functions

This section provides details on fitting different PDFs to a given measurement data. In this case study, wind generation is considered to be the only source of volatility. Note, however, that the procedures utilised in this study are equally applicable to the other sources of volatility as well. The wind measurement data in the time-scale of power system TDSs utilised in this case study are presented in Appendix A.3. The Real-World Cumulative Density Function (RCDF) of the wind speed measurement data is shown in Figure 4.8. The next step is to set up stochastic wind speeds using SDE in (3.12). This is done by employing the procedures described in Section 2.6.

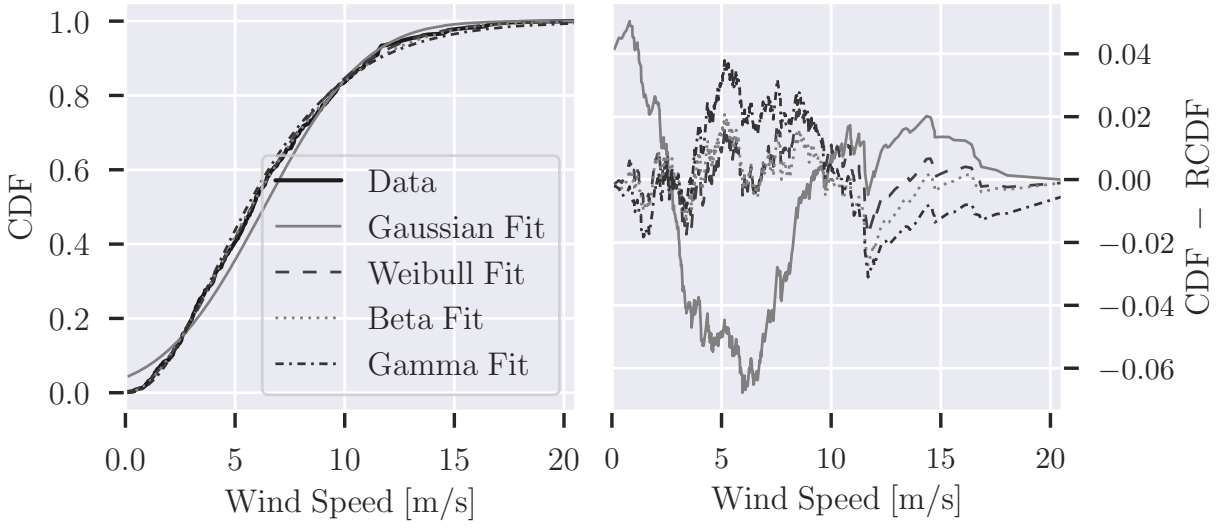

Figure 4.8: RCDF of measurement data and CDF of four PDF fits.

The impact of different PDFs on the overall dynamic response of the system is of interest in this study. With this aim, four PDFs fitting the data of Figure 4.8, namely Gaussian, Weibull, Beta and Gamma are considered. The parameters of the four PDFs are determined through the Maximum Likelihood Estimation method, as mentioned in Section 2.6. The Cumulative Distribution Functions (CDFs) of the fitting PDFs under consideration are illustrated in Figure 4.8, along with the relative error between the CDFs of the PDFs and the RCDF of the wind speed measurement data. Figure 4.8 shows that there are minimal differences between the CDFs and the RCDF. At a first glance, thus, the four PDFs fit reasonably well the data.

4.3.2 Dynamic Simulations

This section studies the impact of different PDF types of correlated stochastic wind speeds on the power system dynamic behavior. The power system considered in this section is the two-area system. The two-area system shown in Figure 4.9 and originally defined in [36], consists of 11 buses, 12 lines/transformers, and four synchronous generators, which are modelled via a 6th-order model and are equipped with IEEE Type-I Automatic Voltage Regulators (AVRs), Turbine Governors (TGs), and an Automatic Generation Control (AGC) that coordinates the four synchronous generators. In this section, the original system is modified to include wind generation. With this aim, the wind generation network is modelled as in Figure 3.1. Then Substation A is connected to bus 9 of the two-area system.

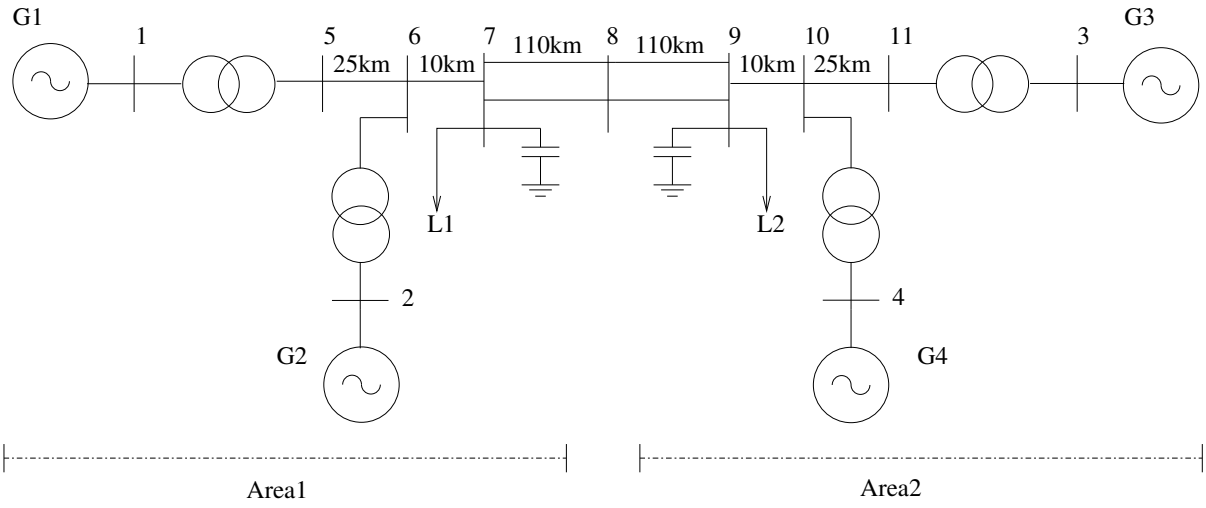

Figure 4.9: Single-line diagram of the two area system.

The detailed dynamic behaviour of the two-area system with inclusion of wind generation is simulated using correlated SDAEs, presented in Section 3.4. The WPPs are modelled through variable-speed doubly-fed induction generators. The correlated stochastic processes are introduced into the wind speeds using the model described in Section 3.5.3. Where the stochastic processes are modelled through all the four PDF types discussed in section 4.3.1. The correlation matrix $\mathbf{R}$ of wind speeds is set up using data given in Table A.2. The power system dynamic simulations are performed using the MC.

The impact of correlated stochastic wind speeds, simulated through different PDF types, on the statistical properties of relevant quantities of the power system at the stationary conditions is analysed first. The only difference in the simulations is the diffusion term in (3.12), which, as mentioned in Section 2.4, defines the PDF of the stochastic processes, in this case, wind speeds.

The drift term, which defines the Autocorrelation Function (ACF), on the other hand, is assumed to be constant and same for all the PDF types. In fact, the ACF of the total wind active power p_{wind} injected at Substation A into the power system is illustrated in Figure 4.10. This figure shows that the ACF of p_{wind} for all the scenarios are similar. This means that the drift terms of the wind speeds remain unaltered while simulating all the scenarios.

The impact of correlated stochastic wind speeds with different PDF types on the relevant power system quantities is quantified in Table 4.1. This table shows the standard

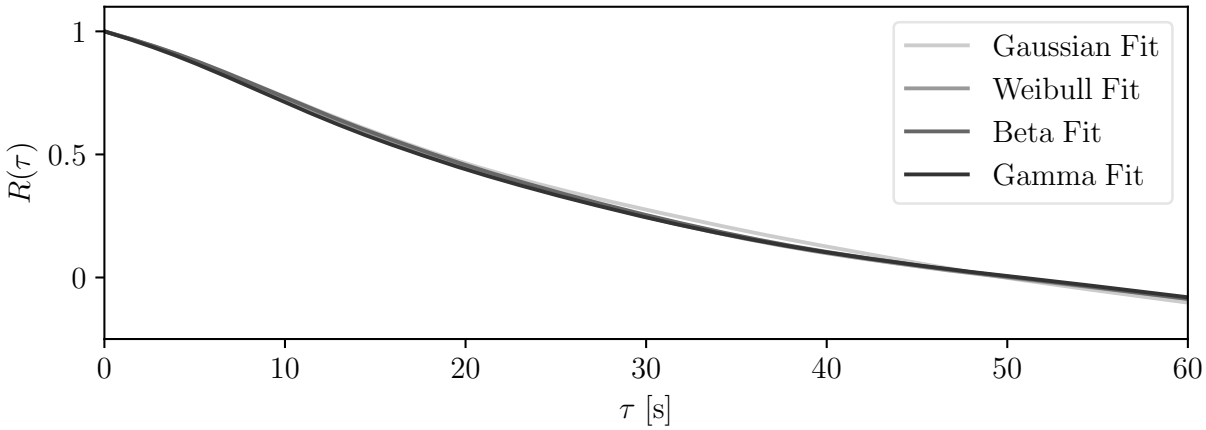

Figure 4.10: Average ACF of thousand trajectories of total wind active power injected into the two-area system with inclusion of wind generation.

deviation of: the bus voltage magnitudes $\sigma(v)$; and the active power injections $\sigma(p_g)$ of the synchronous machines. The results indicate that $\sigma(v)$ and $\sigma(p_g)$ increase from Gaussian to Gamma PDF in both scenarios.

The results in Table 4.1 are noteworthy because the only parameter that varies is the PDF of the wind speed. The changes in the statistical properties of the power system quantities based solely on PDF types of wind speeds are counter intuitive. One would expect to see no differences in the statistical properties of any of the power system quantity based on different PDF types of wind speeds. Especially when the differences between CDFs of the fitting PDF types and the RCDF of data are small.

Further insights on the effect of the PDFs on the dynamic response of the system can be obtained with a frequency domain analysis. Frequency domain analysis is carried out using the procedures, which are described later in Chapter 5. With this regard, the amplitude of the oscillations induced in the inter-area electro-mechanical oscillatory mode of the power system are analysed. The inter-area mode of the two-area system with inclusion of wind generation is first calculated as, eigenvalue -0.075167 ± 3.540781, and frequency 0.563 [Hz]. Then, the frequency spectrum of p_{wind} for the four PDF types, which is illustrated in Figure 4.11, is evaluated. Results show that the amplitude of the frequencies in p_{wind} is dependent on the PDF types of the underlying wind speeds. The amplitudes of frequencies in case of Gaussian PDF are the lowest whereas Gamma PDF shows the highest amplitudes. On the other hand, the amplitudes of frequencies for Weibull and Beta PDF are remarkably similar in the whole frequency spectrum.

The amplitude of oscillations induced in the inter-area oscillatory mode is shown in Figure 4.12, which illustrates the frequency spectrum of voltage magnitude at Bus 8 $v_{\text{Bus 08}}$. Figure 4.12 shows highest amplitude of oscillations in the inter-area oscillatory

Table 4.1: Standard deviations (Std.) of power system quantities of the two-area system with inclusion of wind generation reached at stationary conditions.

Std. [pu]	Gaussian	Weibull	Inc.	Beta	Inc.	Gamma	Inc.
$\sigma(v_{\text{Bus 08}})$	0.0087	0.0091	4.6	0.0092	5.75	0.0095	9.2
$\sigma(v_{\text{Bus 09}})$	0.0058	0.0061	5.17	0.0062	6.9	0.0064	10.34
$\sigma(p_{g_{\text{G1}}})$	0.0136	0.0136	4.08	0.0138	5.97	0.0148	13.1
$\sigma(p_{g_{\text{G2}}})$	0.0135	0.0135	4.07	0.0138	5.96	0.0147	13.08
$\sigma(p_{g_{\text{G3}}})$	0.0134	0.0134	4	0.0137	5.89	0.0146	13.32
$\sigma(p_{g_{\text{G4}}})$	0.0133	0.0133	3.98	0.0136	5.87	0.0145	13.27

Inc.: Normalised increment calculated in % with Gaussian PDF as base.

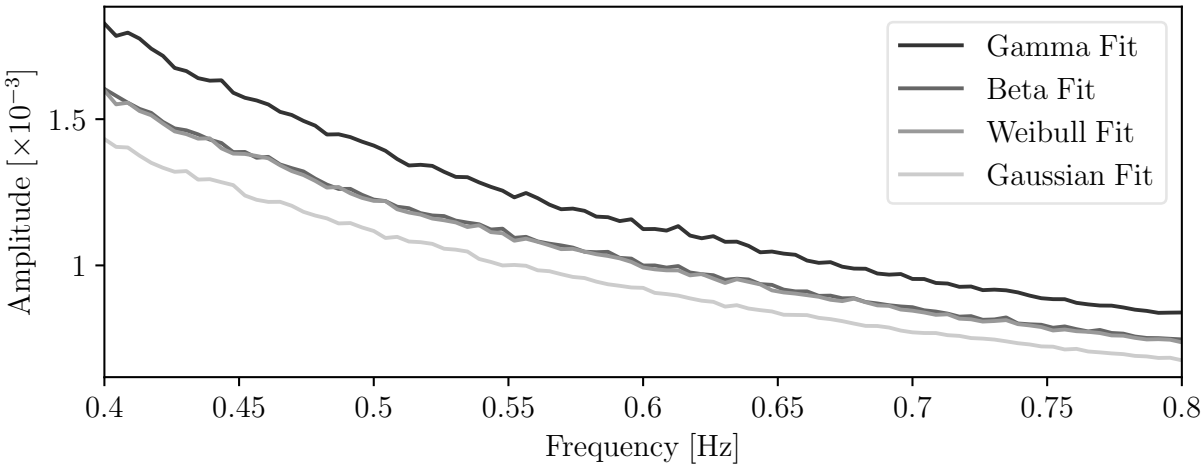

Figure 4.11: Average of frequency spectrum of thousand trajectories of total wind active power injected into the two-area system with inclusion of wind generation.

mode for Gamma PDF with the lowest being the Gaussian PDF. These variations in the amplitudes of the oscillations for different PDF types lead to variations in the statistical properties of the quantities of the power system as seen in Table 4.1.

Next, the impact of the PDF types on the behavior of the system after the occurrence of a contingency is evaluated. This consists in the trip of the line connecting buses 8 and 9 at time $t = 30$ s. The mean trajectories of $v_{\text{Bus 08}}$ obtained for all the PDF types are shown in Figure 4.13. This figure also illustrates the deterministic trajectory of $v_{\text{Bus 08}}$ obtained by simulating the modified two-area system through deterministic DAEs. Figure 4.13 shows that the mean trajectories of $v_{\text{Bus 08}}$ obtained for all the PDF types coincide with the deterministic trajectory of $v_{\text{Bus 08}}$.

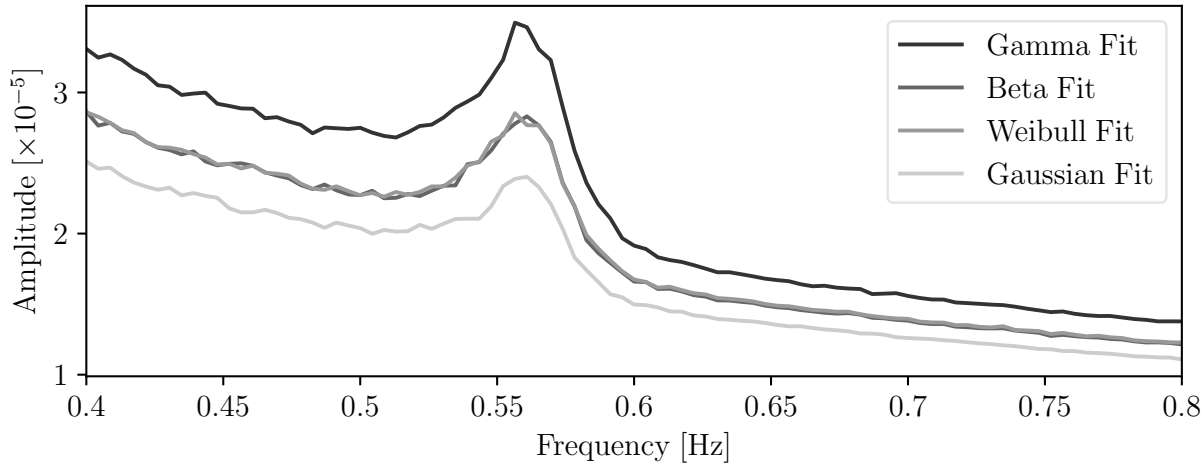

Figure 4.12: Average frequency spectrum of thousand trajectories of voltage magnitude at bus 8 of the two-area system with inclusion of wind generation.

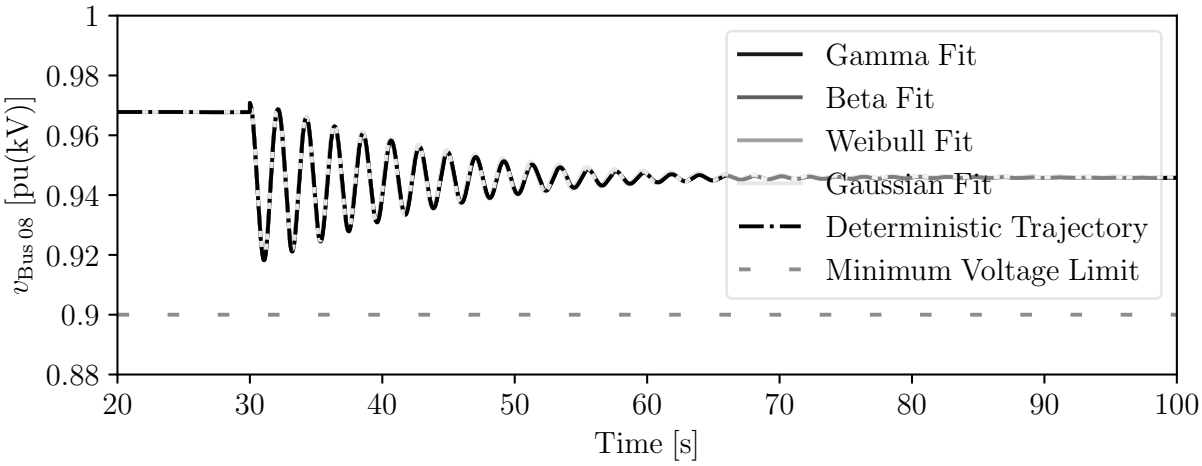

Figure 4.13: Average of thousand trajectories of voltage magnitude at bus 8 of the two-area system with inclusion of wind generation for different PDF types.

Finally, the trajectories of $v_{\text{Bus 08}}$ obtained as a result of simulating correlated wind speeds, through different PDF types, are illustrated in Figure 4.14. While Table 4.1 shows the values of $\sigma(v_{\text{Bus 08}})$ before the contingency. The standard deviation of $v_{\text{Bus 08}}$ is the lowest for the Gaussian and the highest for the Gamma PDF. Figure 4.14 shows that a considerable number of trajectories of $v_{\text{Bus 08}}$ violate the minimum voltage limit. The number of trajectories of $v_{\text{Bus 08}}$ that go below the minimum voltage limit at least once in the period of 30 s $< t <$ 35 s is shown in Table 4.2.

The results shown in Figure 4.14 and Table 4.2 agree with the discussion presented above in this section, i.e., the Gamma PDF leads to the worst dynamic behavior whereas the Gaussian PDF to the best. The Weibull and Beta PDF remain close to each other, which must be expected as the differences in the CDFs of Weibull and Beta PDF vs RCDF as well as in their frequency spectrum are negligible. These results, while being non-intuitive, can be understood by analysing the oscillations induced in the power system by the wind speeds following different PDF types.

Note that the conclusions that can be drawn in this case study do not allow to conclude that the Gamma PDF *always* leads to the worst dynamic response, nor that processes with different PDFs always cause different dynamic impacts. The effect of the PDF depends on the ACF of the stochastic processes, their locations in the network and on the oscillatory modes of the system.

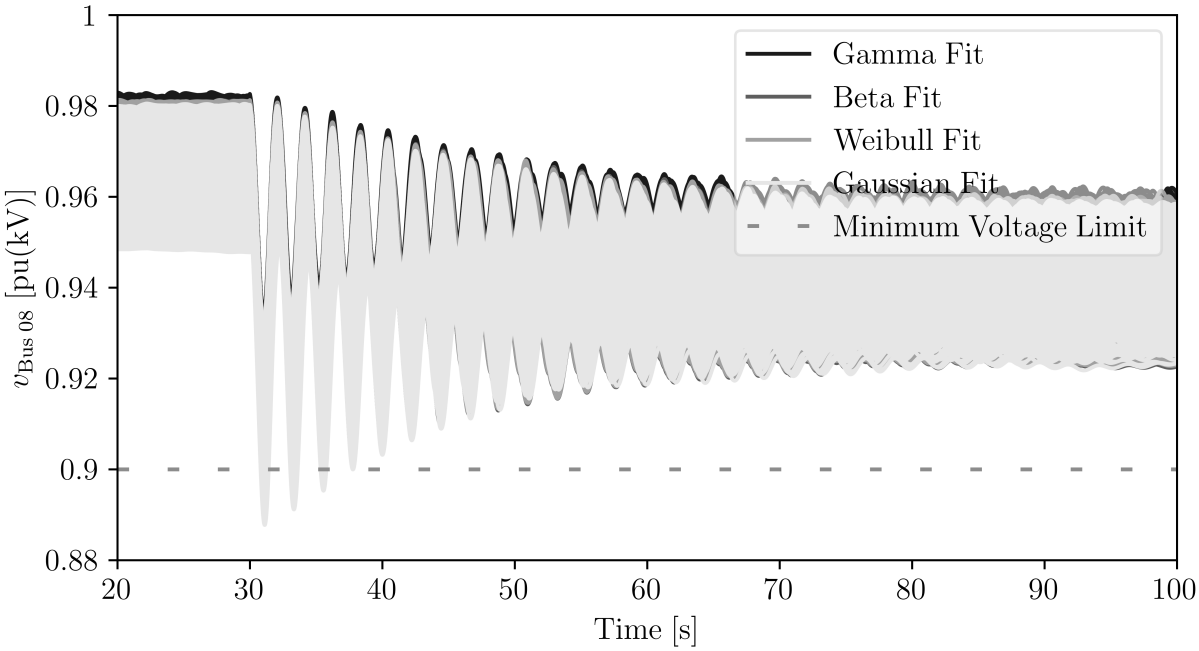

Figure 4.14: Trajectories of voltage magnitude at bus 8 of the two-area system with inclusion of wind generation for different PDF types.

Table 4.2: Trajectories with under-voltages at bus 8 of the two-area system with inclusion of wind generation.

PDF	Trajectories with under-voltages
Gaussian	42 (4.2 %)
Weibull	56 (5.6 %)
Beta	59 (5.9 %)
Gamma	70 (7.0 %)

4.4 Linear Estimation Method

This section presents a direct method to calculate the variances of the power system algebraic variables. The SDAE model introduced in Section 3.4 is the starting point of the power system dynamic model considered in this section. This section models the dynamic behaviour of the power system in the presence of stochastic disturbances as a set of index-1 SDAEs:

$$\boldsymbol{x} = \boldsymbol{f}(\boldsymbol{x}, \boldsymbol{y}, \boldsymbol{\eta})\,, \tag{4.1}$$

$$\mathbf{0}_{m,1} = \boldsymbol{g}(\boldsymbol{x}, \boldsymbol{y}, \boldsymbol{\eta})\,, \tag{4.2}$$

$$\boldsymbol{\eta} = \boldsymbol{a}(\boldsymbol{\eta}) + \boldsymbol{b}(\boldsymbol{\eta}) \circ \boldsymbol{\zeta}\,, \tag{4.3}$$

where all the variables and parameters have the same meaning as in (3.3).

To calculate the variances of the power system algebraic variables $\boldsymbol{y}$, the set of SDAEs are linearized at an equilibrium point $(\boldsymbol{x}_o, \boldsymbol{y}_o, \boldsymbol{\eta}_o)$ as per Method I described in [30]. Where $(\boldsymbol{x}_o, \boldsymbol{y}_o, \boldsymbol{\eta}_o)$ is a point for which (4.2) are satisfied such that $\dot{\boldsymbol{x}} = \mathbf{0}_{n,1}$ and $\boldsymbol{a}(\boldsymbol{\eta}_o) = \mathbf{0}_{p,1}$. The linearization of (4.1)-(4.3) gives:

$$\begin{bmatrix} \hat{\boldsymbol{x}} \\ \mathbf{0}_{m,1} \\ \hat{\boldsymbol{\eta}} \end{bmatrix} = \begin{bmatrix} \boldsymbol{f}_{\boldsymbol{x}} & \boldsymbol{f}_{\boldsymbol{y}} & \boldsymbol{f}_{\boldsymbol{\eta}} \\ \boldsymbol{g}_{\boldsymbol{x}} & \boldsymbol{g}_{\boldsymbol{y}} & \boldsymbol{g}_{\boldsymbol{\eta}} \\ \mathbf{0}_{p,n} & \mathbf{0}_{p,m} & \boldsymbol{a}_{\boldsymbol{\eta}} \end{bmatrix} \begin{bmatrix} \hat{\boldsymbol{x}} \\ \hat{\boldsymbol{y}} \\ \hat{\boldsymbol{\eta}} \end{bmatrix} + \begin{bmatrix} \mathbf{0}_{n,q} \\ \mathbf{0}_{m,q} \\ \boldsymbol{B}(\boldsymbol{\eta}_o) \end{bmatrix} \boldsymbol{\xi}\,, \tag{4.4}$$

where $\boldsymbol{f}_{\boldsymbol{x}}$, $\boldsymbol{f}_{\boldsymbol{y}}$, $\boldsymbol{f}_{\boldsymbol{\eta}}$, $\boldsymbol{g}_{\boldsymbol{x}}$, $\boldsymbol{g}_{\boldsymbol{y}}$, $\boldsymbol{g}_{\boldsymbol{\eta}}$, $\boldsymbol{a}_{\boldsymbol{\eta}}$ are the Jacobian matrices of the system calculated at $(\boldsymbol{x}_o, \boldsymbol{y}_o, \boldsymbol{\eta}_o)$. $\hat{\boldsymbol{x}}$ and $\hat{\boldsymbol{\eta}}$ represent the deterministic and the stochastic states of the linearized system. Eliminating the algebraic variables from (4.4) and defining $\hat{\boldsymbol{z}} = [\hat{\boldsymbol{x}}, \hat{\boldsymbol{\eta}}]^{\mathrm{T}}$ leads to a set of linear SDEs, as follows:

$$\begin{aligned} \begin{bmatrix} \hat{\boldsymbol{x}} \\ \hat{\boldsymbol{\eta}} \end{bmatrix} &= \begin{bmatrix} \boldsymbol{f}_{\boldsymbol{x}} - \boldsymbol{f}_{\boldsymbol{y}}\boldsymbol{g}_{\boldsymbol{y}}^{-1}\boldsymbol{g}_{\boldsymbol{x}} & \boldsymbol{f}_{\boldsymbol{\eta}} - \boldsymbol{f}_{\boldsymbol{y}}\boldsymbol{g}_{\boldsymbol{y}}^{-1}\boldsymbol{g}_{\boldsymbol{\eta}} \\ \mathbf{0}_{p,n} & \boldsymbol{a}_{\boldsymbol{\eta}}\,, \end{bmatrix} \begin{bmatrix} \hat{\boldsymbol{x}} \\ \hat{\boldsymbol{\eta}} \end{bmatrix} + \begin{bmatrix} \mathbf{0}_{n,q} \\ \boldsymbol{b}(\boldsymbol{\eta}_o) \end{bmatrix} \boldsymbol{\xi} \\ &= \mathbf{A}_o\,\hat{\boldsymbol{z}} + \mathbf{B}_o\,\boldsymbol{\xi}\,, \end{aligned} \tag{4.5}$$

Based on the Fokker-Planck equation, the probability distribution $\boldsymbol{\varpi}(\hat{\boldsymbol{z}})$ of all state variables in stationary condition satisfies [72]:

$$\boldsymbol{\varpi}(\hat{\boldsymbol{z}}) = (\det \mid 2\pi\mathbf{D} \mid)^{-1/2} \cdot \exp\!\left(-\frac{1}{2}\hat{\boldsymbol{z}}^{\mathrm{T}}\mathbf{D}^{-1}\hat{\boldsymbol{z}} \right), \tag{4.6}$$

where $\mathbf{D}$ is the variance-covariance matrix of the state variables in (4.5). Matrix $\mathbf{D}$ is symmetric and satisfies the Lyapunov equation:

$$\mathbf{A}_o\mathbf{D} + \mathbf{D}\mathbf{A}_o^{\mathrm{T}} = -\mathbf{B}_o\mathbf{B}_o^{\mathrm{T}}\,, \tag{4.7}$$

which is a special case of the Riccati equation. The diagonal elements of $\mathbf{D}$ are the steady-state variances of the components of the state variables $\hat{\boldsymbol{z}}$. In particular, if the stochastic processes $\boldsymbol{\eta}$ are not correlated, the last p diagonal elements of $\mathbf{D}$ can be written

as:

$$\sigma_k^2 = \frac{b_k^2}{2a_k}, \qquad k = 1, \ldots, p\,,$$

where a_k and b_k are k-th diagonal elements of $\boldsymbol{a_\eta}$ and $\mathbf{B}_o$, respectively, and σ_k^2 are the variances of the p stochastic processes $\hat{\boldsymbol{\eta}}$.

From (4.5), it is observed that $\hat{\boldsymbol{x}}$ can be written as a linear combination of the entries of $\hat{\boldsymbol{z}}$. Hence, also the elements of $\hat{\boldsymbol{x}}$ are Gaussian processes. Furthermore, the covariance matrix $\mathbf{K}$ of the small-signal algebraic variables can be written as [61]:

$$\mathbf{K} = \mathbf{G}_o\, \mathbf{D}\, \mathbf{G}_o^{\mathrm{T}}\,, \tag{4.8}$$

where

$$\mathbf{G}_o = -\boldsymbol{g_y}^{-1} \begin{bmatrix} \boldsymbol{g_x} & \boldsymbol{g_\eta} \end{bmatrix}. \tag{4.9}$$

The diagonal elements of $\mathbf{K}$ are the sought variances of the algebraic variables $\hat{\boldsymbol{y}}$.

Note that if $p \ll n$, i.e., the number of sources of stochastic disturbances is much smaller than the number of state variables, the covariance matrices $\mathbf{D}$ and, hence, $\mathbf{K}$ might not be full rank. A zero element in the k-th position of the diagonal of $\mathbf{D}$ ($\mathbf{K}$) indicates that the associated $\tilde{x}_k$ ($\tilde{y}_k$) are not affected by stochastic disturbances. In this case, the vector of stochastic processes $\hat{\boldsymbol{z}}$ is said to be degenerate [27].

4.5 Case Study

This section illustrates the accuracy and numerical efficiency of the LE to calculate the variances of algebraic variables of the power system. All results are compared to the ones obtained through the MC. The power systems utilised in this case study are the IEEE 14-bus system and the All-Island Irish Transmission System (AIITS). Equation (4.7) is solved using the open-source library SLICOT [10].

In both power systems, the sources of stochastic disturbances are modeled as independent OU processes and included in the loads and, for the AIITS, also in the wind speeds. Where the stochastic load consumption model described in Section 3.5.1 is used to model load consumption, and the wind speeds are modeled through the stochastic wind speed model in Section 3.5.3.

The accuracy of the LE is measured by calculating the closeness of the values of standard deviation of the power system variables obtained through the MC with those obtained through the LE. With this aim, a *measure of closeness* index, ϵ_σ, is defined as follows:

$$\epsilon_\sigma\ (\%) = \frac{\sigma_{\mathrm{MC}} - \sigma_{\mathrm{LE}}}{\sigma_{\mathrm{MC}}} 100\,. \tag{4.10}$$

where σ_{MC}, and σ_{LE} are the standard deviations of the variables obtained through the MC and the LE, respectively. Note that the choice of σ_{MC} as base for ϵ_σ is arbitrary. Also note that ϵ_σ is calculated for a large number of power system algebraic variables. A detailed description of the variables utilised is provided in Table 4.3.

Table 4.3: List and description of power system variables.

Variable	Description
η_p	Stochastic disturbance on load active power consumption
η_q	Stochastic disturbance on load reactive power consumption
δ	Rotor angle of the synchronous machine
ω	Rotor speed of the synchronous machine
p_g	Active power injection of the synchronous machine
q_g	Reactive power injection of the synchronous machine
I_d	d-axis current of the synchronous machine
I_q	q-axis current of the synchronous machine
v_d	d-axis voltage of the synchronous machine
v_q	q-axis voltage of the synchronous machine
v	Bus voltage magnitude
θ	Bus voltage angle
p_{fr}	Active power injections at the sending-end bus
p_{to}	Active power injections at the receiving-end bus
q_{fr}	Reactive power injections at the sending-end bus
q_{to}	Reactive power injections at the receiving-end bus

4.5.1 IEEE 14 Bus System

The IEEE 14-bus system, shown in Figure 4.15, contains 14 buses with 11 loads, 20 lines/transformers, and 5 synchronous machines. The synchronous generators are described by a sixth-order model, and are equipped with TGs and IEEE Type-I AVRs. An AGC is also included in the model [49].

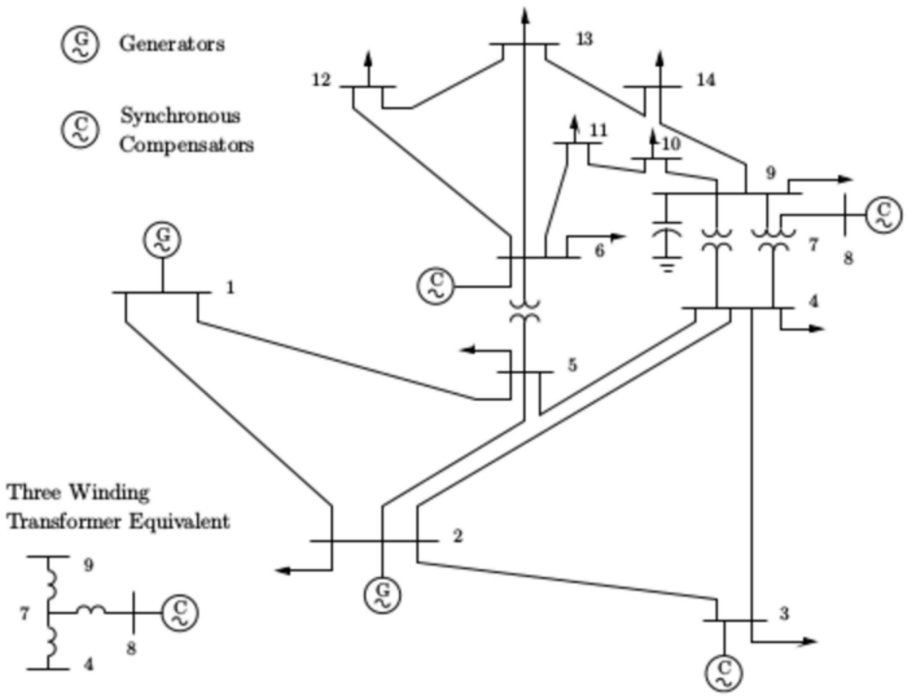

Figure 4.15: Single line diagram of the IEEE 14-bus system.

The stochastic load consumption is modeled through (3.5) with the following parameters: the autocorrelation coefficients of η_p and η_q are $\alpha_p = \alpha_q = 0.01$ s^{-1}, respectively; and the standard deviation of η_p and η_q are $\sigma(\eta_p) = 5\%$ of p_{L_0} and $\sigma(\eta_q) = 5\%$ of q_{L_0}, respectively. The simulation time t_f for each realization is chosen as $t_f = 2/\alpha = 200$ s. The integration of the deterministic part of SDAEs is performed with with a time step $\Delta t = 0.01$ s. The OU processes are integrated using a step size $h = 0.01$ s.

Figure 4.16 shows the box plot of the values of ϵ_σ obtained in the case of the IEEE 14-bus system through the MC and the LE. Results indicate that LE yields σ_{LE} that are very close to σ_{MC}. Note that the box plot is drawn such that the thick horizontal grey lines show the median of the data, the top and bottom notches contain 5% to 95% percentile of the data, and the black circles show the outliers.

Note that as η_p and η_q are modeled through the OU process, which is linear and has a constant diffusion term, the LE yields the variances of η_p and η_q, which are exactly the same to those obtained from the MC. This is confirmed by the results shown in Figure 4.16, which shows a very close match between the LE and the MC for the stochastic processes η_p and η_q. Also note that, to test the accuracy of the LE against the nonlinearity of the SDAEs, a wide range of standard deviation of the process, $\sigma(\eta_p) = \sigma(\eta_q)$, ranging

from 1% to 10% of the initial load consumption is considered. The variations in the values of ϵ_σ for all the variables were found to be in the same range as in Figure 4.16. In fact, the standard deviation $\sigma(\epsilon_\sigma)$ and mean $\mu(\epsilon_\sigma)$ of the measure of closeness index for a few variables are illustrated in Figure 4.17. It is fair to conclude, thus, that the LE works with

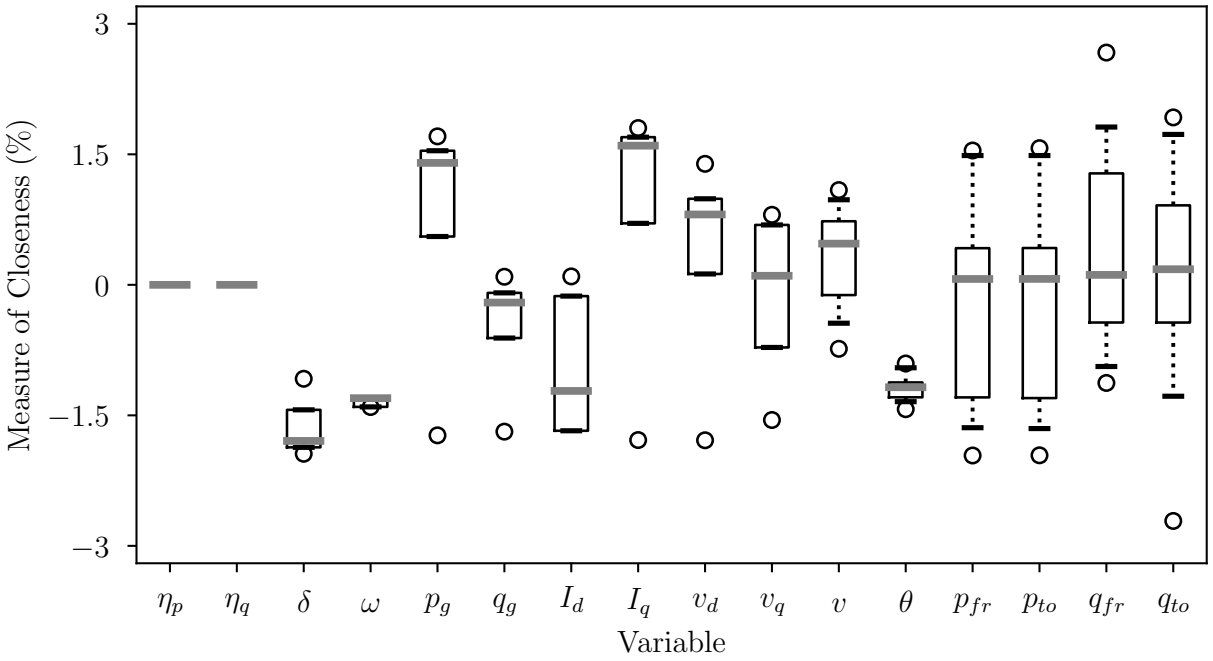

Figure 4.16: Box plot of measure of closeness index for the IEEE 14-bus system.

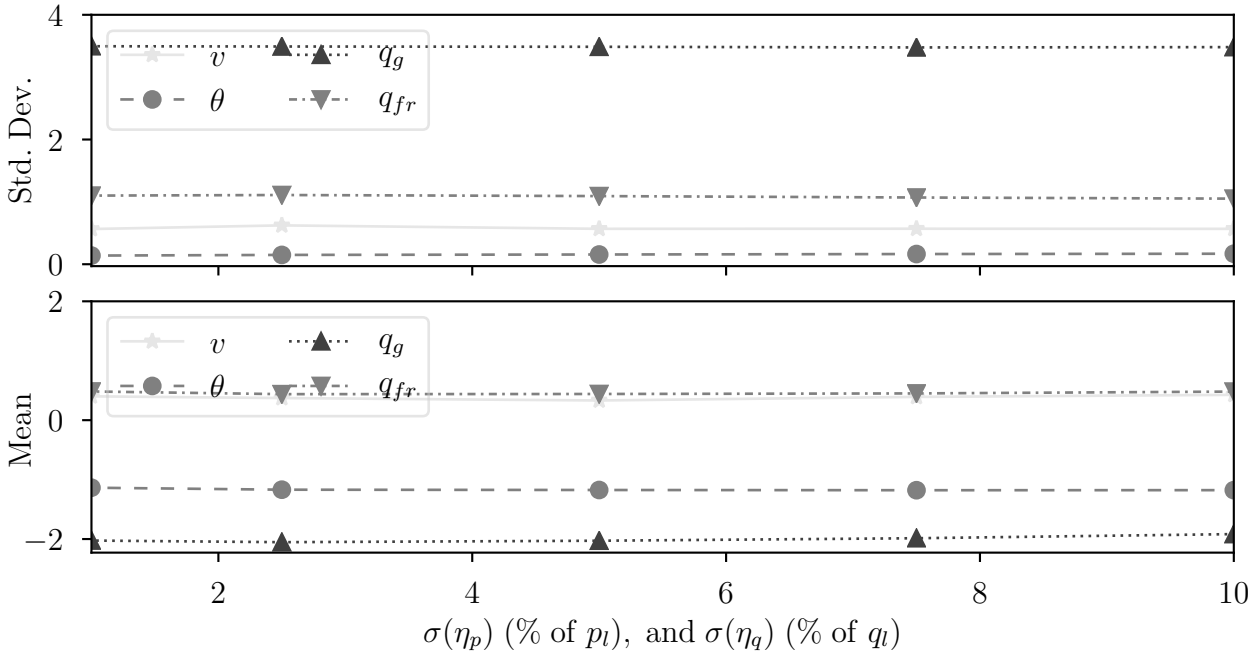

Figure 4.17: Standard deviation and mean of the measure of closeness index for a few variables of the IEEE 14-bus system.

an exceptionally good accuracy for a wide range of standard deviation of the stochastic processes.

4.5.2 All-Island Irish Transmission System

This section demonstrates the robustness and light computational burden of the LE when applied to the real-world complex systems. For this reason, a dynamic model of the All-Island Irish Transmission System (AIITS) is considered. The schematic map of the AIITS is shown in Figure 4.18. The AIITS consists of 1479 buses, 1851 lines/transformers, and 22 synchronous generators that are modeled through a VI-order model and are equipped with IEEE ST1a AVRs, and TGs to ensure a secure operation of the grid. Six conventional power plants also include a Power System Stabilizer. The AIITS includes 246 load devices. The AIITS has two 500 MW high-voltage direct-current interconnections with Scotland and Wales. The AIITS also includes 176 wind power plants, 34 of which are equipped with constant-speed and 142 with doubly-fed induction generators.

The MC, which is comprised of 1000 TDSs, is employed first to calculate σ_{MC}. The stochastic disturbances are introduced on load consumption through the load model in (3.5), using independent OU processes. The parameters of $\boldsymbol{\eta}$ in (3.5) are chosen such that $\alpha_p = \alpha_q = 0.01\text{s}^{-1}$; $\sigma(\eta_p) = 5\%$ of p_{L_0}; and $\sigma(\eta_q) = 5\%$ of q_{L_0}. The wind speed is modeled as a OU process through (3.11) with a standard deviation 5 % of the average wind speed. The final simulated time for the AIITS is calculated as $t_f = 2/\alpha = 200$ s. Each realization of the MC is simulated with a time step of 0.01 s.

The box plot of ϵ_σ for the AIITS is shown in Figure 4.19. The following remarks are relevant. The measure of closeness index, ϵ_σ, indicates that the LE deviates more with respect to the MC for the AIITS than for the IEEE 14-bus system. The values of the ϵ_σ of the algebraic variables are larger for the AIITS than for the IEEE 14-bus system. These deviations, however, are not due to numerical inaccuracies but to the fact that ϵ_σ is a relative measure. Larger ϵ_σ refer to very small values of the standard deviation of the algebraic variables.

On the other hand, the LE shows a clear advantage with respect to the MC, at least for large power system models. That is, the LE is characterized by significantly smaller computational times than the MC. In the case of the AIITS, the total CPU time required

by the MC was 14763 s, i.e., more than 4 hours, whereas the LE took 54 s, i.e., less than a minute.

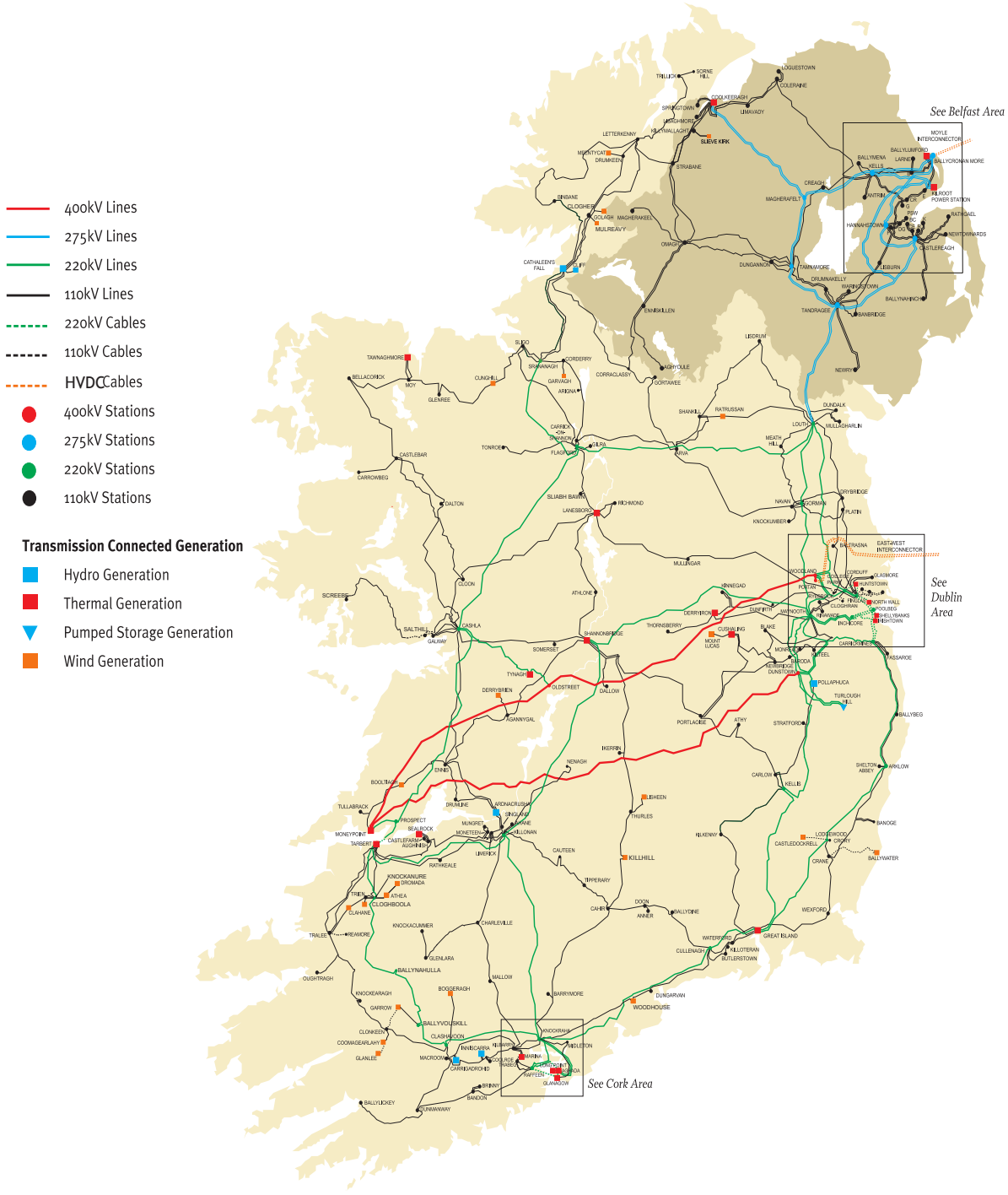

Figure 4.18: The schematic map of the All-Island Irish Transmission System [18].

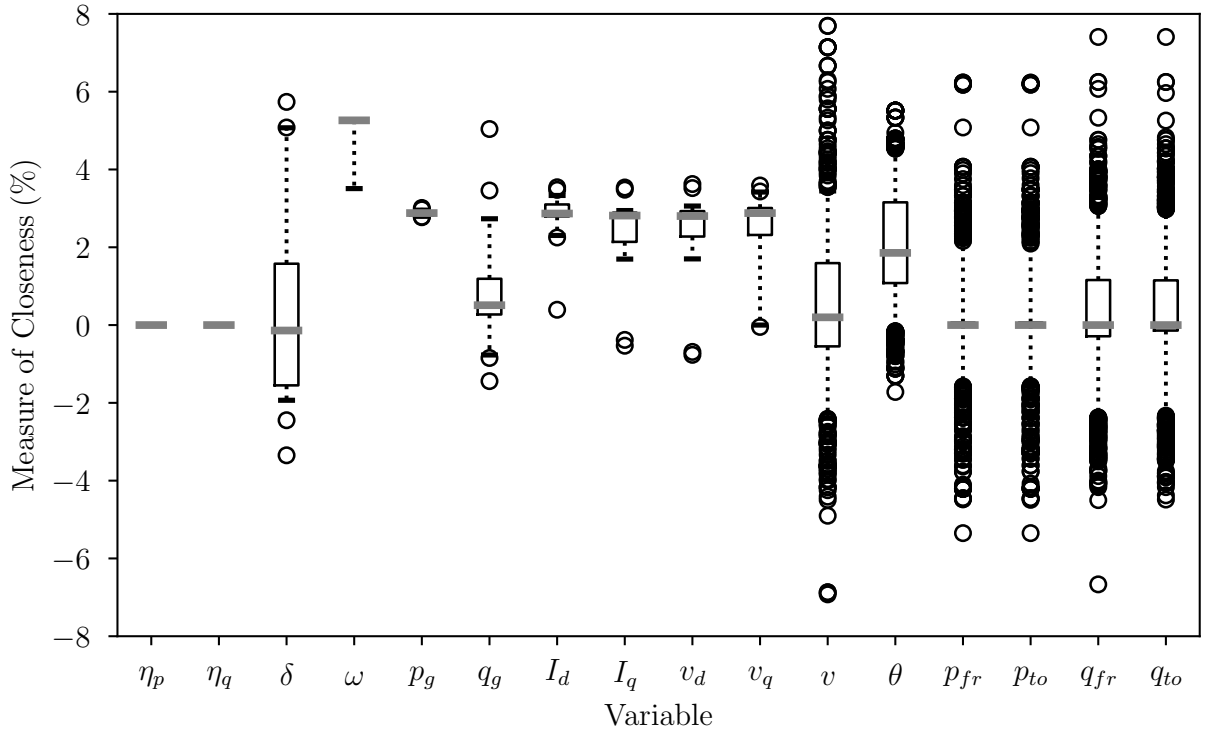

Figure 4.19: Box plot of measure of closeness index for the AIITS.

4.6 Conclusions

This chapter presents methods to calculate the variances of the algebraic variables of power system modeled as SDAEs. With this regard, the conventional MC and a newly proposed method, named the LE, are used. The chapter also discuses the impact of modelling stochastic processes with various PDFs on the variances of the algebraic variables and the dynamic behaviour of the power system.

The MC is illustrated with the help of case study utilising a 9-bus system. The case study demonstrates that the computational burden of the MC is dependent on the autocorrelation coefficient of the stochastic processes; the time-step of the integration scheme; the number of realizations of the processes; and complexity and size of the power system.

The impact of modelling stochastic processes with various PDF types on power system dynamic is demonstrated by simulating a distribution network. It is shown that some PDF types, despite having similar statistical properties, might have severe impact on the variances of the power system quantities and as a result the probability that system physical limits are violated after a contingency is affected. This result is counter intuitive and cannot be known without actually simulating the system. Note that in this case study

the results were obtained using the MC. These results cannot be obtained through a direct method because direct methods can study the system only at stationary conditions.

The proposed direct method, i.e., LE, is based on the solution of the Lyapunov equation and a linearized method. The LE finds its usage in providing a realistic estimate of variances of the algebraic variables at stationary conditions, which is crucial to ensure that none of the system physical limits are violated in normal grid operation. Simulation results show that the proposed technique has a high accuracy for a wide range of standard deviation of stochastic processes, and significantly reduced computational time as compared to the conventional MC.

It is relevant to note that the LE, despite a high accuracy and a clear advantage over the MC in terms of computational efficiency, is not suitable for the dynamic analyses of the power systems. The dynamic analyses consist of monitoring the individual trajectories of the MC for violations of the system limits such as bus voltage limits, or any instabilities such as loss of synchronism. Such analyses cannot be conducted through a direct method. Furthermore, the LE is valid only if linearization is valid and cannot consider the nonlinearities, the hard limits, saturations etc.

Chapter 5

Autocorrelation

5.1 Introduction

The impact of autocorrelation of the stochastic disturbances on the power system's dynamic behavior is the objective of this chapter. For this reason, modelling the power system as a set of nonlinear Stochastic Differential Algebraic Equations (SDAEs) is the best formulation choice available [41, 51, 73]. The SDAE models power system's dynamic behaviour independent of its size or complexity. Therefore, no simplification or linearization is required. A byproduct of this modelling approach, however, is that no analytical solutions, of the resulting SDAEs that describe the power system model, are available. For this reason, numerical methods mentioned in Chapter 3 are utilised to integrate the nonlinear SDAEs.

The goal in this chapter is twofold. To study the impact of autocorrelation of stochastic disturbances on the stability of the power system; and to study the dynamic coupling between the drift of stochastic disturbances and the electro-mechanical modes of the power system. With this regard, two techniques, namely, time- and frequency-domain analysis are utilised. For simplicity but without loss of generality, this chapter focuses on the stochastic disturbances introduced into the power system in load consumption. Stochastic disturbances are modelled using stochastic load model in (3.5).

The discussion presented in this chapter models net load at distribution level. Where the net load is obtained by subtracting the power injections of non-synchronous Renewable Energy Sources (RES) from actual load demand. In the remainder of this chapter, stochastic disturbances are modelled as independent processes, i.e., $\mathbf{R} = \mathbf{I}$ and are

described by Ornstein-Uhlenbeck (OU) processes. This assumption allows simplifying the discussion of the case studies but does not impact on the generality of the conclusions.

The remainder of the chapter is organized as follows. Section 5.2 analyses the transient behaviour of power system subjected to stochastic disturbances in time-domain. With this regard, Subsection 5.2.1 presents a detailed discussion on the impact of atutocorrelation of a stochastic process on its dynamic response. Whereas Subsection 5.2.2 discusses the impact of autocorrelation of the stochastic disturbances on the dynamic behaviour of the power system. Section 5.3 focuses on another relevant feature of the autocorrelation, i.e., the dynamic coupling between the drift of stochastic disturbances and the electro-mechanical modes of the systems. Finally, conclusions are drawn in Section 5.4.

5.2 Time Domain Analysis

This section studies the impact of autocorrelation of stochastic disturbances on the transient behaviour of power system in time-domain. With this aim, at first, the impact of autocorrelation of a stochastic process on the dynamic behaviour of the stochastic process itself is analysed in Section 5.2.1. Finally, Section 5.2.2 studies the effect of autocorrelation of the stochastic disturbances on the dynamic behaviour, and hence, stability of power system. The discussion in this section was originally presented in [4].

5.2.1 Dynamic Response of Stochastic Process

This section presents a detailed discussion on the dynamic analysis of the stochastic process in time domain. This analysis considers the autocorrelation, i.e., Autocorrelation Function (ACF) and standard deviation, i.e., Probability Density Function (PDF) of the stochastic process. For simplicity but without loss of generality, a OU process is chosen. Note that the discussion presented in this section is valid for other stochastic processes as well.

The OU process is a linear implementation of the SDE in (2.9) and/or (2.20). Hence, both drift and diffusion terms can independently modify the dynamic behavior of a OU process. As a result, the power system dynamic will behave differently dependent on the modifications in the two terms. The OU process is mean-reverting, i.e., it tends to its mean value and shows constant standard deviation in stationary conditions. A OU

process is defined as:

$$\dot{\eta} = -\alpha(\eta - \mu) + \beta\xi\,, \tag{5.1}$$

where α is the autocorrelation coefficient or the speed of the mean reversion; β is the coefficient of the diffusion term; μ is the mean value; and ξ is the white noise. The process resulting from (5.1) is a real-valued process that follows a Gaussian PDF given by $\mathcal{N}(\mu, \sigma^2)$, and $\beta = \sigma\sqrt{2\alpha}$.

The process defined in (5.1) is a linear combination of two terms: drift and diffusion. This allows for both terms to be adjusted independently. As a result, OU processes with different values of α and, hence, different dynamic behavior, can have same PDF in stationary conditions. In fact, the PDF of (5.1) is defined as in (2.6), which does not depend on α.

Table 5.1 shows a set of parameters of OU processes. Figure 5.1 illustrates the time series of OU processes generated from the parameters in Table 5.1. It is important to note that the processes shown in the top panel Figure 5.1 have the same PDF in stationary conditions. However, their transient behavior is significantly different because of the different values of α. On the other hand, the bottom panel of Figure 5.1 illustrates OU processes generated with different values of σ but same values of α. Comparing the upper and lower panel of Figure 5.1, it is evident that from the dynamic point of view, a process with high α and low standard deviation has a similar effect as a process with low α and high standard deviation.

The autocorrelation coefficient of a stationary stochastic process is calculated from the ACF. As explained in Chapter 2, the ACF of a stationary stochastic process measures the dependence of present values, of a given time series, on the past values, of the same time series, as a function of time lag, and is calculated using (2.13). Figure 5.2 illustrates the ACFs, calculated using (2.13), of the OU processes shown in Figure 5.1. The ACF is always equal to 1 for $\tau = 0$ by definition. As τ increases the correlation of the OU processes between current and future values decreases exponentially and decreases the

Table 5.1: Parameters of OU processes.

Parameters	η_1	η_2	η_3	η_4	η_5	η_6
α	1	0.1	0.01	0.01	0.01	0.01
σ	0.1	0.1	0.1	0.4	0.3	0.2

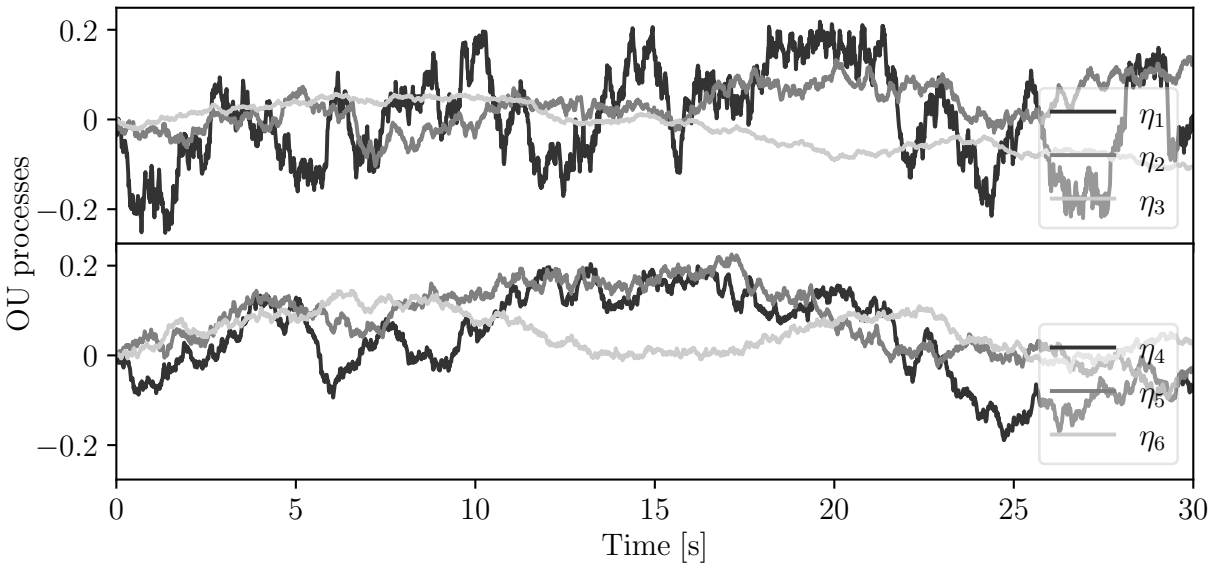

Figure 5.1: Single trajectory of OU processes defined in Table 5.1.

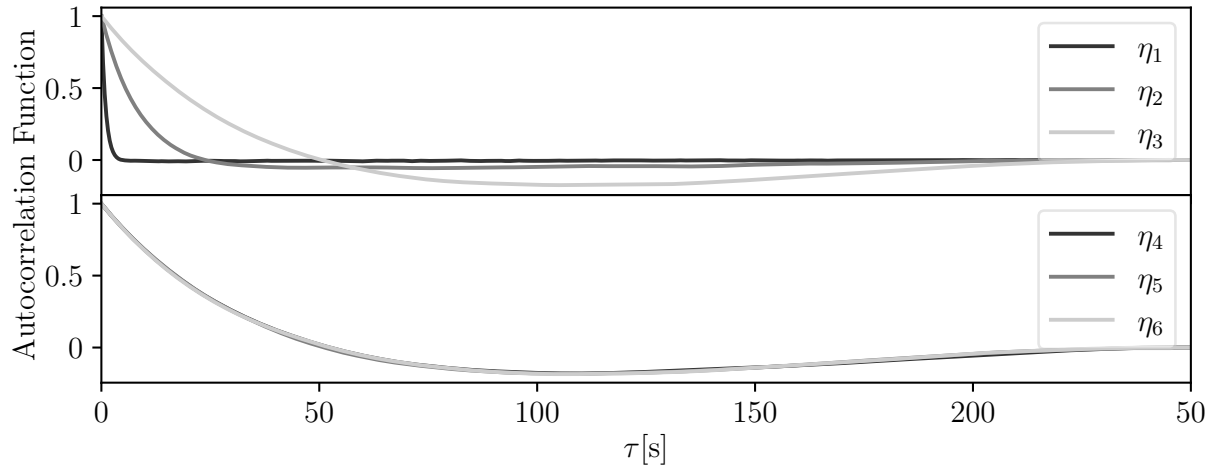

Figure 5.2: Exponentially decaying ACFs of OU processes defined in Table 5.1.

faster the higher the value of α. In fact, the analytical expression of ACF of a OU process is given as $R(\tau) = e^{-\alpha\tau}$. Note, however, that processes with different σ and same α show similar time evolution of the ACF (see bottom panel of Figure 5.2).

It is interesting to note that, taken alone, neither the time series of the OU processes, shown in Figure 5.1, nor the dynamic behavior of the ACF, shown in Figure 5.2, allow to distinguish between the OU processes. A more effective way to visualize the behavior of stochastic processes is through the MC. With this aim, 1,000 trajectories of each process of Table 5.1, with initial condition $\eta_i(0) = 0$ and a time step $h = 0.01$ s for the increments of the Wiener process, are simulated. The spread of the 1,000 trajectories of the OU processes can be visualized in Figure 5.3. Top panel of Figure 5.3 shows that the

OU processes reach same standard deviation at stationary conditions, i.e., $\sigma(t) = \sigma$, at separate times depending on α. Whereas the OU processes with same α but different σ reach different standard deviation at the stationary conditions all at the same time.

For the proof of concept, the standard deviation of all the trajectories for each process is calculated at every time step and plotted against time in Figure 5.4. The results shown in Figure 5.4 indicate that the time at which a stochastic process becomes stationary depends only on α of the process. In fact, the expression for a stochastic process to reach stationarity is given by $t_f = 2/\alpha$, which is not dependent on σ. On the other hand, the spread of the trajectories in stationary conditions depends only on the value of the standard deviation.

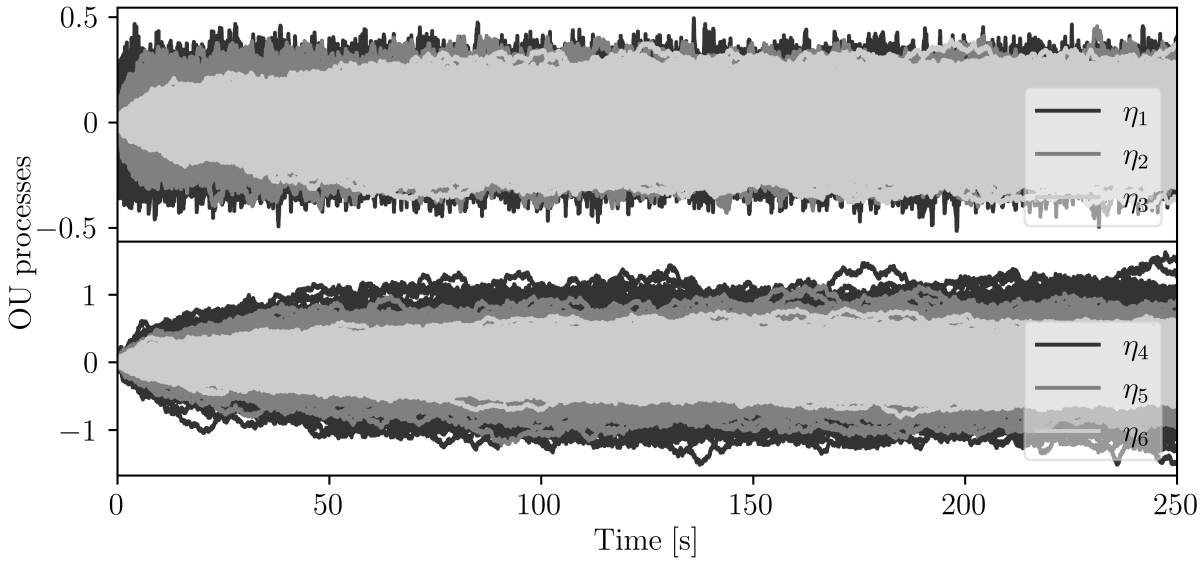

Figure 5.3: 1,000 trajectories of OU processes defined in Table 5.1.

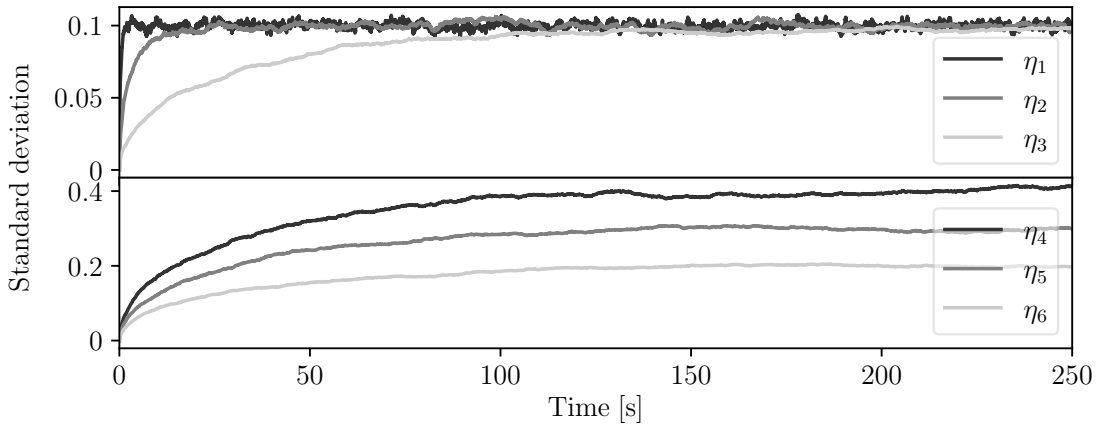

Figure 5.4: Standard deviations of 1,000 trajectories of OU processes defined in Table 5.1.

So far, independent OU processes have been considered. In the SDAE model in (3.3), however, the OU processes are dynamically coupled with the rest of the system. Common sense would suggest that ACFs of the OU processes affect exclusively the transient, while the standard deviation affects only the stationary conditions. However, since the variables $\boldsymbol{\eta}$ appear in the nonlinear differential-algebraic equations, this intuition is not always correct. The next subsection of this section shows that the ACF of the OU processes also impact on the stationary conditions of the system.

5.2.2 Dynamic Response of Power Systems

This section analyses the impact of the autocorrelation of stochastic disturbances on the dynamic behavior of the power system in time domain. This analysis is performed considering the evolution in time of the standard deviation of relevant variables of the system. With this aim, the MC is employed to extract meaningful statistical properties, such as the standard deviation and the autocorrelation of the trajectories of relevant variables, and also to assess the stability of the power system subject to stochastic disturbances. The MC utilises the dynamic model of two power systems, namely the well-known Kundur's two-area system and the dynamic model of the real-world All-Island Irish Transmission System (AIITS).

With the aim of studying the impact of autocorrelation coeficient α, six scenarios with various combinations of α and σ of the OU processes that describe the loads are defined in Table 5.2. The MC simulates $1,000$ trajectories for each scenario in Table 5.2. The numerical integration schemes utilise a time step of $h = 0.01$ s to integrate the Wiener

Table 5.2: Autocorrelation α and standard deviation σ of stochastic load consumption for different cases.

Scenarios	α [s^{-1}]	$\sigma(\eta_p)$ [% of p_{L0}]	$\sigma(\eta_q)$ [% of q_{L0}]
S1a	0.01	0.4	0.4
S1b	0.1	0.4	0.4
S1c	1	0.4	0.4
S2a	0.01	0.6	0.6
S2b	0.1	0.6	0.6
S2c	1	0.6	0.6

process in the non-linear SDAEs, while the deterministic part is integrated with a step size of $\Delta t = 0.01$ s. The total simulated time for each trajectory is $t = 200$ s.

5.2.2.1 Two-Area System

The original two-area system introduced in Section 4.3.2 and shown in Figure 4.9 is used in this case study. The impact of standard deviations of the stochastic disturbances on the power system algebraic variables is considered first. For this reason, the values of standard deviation of bus voltage magnitude $\sigma(v)$; and of active $\sigma(p_g)$ and reactive $\sigma(q_g)$ power generation of the synchronous generators calculated for scenarios S1a, S2a, S1b, and S2b are shown in Table 5.3. The values of $\sigma(v)$, $\sigma(p_g)$ and $\sigma(q_g)$ reported in Table 5.3 show an increase of 50% from scenario S1a to S2a and scenario S1b to S2b. Note that in the scenarios compared in Table 5.3, α of stochastic processes remains constant while σ is increased by 50% from the base scenario. The results indicate that in stationary conditions, the variations in σ of stochastic processes while keeping α constant lead to variations in σ of the power system variables in the same proportion. This behaviour is expected from a power system in stationary conditions.

Table 5.3: Standard deviation (Std.) of power system algebraic variables of the two-area system with stochastic loads for scenarios S1a, S2a, S1b, and S2b.

Std.	S1a	S2a	% increase	S1b	S2b	% increase
$v_{\text{Bus 1}}$	0.0008	0.0012	50	0.0023	0.0034	47.83
$v_{\text{Bus 2}}$	0.001	0.0016	60	0.0029	0.0044	51.72
$v_{\text{Bus 3}}$	0.0008	0.0012	50	0.0021	0.0032	52.38
$v_{\text{Bus 4}}$	0.001	0.0016	60	0.0028	0.0042	50
$v_{\text{Bus 7}}$	0.0021	0.0032	52.38	0.0046	0.007	52.17
$v_{\text{Bus 9}}$	0.0023	0.0035	52.17	0.0046	0.007	52.17
$p_{g_{\text{G1}}}$	0.0224	0.0333	48.66	0.0267	0.0394	47.57
$p_{g_{\text{G2}}}$	0.0222	0.033	48.65	0.0252	0.0371	47.22
$p_{g_{\text{G3}}}$	0.0223	0.033	47.98	0.0248	0.0366	47.58
$p_{g_{\text{G4}}}$	0.0223	0.033	47.98	0.025	0.0368	47.20
$q_{g_{\text{G1}}}$	0.0306	0.0463	51.31	0.0531	0.079	48.78
$q_{g_{\text{G2}}}$	0.0479	0.0725	51.36	0.0711	0.1056	48.52
$q_{g_{\text{G3}}}$	0.0321	0.0487	51.71	0.05	0.0745	49
$q_{g_{\text{G4}}}$	0.0526	0.0796	51.33	0.0708	0.1051	48.45

Next, the impact of α of stochastic processes on the statistical properties, i.e., mean and variance, of power system variables in stationary conditions is considered. With this regard, the time evolution of $\sigma(v)$ at load buses 7 and 9 are shown in Figures 5.5 and 5.6, respectively. By observing the Figures 5.5 and 5.6, it is obvious that α of the underlying stochastic processes has a significant impact on $\sigma(v)$ in stationary conditions. The actual values of $\sigma(v)$ at generator and load buses for base scenario, which is $\alpha = 0.01\text{s}^{-1}$, and their % increase calculated from the base scenarios are shown in Tables 5.4 and 5.5. Note

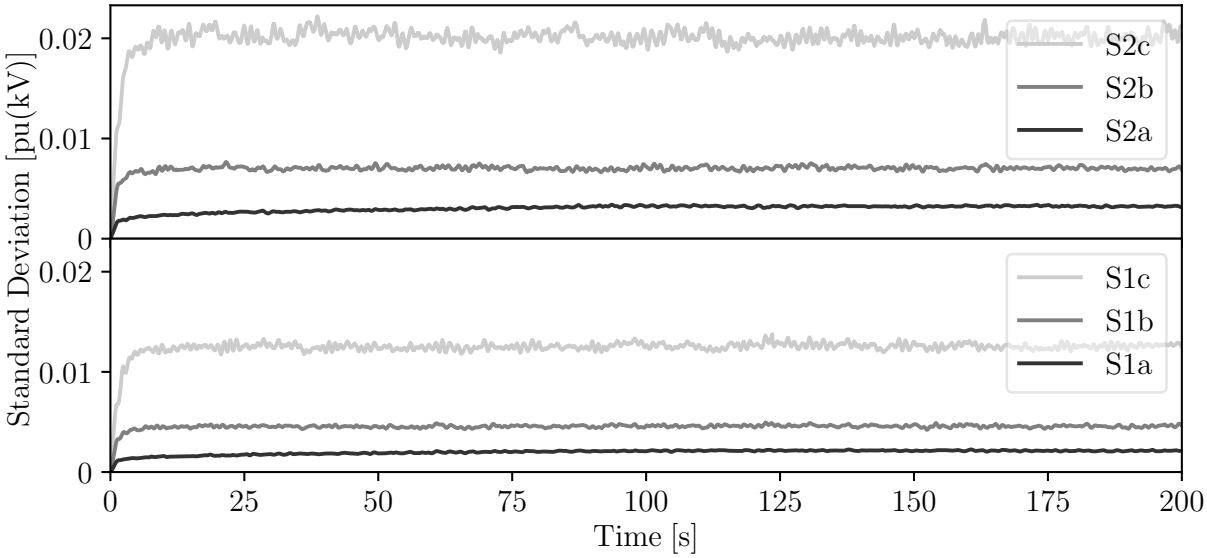

Figure 5.5: Standard deviation of voltage magnitude at load bus 7 of the two-area system with stochastic loads.

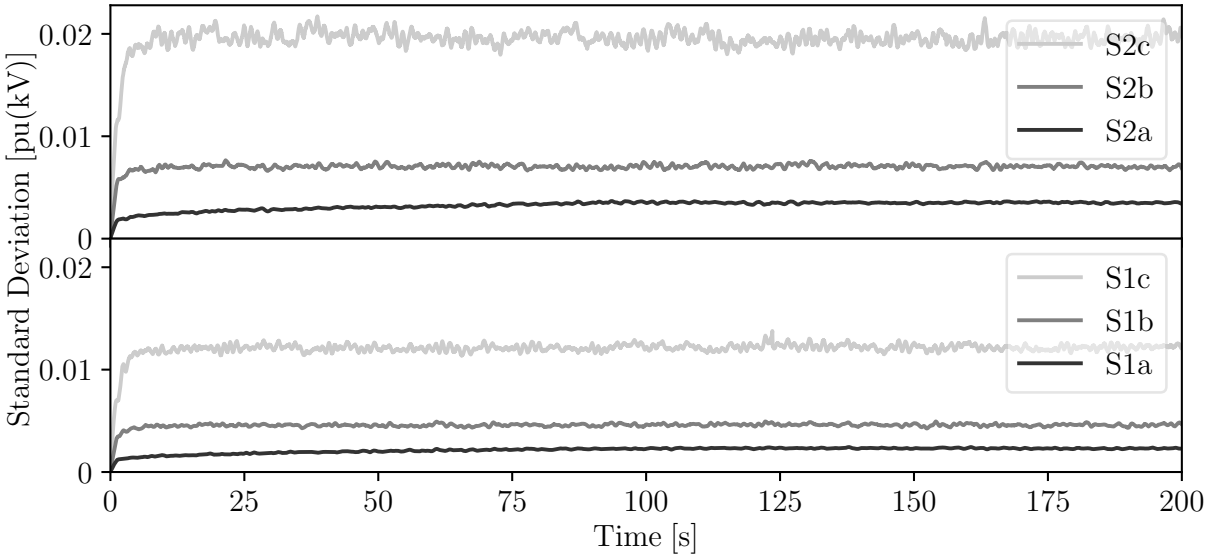

Figure 5.6: Standard deviation of voltage magnitude at load bus 9 of the two-area system with stochastic loads.

that the results presented in Tables 5.4 and 5.5 indicate that $\sigma(v)$ varies from 100% to 775% for a variation in α from 0.01 to $1s^{-1}$. These variations in $\sigma(v)$ are dependent only on α of the underlying stochastic processes and are independent of σ of the stochastic processes.

Finally, the variations in $\sigma(p_g)$ and $\sigma(q_g)$ for variations in α of stochastic processes are observed. Figures 5.7 and 5.8 illustrate the time evolution of $\sigma(p_g)$ of generators G1 and G3, respectively. Whereas the time evolution of $\sigma(q_g)$ of generators G2 and G4 are shown in Figures 5.9 and 5.10, respectively. These figures show an increase in σ for an increase in α. The actual values of $\sigma(p_g)$ and $\sigma(q_g)$ along with their % increase are shown in Tables 5.4 and 5.5. The results in both tables indicate that the $\sigma(p_g)$ and $\sigma(q_g)$ increase from 85% to 330%, as α is increased from 0.01 to $1s^{-1}$.

It is also interesting to note that 197 simulations were found to be unstable for scenario S2c. For illustration, a selection of the unstable trajectories from scenario S2c are shown in Figures 5.11 to 5.13. These figures indicate that the loss of stability in scenario S2c are

Table 5.4: Standard deviation of power system algebraic variables of the two-area system with stochastic loads for scenarios S1a, S1b and S1c.

Standard deviation	S1a absolute [pu]	S1b % increase[1]	S1c % increase[1]
$v_{\text{Bus 1}}$	0.0008	187.5	712.5
$v_{\text{Bus 2}}$	0.001	190	740
$v_{\text{Bus 3}}$	0.0008	162.5	637.5
$v_{\text{Bus 4}}$	0.001	180	680
$v_{\text{Bus 7}}$	0.0021	119.05	504.76
$v_{\text{Bus 9}}$	0.0023	100	434.78
$p_{g_{\text{G1}}}$	0.0224	19.2	120.09
$p_{g_{\text{G2}}}$	0.0222	13.51	87.39
$p_{g_{\text{G3}}}$	0.0223	11.21	82.96
$p_{g_{\text{G4}}}$	0.0223	12.11	87.89
$q_{g_{\text{G1}}}$	0.0306	73.53	336.27
$q_{g_{\text{G2}}}$	0.0479	48.43	244.05
$q_{g_{\text{G3}}}$	0.0321	55.76	260.44
$q_{g_{\text{G4}}}$	0.0526	34.6	181.37

[1] Note: % increase is calculated based on S1a.

Table 5.5: Standard deviation of power system algebraic variables of the two-area system with stochastic loads for scenarios S2a, S2b, and S2c.

Standard deviation	S2a absolute [pu]	S2b % increase[2]	S2c % increase[2]
$v_{\text{Bus 1}}$	0.0012	183.33	775
$v_{\text{Bus 2}}$	0.0016	175	743.75
$v_{\text{Bus 3}}$	0.0012	166.67	708.33
$v_{\text{Bus 4}}$	0.0016	162.5	700
$v_{\text{Bus 7}}$	0.0032	118.75	543.75
$v_{\text{Bus 9}}$	0.0035	100	471.43
$p_{g_{\text{G1}}}$	0.0333	18.32	133.33
$p_{g_{\text{G2}}}$	0.033	12.42	97.88
$p_{g_{\text{G3}}}$	0.033	10.91	94.24
$p_{g_{\text{G4}}}$	0.033	11.52	95.45
$q_{g_{\text{G1}}}$	0.0463	70.63	364.36
$q_{g_{\text{G2}}}$	0.0725	45.66	265.93
$q_{g_{\text{G3}}}$	0.0487	52.98	286.86
$q_{g_{\text{G4}}}$	0.0796	32.04	202.01

[2]Note: % increase is calculated based on S2a.

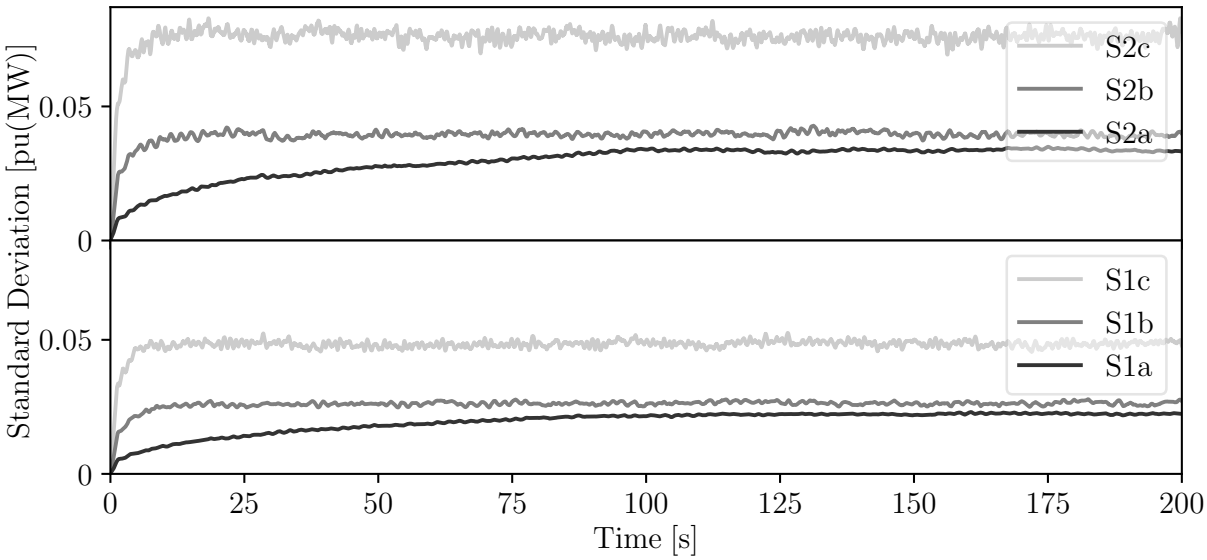

Figure 5.7: Standard deviation of active power injection of synchronous generator G1 of the two-area system with stochastic loads calculated against time for all the cases.

due to shortage of reactive power that leads to voltage collapse. On the other hand, no instability occurs for scenarios S2a and S2b. These results indicate that α of stochastic processes, not σ and PDFs alone, are crucial parameters for the stability analysis of power systems. In fact, high σ might not be dangerous for the system if α is sufficiently low. On the other hand, if α of the stochastic processes are sufficiently high, even if their σ are low, instability can occur.

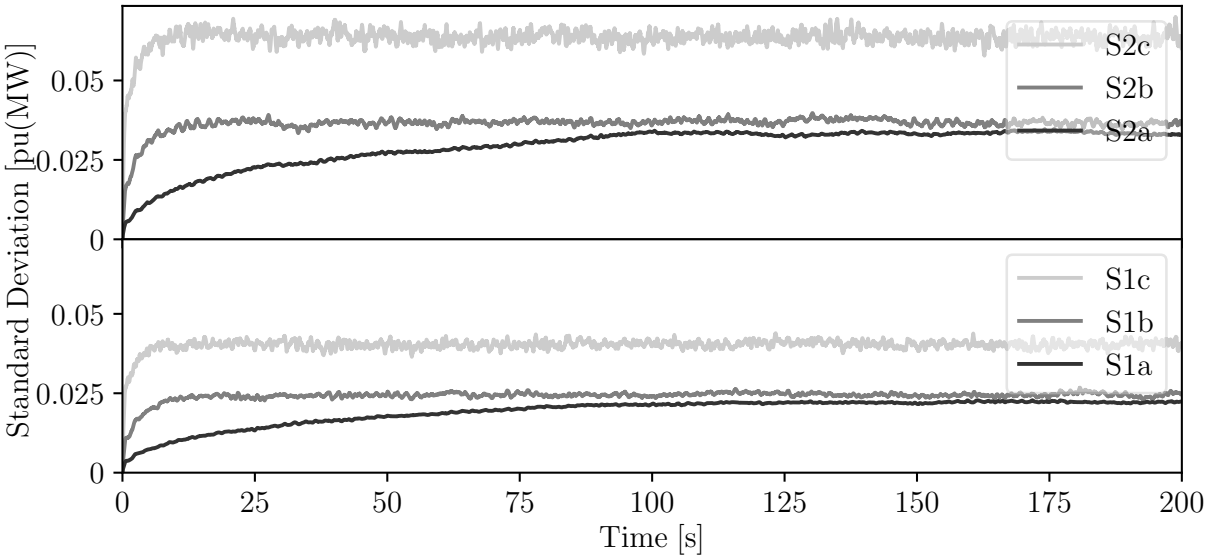

Figure 5.8: Standard deviation of active power injection of synchronous generator G3 of the two-area system with stochastic loads calculated against time for all the cases.

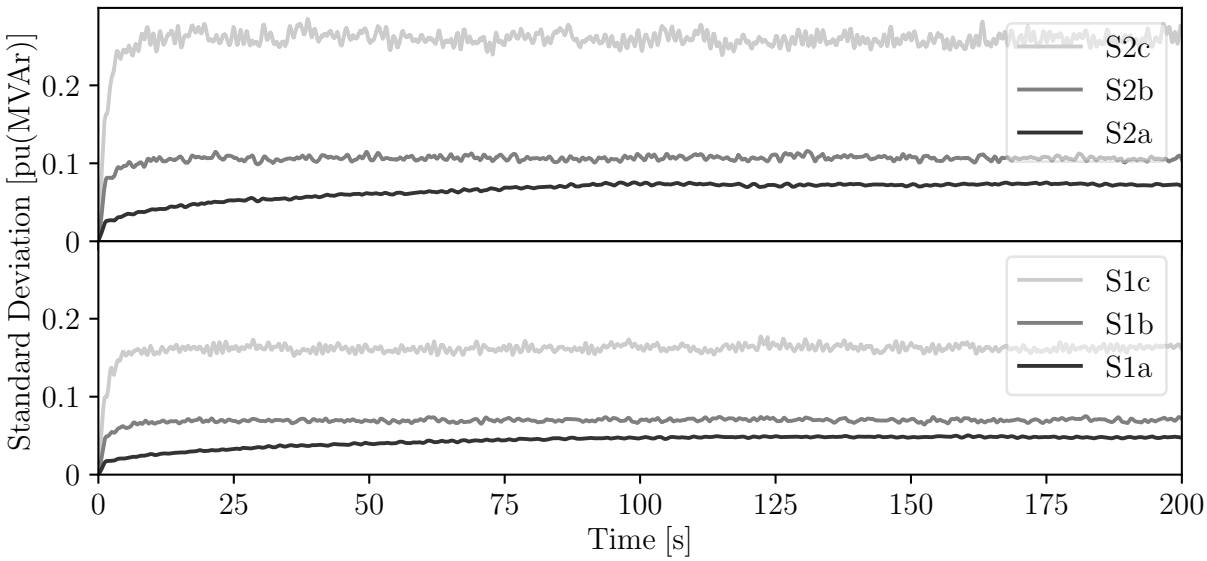

Figure 5.9: Standard deviation of reactive power injection of synchronous generator G2 of the two-area system with stochastic loads calculated against time for all the cases.

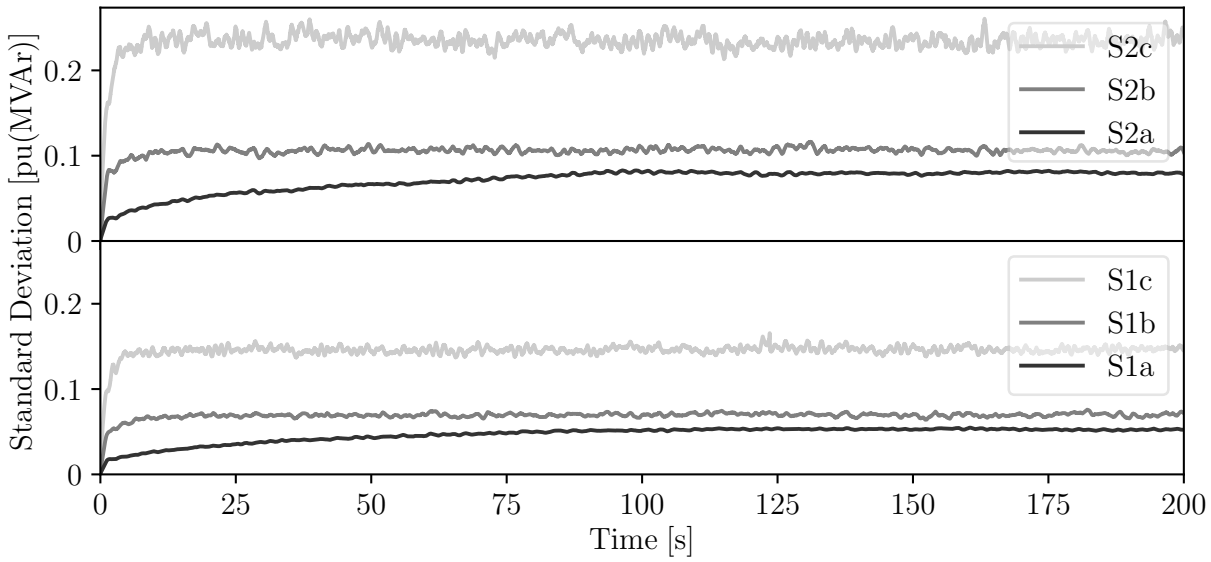

Figure 5.10: Standard deviation of reactive power injection of synchronous generator G4 of the two-area system with stochastic loads calculated against time for all the cases.

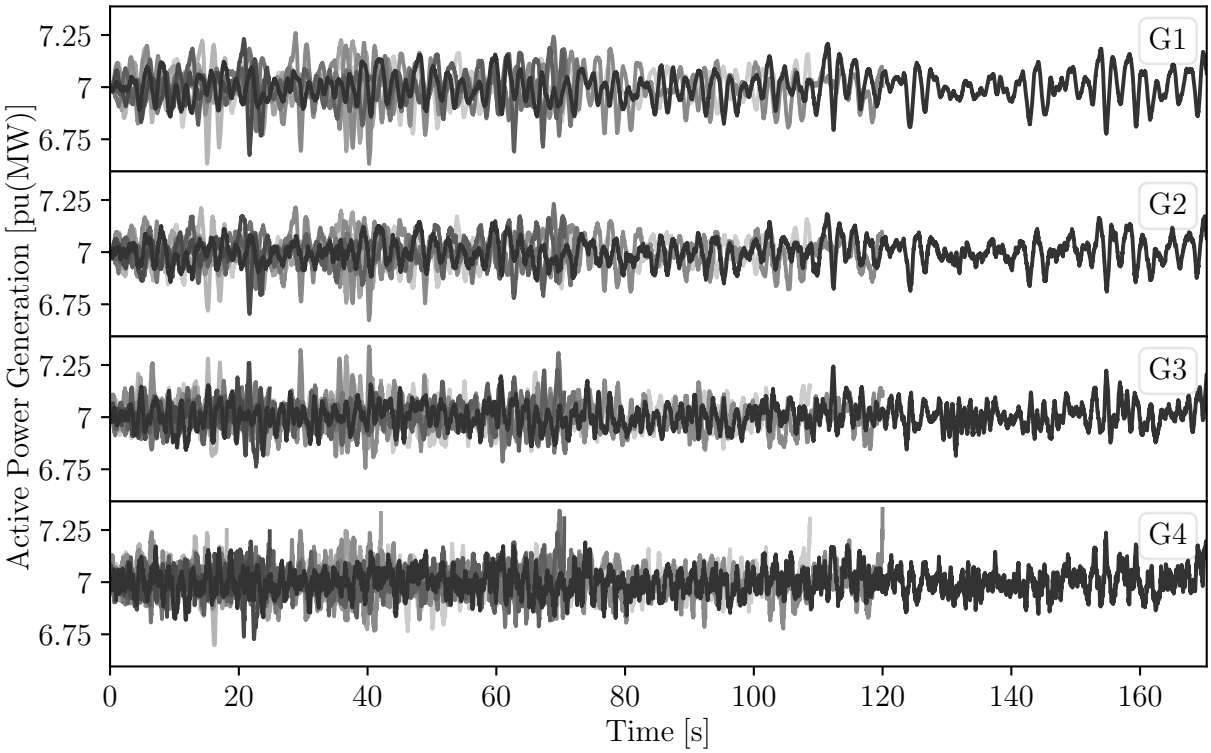

Figure 5.11: Few unstable trajectories of the active power generation of all synchronous machines of the two-area system with stochastic loads from scenario S2c.

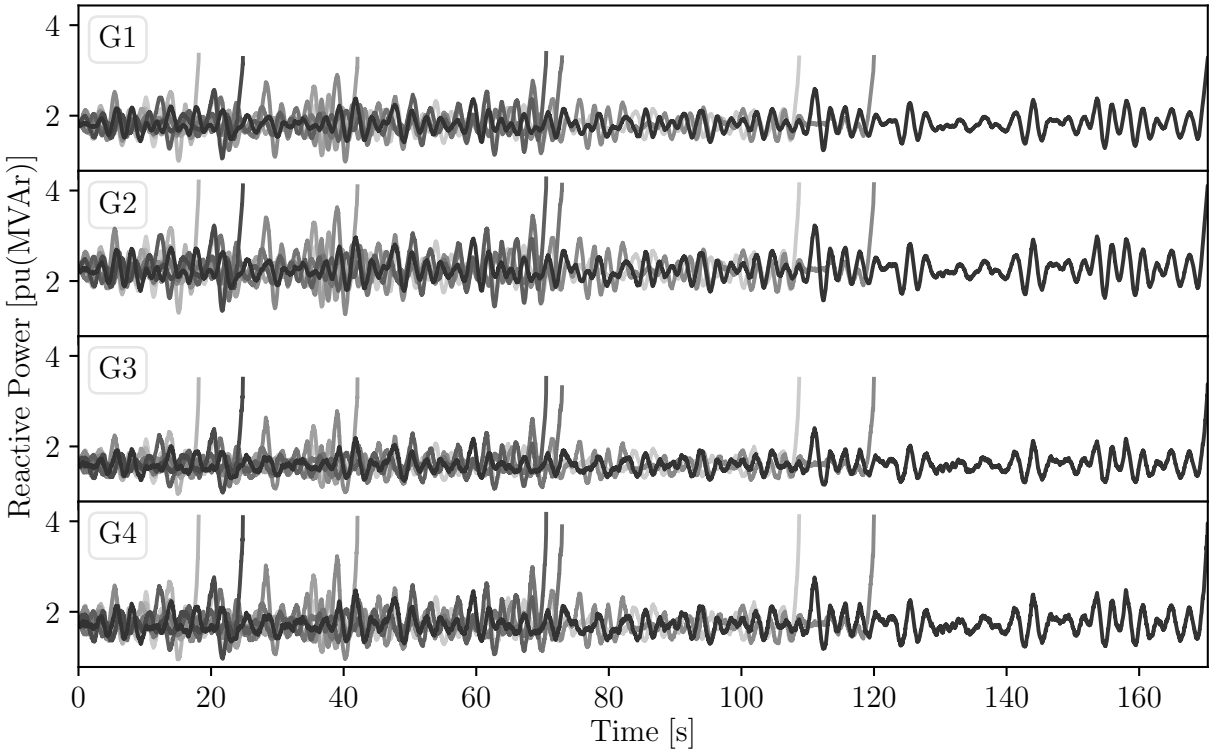

Figure 5.12: Few unstable trajectories of the reactive power generation of all synchronous machines of the two-area system with stochastic loads from scenario S2c.

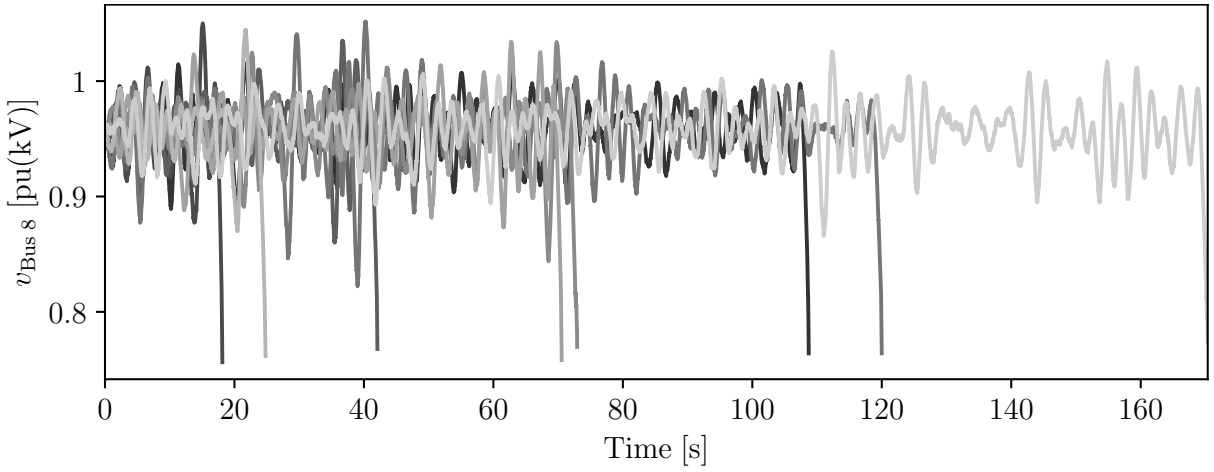

Figure 5.13: Few unstable trajectories of the voltage magnitude at bus 8 of the two-area system with stochastic loads from scenario S2c.

5.2.2.2 All-Island Irish Transmission System

The power system chosen in this section is the AIITS, presented in Section 4.5.2. The impact of stationary probability distributions of stochastic processes on the power system algebraic variables is considered first. For this reason, the values of $\sigma(v)$ at few buses, and values of $\sigma(p_g)$ and $\sigma(q_g)$ of a few synchronous generators obtained for scenarios S1a, S2a,

S1b, and S2b are shown in Table 5.6. The % increase in the values of $\sigma(v)$, $\sigma(p_g)$ and $\sigma(q_g)$ calculated using scenarios S1a and S2a as base are also reported in Table 5.6. From Table 5.6, it is evident that $\sigma(v)$, $\sigma(p_g)$ and $\sigma(q_g)$ show an increase of 50% for an increase of 50% in σ of the stochastic processes, when α is kept constant. This result substantiates the results obtained for the two-area system, see Table 5.3.

Next, the impact of the autocorrelation of stochastic processes on the statistical properties of algebraic variables of the AIITS in stationary conditions is observed. With this regard, the values of $\sigma(v)$, $\sigma(p_g)$ and $\sigma(q_g)$ obtained for the six scenarios, in Table 5.2, are presented in Tables 5.7 and 5.8. From the results in Tables 5.7 and 5.8, it can be seen that σ of power system algebraic variables increases for an increase in α of the

Table 5.6: Standard deviation of power system algebraic variables of the AIITS with stochastic loads for scenarios S1a, S2a, S1b, and S2b.

Standard	S1a	S2a		S1b	S2b	
deviation	$\times 10^{-4}$ [pu]	$\times 10^{-4}$ [pu]	% increase	$\times 10^{-4}$ [pu]	$\times 10^{-4}$ [pu]	% increase
$v_{\text{Bus 1}}$	0.013	0.0194	49.23	0.0134	0.0201	50
$v_{\text{Bus 2}}$	0.01	0.0149	49	0.0106	0.0158	49.06
$v_{\text{Bus 13}}$	0.0115	0.0173	50.43	0.0115	0.0173	50.43
$v_{\text{Bus 170}}$	0.0101	0.0151	49.5	0.0108	0.0163	50.93
$v_{\text{Bus 1000}}$	0.0119	0.0178	49.58	0.0119	0.0178	49.58
$v_{\text{Bus 1479}}$	0.024	0.036	50	0.0239	0.0359	50.21
$p_{g_{\text{G1}}}$	5.7601	8.6401	50	5.8416	8.7624	50
$p_{g_{\text{G2}}}$	2.4508	3.6762	50	2.4824	3.7237	50
$p_{g_{\text{G3}}}$	8.5706	12.8559	50	8.7562	13.1343	50
$p_{g_{\text{G4}}}$	4.6096	6.9144	50	4.6019	6.9029	50
$p_{g_{\text{G5}}}$	8.0003	12.0004	50	7.9359	11.9039	50
$p_{g_{\text{G6}}}$	1.9401	2.9101	50	1.975	2.9625	50
$p_{g_{\text{G7}}}$	2.9027	4.354	50	2.8731	4.3097	50
$q_{g_{\text{G1}}}$	0.2049	0.3073	49.98	0.2018	0.3027	50
$q_{g_{\text{G2}}}$	0.4183	0.6275	50.01	0.4343	0.6515	50.01
$q_{g_{\text{G3}}}$	0.2354	0.3531	50	0.2876	0.4313	49.97
$q_{g_{\text{G4}}}$	0.2455	0.3683	50.02	0.2998	0.4497	50
$q_{g_{\text{G5}}}$	1.2566	1.885	50.01	1.2145	1.8217	50
$q_{g_{\text{G6}}}$	1.5121	2.2682	50	1.4179	2.1268	50
$q_{g_{\text{G7}}}$	5.7973	8.6959	50	5.6656	8.4985	50

stochastic processes regardless the fact that the stationary probability distribution of the stochastic process remains unaltered.

Note that the results presented in Tables 5.7 and 5.8 show that $\sigma(v)$, $\sigma(p_g)$ and $\sigma(q_g)$ in the AIITS increase by a small percentage as compared to the two-areas system in Section 5.2.2.1. This slight increase in $\sigma(v)$, $\sigma(p_g)$ and $\sigma(q_g)$ in the AIITS is because loads are well distributed throughout the system, and the eigenvalues are very well damped. Whereas this is not the case in the two-area system where the loads are concentrated in large amount only on the two buses, and the eigenvalues of the system are poorly damped. The eigenvalues of the critical modes are shown in Section 5.3 later in this chapter.

Table 5.7: Standard deviation of power system algebraic variables of the AIITS with stochastic loads for scenarios S1a, S1b and S1c.

Standard deviation	S1a absolute $\times 10^{-4}$ [pu]	S1b % increase[3]	S1c % increase[3]
$v_{\text{Bus 400}}$	0.0403	71.22	203.72
$v_{\text{Bus 450}}$	0.0551	57.17	171.87
$v_{\text{Bus 500}}$	0.187	29.52	169.63
$v_{\text{Bus 550}}$	0.187	29.52	169.63
$v_{\text{Bus 600}}$	0.0408	51.96	142.89
$v_{\text{Bus 650}}$	0.1542	22.96	139.75
$p_{g_{\text{G4}}}$	3.6837	1.62	37.71
$p_{g_{\text{G5}}}$	1.5446	3.16	37.14
$p_{g_{\text{G6}}}$	1.9401	1.8	36.47
$p_{g_{\text{G7}}}$	8.5706	2.17	35.54
$p_{g_{\text{G8}}}$	2.4508	1.29	34.92
$p_{g_{\text{G9}}}$	5.7601	1.41	18.33
$q_{g_{\text{G4}}}$	0.2354	22.18	21.11
$q_{g_{\text{G5}}}$	0.244	22.99	20.25
$q_{g_{\text{G6}}}$	0.2455	22.12	19.47
$q_{g_{\text{G7}}}$	0.1625	12.86	16.55
$q_{g_{\text{G8}}}$	0.5555	16.11	16.11
$q_{g_{\text{G9}}}$	0.8684	4.17	15.63

[3] Note: % increase is calculated based on S1a.

Table 5.8: Standard deviation of power system algebraic variables of the AIITS with stochastic loads for scenarios S2a, S2b, and S2c.

Standard deviation	S2a absolute $\times 10^{-4}$ [pu]	S2b % increase[4]	S2c % increase[4]
$v_{\text{Bus 400}}$	0.0827	57.19	171.7
$v_{\text{Bus 450}}$	0.2805	29.48	169.63
$v_{\text{Bus 500}}$	0.0612	52.12	142.97
$v_{\text{Bus 550}}$	0.2312	22.97	139.84
$v_{\text{Bus 600}}$	0.1832	18.45	117.74
$v_{\text{Bus 650}}$	0.1323	15.04	103.33
$p_{g_{\text{G4}}}$	4.0811	11.46	114.52
$p_{g_{\text{G5}}}$	5.5255	1.63	37.72
$p_{g_{\text{G6}}}$	2.3168	3.16	37.15
$p_{g_{\text{G7}}}$	2.9101	1.8	36.48
$p_{g_{\text{G8}}}$	12.8559	2.17	35.54
$p_{g_{\text{G9}}}$	13.6762	1.29	34.92
$q_{g_{\text{G4}}}$	2.2397	16	49.85
$q_{g_{\text{G5}}}$	2.7262	30.82	37.45
$q_{g_{\text{G6}}}$	0.3531	22.15	21.13
$q_{g_{\text{G7}}}$	0.3659	23.04	20.28
$q_{g_{\text{G8}}}$	0.3683	22.1	19.47
$q_{g_{\text{G9}}}$	0.2437	12.88	16.58

[4] Note: % increase is calculated based on S2a.

5.2.2.3 Discussion

From the results presented above in this section, it is evident that the standard deviation σ, while keeping autocorrelation coefficient α constant, of the power system output variables increases in the same proportion as the σ of the stochastic processes. The standard deviation of output variables is also directly impacted by α of the stochastic processes. This occurs despite the fact that the processes have the same probability distribution in stationary conditions, as shown in Figure 5.4. Note that all the scenarios reach the same mean value.

It is important to note that the variables v, p_g and q_g belong to the vector of algebraic variable $\boldsymbol{y}$ of (3.3), i.e., their stochastic behavior is the result of the inclusion in $\boldsymbol{f}$ and $\boldsymbol{g}$ of the stochastic variable $\boldsymbol{\eta}$. It is observed that high values of the autocorrelation can

drive the system to instability even if the standard deviation of the stochastic processes is small, and acceptable in stationary conditions. This non-intuitive result is due to the dynamic coupling of the autocorrelation of stochastic processes with the nonlinearity of the SDAEs that define the power system model.

5.3 Frequency Domain Analysis

This section investigates whether stochastic processes can trigger the electro-mechanical modes of the power system and hence, modify its dynamic response. With this aim, at first, the electro-mechanical modes are identified by calculating the dominant eigenvalues and their participation factors. Then, the frequency spectrums of relevant variables of the system are analysed to quantify the impact of the autocorrelation of stochastic processes on the overall system dynamic response.

This approach is conceptually similar to the signal probing technique, e.g., [62, 85, 86], which utilises a Fourier analysis of measurement data to determine the frequency, damping, and participation factors associated with the inter-area oscillatory modes of the power system. The results discussed in this section were presented in [5].

5.3.1 Dynamic Response of Stochastic Processes

It is relevant to analyse the effect of α on the dynamic response of stochastic process, which is modelled as a OU process using (5.1). Top panel of Figure 5.1 shows three realizations of (5.1), obtained for $\mu = 0$, $\sigma = 0.1$ and different values of α.

The three processes shown in top panel of Figure 5.1 have the same PDFs in stationary condition. However, their dynamic behavior is significantly different because of the different value of α and, hence, of their autocrrelation. This can be observed in top panel of Figure 5.1: the higher the value of α, the faster the variations in the stochastic process in the unit of time.

An effective way to differentiate stochastic processes having same PDFs but different α is offered by the frequency spectrum of the time series obtained by Fourier Transform. Figure 5.14 illustrates the frequency spectrum of the time series observed in the top panel of Figure 5.1. Figure 5.14 shows that the higher the value of α, the bigger the amplitudes

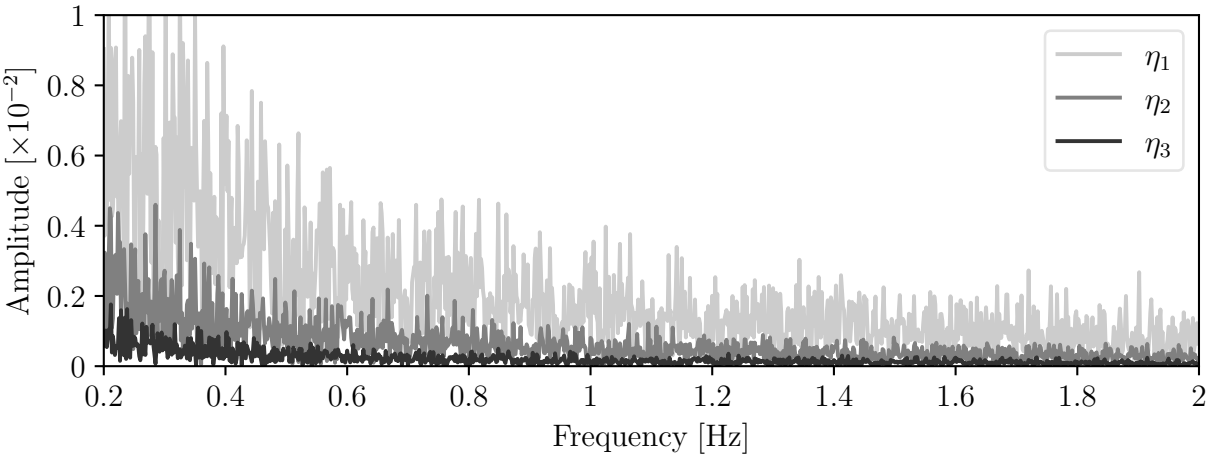

Figure 5.14: Frequency spectrum of realizations of OU processes with $\mu = 0$; $\sigma = 0.1$; and $\alpha_1 = 0.01\ \mathrm{s}^{-1}$, $\alpha_2 = 0.1\ \mathrm{s}^{-1}$, and $\alpha_3 = 1\ \mathrm{s}^{-1}$.

of the frequencies of which a OU process is composed. Thus, the amplitudes of the frequencies, of which a OU process is composed, is directly proportional to the α.

5.3.2 Dynamic Response of Power Systems

This section studies two power systems, namely, the well-known Kundur's two-area system and a dynamic model of the AIITS. Both systems are modelled as a set of nonlinear SDAEs. In all simulations, the realizations of the Wiener processes are integrated with a sufficiently small step size of $h = 0.01$ s, whereas the integration of the deterministic part utilises a step length $\Delta t = 0.01$ s. Each trajectory simulated for a total simulation time of 200 s. In this time period, the stochastic processes reach stationarity.

Three scenarios where stochastic processes are characterized by low-, medium- and high-speed exponentially decaying autocorrelations, respectively, are defined as follows:

- S1: $\alpha = 0.01\ \mathrm{s}^{-1}$.
- S2: $\alpha = 0.1\ \mathrm{s}^{-1}$.
- S3: $\alpha = 1\ \mathrm{s}^{-1}$.

The values above are in the range of real-world stochastic processes that are found in power systems.

5.3.2.1 Two-Area System

The two-area system introduced in Section 4.3.2, and shown in Figure 4.9, is simulated using the SDAE model described in (3.3). Stochastic processes are introduced through stochastic load model in (3.5). Stochastic processes $\boldsymbol{\eta}$ in (3.5) are modelled as independent OU processes using (5.1). Note that (3.5) models net load. The impact of the stochastic processes on the dynamic response of the system is studied considering each area independently.

Stochastic Loads only in area 1

The dominant electro-mechanical modes of the system along with the participation factors of the machines after introducing stochastic processes in area 1 are shown in Table 5.9. These modes are calculated as a result of including stochastic processes in load power consumption in area 1 through OU processes. The standard deviation of OU processes is set to $\sigma = 1\%$ of the mean load value for all scenarios. For each scenario, the OU processes have the same frequency spectrum as shown in Figure 5.14.

The impact of the autocorrelations of stochastic processes on the bus voltage magnitude v at load buses is analysed first. With this regard, the time domain profile of v at load buses 7 and 9 is shown in Figure 5.15. From Figure 5.15, it is evident that v at bus 7 experiences higher variations in time as compared to v at bus 9. While the amplitude of the variations in v at both buses is dependent on the value of α. This is further confirmed by analysing the frequency spectrum of the time domain profile of v. Figure 5.16 illustrates the frequency spectrum of v at buses 7 and 9. This figure shows that the amplitude of the oscillation of the dominant electro-mechanical mode is dependent on α of the stochastic process. Note that v on both buses observes oscillations only in the inter-area oscillatory mode i.e, mode 1 in Table 5.9. Since stochastic processes are modelled only in area 1, v at bus 7, which is in area 1, experiences higher amplitude oscillations as compared to v at bus 9, which is in area 2.

Next, the reactive power generation q_g of the synchronous generators in the two-area system is analysed in both time- and frequency-domain. Figure 5.17 illustrates the time profile of q_g of all the synchronous generators. By observing Figure 5.17, it is clear that the synchronous generators in area 1, i.e., G1 and G2, provide more reactive power support than those in area 2, i.e., G3 and G4. For the proof of concept, the frequency spectrum

of q_g of all the generators is shown in Figure 5.18. From Figure 5.18, it is evident that generators in area 1 experience higher amplitude oscillations for higher α as compared to

Table 5.9: Electro-mechanical modes and corresponding participation factors of the two-area system with stochastic load in area 1.

Mode	Eigenvalue	Freq. [Hz]	Participation Factors			
			G1	G2	G3	G4
1	-0.063±j3.866	0.615	19.05	11.01	34.86	21.85
2	-0.300±j7.112	1.132	42.07	52.93	1.63	1.25
3	-0.300±j7.392	1.176	1.02	1.47	37.7	57.52

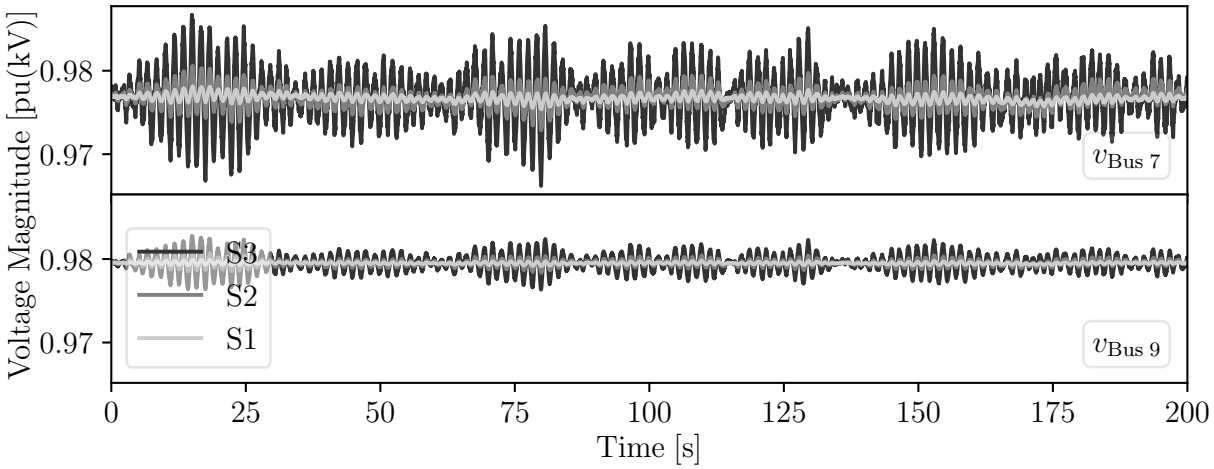

Figure 5.15: Time profile of voltage magnitude at load buses 7 and 9 of the two-area system with stochastic load in area 1.

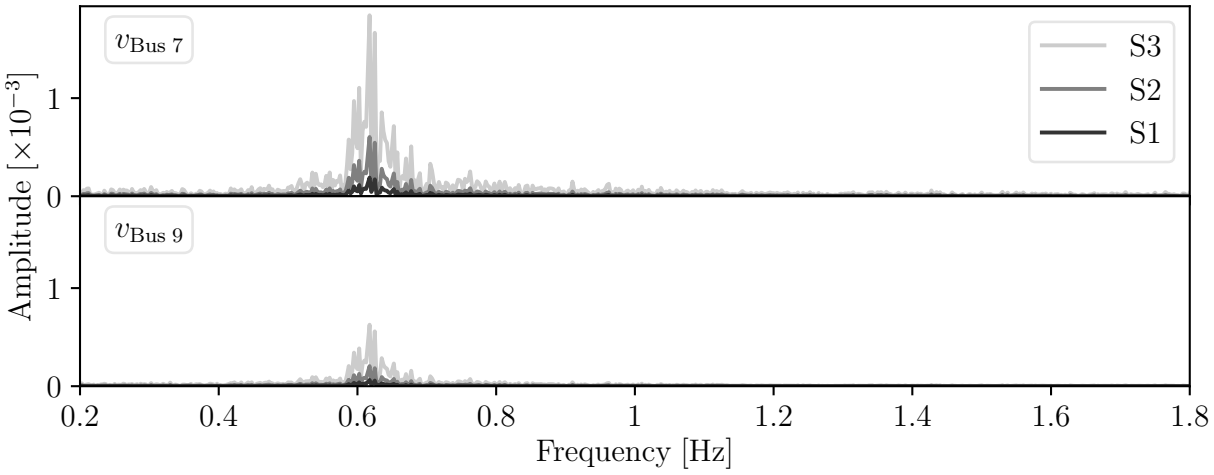

Figure 5.16: Frequency spectrum of voltage magnitude at load buses 7 and 9 of the two-area system with stochastic load in area 1.

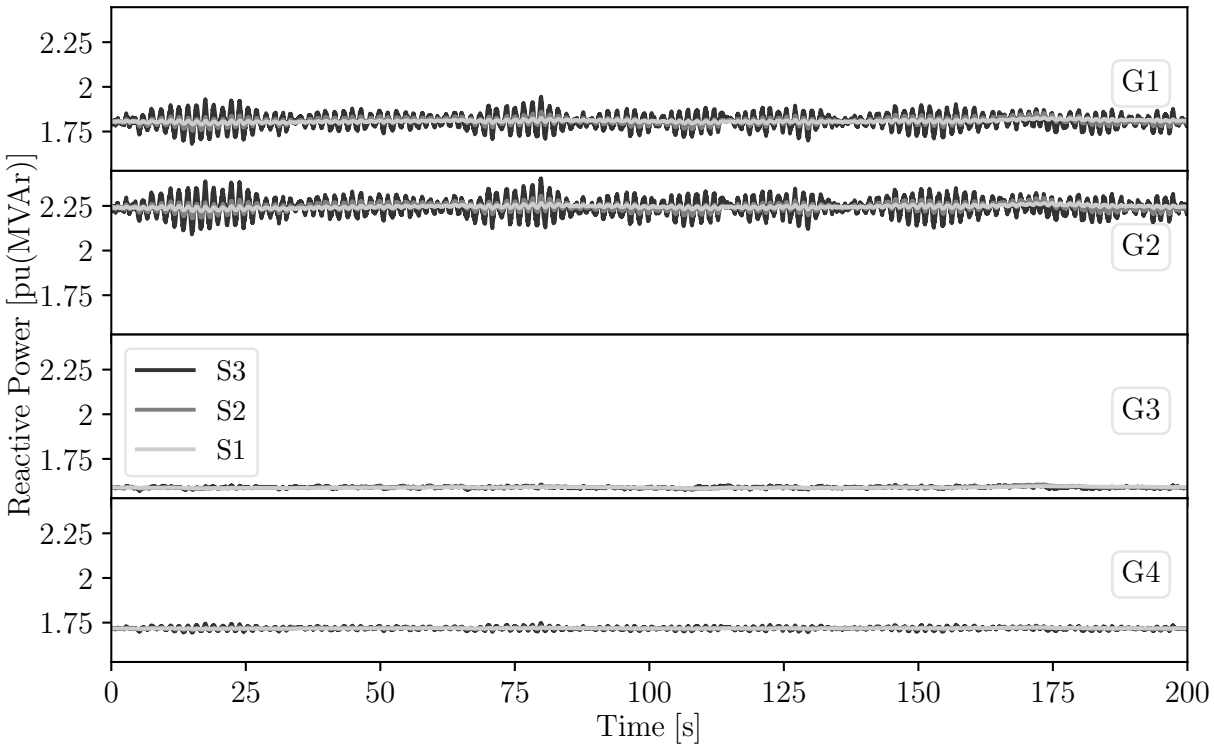

Figure 5.17: Time profile of reactive power injections of all the synchronous generators of the two-area system with stochastic load in area 1.

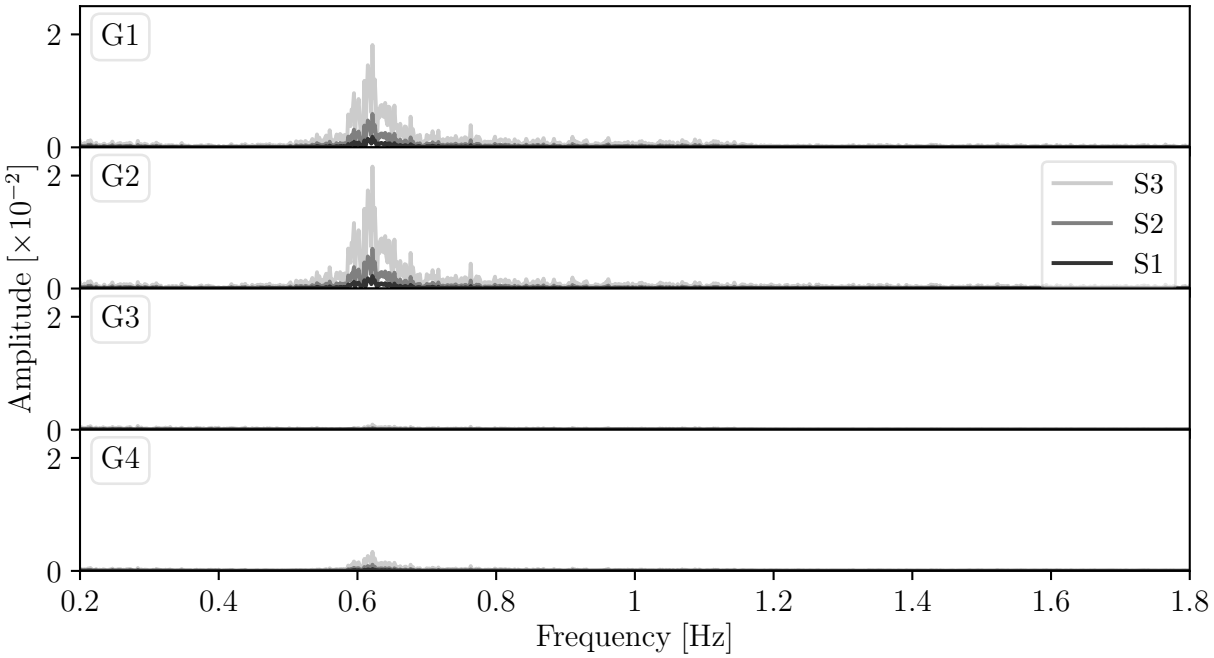

Figure 5.18: Frequency spectrum of reactive power injections of all the synchronous generators of the two-area system with stochastic load in area 1.

generators in area 2. Note that q_g experiences oscillations only in the inter-area oscillatory mode, which is the same as with v.

Next, the impact of the autocorrelation of the stochastic processes on the active power injections p_g of the synchronous generators is observed. The time profile of p_g of all the synchronous generators is shown in Figure 5.19. The oscillations of these generators are higher the higher the value of α of the stochastic processes included in the load consumption. Figure 5.20 illustrates the frequency spectrum of p_g of the synchronous generators. By comparing the frequencies of the dominant electro-mechanical modes shown in Table 5.9 with the frequency spectrum shown in Figure 5.20, it is clear that an increase in α causes an increase in the amplitude of the oscillations in the dominant electro-mechanical modes. Note also that the frequency spectrum of p_g shows well the coupling of the oscillatory modes of the two-area system with the values of α.

The amplitudes of the oscillations observed in p_g also depend on the participation factors of the machines. This is particularly evident for the inter-area oscillatory mode, which shows significant participation from all the generators. The amplitude of the inter-area oscillatory mode observed in all the generators is proportional to their participation factors. This behavior can be verified by observing the participation factors of generators in modes 2 and 3. Since mode 2 has significant participation from G1 and G2, and provided that the disturbance originates in area 1, negligible oscillations are observed in mode 2 in the generators G3 and G4, located in area 2. Whereas mode 3 has significant participation from G3 and G4. Hence, negligible oscillations are observed in mode 3 from all the generators. This is due, again, to the fact that the disturbance is located in area 1.

Finally, the impact of the autocorrelation coefficient on the stability of power system is analysed with MC. With this aim, 1,000 Time Domain Simulations (TDSs) are carried out. The results of these simulations are presented in Table 5.10, which indicates that none of the trajectories were found to be unstable for the three scenarios.

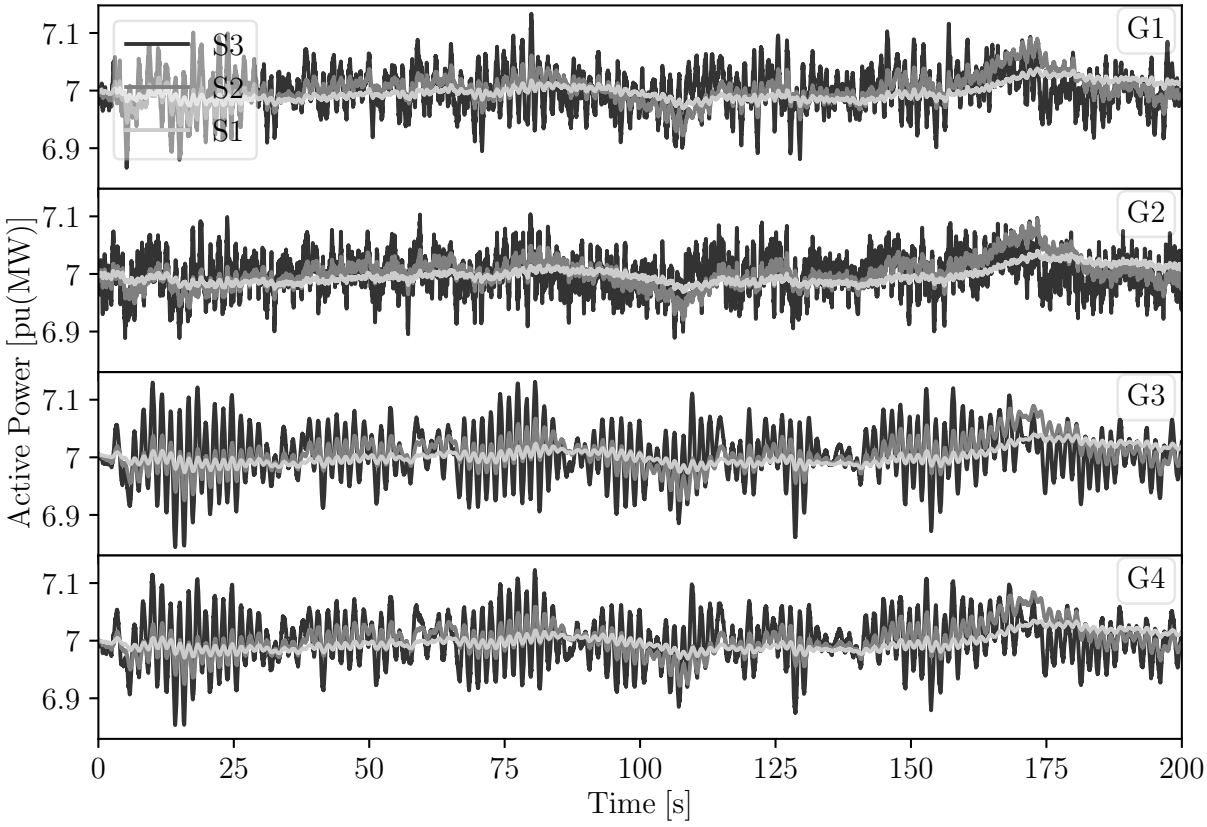

Figure 5.19: Time profile of active power injections of all the synchronous generators of the two-area system with stochastic load in area 1.

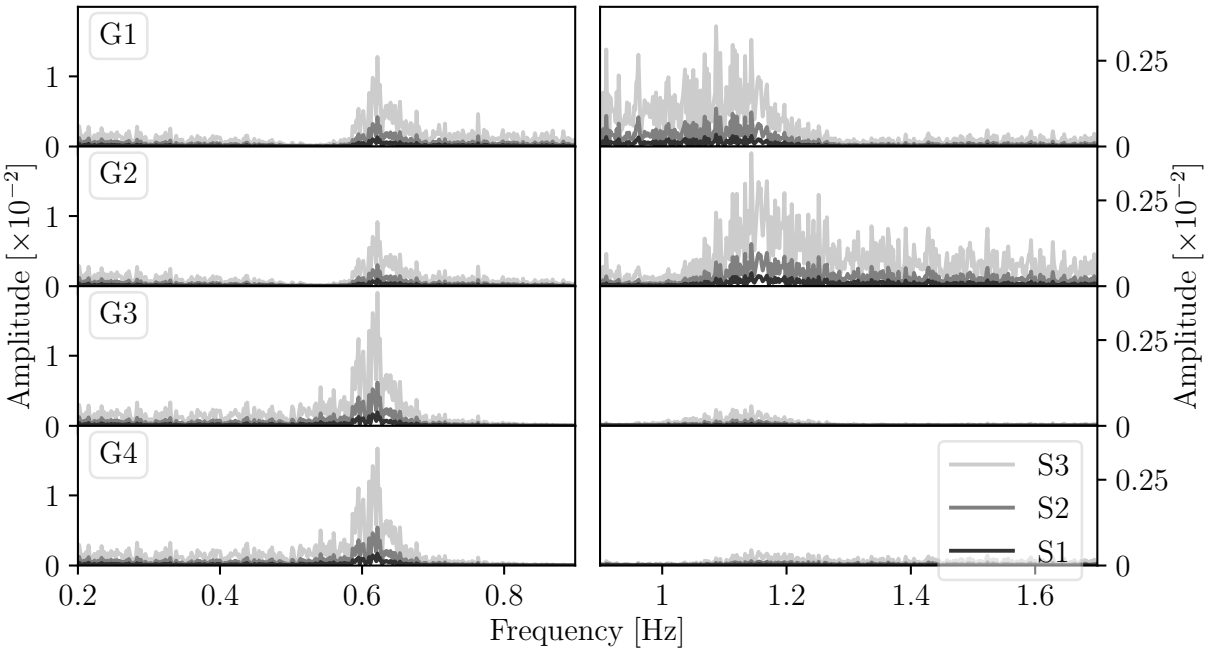

Figure 5.20: Frequency spectrum of active power injections of all the synchronous generators of the two-area system with stochastic load in area 1.

Table 5.10: Unstable trajectories for the two-area system with stochastic loads.

Scenario	Stochastic Processes in area 1 Unstable trajectories	Stochastic Processes in area 2 Unstable trajectories
S1	0	0
S2	0	0
S3	0	521 (52.1%)

Stochastic Loads only in area 2

The dominant electro-mechanical modes of the system along with the participation factors of the machines after introducing stochastic processes in area 2 are shown in Table 5.11. The parameters of the stochastic loads are the same as those utilised in the example above except for the standard deviation that is set to $\sigma = 0.5\%$ of the mean load consumption.

The time domain profile and frequency spectrum of v at load buses 7 and 9 are illustrated in Figures 5.21 and 5.22, respectively. These figures show that higher amplitude oscillations are observed for higher values of α. These figures also show that the oscillations are observed only in the inter-area oscillatory mode with similar amplitude in v at buses 7 and 9 in Areas 1 and 2, respectively. Note that this result is different from that obtained by considering that stochastic processes are modelled only in area 1, as can be seen in Figures 5.15 and 5.16. The rationale for this difference is as follows.

Figures 5.23 and 5.24 illustrate the time- and frequency-domain profile of q_g of all the synchronous generators, respectively. Note that the generators in both areas observe oscillations with similar amplitudes. This behaviour of q_g coincides with the behaviour observed in v, seen in Figures 5.21 and 5.22. This happens despite the fact that disturbance is only in area 2. The reason behind this is that the generators in area 1 are providing more reactive power support than the generators in area 2. This causes reactive power being exported from area 1 to area 2, which makes the generators in area 1 experience oscillations with amplitudes similar to those in area 2.

Next, the time domain profile of p_g of all the synchronous generators is illustrated in Figure 5.25. While Figure 5.26 shows the frequency spectrum of all the synchronous generators in the two-area system. The results show that generators G3 and G4 in area 2 show higher amplitude oscillations as compared to generators G1 and G2 in area 1. The rationale of this result is given by the participation of the generators to the inter-area mode (see Table 5.11). These results are consistent with those discussed in the example

above, i.e., the higher the α the higher the oscillations observed in the generators of area 2. Note that even though modes 2 and 3 have similar frequency, only the p_g of machines

Table 5.11: Electro-mechanical modes and corresponding participation factors of the two-area system with stochastic load in area 2.

Mode	Eigenvalue	Freq. [Hz]	Participation Factors			
			G1	G2	G3	G4
1	-0.139±j2.690	0.428	5.20	7.62	27.07	34.64
2	-0.292±j7.154	1.139	38.67	52.67	2.82	2.62
3	-0.331±j7.214	1.148	2.03	4.16	42.97	46.4

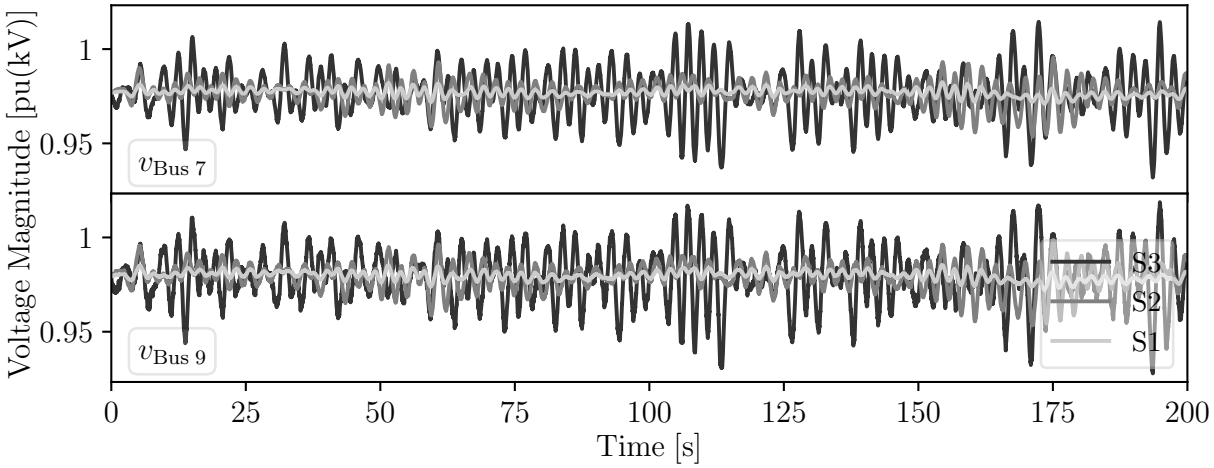

Figure 5.21: Time profile of voltage magnitude at load buses 7 and 9 of the two-area system with stochastic load in area 2.

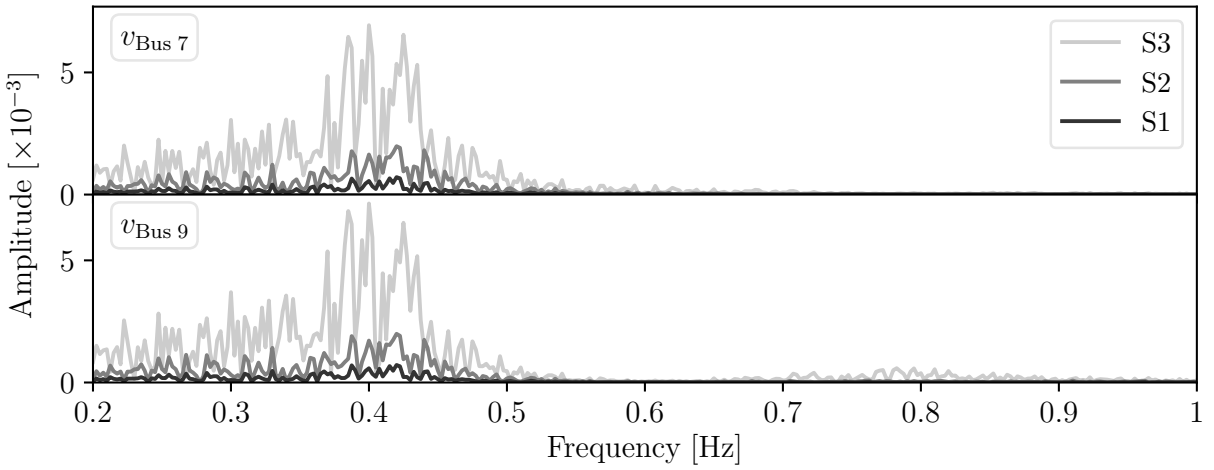

Figure 5.22: Frequency spectrum of voltage magnitude at load buses 7 and 9 of the two-area system with stochastic load in area 2.

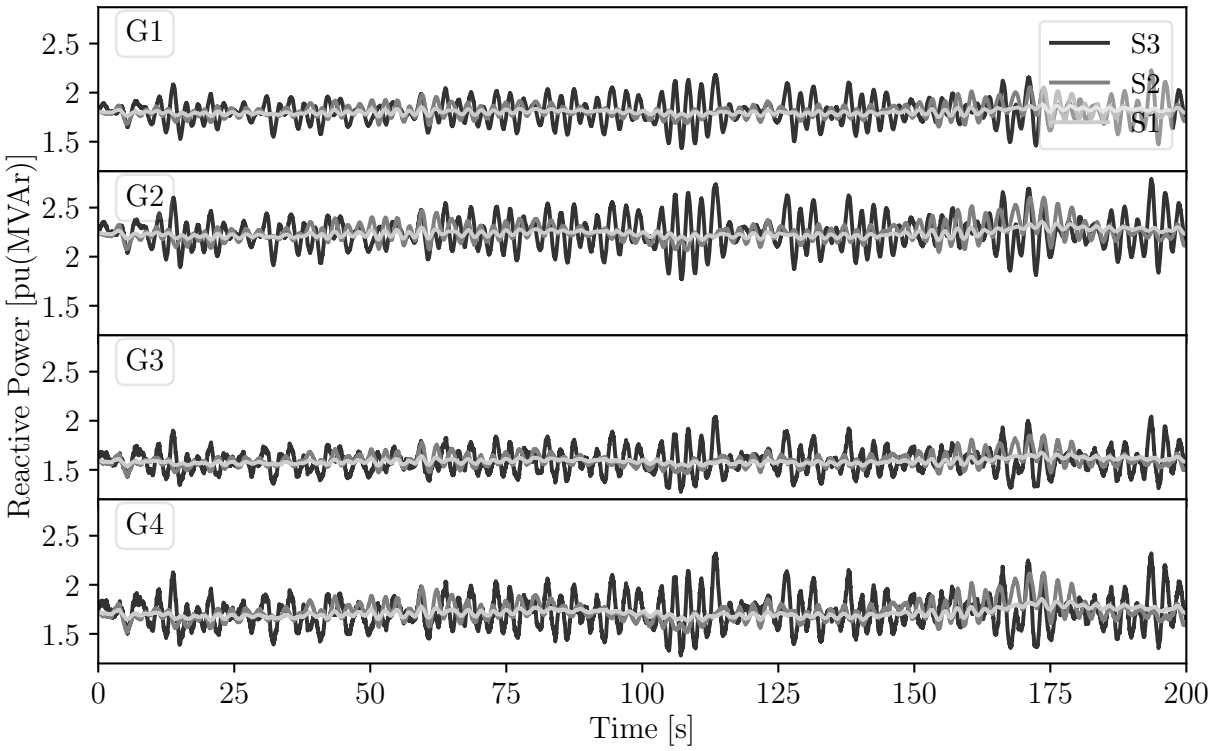

Figure 5.23: Time profile of reactive power injections of all the synchronous generators of the two-area system with stochastic load in area 2.

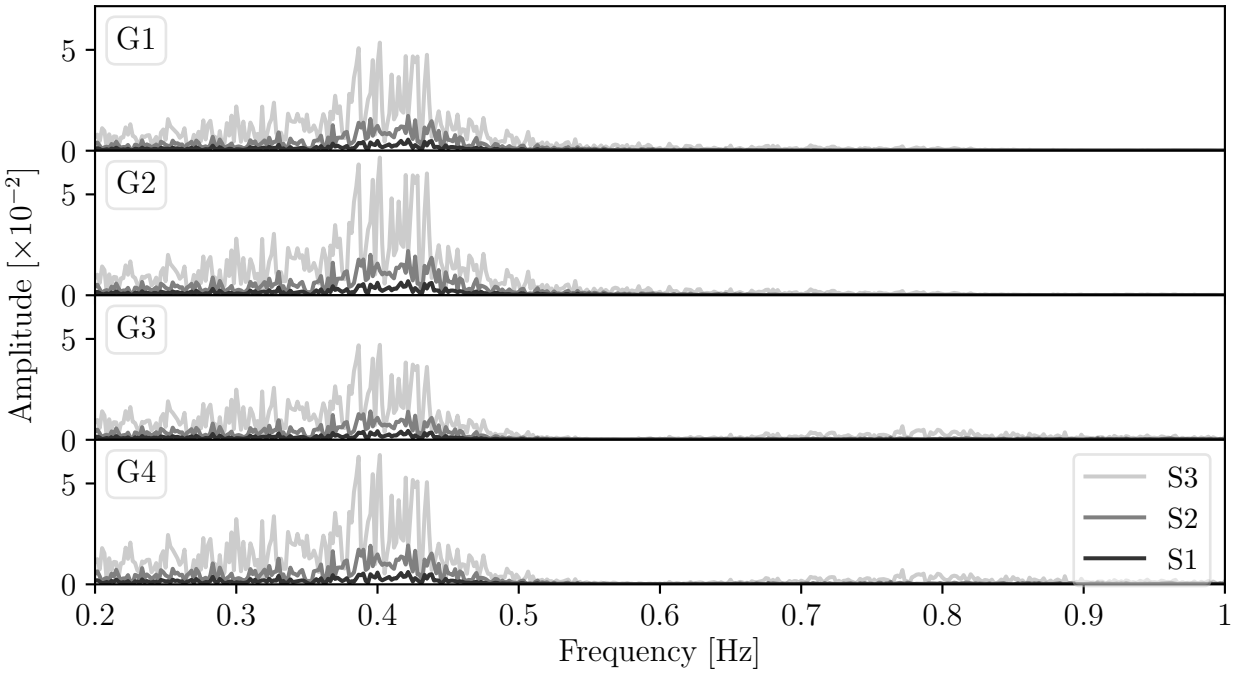

Figure 5.24: Frequency spectrum of reactive power injections of all the synchronous generators of the two-area system with stochastic load in area 2.

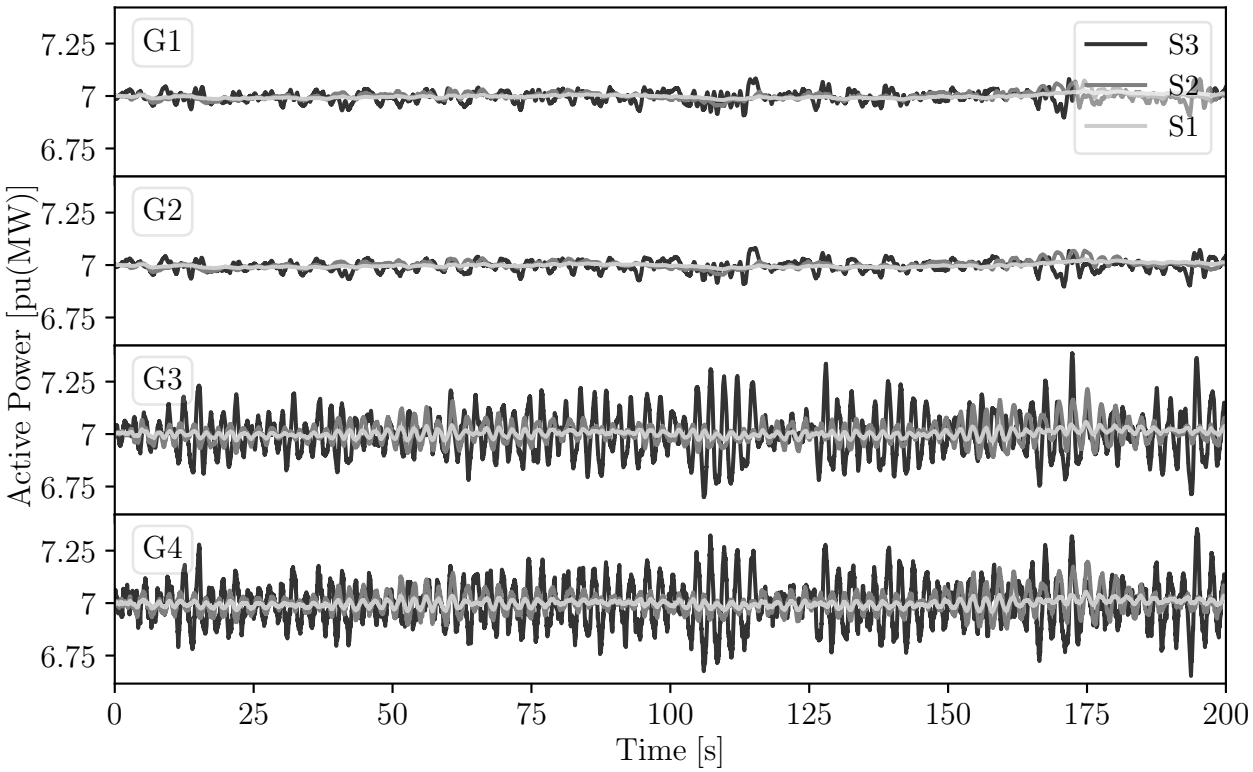

Figure 5.25: Time profile of active power injections of all the synchronous generators of the two-area system with stochastic load in area 2.

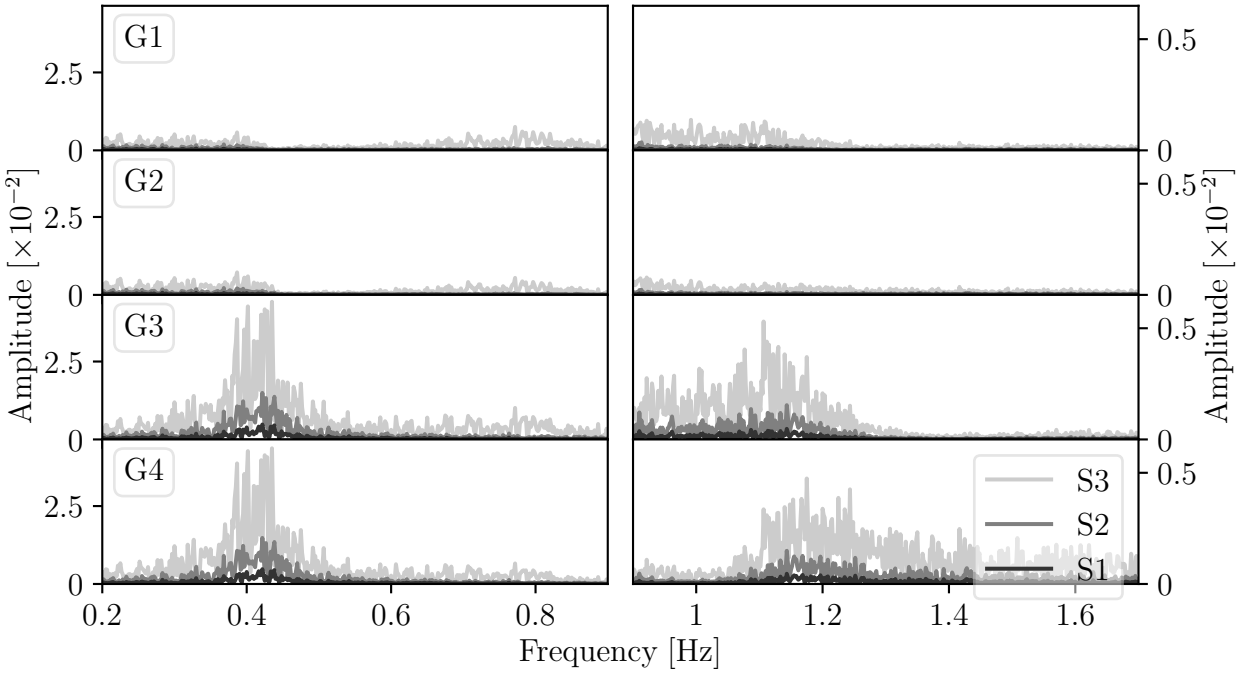

Figure 5.26: Frequency spectrum of active power injections of all the synchronous generators of the two-area system with stochastic load in area 2.

G3 and G4 show a relevant increase in the amplitude of the frequency of mode 3 because the sources of stochastic disturbances are in area 2.

Finally, the effect on the stability of the two-area system of the autocorrelation of the stochastic processes included in area 2 is analysed using MC, which comprises of 1,000 simulations. The trajectories of v, p_g and q_g are observed and the results for unstable trajectories are presented in Table 5.10. Table 5.10 shows that 52.1% of trajectories are unstable for scenario S3. For illustration purposes, a few unstable trajectories of the selected power system variables are shown in Figures 5.27 to 5.29. From the results the two-area system appears to have run out of reactive power support. It is important to note that, for all scenarios, the standard distribution of the processes is kept the same while the autocorrelation coefficient of the processes is varied. This implies that sufficiently high values of the autocorrelation coefficient of the stochastic processes, which may originate only in one area of the system, may drive a system to instability, which may lead to a voltage collapse.

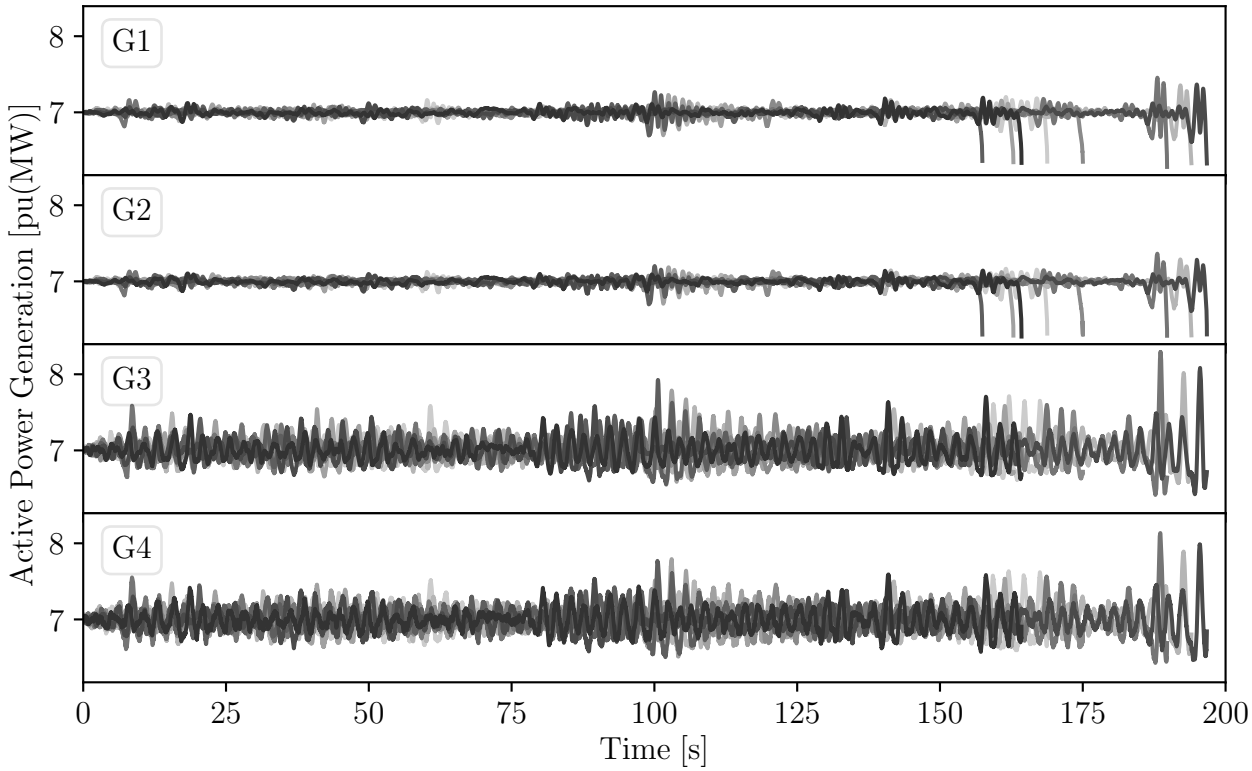

Figure 5.27: Few unstable trajectories of the active power injections of the synchronous generators of the two-area system with stochastic load in area 2 for scenario S3.

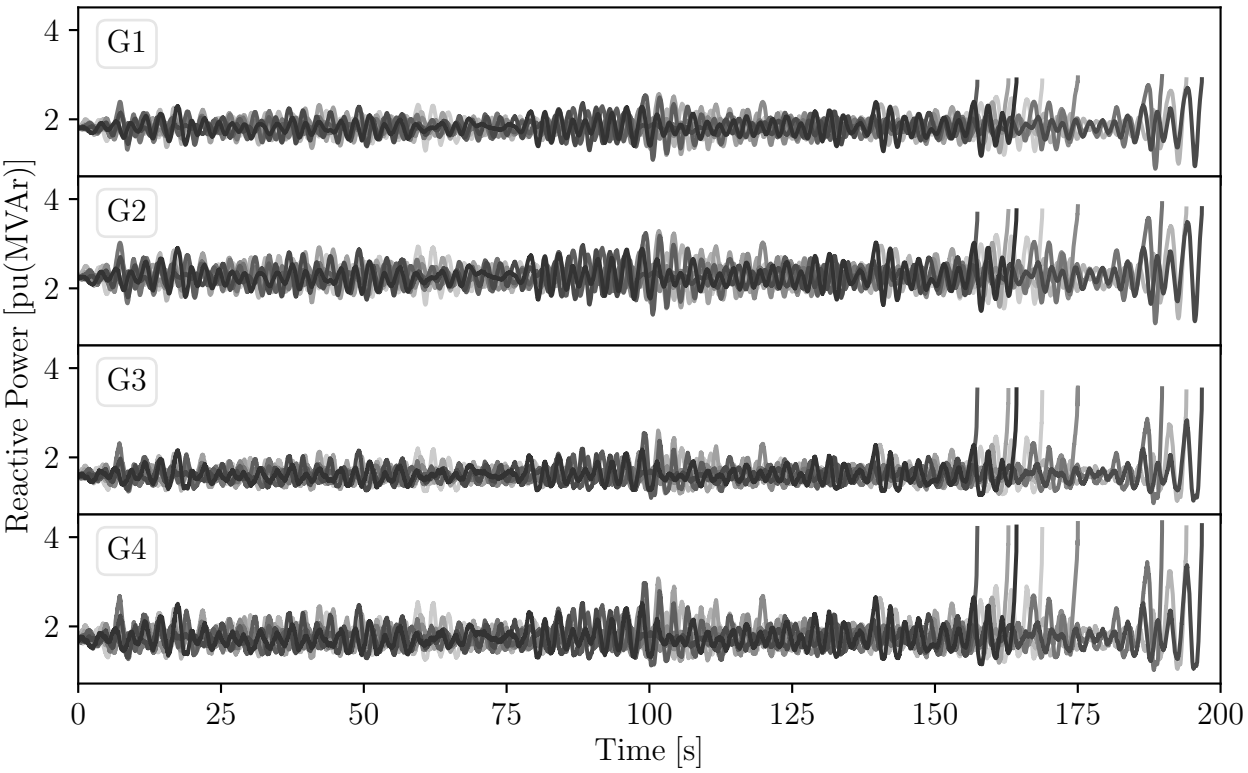

Figure 5.28: Few unstable trajectories of the reactive power injections of the synchronous generators of the two-area system with stochastic load in area 2 for scenario S3.

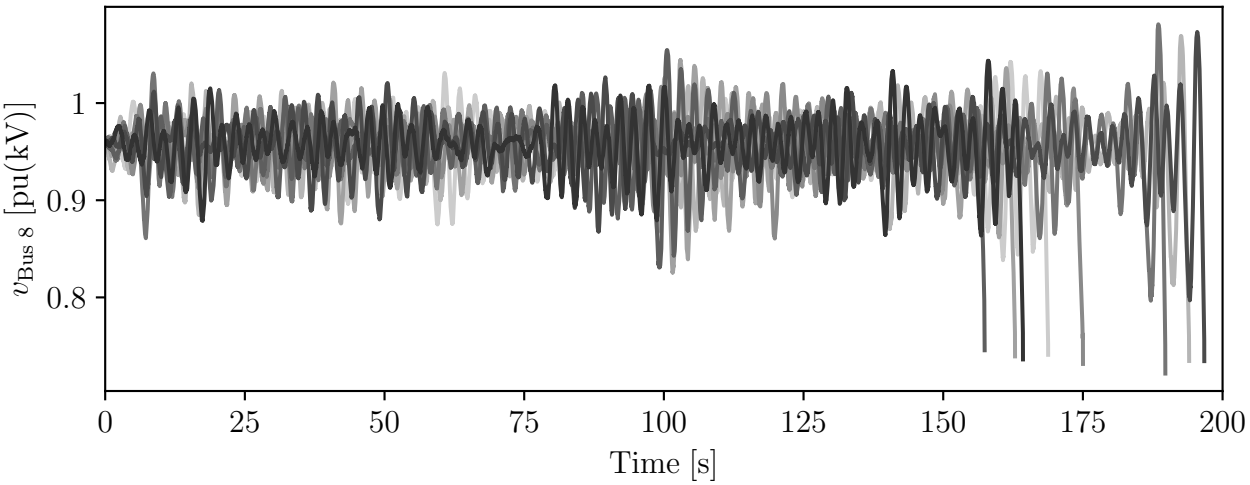

Figure 5.29: Few unstable trajectories of the voltage magnitude at bus 8 of the two-area system with stochastic load in area 2 for scenario S3.

5.3.2.2 All-Island Irish Transmission System

In this section, a dynamic model of the AIITS introduced in Section 4.5.2 is considered. The AIITS is modelled as a set of non-linear SDAEs in (3.3). Stochastic processes are

included in the load consumption using the stochastic load model provided in Section 3.5.1.2, with $\mathbf{R} = \mathbf{I}$, where stochastic processes are modelled as OU processes.

The dominant electro-mechanical oscillation modes of the AIITS are shown in Table 5.12. Whereas the frequency spectrum of p_g of a few synchronous generators of the AIITS are shown in Figures 5.30 and 5.31. The results show that the amplitude of the oscillations induced in p_g are dependent not only on the participation factors of the generators but also on the damping of the relevant mode.

Figure 5.30 illustrates that generator G3 shows low amplitude oscillations in the relevant mode, despite the fact that it has the highest participation factor as compared to generators G1 and G2. Whereas the generators G1 and G2 show higher amplitude

Table 5.12: Electro-mechanical modes and corresponding participation factors of the AIITS with stochastic loads.

Mode	Eigenvalue	Freq. [Hz]	Damp. [%]	Participation Factors					
				G1	G2	G3	G4	G5	G6
1	-0.392±j4.689	0.746	8.33	54.5	29.73	–	–	–	–
2	-0.826±j4.595	0.731	17.7	2.6	14.8	73.9	–	–	–
3	-1.059±35.948	0.971	17.10	–	–	–	21.1	73.6	–
4	-1.150±j6.368	1.013	17.78	–	–	–	–	–	91.26

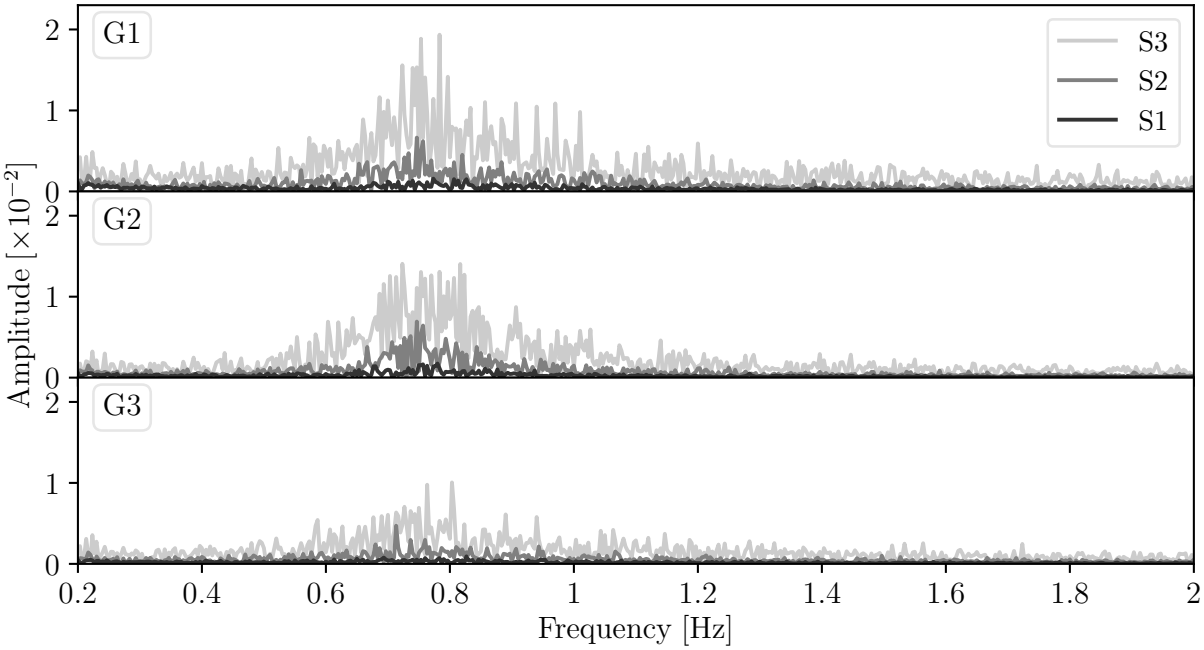

Figure 5.30: Frequency spectrum of active power injections of the synchronous generators G1, G2 and G3 of the AIITS with stochastic loads.

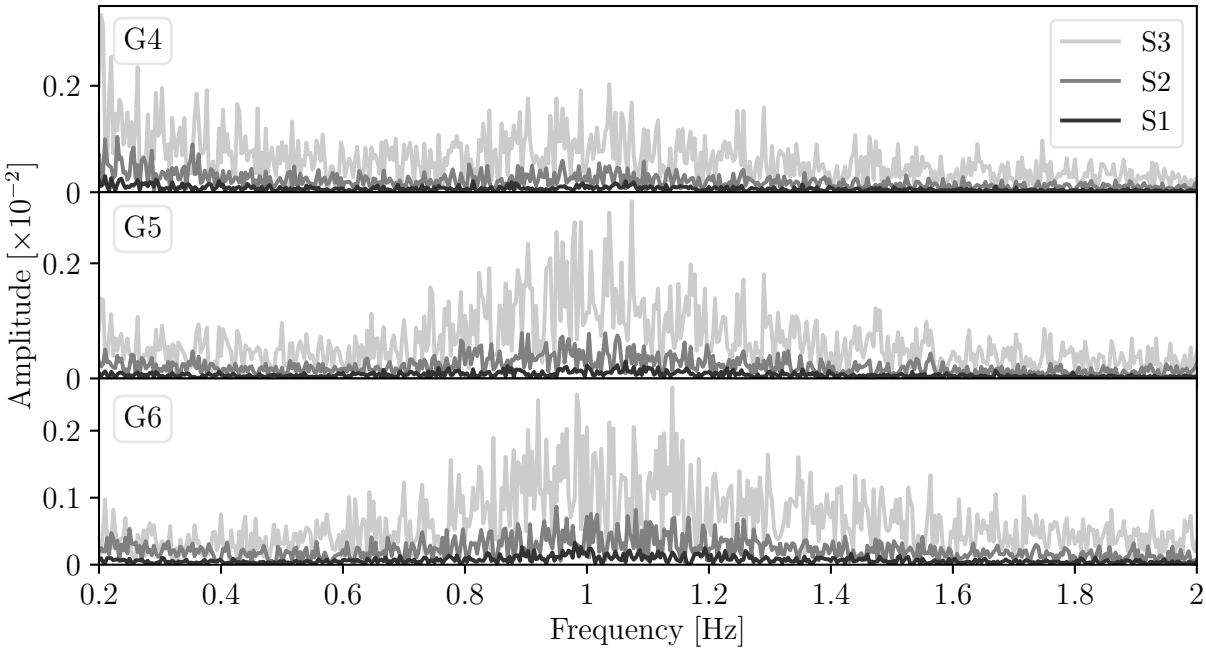

Figure 5.31: Frequency spectrum of active power injections of the synchronous generators G4, G5 and G6 of the AIITS with stochastic loads.

oscillations in their relevant modes despite having low participation as compared to G3. The rationale behind this result is that the damping of mode related to G3 is exceedingly high as compared to the damping of mode related to G1 and G2 (see Table 5.12). Similar behaviour is observed in generators G4 to G6 in Figure 5.31, where the relevant modes have higher damping. The results shown in Figures 5.30 and 5.31 are similar to those obtained for the two-area system, i.e., the amplitude of the frequency of the electro-mechanical oscillation modes is increased by increasing the autocorrelation coefficient α.

5.4 Conclusions

This chapter analyses the impact of the autocorrelation coefficient of the stochastic disturbances originating in power systems from sources of volatility such as load power consumption and non-synchronous RES penetration. With this regard, two methods, namely, time- and frequency-domain analysis, are utilised.

The time-domain analysis focuses on the power system output variables in stationary conditions. The results show that the standard deviations of the power system variables depend not only on the stationary distributions of the stochastic disturbances but also on the autocorrelation coefficient. Whereas the frequency-domain analysis studies the effect

of time-dependence of the stochastic disturbances on the dynamic response of the power system in the time-scale of power system transient. This method particularly focuses on the electro-mechanical oscillations in the power system triggered by these disturbances. The results of the frequency-domain analysis allow drawing the following relevant remarks.

- The higher the autocorrelation coefficient of the stochastic disturbances, the higher the amplitude of the frequency of dominant electro-mechanical modes.
- Stochastic disturbances originated in an area propagate to other areas through inter-area modes or through reactive power transfer from one area to another.
- The presence of stochastic disturbances in an area of the system has a reduced effect on the local modes of other areas. This is due to the fact that the noise originated in an area propagates to other areas through inter-area modes.
- Stochastic disturbances included in an area and exhibiting high values of autocorrelation coefficients may cause instability in the power system than those included in another area with the same statistical properties. Hence, it is crucial to know the autocorrelation coefficient of the stochastic processes along with their stationary distribution.

The case studies indicate that it is important to assess the instability probability of a power system subjected to stochastic disturbances based not only on the stationary PDF but also on the autocorrelation coefficient. With this result, the case study highlights the importance of solving TDSs with the actual values of the autocorrelation coefficients of all the stochastic processes present in a power system. It can also be observed that with the increasing penetration of non-synchronous RES and flexible loads, instabilities originated due to their stochastic nature are going to be increasingly likely in the future.

Note that the results presented in this chapter have been verified with various numerical integration schemes. This allows concluding that the instabilities observed for some scenarios are in effect due to the actual behavior of the system and not to numerical issues.

Chapter 6

Correlation

6.1 Introduction

This chapter illustrates several case studies based on the set of correlated Stochastic Differential Algebraic Equations (SDAEs) introduced in Chapter 3, to quantify the impact of correlated stochastic disturbances on the dynamic behaviour of the power system. The construction of the correlation matrix, which is the fundamental element to set up correlated SDAEs, based on measurement data is discussed first. Then the impact of modelling correlated stochastic processes on load active and reactive power consumption and wind speed fluctuations is demonstrated. Finally, the chapter presents several case studies that model correlation on different sources of volatility, i.e., stochastic load consumption, bus voltage phasors, and renewable energy sources penetrations, i.e., wind generation, and study their impact on the power system dynamic behaviour.

The remainder of the chapter is organized as follows. The construction of correlation matrix based on measurement data is discussed in Section 6.2. The scenarios of correlation utilised for the case studies are presented in Section 6.3. The impact of correlated active and reactive power, and correlated wind speeds on the standard deviation of the power system variables is discussed in Sections 6.4 and 6.5, respectively. Section 6.6 presents a case study utilising three power systems including the model of the real-world dynamic All-Island Irish Transmission System (AIITS) to assess the impact of correlated volatility on the power system dynamic. Conclusions are drawn in Section 6.7.

6.2 Correlation Matrix

This section utilises the methods described in Section 2.5.2 to illustrate the construction of correlation matrix based on measurement data. With this regard, at first, Section 6.2.1 provides details on the measurement data and the calculation of the noise elements from the data. The noise elements obtained from data are utilised to build the correlation matrix in Section 6.2.2.

6.2.1 Extraction of Noise Elements from Measurement Data

This section illustrates the procedure presented in Section 2.5.2 to extract the noise elements $d\psi$ from the measurement data. For this purpose, a variety of wind speed measurement data exhibiting different fitting PDF types and different time scales ranging from 1 second to 1 hour, presented in Appendix A.3, are utilised. Since the Irish system has a very high share of wind penetration, the wind speed measurement data was easily available. Nonetheless, the method utilised in this section is equally applicable to the measurement data from other sources as well.

For the extraction of $d\psi$ from the wind speed measurement data the following elements are the fundamental requirement: the fitting PDF; the parameters of the fitting PDF; and the Autocorrelation Function (ACF), i,e., autocorrelation coefficient, of the measurement data. These are obtained utilising the procedures described in Section 2.6. The $d\psi$ are then extracted from the data by employing the method provided in Section 2.5.2. The PDFs of $d\psi$ obtained from the measurement data, presented in Table A.1, are shown in Figure 6.1. This figure illustrates that the PDF of $d\psi$ is independent of the ACF, PDF and time-scale of the process; and follows the normal random variable with zero mean and unit variance, and is in accordance with the discussion in Section 2.5.2.

6.2.2 Construction of the Correlation Matrix

This section demonstrates the construction of the correlation matrix $\mathbf{R}$ from the measurement data. The elements of $\mathbf{R}$ represent the spatio-temporal correlation between the increments of the noise elements, i.e., $d\psi_i$ and $d\psi_j$. The noise elements are calculated from the measurement data as illustrated in Section 6.2.1. Once the time series of $d\psi$ is

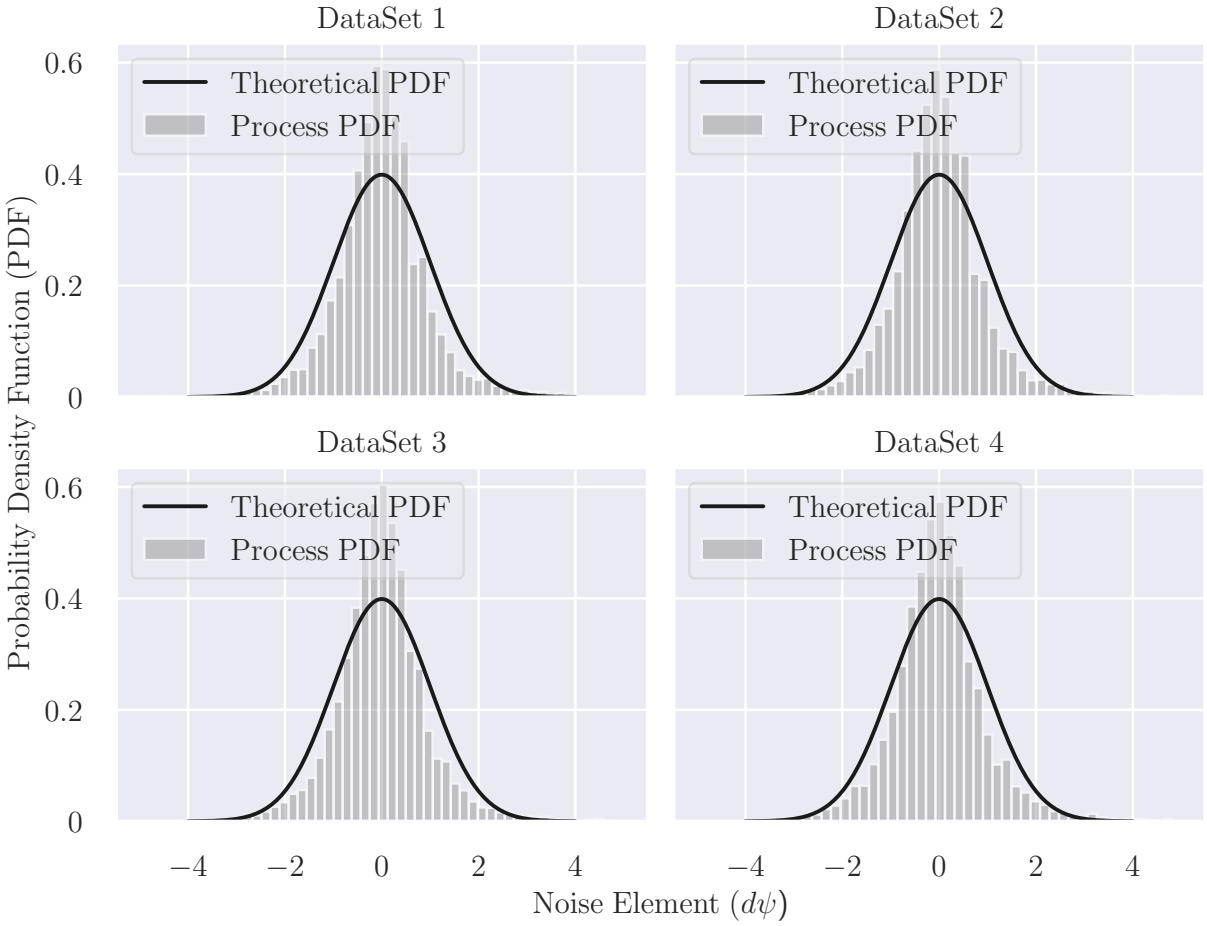

Figure 6.1: PDFs of $d\psi$ obtained from wind data, in Table A.1, using (2.29).

obtained, each element of $\mathbf{R}$, i.e., $r_{i,j} = \text{corr}[d\psi_i, d\psi_j]$ is calculated by employing Pearson's correlation coefficient, presented in Appendix B.2.1.

In this section, $\mathbf{R}$ is constructed for the ten wind sites of the distribution network shown in Figure 3.1. The scatter plot of $d\psi$ of selected wind sites is illustrated in Figure 6.2. This figure shows that some wind sites show a stronger correlation between them as compared to the others. This correlation depends on the distance between the sites. The scatter plot in Figure 6.2 accounts only for the spatial correlation, i.e., correlation with respect to distance. This correlation between the wind sites remains fixed because the distance between any two wind sites will always remain the same. To account for the temporal correlation large amount of data spanning over several years in the time-scale of power system dynamic will be required. This will help in understanding if the correlation between any two wind sites is a function of time or not. These data are not available at this stage.

Figure 6.2: Scatter plot of $d\psi$ obtained from wind data, for the wind sites in the distribution network in Figure 3.1.

Once the scatter plots are obtained, which are provided for illustration purposes only. The Pearson's correlation coefficient is applied to calculate linear correlation between any two wind sites. These correlations are then populated in $\mathbf{R}$ in their respective positions, i.e., $r_{i,j} = \text{corr}[d\psi_i, d\psi_j]$. The wind correlation matrix for the distribution network of Figure 3.1 is presented in Table A.2. For illustration purposes the correlation values obtained from the wind measurement data are plotted against the distance and are shown in Figure 6.3. Figure 6.3 shows that the correlation between the wind sites depends exponentially on the distance between them. The trend observed for the wind correlation in Figure 6.3 is consistent with the results reported in other studies [24, 45, 65].

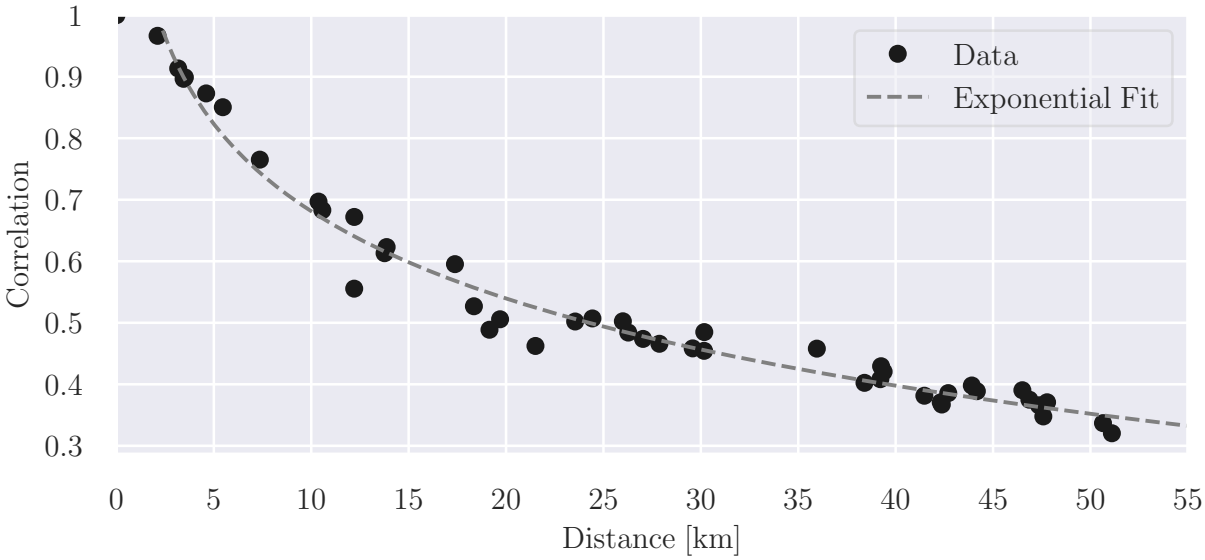

Figure 6.3: Correlation against distance between the wind sites in the distribution network in Figure 3.1.

6.3 Correlation Scenarios

The correlation matrix $\mathbf{R}$ is the fundamental tool required to set up correlated SDAEs. The entries of $\mathbf{R}$ represent the correlation between two given stochastic processes. This correlation is calculated using the measurement data. As explained in Section 6.2, a limited amount of data are available to account for correlation in the time-scale of power system dynamic simulations. This makes it almost impossible to construct $\mathbf{R}$.

In the remainder of this chapter, a sensitivity analysis is performed. Three scenarios of correlation are defined as follows:

- Scenario 1 (S1) represents the fully uncorrelated SDAE model, i.e., the correlation between any two stochastic processes i and j is $r_{i,j} = 0$.
- Scenario 2 (S2) considers a low level of correlation among processes, i.e., the correlation between any two stochastic processes i and j is set to $r_{i,j} = 0.4$.
- Scenario 3 (S3) considers a high level of correlation among processes, i.e., the value of correlation between any two stochastic processes i and j is set to $r_{i,j} = 0.8$.

6.4 Correlated Stochastic Active and Reactive Power

This section studies the impact of modelling correlation on stochastic active p_{L} and reactive q_{L} power consumption of loads on the statistical properties of power system relevant quantity, i.e., bus voltage magnitude v at the load buses. For this reason, the detailed dynamic model of the 9-bus system introduced in Section 4.2 is simulated through correlated SDAEs in 3.3. Where, the loads are modelled as described in Section 3.5.1.1.

The three scenarios of correlation defined in Section 6.3 are considered. The stochastic disturbances at load consumption are defined through the correlated Ornstein-Uhlenbeck (OU) processes introduced in Section 2.7.1. The values of the parameters are chosen as follows: $\alpha_p = \alpha_q = 1\mathrm{s}^{-1}$; $\sigma(\eta_p) = 4\%$ of p_{L0}; and $\sigma(\eta_q) = 4\%$ of q_{L0}. The MC is chosen to simulate the 9-bus system.

The stationary PDFs of the stochastic processes are not altered when correlating processes using (2.20), as explained in Section 2.5. The time domain trajectories and stationary PDFs of the correlated OU processes are shown in Section 2.7.1. The standard deviations of correlated p_{L} and q_{L}, obtained through the MC, at load buses are illustrated in Figures 6.4 and 6.5, respectively. These figures show that the standard deviation of p_{L} and q_{L}, in stationary conditions, remain the same despite being correlated.

The time profiles of v at load buses are illustrated in Figure 6.6. This figure shows a slight increase in v for an increase in correlations between p_{L} and q_{L}. An effective way to differentiate between the time profiles of v shown in Figure 6.6 is through the standard

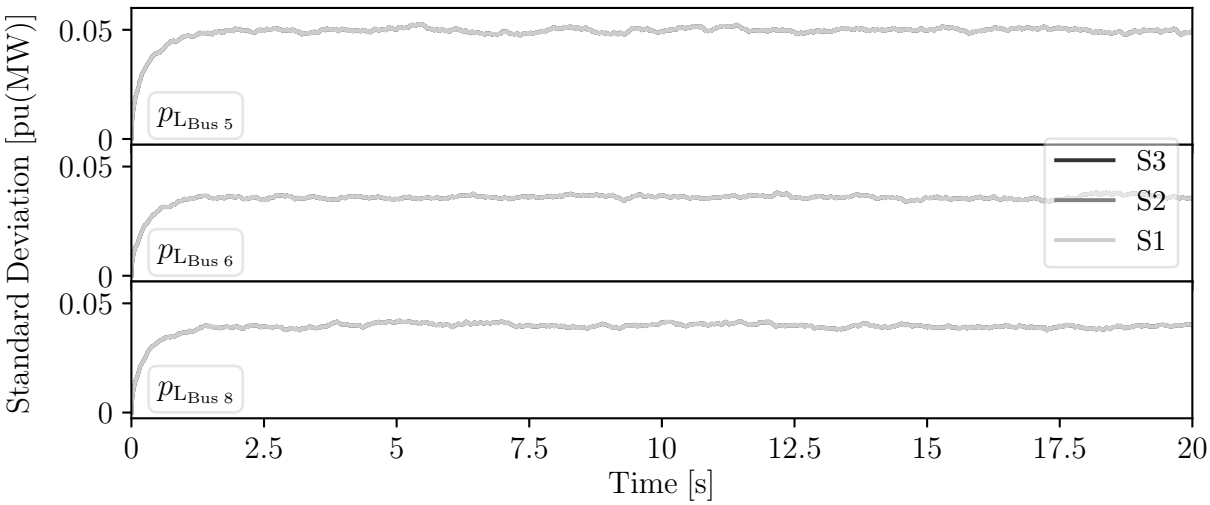

Figure 6.4: Standard deviation of active power consumption at load buses of the 9-bus system with correlated active and reactive power loads.

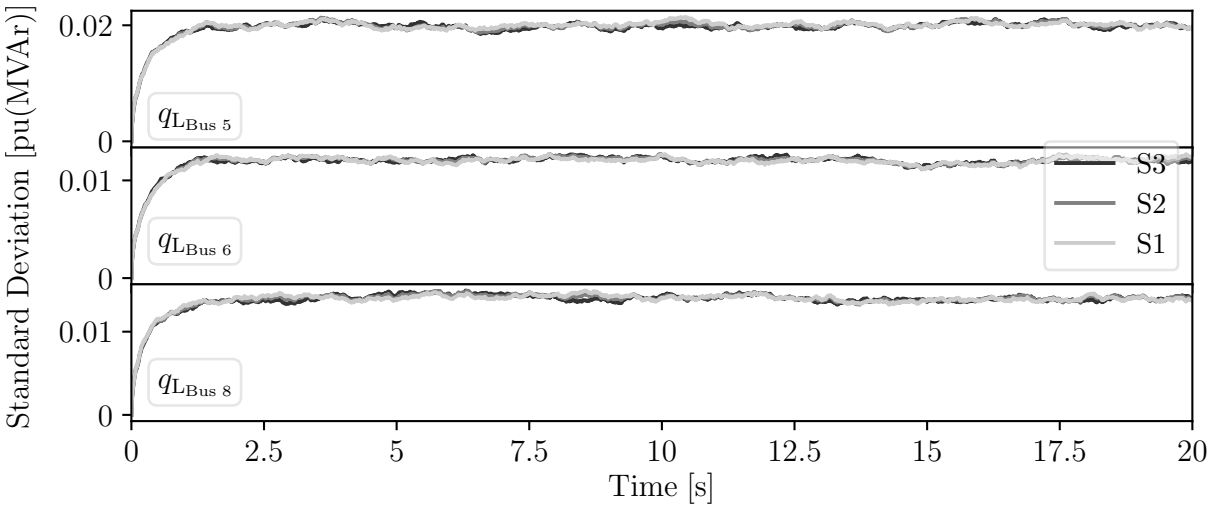

Figure 6.5: Standard deviation of reactive power consumption at load buses of the 9-bus system with correlated active and reactive power loads.

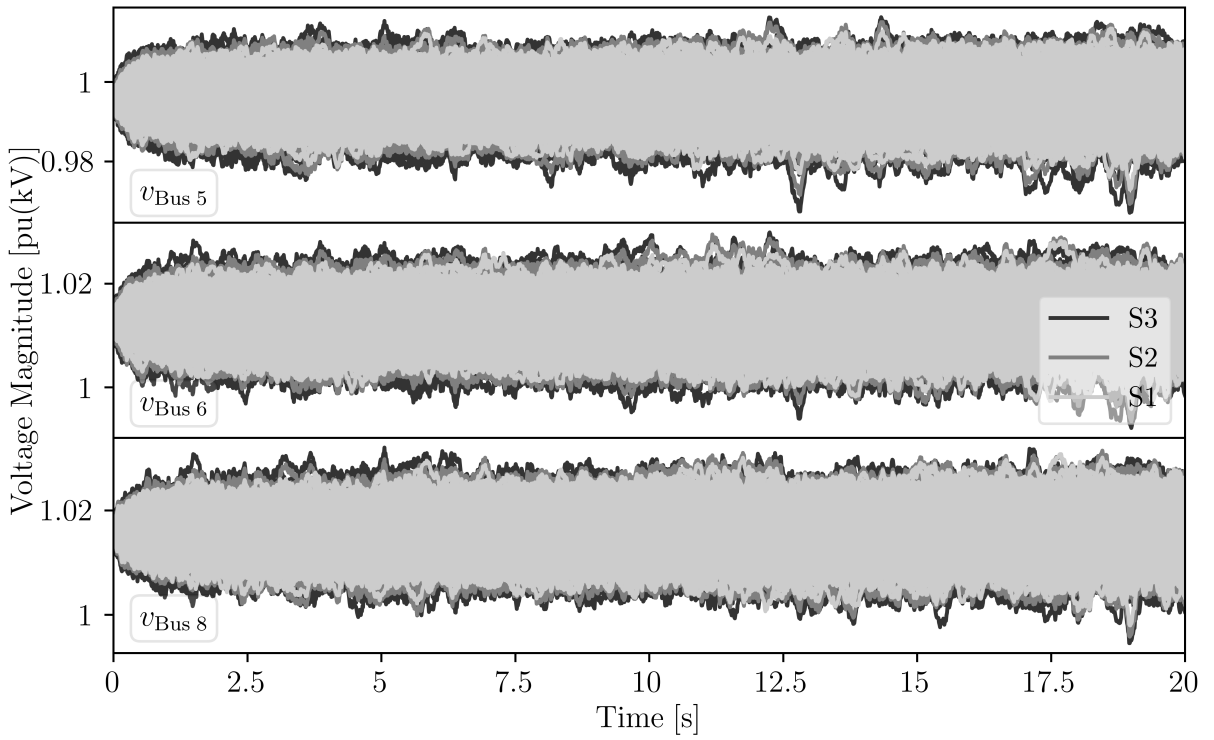

Figure 6.6: Trajectories of voltage magnitude at load buses of the 9-bus system with correlated active and reactive power loads.

deviation. For this reason, the standard deviation of v at the load buses is calculated against time and illustrated in Figure 6.7. This figure shows that the standard deviation of v at load buses is directly proportional to the level of correlation between p_{L} and q_{L}. The effect of the correlation on p_{L} and q_{L} in stationary conditions as well as during a transient is discussed in detail in Section 6.6.1.

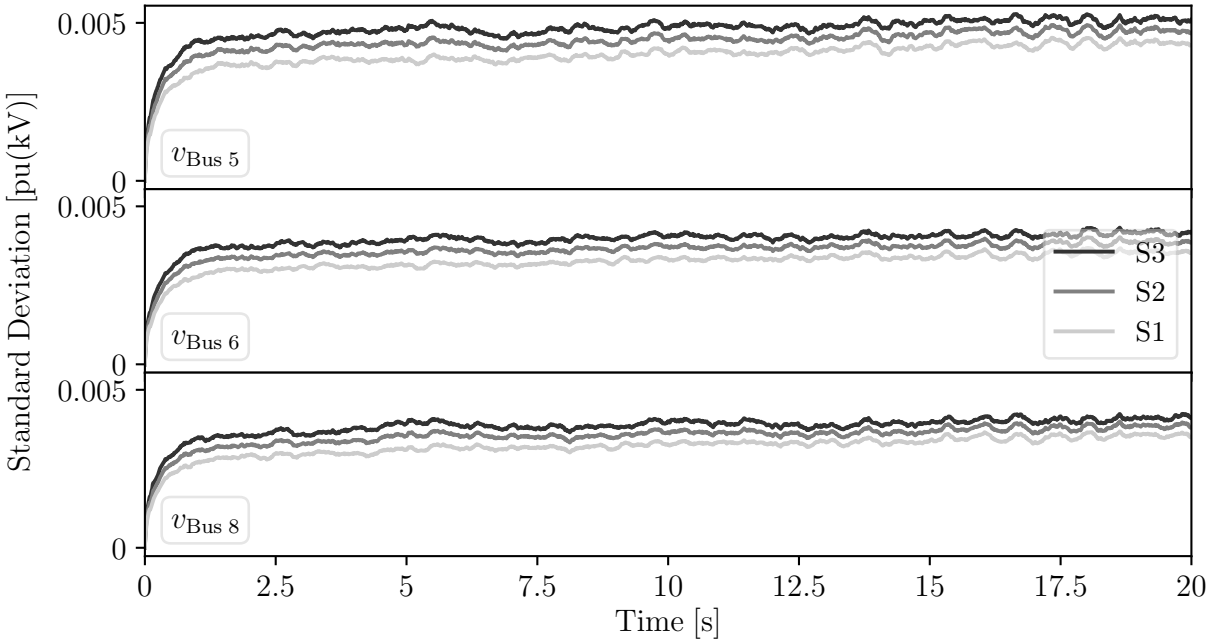

Figure 6.7: Standard deviation of voltage magnitude at load buses of the 9-bus system with correlated active and reactive power loads.

6.5 Correlated Stochastic Wind Speeds

This section studies the impact of correlated wind speeds on the dynamic behaviour of the active power injections p_e of the WPPs in the distribution network. The distribution network utilised in this section is the one introduced in Section 3.6 and shown in Figure 3.1. The wind speeds of the WPPs connected to bus Trien in the distribution network are correlated using the model described in Section 3.5.3. The correlated wind speeds are modelled through Gamma distribution as introduced in Section 2.7.2.2. Note that it is important to model the wind speeds with the right PDFs obtained through the measurements, as discussed in Section 4.3.1.

The dynamic behaviour of the processes being correlated depends on the level of correlation between them, see Figure 2.10. Note that the dynamic behaviour of the processes is modified without altering the stationary PDFs of the processes, as explained in Section 2.7.2.3. The effect of correlation between wind speeds is transferred to p_e of the WPPs. Figure 6.8 illustrates the time profile of p_e for distinct levels of correlation modelled on the underlying wind speeds. In Figure 6.8, it can be observed that, as the level of correlation between the wind speeds is increased, the time profiles of p_e come closer to each other, which modifies the dynamic behavior of p_e. However, this does not

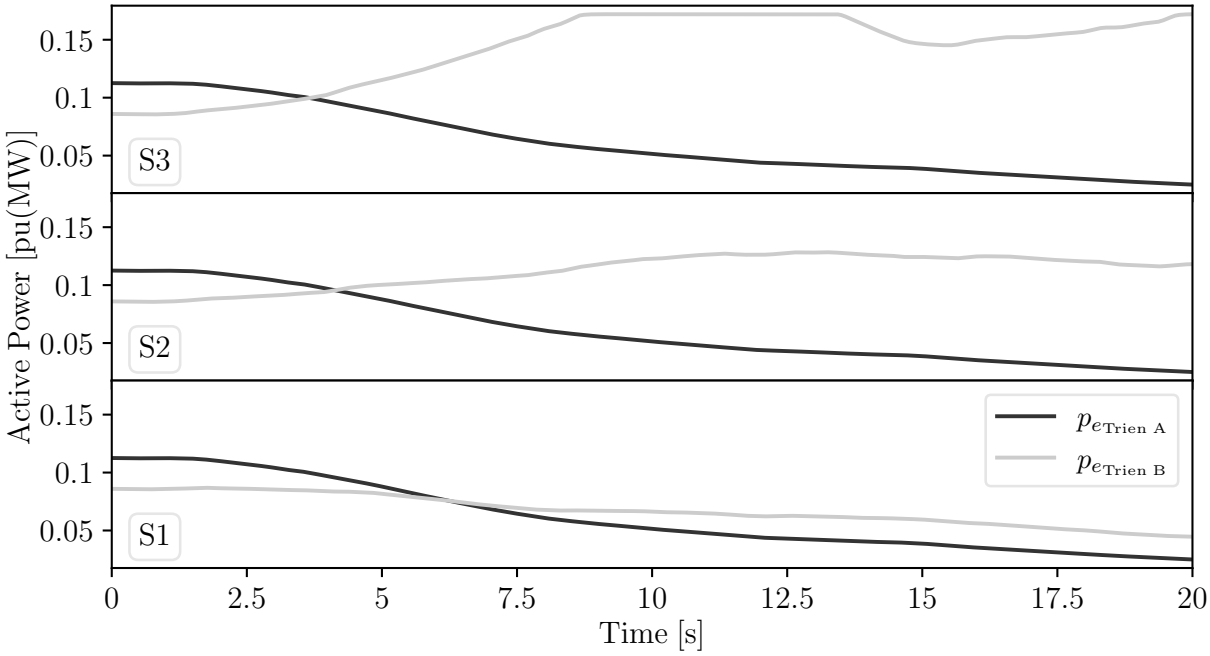

Figure 6.8: Active power injections of the WPPs connected to bus Trien for various levels of correlation between wind speeds.

modify the statistical properties of p_g, as the statistical properties of the wind speeds remain unaltered.

To show that standard deviation of p_e is not affected by the correlation between the wind speeds, the MC is adopted. The MC simulates 1,000 trajectories of the active power p_e. The standard deviations of p_e of the WPPs at bus Trien are calculated against time and illustrated in Figure 6.9. This figure shows that standard deviation of p_e of the WPPs remains the same at any level of correlation. Conversely, the standard deviation of total p_e injected at bus Trien is dependent on the level of correlation between the underlying wind speeds. The standard deviation of total p_e injected at bus Trien is illustrated in Figure 6.10. The rationale behind this is that p_e of each WPP being correlated will show similar variations in time dependent on the correlation between the underlying wind speeds. This makes the sum of p_e rise or fall dependent on the correlation, which causes p_e injected at the bus to have a higher standard deviation for higher correlation.

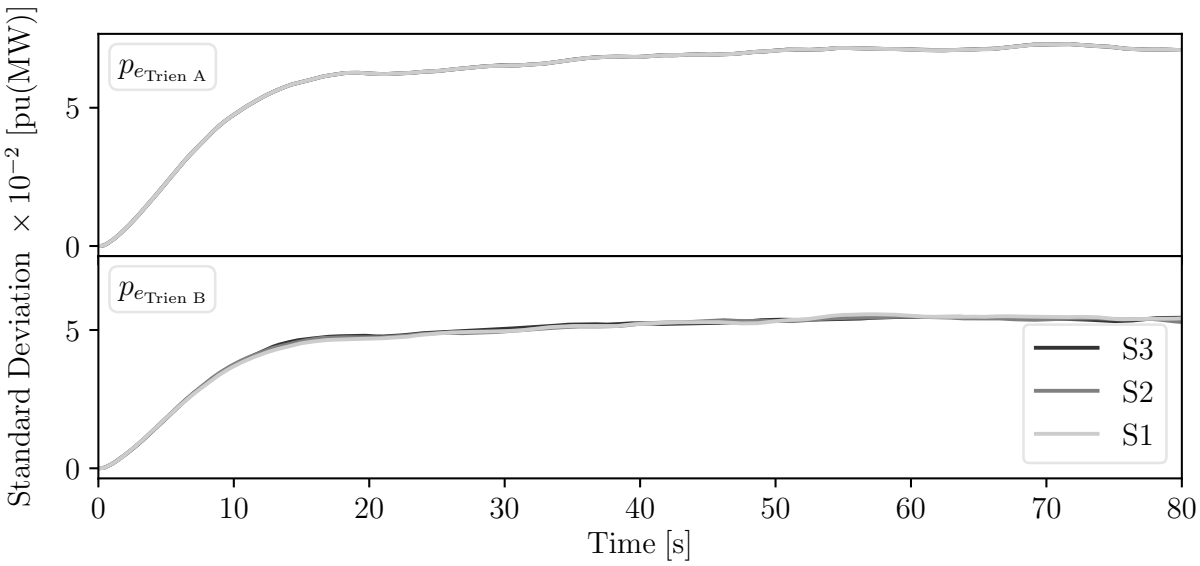

Figure 6.9: Standard deviation of the active power of WPPs connected to bus Trien.

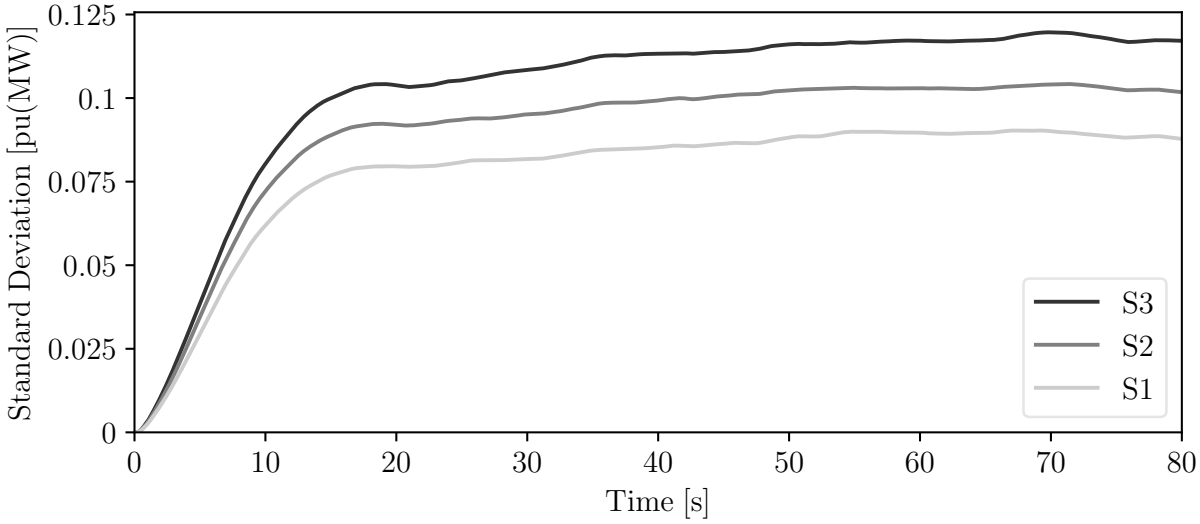

Figure 6.10: Standard deviation of the active power injected at bus Trien.

6.6 Case Study

This case study aims at evaluating the effect of the correlated stochastic disturbances on the dynamic behavior of power systems. With this goal, the standard deviations of the trajectories of system variables such as the active power of synchronous generators and bus voltage magnitudes considering the cases of correlated and uncorrelated disturbances are compared. The power systems considered are (i) the two-area system, (ii) the two-area system with inclusion of wind generation, and (iii) a dynamic model of the All-Island Irish Transmission System (AIITS).

The impact of the correlation of disturbances is evaluated by observing the trajectories of relevant quantities of the system. With this aim, the MC is chosen. Each simulation requires about 8,000 realizations of the Wiener processes for all wind speeds, bus voltage phasors, and load active and reactive power consumption.

6.6.1 Two-Area System

The two-area system introduced in Section 4.3.2 is modified as shown in Figure 6.11. Correlated disturbances in the two-area system are modelled as correlated OU processes using the procedure described in Section 2.7.1. These are included into the modified two-area system through stochastic load consumption, and bus voltage phasors, with the following parameters: $\alpha_p = \alpha_q = \alpha_v = \alpha_\theta = 1\text{s}^{-1}$; $\sigma(\eta_p) = 0.6\%$ of p_{L0}; $\sigma(\eta_q) = 0.6\%$ of q_{L0}; $\sigma(\eta_v) = 0.3\%$ of v_0; and $\sigma(\eta_\theta) = 0.3\%$ of θ_0. The results discussed in this section were originally presented in [3].

First, the correlated stochastic disturbances are introduced in stochastic load consumption using the load model (3.5). The correlation matrix $\mathbf{R}$ utilised to model correlation on stochastic load consumption is shown in Table 6.1, where r represents the correlation between any two given quantities. The value of r is chosen based on the scenarios described in Section 6.3. The case study considers correlation between the load devices connected in the same area. Hence, inter-area correlation is not considered.

The trajectories of the voltage profile at bus 8 are observed for the three scenarios simulated, and the results are presented in Table 6.2. Results indicate that the higher

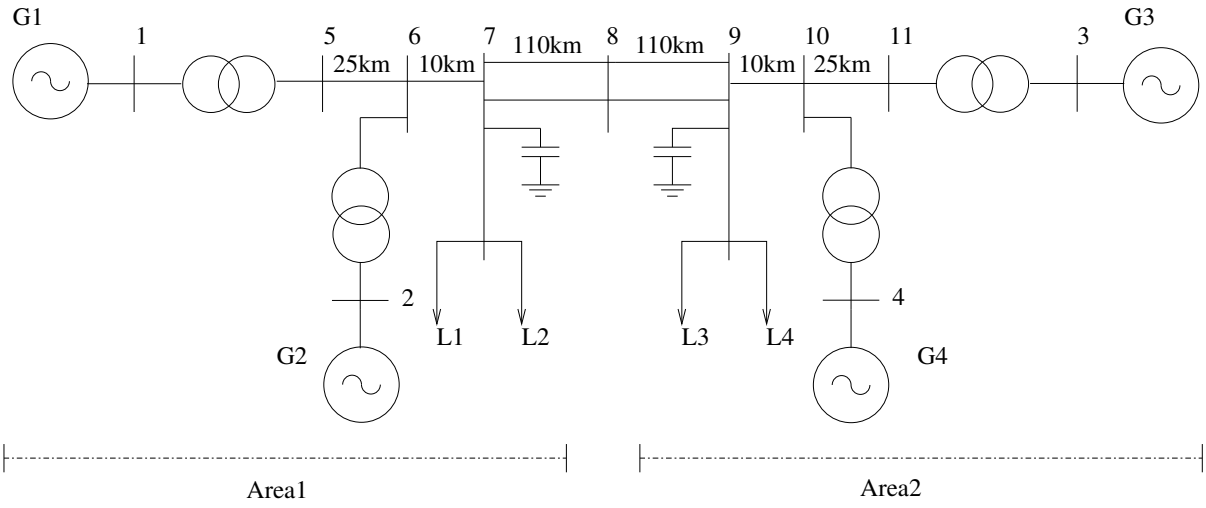

Figure 6.11: Single-line diagram of the modified two-area system [3].

the correlation among processes, the higher the probability that the system becomes unstable. This result can be explained as follows: the loads will require more/less power from generators if they all increase/decrease in a coordinated manner. For illustration purposes, a selection of the unstable trajectories from scenarios S2 and S3, are shown in Figures 6.12-6.14 and Figures 6.15-6.17, respectively. Simulations indicate that the loss of stability, in this case, is due to a shortage of reactive power that leads to voltage collapse.

Table 6.1: Correlation matrix of the stochastic loads of the modified two-area system.

	p_1	p_2	p_3	p_4	q_1	q_2	q_3	q_4
p_1	1	r	0	0	r	r	0	0
p_2	r	1	0	0	r	r	0	0
p_3	0	0	1	r	0	0	r	r
p_4	0	0	r	1	0	0	r	r
q_1	r	r	0	0	1	r	0	0
q_2	r	r	0	0	r	1	0	0
q_3	0	0	r	r	0	0	1	r
q_4	0	0	r	r	0	0	r	1

Table 6.2: Unstable trajectories of the modified two-area system with correlated stochastic loads.

Scenario	Unstable trajectories	Disconnection of load L_3: Unstable trajectories
S1	0	0
S2	68 (6.8%)	19 (1.9%)
S3	369 (36.9%)	68 (6.8%)

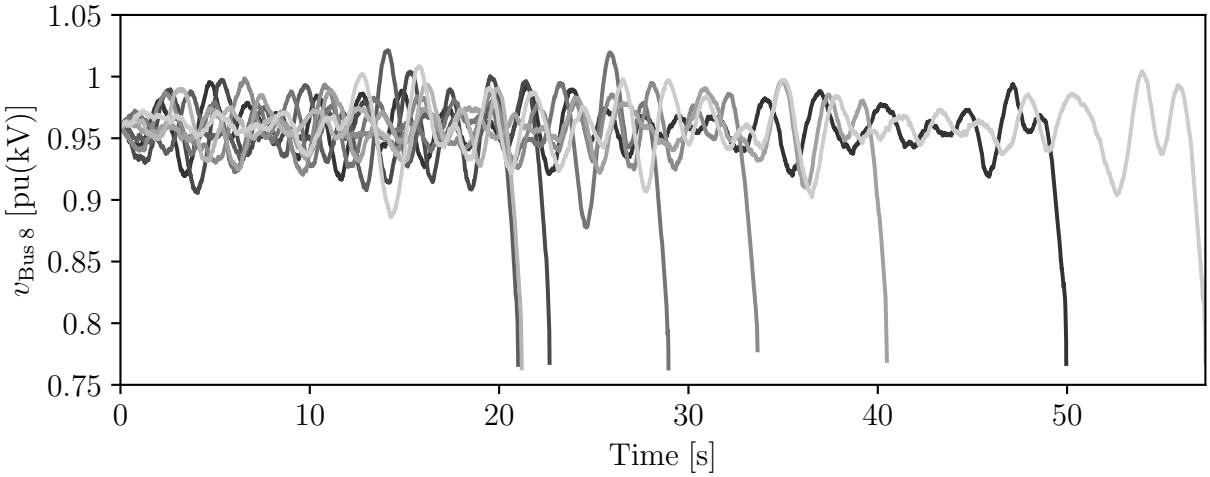

Figure 6.12: Few unstable trajectories of voltage magnitude at bus 8 of the modified two-area system with correlated stochastic loads for selected unstable trajectories for scenario S2.

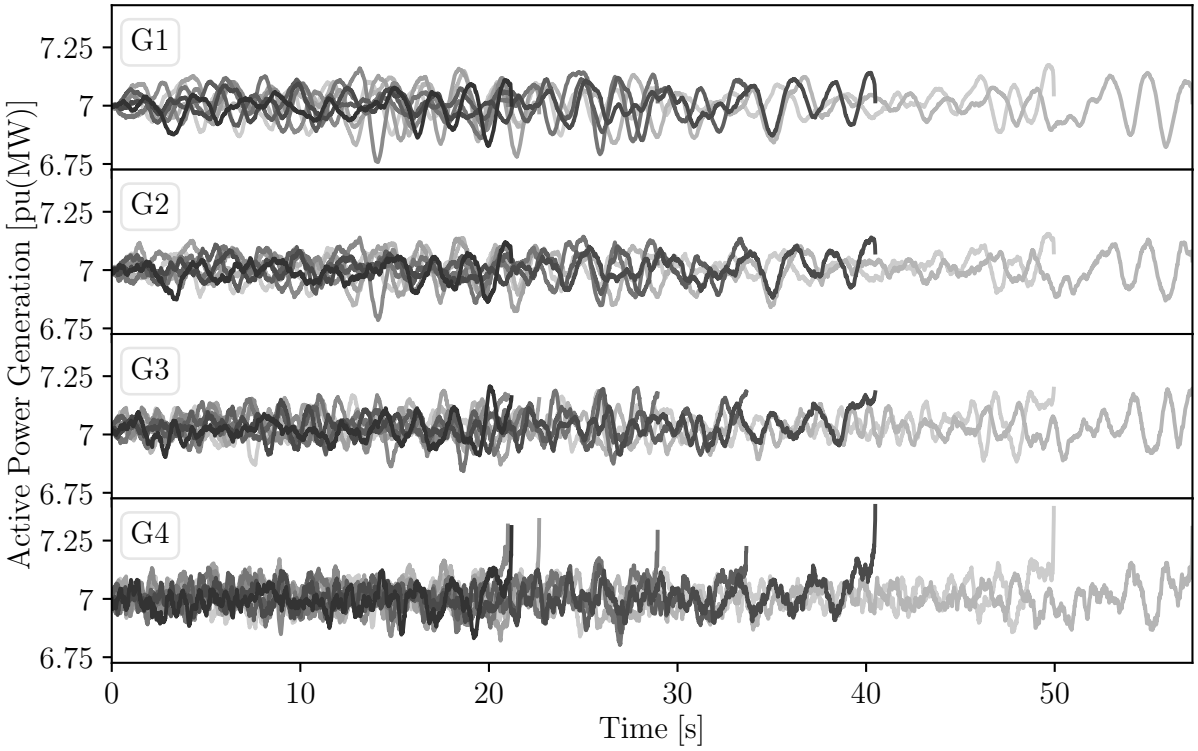

Figure 6.13: Few unstable trajectories of active power injections of the synchronous generators of the modified two-area system with correlated stochastic loads for scenario S2.

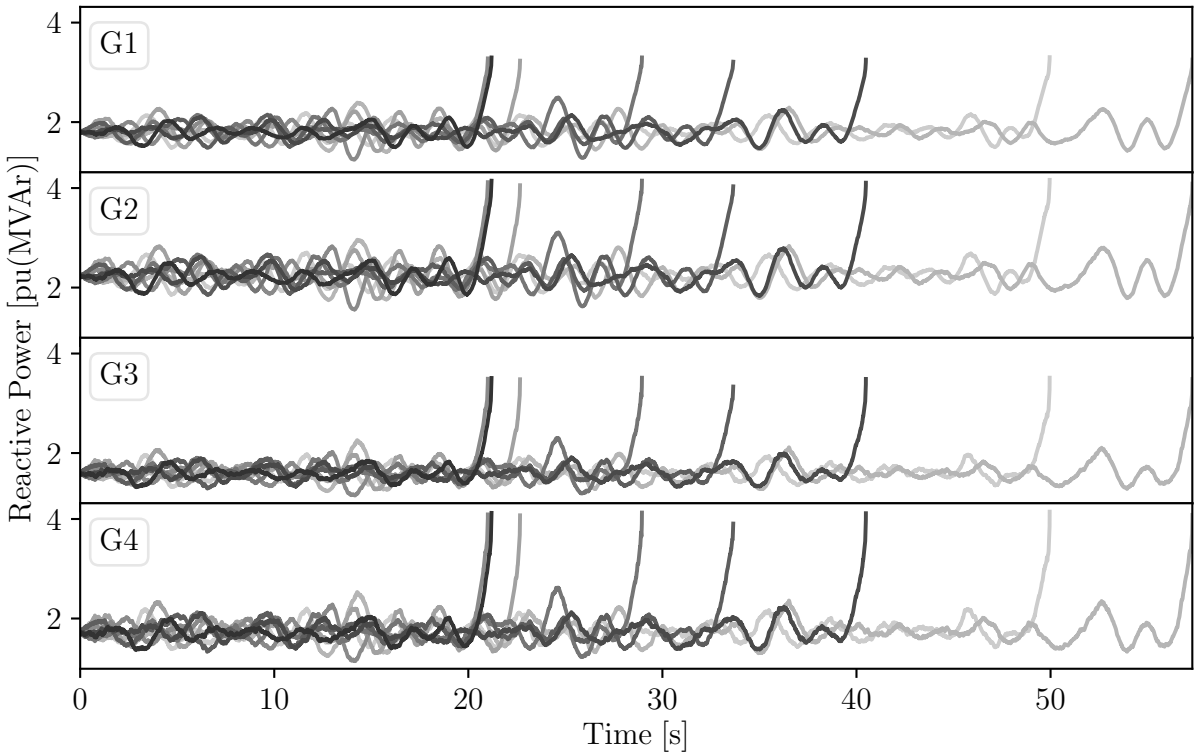

Figure 6.14: Few unstable trajectories of reactive power injections of the synchronous generators of the modified two-area system with correlated stochastic loads for scenario S2.

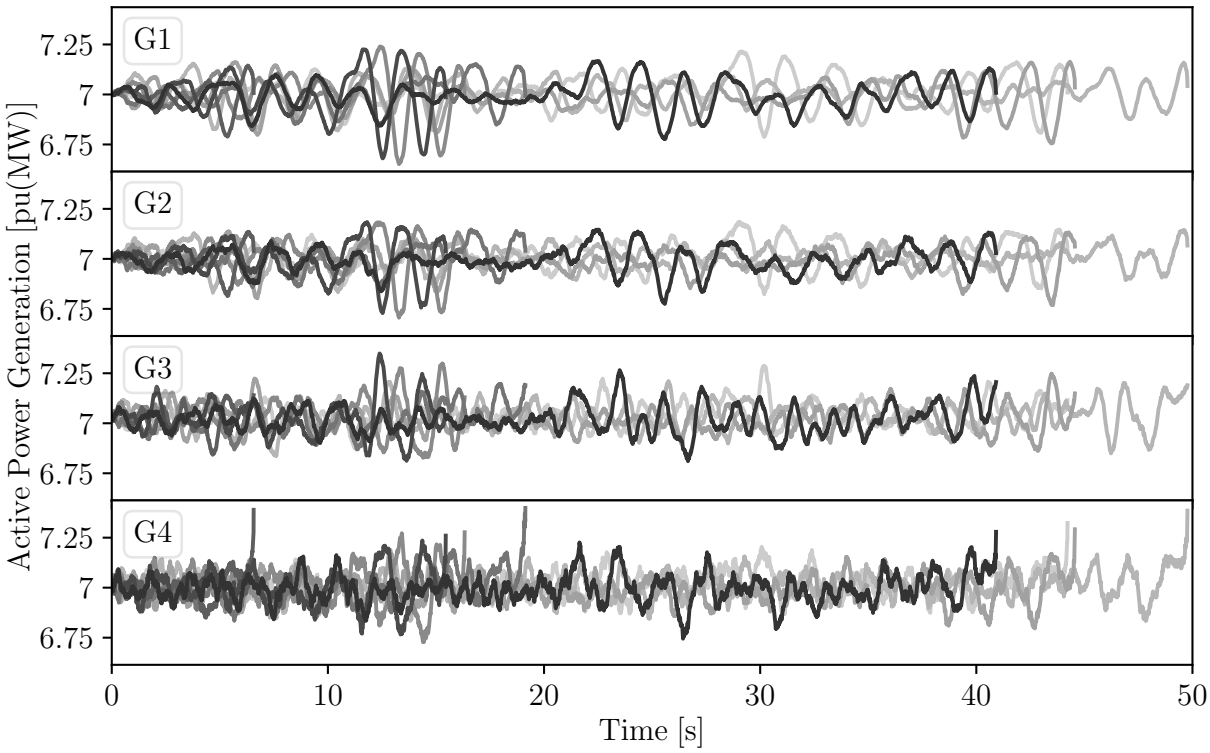

Figure 6.15: Few unstable trajectories of active power injections of the synchronous generators of the modified two-area system with correlated stochastic loads for scenario S3.

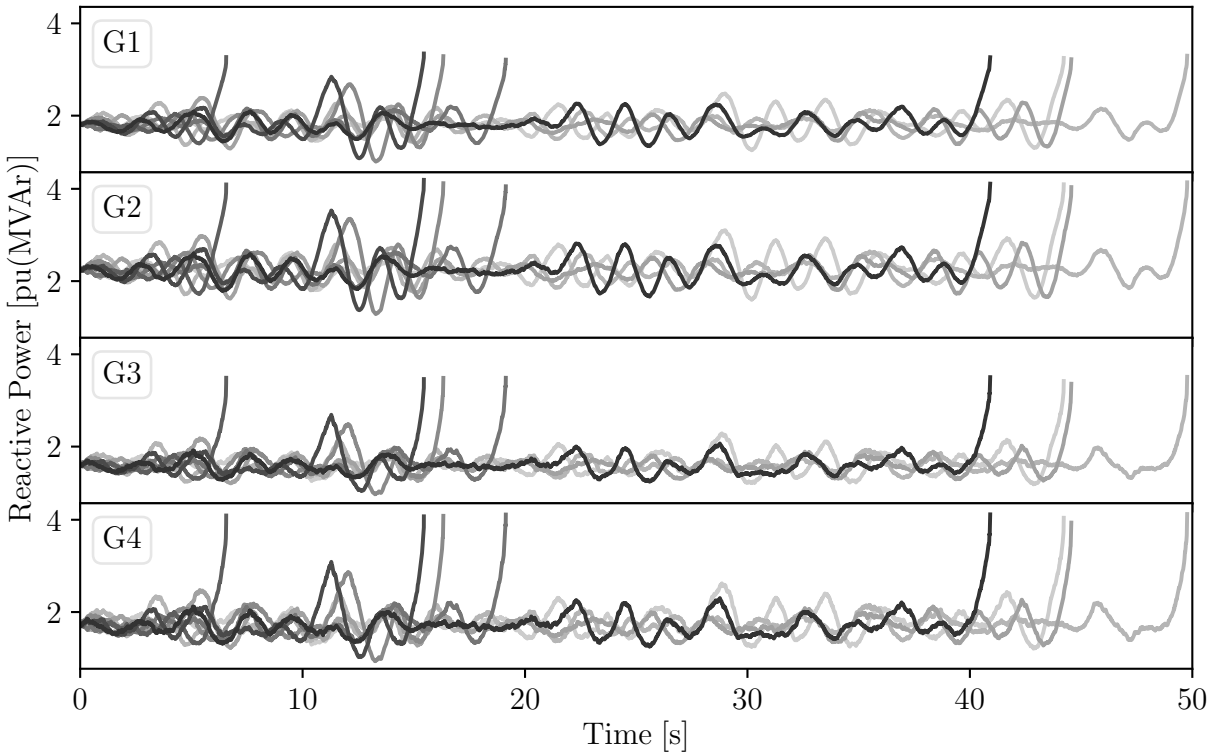

Figure 6.16: Few unstable trajectories of reactive power injections of the synchronous generators of the modified two-area system with correlated stochastic loads for scenario S3.

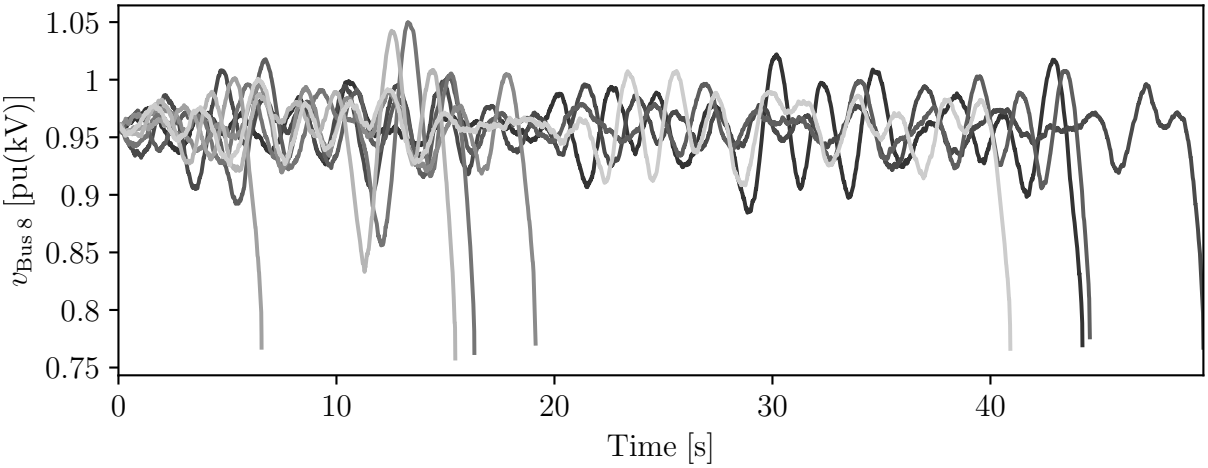

Figure 6.17: Few unstable trajectories of voltage magnitude at bus 8 of the modified two-area system with correlated stochastic loads for selected unstable trajectories for scenario S3.

An effective way to evaluate the effect of correlation between the loads is through observing the statistical properties of the relevant quantities. The statistical property, and the quantity chosen in this case study is the standard deviation of the active and reactive power generation of synchronous generators, namely, $\sigma(p_g)$ and $\sigma(q_g)$, respectively. The standard deviation of stable trajectories of active p_g and reactive q_g power generation of synchronous generators obtained from the simulations presented above in this section is calculated and presented in Table 6.3. This table indicates that the values of $\sigma(p_g)$ and

Table 6.3: Standard deviation of active and reactive powers of synchronous generators for the modified two-area system with correlated stochastic loads.

Standard deviation	S1 absolute	S2 % increase [1]	S3 % increase[1]
$p_{g_{\text{G1}}}$	0.0519	22.73	45.04
$p_{g_{\text{G2}}}$	0.0439	22.34	44.15
$p_{g_{\text{G3}}}$	0.0432	22.76	45.03
$p_{g_{\text{G4}}}$	0.0442	21.94	42.53
$q_{g_{\text{G1}}}$	0.1399	24.37	48.88
$q_{g_{\text{G2}}}$	0.1726	24.37	48.89
$q_{g_{\text{G3}}}$	0.1215	25.22	50.82
$q_{g_{\text{G4}}}$	0.1554	25.13	50.55

[1] Note: % increase is calculated based on scenario S1.

$\sigma(q_g)$ increase by about 25% comparing scenarios S1 to S2 and by about 50% comparing scenarios S1 and S3.

Next, the impact of correlated stochastic disturbances in bus voltage phasors on $\sigma(p_g)$ and $\sigma(q_g)$ of the synchronous generators is evaluated by modelling the correlated stochastic disturbances on the bus voltage phasors through the model introduced in Section 3.5.2. The correlation matrix is built in such a way that stochastic processes modelled on intra area buses are considered to be correlated, whereas no correlation is considered between the inter area buses. In this example, load power consumption does not include stochastic disturbances. Table 6.4 shows $\sigma(p_g)$ and $\sigma(q_g)$ of synchronous generators calculated for the three scenarios S1, S2, and S3. It appears that the correlation among the stochastic bus voltage phasors is inversely proportional to the $\sigma(p_g)$ and $\sigma(q_g)$ of the generators. Note that none of the trajectories were found to be unstable. This effect is thus the opposite as the one obtained when varying the correlation of the load power consumption.

Finally, the impact of correlated stochastic disturbances on the transient behaviour of the power system undergoing a contingency is considered. With this aim, the two-area system is simulated using correlated stochastic loads with the following parameters: $\alpha_p = \alpha_q = 1\text{s}^{-1}$; $\sigma(\eta_p) = 0.5\%$ of p_{L0}; and $\sigma(\eta_q) = 0.5\%$ of q_{L0}. The contingency planned is the disconnection of loads connected to bus 9 at $t = 10s$. The simulation results for unstable trajectories for the three scenarios of correlation are shown in Table 6.2. The

Table 6.4: Standard deviation of active and reactive powers of synchronous generators for the modified two-area system with correlated stochastic voltages.

Standard deviation	S1 absolute	S2 % increase [1]	S3 % increase[1]
$p_{g_{\text{G1}}}$	0.0495	-20.06	-47.24
$p_{g_{\text{G2}}}$	0.0547	-20.68	-49.20
$p_{g_{\text{G3}}}$	0.0908	-17.51	-39.67
$p_{g_{\text{G4}}}$	0.0909	-18.22	-41.70
$q_{g_{\text{G1}}}$	0.0598	-18.75	-42.93
$q_{g_{\text{G2}}}$	0.0705	-17.63	-40.22
$q_{g_{\text{G3}}}$	0.0420	-21.49	-50.79
$q_{g_{\text{G4}}}$	0.0516	-20.75	-49.49

[1] Note: % increase is calculated based on scenario S1.

results show that the system experiences increased number of unstable trajectories for higher values of correlation. A section of unstable trajectories of rotor angle δ of all the synchronous machines for scenario S2 are shown in Figure 6.18, whereas the stable trajectories of δ obtained for scenario S3 are shown in Figure 6.19.

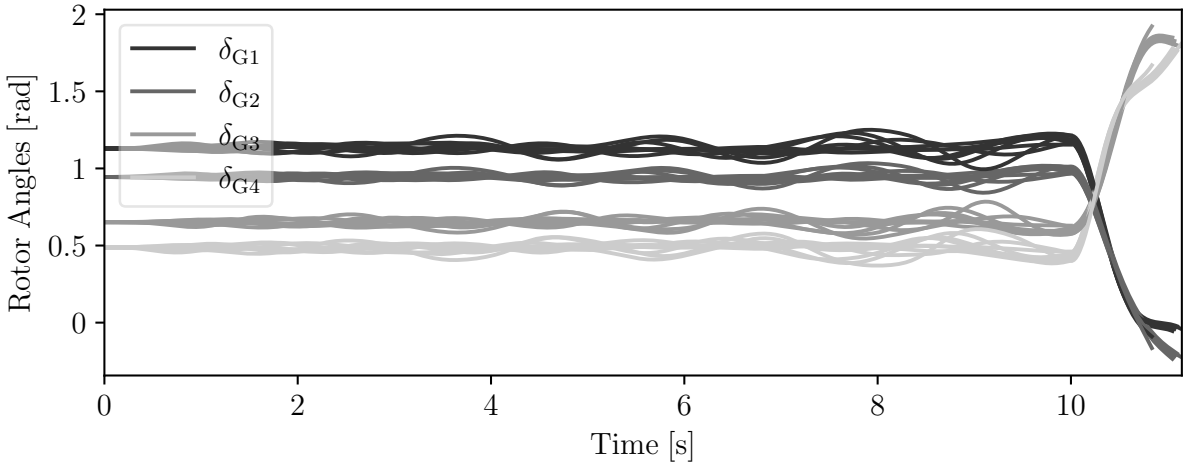

Figure 6.18: Few unstable trajectories of rotor angles of all the synchronous machines of the modified two-area system for scenario S2.

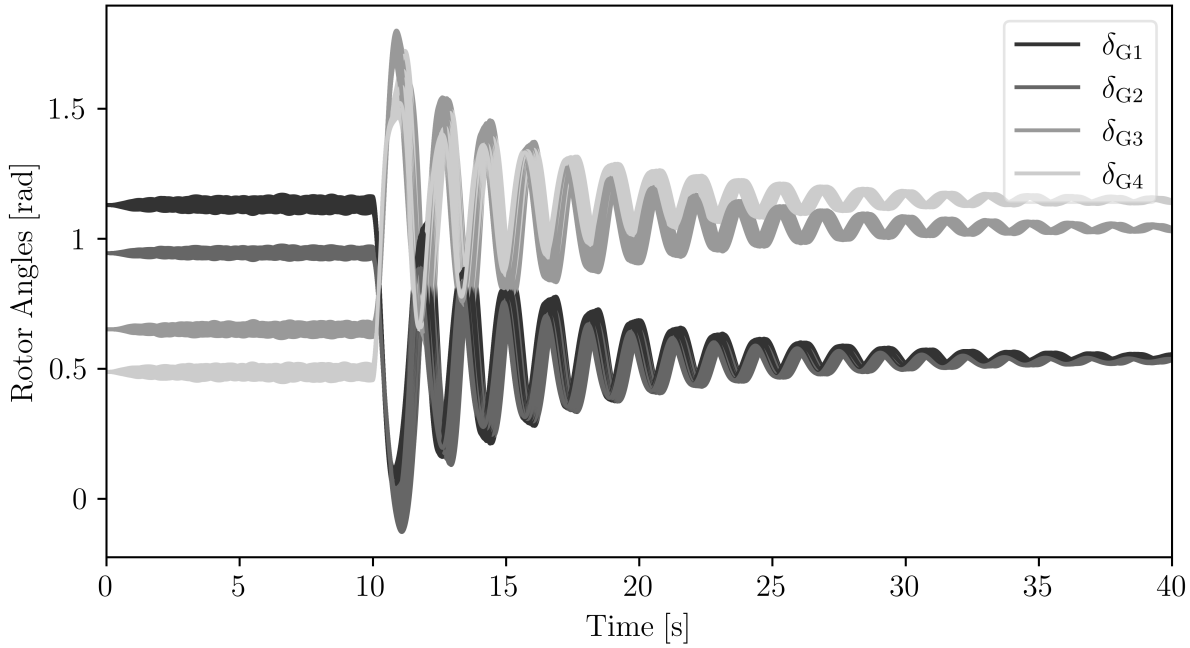

Figure 6.19: Stable trajectories of rotor angles of all the synchronous machines of the modified two-area system for scenario S3.

6.6.2 Two-Area System With Wind Generation

The power system utilised in this section is the well-known two-area system with inclusion of wind generation network, which was presented in Section 4.3.2. The results presented in this section were originally discussed in [6]. The WPPs are modelled through variable-speed doubly-fed induction generators. The correlated stochastic disturbances are introduced into the wind speeds using the model described in Section 3.5.3. As discussed in Section 6.5, the wind speeds are modelled using Gamma distribution. The correlation matrix $\mathbf{R}$ of wind speeds is provided in Table A.2. The power system dynamic simulations are performed using the MC.

To study the impact of correlated wind speeds on the power system dynamic, a sensitivity analysis is adopted. With this aim, the following scenarios are considered:

- Scenario 1 (S1) considers no correlation among wind speeds.
- Scenario 2 (S2) considers correlation among all wind speeds.

Firstly, the impact of modelling correlation on the standard deviation of the power system variables is quantified. The standard deviation of the frequency of the center of inertia ω_{Coi} for both scenarios is illustrated in Figure 6.20. while the standard deviations of bus voltage magnitude $\sigma(v)$, and active power $\sigma(p_g)$ injections of the synchronous machines are shown in Table 6.5. Figure 6.20 and Table 6.5 show that the standard deviations of the power system variables are increased with an increase in the level of correlation among the

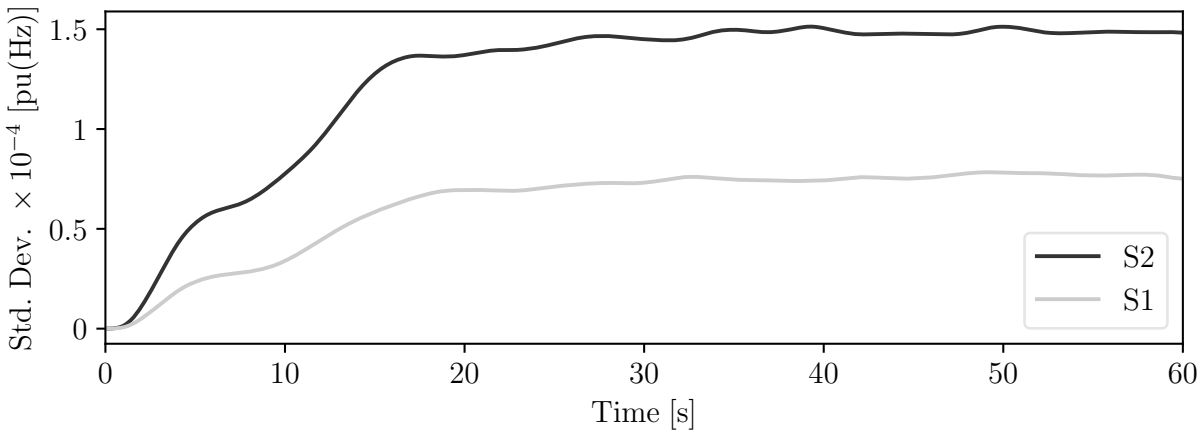

Figure 6.20: Standard deviation of the frequency of the center of inertia of the two-area system with inclusion of correlated wind fluctuations.

Table 6.5: Standard deviation of bus voltage magnitudes and active power injections of the synchronous generators in the two-area system with inclusion of correlated wind fluctuations.

Std. [pu]	S1	S2	% increase
$\sigma(v_{\text{Bus 08}})$	0.0049	0.0095	93.88
$\sigma(v_{\text{Bus 09}})$	0.0033	0.0064	93.94
$\sigma(p_{\text{G1}})$	0.0075	0.0148	97.33
$\sigma(p_{\text{G2}})$	0.0074	0.0147	98.65
$\sigma(p_{\text{G3}})$	0.0075	0.0146	94.67
$\sigma(p_{\text{G4}})$	0.0074	0.0145	95.95

wind speeds. This indicates that correlated wind speeds can modifying the distribution of power system quantities without modifying the distribution of power injections of WPPs.

In this second case, the two-area system modified to include wind generation is subjected to both correlated wind speeds and a contingency. The contingency consists of the trip of the line connecting buses 8 and 9 at time $t = 30$ s. The voltage profile at Bus 8 for the two scenarios of correlation is illustrated in Figures 6.21 and 6.22. These figures show the trajectories of the bus voltage magnitude v at bus 8 along with the mean of the trajectories for the system modelled through correlated SDAEs, for the two scenarios.

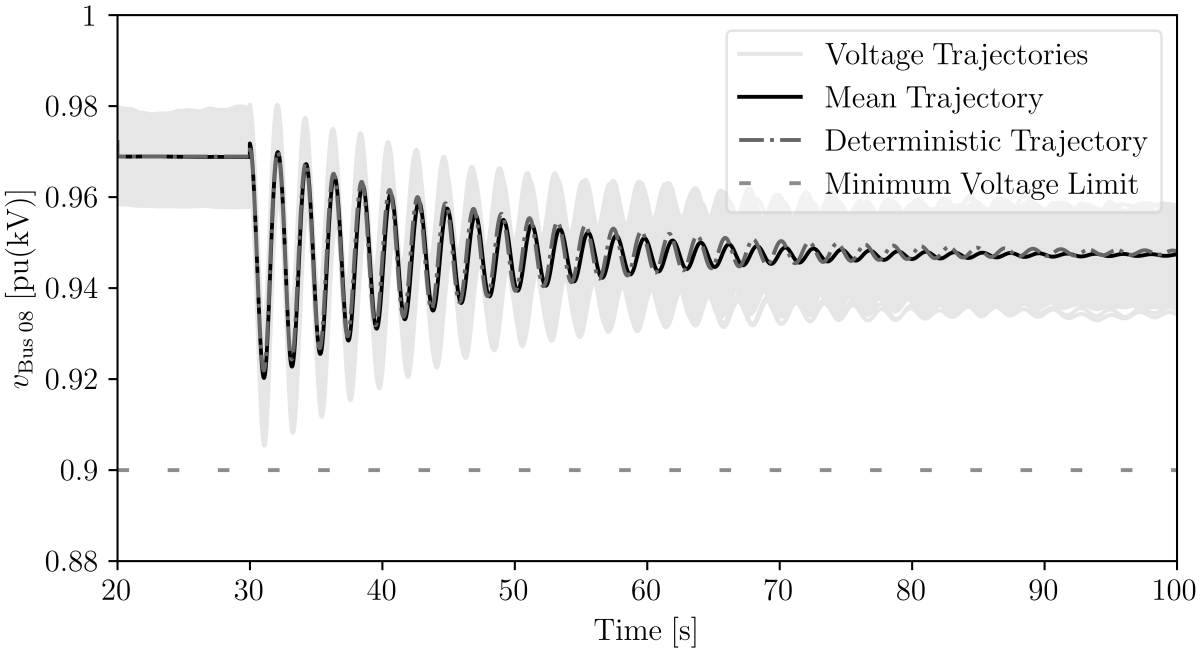

Figure 6.21: Voltage profile at bus 8 for scenario S1 for the two-area system with inclusion of correlated wind fluctuations.

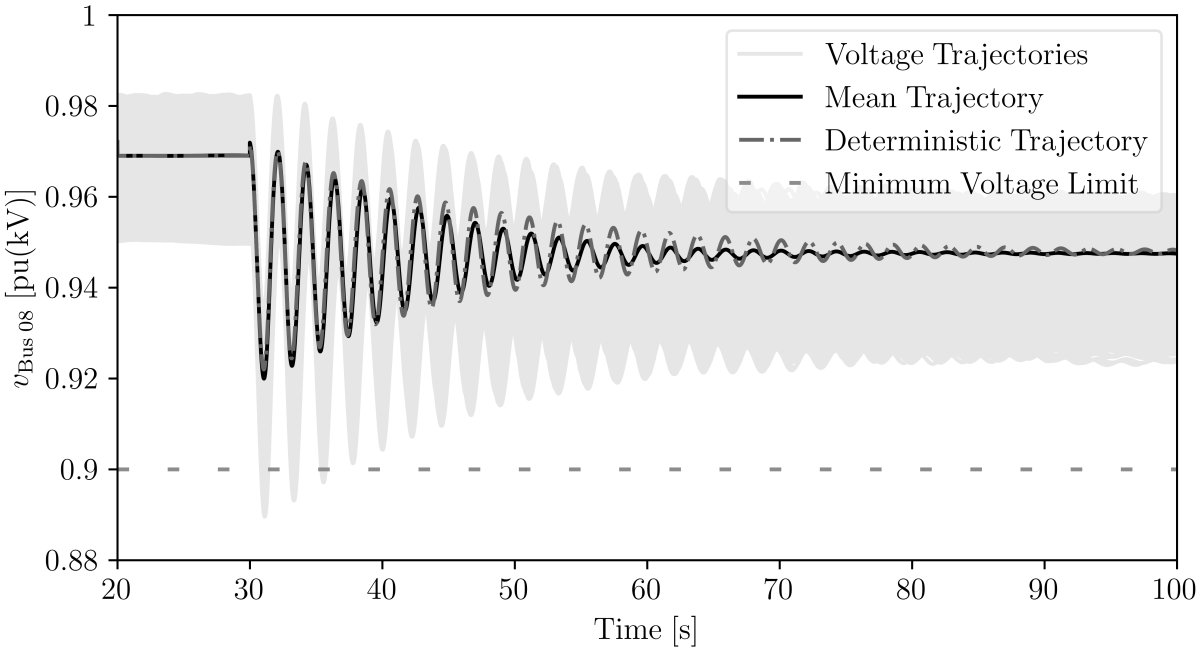

Figure 6.22: Voltage profile at bus 8 for scenario S2 for the two-area system with inclusion of correlated wind fluctuations.

The trajectory of the bus voltage magnitude at bus 8 for the system modelled through set of deterministic DAEs using constant wind speeds is also shown in Figures 6.21 and 6.22.

The mean trajectory of v coincides with the deterministic trajectory in both scenarios. This was to be expected as the level of correlation among wind speeds does not impact on the wind speed average values. On the other hand, the standard deviation of v increases as the wind correlation increases. This increase of the standard deviation causes 70 (7.0 %) trajectories of v to violate the minimum voltage limit for at least 5 s for case 2 (see Figure 6.22).

The results presented in this section were obtained by simulating the wind generation network in detail as in Figure 3.1. The wind generation network of WPPs in Figure 3.1 is formed in a hierarchical manner. In such a network the WPPs can be aggregated at different hierarchical levels of the network, i.e., bus, distribution, and transmission. The aggregated WPPs can then be driven by an aggregated wind speed process, presented in Section 3.6. This new network, when driven by the aggregated wind speed should produce results similar to those obtained above in this section.

The accuracy of the wind speed aggregation model, in Section 3.6, is measured by comparing the standard deviation of the trajectories of active power $\sigma(p_e)$ generated at various levels of the grid by simulating the entire network to $\sigma(p_e)$ generated by the

aggregated WPP driven by the aggregated wind speed process. The wind aggregation model is considered to work with high accuracy if $\sigma(p_e)$ of wind generation obtained through aggregating WPPs in different regions of the grid is close to $\sigma(p_e)$ obtained by individually modelling WPPs in the network. The values of $\sigma(p_e)$ calculated for detailed and aggregated WPPs along with the errors are presented in Table 6.6. The low values of the errors shown in Table 6.6 is an evidence of the accuracy of the proposed aggregated wind speed model.

Table 6.6: Standard deviation of active power generation of aggregated WPP.

Aggregation Level	Location	SPM		Error
		Detailed	Aggregated	
Bus	Tralee	57.73	60.71	2.78
	Garrow	61.8	63.72	3.1
	Trien	62.31	64.4	3.35
Distribution	Substation B	44.21	45.53	2.88
	Substation C	51.66	52.59	1.8
Transmission	Substation A	46.64	47.36	1.53

SPM: Standard deviation of p_g expressed in percent of the mean value.
Error: Absolute normalised error in % between detailed and aggregated.

6.6.3 All-Island Irish Transmission System

In this section, the AIITS introduced in Section 4.5.2 is considered. Correlated stochastic disturbances are introduced in stochastic load consumption, and power flow equations. The wind speeds driving the WPPs are modelled using correlated wind speeds explained in Section 3.5.3. The results discussed in this section were originally presented in [3].

Stochastic disturbances are modelled as correlated OU processes. The parameters for stochastic load consumption, stochastic bus voltage phasors, and stochastic wind speeds are as follows: $\alpha_p = \alpha_q = \alpha_v = \alpha_\theta = \alpha_w = 1\text{s}^{-1}$; $\sigma(\eta_p) = 0.5\%$ of p_{L0}; $\sigma(\eta_q) = 0.5\%$ of q_{L0}; $\sigma(\eta_w) = 0.5\%$ of w_0; $\sigma(\eta_v) = 0.3\%$ of v_0; and $\sigma(\eta_\theta) = 0.3\%$ of θ_0. Note that the correlation matrix in the case study in this section is constructed in such a way that stochastic disturbances on every device connected in same area are correlated whereas no correlation is considered among the devices connected in different areas.

The impact of correlated load consumption on $\sigma(p_g)$ and $\sigma(q_g)$ of the synchronous generators is discussed first. In this example, wind, and bus voltage phasors do not include stochastic disturbances. Table 6.7 shows $\sigma(p_g)$ and $\sigma(q_g)$ of selected synchronous generators calculated for the three scenarios S1, S2, and S3. The correlation among the stochastic loads has a direct impact on $\sigma(p_g)$ and $\sigma(q_g)$ of the generators. The values of $\sigma(p_g)$ and $\sigma(q_g)$ almost double when the correlation among stochastic loads is doubled. This is a noteworthy result as the standard deviation of the loads remains the same in all three scenarios. This result also substantiates the results obtained for the two-area system.

Next, the impact of correlated stochastic disturbances modelled on bus voltage phasors, using the procedure described in Section 3.5.2, on $\sigma(p_g)$ and $\sigma(q_g)$ of the synchronous generators is considered. In this example, wind, and load power consumption do not include stochastic disturbances. Table 6.8 shows $\sigma(p_g)$ and $\sigma(q_g)$ of selected synchronous generators calculated for the three scenarios S1, S2, and S3. These results corroborate the results obtained in Table 6.4. Henceforth, modelling correlation on stochastic bus voltage phasors leads to reduction in the values of $\sigma(p_g)$ and $\sigma(q_g)$ of the generators. This effect is thus the opposite as the one obtained when varying the correlation of the load power consumption.

Table 6.7: Standard deviation of active and reactive powers of synchronous generators in the AIITS simulated with correlated stochastic loads.

Standard deviation	S1 absolute	S2 % increase [1]	S3 % increase[1]
$\sigma(p_{g_{\mathrm{G1}}})$	0.0025	44	76
$\sigma(p_{g_{\mathrm{G2}}})$	0.0037	56.76	94.59
$\sigma(p_{g_{\mathrm{G3}}})$	0.0013	53.85	92.31
$\sigma(p_{g_{\mathrm{G4}}})$	0.0012	58.33	100
$\sigma(p_{g_{\mathrm{G5}}})$	0.002	55	90
$\sigma(q_{g_{\mathrm{G1}}})$	0.0004	25	50
$\sigma(q_{g_{\mathrm{G2}}})$	0.001	50	80
$\sigma(q_{g_{\mathrm{G3}}})$	0.0003	33.33	66.67
$\sigma(q_{g_{\mathrm{G4}}})$	0.0004	50	75
$\sigma(q_{g_{\mathrm{G5}}})$	0.0006	50	83.33

[1] Note: % increase is calculated based on scenario S1.

Table 6.8: Standard deviation of active and reactive powers of synchronous generators in the AIITS simulated with correlated stochastic bus voltage phasors.

Standard deviation	S1 absolute	S2 % increase [1]	S3 % increase[1]
$\sigma(p_{g_{\mathrm{G1}}})$	0.0193	-22.8	-42.49
$\sigma(p_{g_{\mathrm{G2}}})$	0.0234	-18.8	-32.48
$\sigma(p_{g_{\mathrm{G3}}})$	0.01	-20	-41
$\sigma(p_{g_{\mathrm{G4}}})$	0.0099	-20.2	-40.4
$\sigma(p_{g_{\mathrm{G5}}})$	0.0127	-18.11	-34.65
$\sigma(q_{g_{\mathrm{G1}}})$	0.0176	-19.89	-50.57
$\sigma(q_{g_{\mathrm{G2}}})$	0.0298	-18.79	-48.32
$\sigma(q_{g_{\mathrm{G3}}})$	0.0159	-22.64	-49.06
$\sigma(q_{g_{\mathrm{G4}}})$	0.0148	-20.27	-41.89
$\sigma(q_{g_{\mathrm{G5}}})$	0.0188	-16.49	-40.43

[1] Note: % increase is calculated based on scenario S1.

In the following example, the AIITS incorporating the correlated stochastic disturbances, i.e., correlated stochastic loads, and correlated wind speeds, using the parameter values presented above in this section is considered. The effect of correlation between different stochastic disturbances on the system dynamics is studied by considering the sum of the trajectories of the relevant quantities such as active power consumption and generation of all the devices connected in the same area. Figure 6.23 illustrates the sum of the active powers p_{load} consumed by all loads; the sum of the active powers p_{wind} generated by all wind power plants; and the sum of the active powers p_{syn} generated by all synchronous generators for the three scenarios of correlation, i.e., S1, S2, and S3. Even though the standard deviation of the individual stochastic processes remains the same regardless of the level of correlation being used, Figure 6.23 shows that the spread, in terms of standard deviation, of the sum of the quantities above increases as the correlation between the stochastic process is increased.

Finally, a model of the AIITS that incorporates all stochastic disturbances, i.e., correlated stochastic loads, correlated stochastic bus voltage phasors, and correlated wind speeds, using the parameter values presented above in this section is considered. In addition to the stochastic disturbances, the AIITS undergoes a disconnection of a load connected to the interconnector between Ireland and Wales at $t = 10$ s.

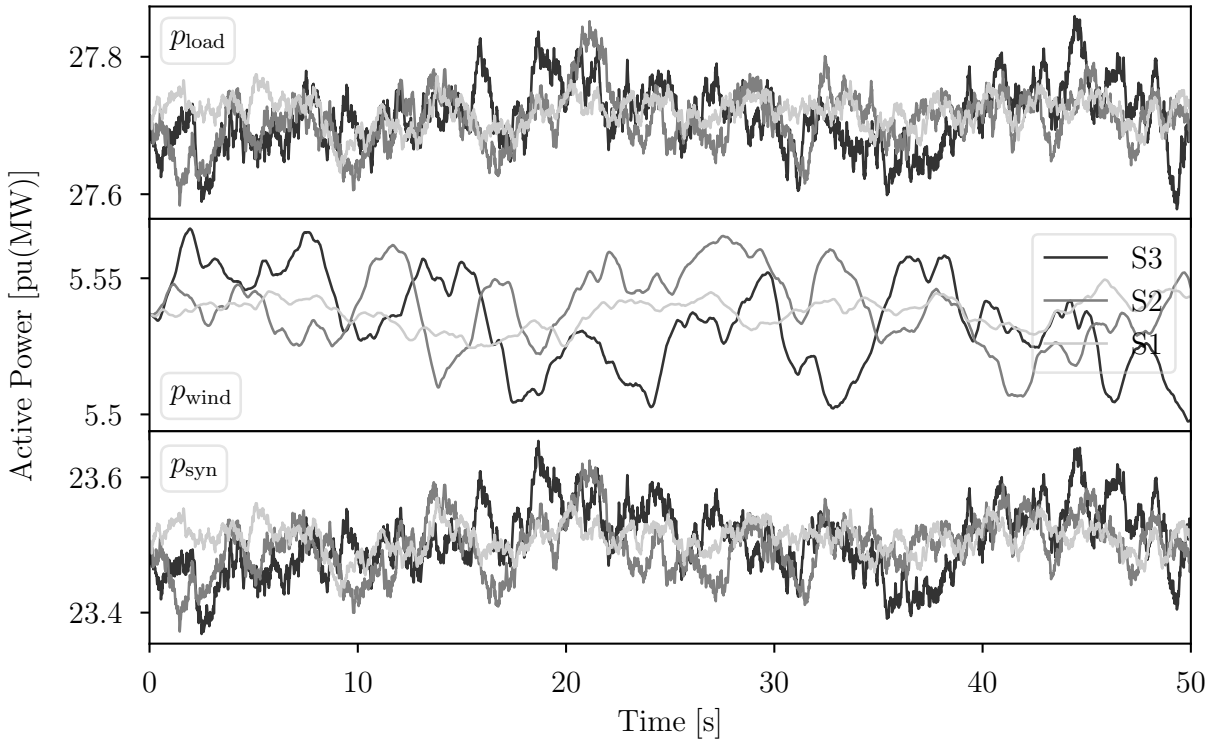

Figure 6.23: Total active power consumed by loads; total active power generated by WPPs; total active power generated by synchronous generators in the AIITS simulating correlated stochastic processes for the three scenarios of correlation, i.e., S1, S2 and S3.

Figure 6.24 shows the time domain profile of voltage magnitude at bus Woodland, for the 1,000 simulations, for S1, i.e., for the fully uncorrelated SDAE model. The black solid line shows the mean value of the 1,000 trajectories, which reflects the voltage profile of a deterministic solution, since all Wiener processes have zero average. This is evident from Figure 6.24 that the mean trajectory coincides with the deterministic trajectory. The deterministic trajectory is obtained for simulating the AIITS for same fault conditions using deterministic DAEs. Figure 6.24 indicates that the voltage profile for the deterministic solution is below the maximum voltage limit, which is shown by a dashed line. It is also relevant to note that 24.4% of the trajectories exceed the maximum voltage limit at least once in the period $10\text{ s} < t < 30\text{ s}$.

Figures 6.25 and 6.26 illustrate the 1,000 trajectories of voltage magnitude at bus Woodland, for scenarios S2 and S3, respectively. Results indicate that the higher the correlation among the processes the lower the standard deviation of the trajectories. For scenario S3, i.e., for the maximum correlation considered in this case study, no trajectory crosses the maximum voltage limit. These results are summarized in Table 6.9. In this

example, the uncorrelated stochastic model shows more conservative results than the scenarios that take into account correlation.

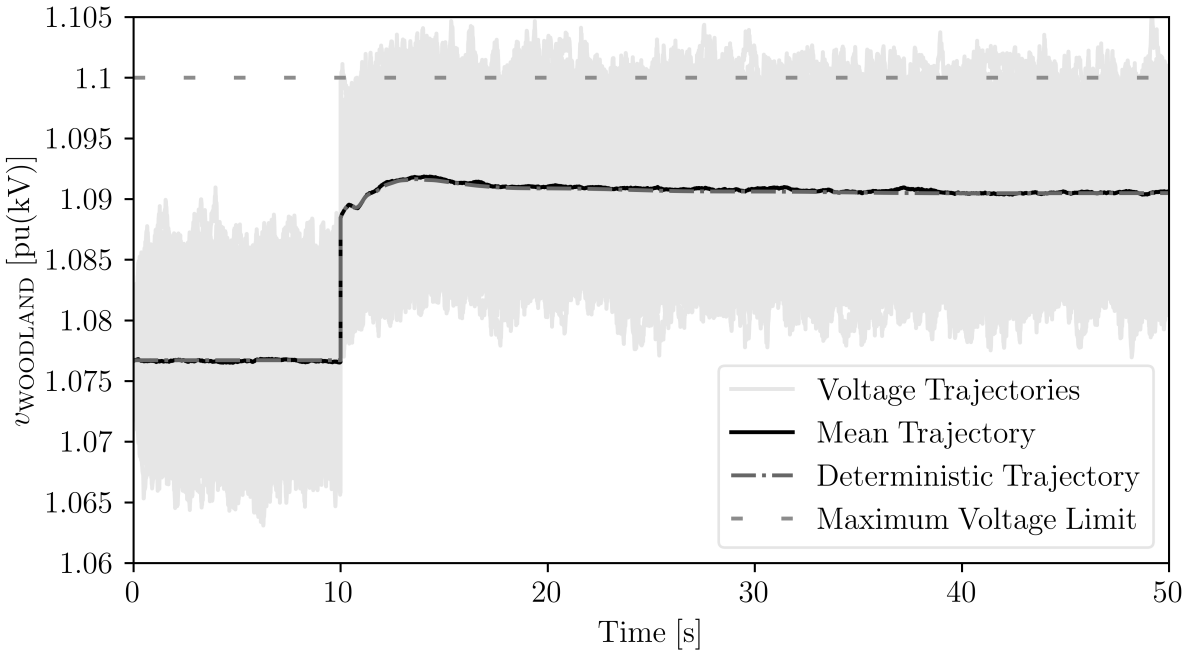

Figure 6.24: Bus voltage magnitude at bus Woodland in the AIITS simulating correlated stochastic processes for scenario S1.

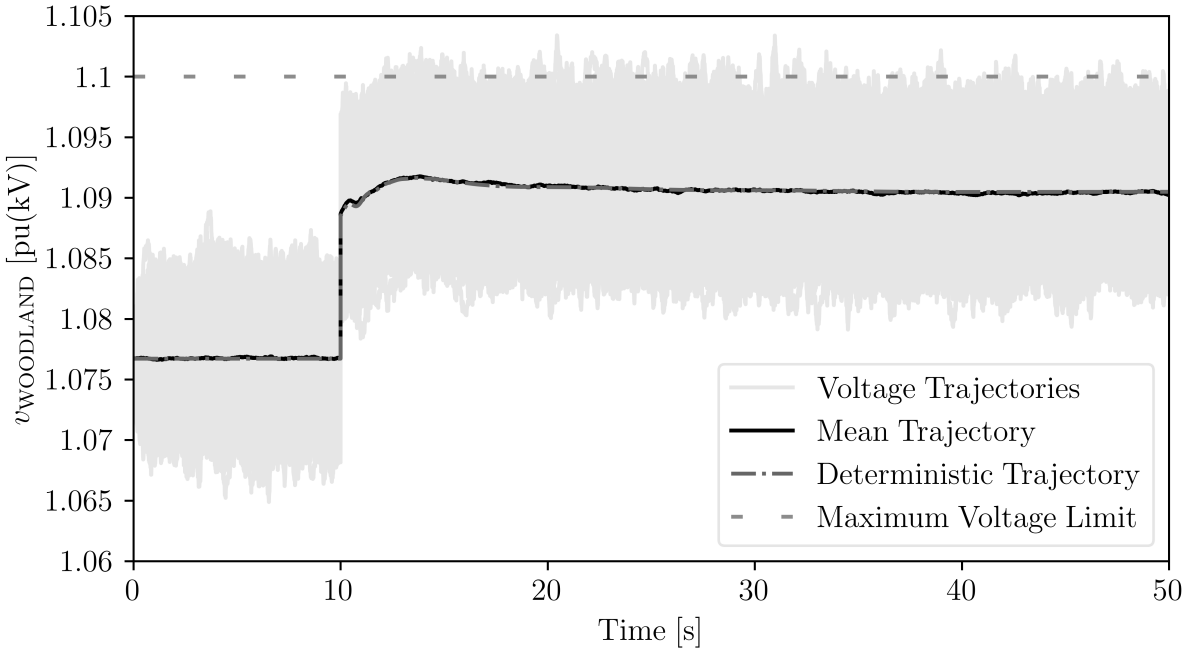

Figure 6.25: Bus voltage magnitude at bus Woodland in the AIITS simulating correlated stochastic processes for scenario S2.

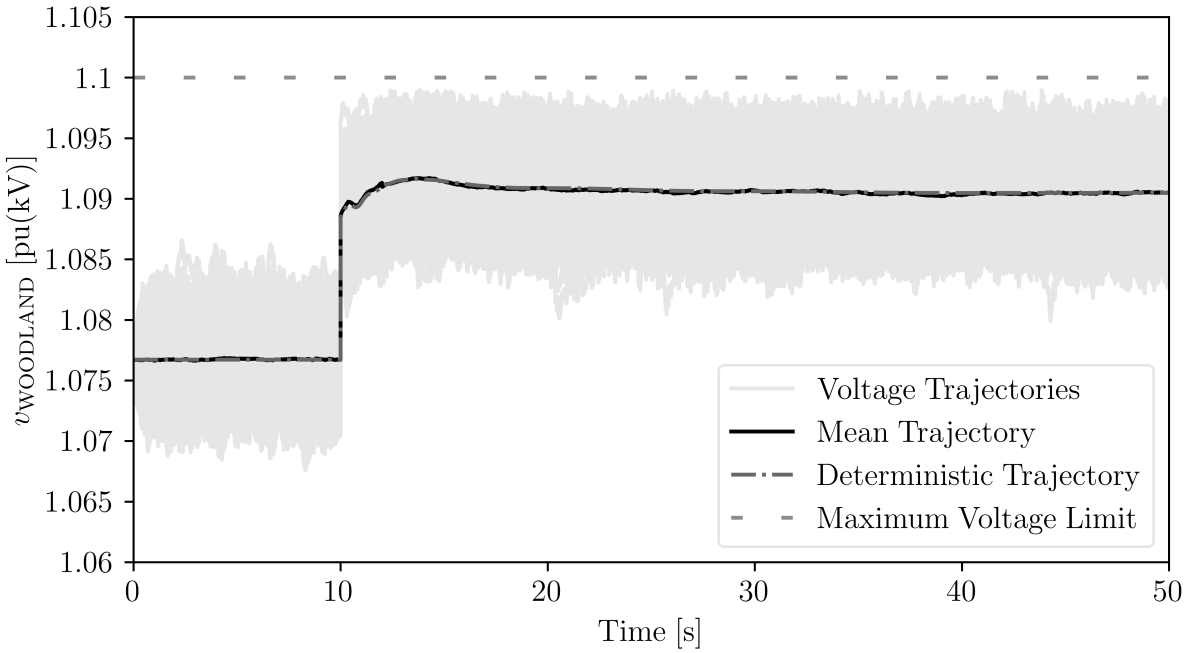

Figure 6.26: Bus voltage magnitude at bus Woodland in the AIITS simulating correlated stochastic processes for scenario S3.

Table 6.9: Trajectories with over-voltages at bus Woodland in the AIITS simulating correlated stochastic processes.

Scenarios	Trajectories with over-voltages
S1	244 (24.4%)
S2	70 (7%)
S3	0

6.7 Conclusions

This chapter discusses the impact of correlated stochastic disturbances on the dynamic behaviour of the power system. With this regard the construction of the correlation matrix required to set up correlated SDAEs is discussed first. Then, the effect of correlated active and reactive power consumption, and correlated wind speeds on the dynamic behaviour of the power system is studied. Finally, the case study models correlation on a variety of sources of correlated stochastic disturbances such as load consumption, bus voltage phasors and wind generation and studies their impact on the power system dynamic through a sensitivity analysis. The case study in this chapter utilises three different power systems including the real-world model of the AIITS to perform power system dynamic simulations.

The examples discussed in the case study lead to conclude that the correlation among stochastic disturbances has a significant impact on the dynamic response of the system and that such an impact is not known *a priori* as, in some cases, considering correlation leads to more conservative results and in others to less conservative results than assuming fully uncorrelated processes. For example, modelling correlation on load consumption and wind speeds increases the standard deviation of the power system quantities and amplifies the effect of contingencies. Whereas modelling correlation on bus voltage phasors causes a reduction in the standard deviation of power system quantities and alleviates the effect of the contingencies. Correlation has thus to be modelled correctly to properly estimate the standard deviation of variables and the instability probability of the system.

Note that the case studies in this chapter perform a sensitivity analysis to quantify the impact of the correlated stochastic disturbances on the dynamic behaviour of the power system. Due to the lack of measurement data, this is only possible to study at this stage. Even though wind speed measurement data is utilised to demonstrate the construction of the correlation matrix. The available wind speed data is limited to a few wind sites and, hence, cannot be utilised to construct the correlation matrix for the higher order system such as the AIITS.

Chapter 7

Conclusions and Future Work

7.1 Summary

This thesis provides generalised data-driven methods to model the sources of stochastic disturbances in power system dynamic studies. Correlated Stochastic Differential Equations (SDEs) are utilised to model correlated stochastic disturbances independent of their statistical properties and time-scales.

A generalised method to construct the correlation matrix, which is the fundamental tool to set up correlated SDEs, from measurement data is discussed. The proposed correlated SDE models are general in the sense that they can model correlation on stochastic processes with arbitrary Autocorrelation Functions (ACFs), Probability Density Functions (PDFs), time-scales, and dimensions. The correlated SDEs are then included into the power system dynamic modelled through a deterministic set of differential-algebraic equations to generate non-deterministic correlated Stochastic Differential Algebraic Equations (SDAEs). Correlated SDAEs are systematic and general and can be used to model any source of volatility such as load consumption or Renewable Energy Sources (RES) generations. Correlated SDAEs are utilised throughout the thesis to study the impact of stochastic disturbances on the short-term dynamic of power system.

A direct method based on the solution of Lyaponov equation to evaluate the standard deviation of the power system algebraic variables in the presence of stochastic disturbances in stationary conditions is also presented. This method is useful when the assessment of the probability of the violation of any system physical limit is of interest. Using the real-world Irish system as a bench mark the thesis shows that the direct method works

with much higher accuracy for a wide range of stationary distributions of the stochastic disturbances. Another advantage of the direct method is the considerable reduction in computational time for systems of large order such as the Irish system.

The impact of ACF of stochastic disturbances on power system dynamic is illustrated in time- and frequency-domain. Results show that for normal operation an increase in the value of autocorrelation coefficient of the stochastic disturbances causes an increase in the standard deviation of the system variables. The results also illustrate that the higher value of autocorrelation coefficient can drive the system to instability even if the standard deviation of the stochastic process is acceptable in stationary conditions.

A case study in this thesis illustrates the method to build the correlation matrix based on measurement data.The thesis demonstrates that the stochastic processes constructed using different types of PDFs have different impact on the standard deviation of the power system quantities and, consequently, the probability that a bus voltage magnitude violates the system limits after a contingency. The thesis also validates the accuracy of the presented model to set up aggregated wind speeds using correlated SDAEs against the detailed model.

The impact of correlation of stochastic disturbances on the power system dynamic is analysed. The results illustrate that correlated stochastic disturbances when modelled on stochastic loads, and wind speeds tend to increase the standard deviation of power system variables in stationary conditions. Such disturbances also pose a worsening effect on the contingencies. On the contrary, the correlation modelled on bus voltage phasors reduces the standard deviation of the power system variables in stationary conditions and alleviates the effect of contingencies.

The results above cannot be obtained without simulating the detailed dynamic model of the system because of the non-linearity of the power system, control hard limits, saturations, etc. The novel contribution of the presented case studies is the identification that the autocorrelation and correlation coefficients of the stochastic disturbances play a significant role in the dynamic behavior of the system and are thus crucial parameters as much as the standard deviation. The fact that the identification of the effect of the autocorrelation and correlation coefficients can be obtained with well- assesssed techniques makes the illustrated approach general and, hopefully, easy to adopt by TSOs.

7.2 Conclusions and Recommendations

The main take-aways from the thesis are as follows.

An increase in either of the value of autocorrelation or correlation coefficient of the stochastic disturbances causes an increase in the standard deviation of the system variables in stationary conditions. This means that the TSOs will have to consider this increase in the standard deviation of the concerned variables such as bus voltage magnitudes, and line current flows, in the normal operation of the grid to make sure that none of the limits are violated by this simple increase in the standard deviation of the concerned variables during usual operation of the grid. Moreover, a higher value of autocorrelation and/or correlation coefficient coupled with a lower value of standard deviation, which might be acceptable in stationary conditions, may lead the system towards instability after a contingency. Due to non-linearity, this result cannot be known without actually simulating the system based on actual parameter values.

Another relevant aspect that has been illustrated in this thesis is that it is important to not only know the statistical parameters of the stochastic disturbances in the time-scale of power system transient in stationary condition but also which PDF type should be used to model such data. The thesis shows that certain PDFs may lead to more conservative results than others. Thus, it is essential to model the stochastic disturbances with the right PDF type based on measurement data and power system dynamic analysis.

Assessing the effect of a specific PDF type on the dynamic behavior of the system is not a straightforward task to solve as both system equations and the diffusion terms of the processes are nonlinear. In this thesis, Time Domain Simulations (TDSs) are performed utilising the cumbersome Monte Carlo Method (MC). These are computationally expensive, as the scenarios for each PDF type should be simulated separately. The thesis shows that the analysis of the spectra of random processes characterized by different although remarkably similar PDF types is a promising alternative approach. Even if the PDFs are similar, in fact, the spectra are different and so might be their impact on the dynamic of the system. How to exactly quantify this impact is currently an open question.

An analytical method to assess the probability that the system variables violate the system physical limits when power systems are subjected to stochastic disturbances is presented in the thesis. This method works with high accuracy for a wide range of

standard deviation of stochastic disturbances independent of the size and complexity of the system.

Note that the analytical methods available in the literature model the power system subject to stochastic disturbances in stationary conditions only. Such methods are incapable of defining the dynamic behavior of power systems subject to stochastic disturbances in such detail as defined in this thesis. Hence, the only choice available is to use numerical methods to understand the effect of the stochastic disturbances on the dynamic behavior of power systems.

Indeed, the main recommendation that can be drawn from this thesis is that the TSOs should perform TDSs through the MC for power systems subject to stochastic disturbances using the actual values of the parameters obtained through measurement data. Using correct values can prevent overlooking some potential instabilities that may arise due to fast-varying stochastic processes. The results presented in this thesis indicate that with the increasing penetration of flexible loads and RES in power systems, instabilities originated by stochastic processes are going to be progressively likely in the future.

At the time of authoring this thesis, however, it is exceedingly difficult to obtain measurement data that can be actually utilised to calculate the correlation matrix for a real-world system. The data made available by the TSOs, in fact, are either detailed but spanning short periods, i.e., considering only specific events (and thus not allowing calculating correlation matrix) or large time series but consisting of values averaged over several minutes, e.g., 15 minutes (and thus inadequate for short-term dynamic analysis). It is our understanding that TSOs have access to such detailed data through Supervisory Control And Data Acquisition systems, as mentioned in the websites, but is not being stored in such a detail because it requires large amount of storage and till date it was not required by a modelling scheme such as the ones introduced in this thesis. Once, TSOs realise the importance of modelling correlated stochastic processes in power systems, the TSOs will make data available in such detail. So that it can be used for the evaluation of statistical properties that can then be utilised to model accurately correlated processes for dynamic analysis.

In conclusion, this thesis provides with the systematic and generalised methods to set up correlated stochastic processes. These models are based on measurement data and can be conveniently included into the existing power system dynamic equations for dynamic

and transient security assessment. Thus, the the modelling techniques presented in this thesis can (and hopefully will) be adopted by the TSOs to study the stability of the power systems in the scenarios with high penetration of stochastic loads and non-synchronous renewable energy sources.

7.3 Future Work

The work presented in this thesis can be extended in various directions. For example, the methods to model correlated stochastic disturbances on sources of volatility, presented in this thesis, are systematic and general, and can be conveniently extended to other sources of volatility such as photovoltaic, tidal generation etc. Furthermore, the power system dynamic analyses in this thesis considers a spatial correlation due to limited amount of data available. However, the method presented to correlate the processes is general, and can be easily extended to temporal correlation, i.e., correlation as a function of time.

The data to account for correlation and the statistical parameters of the processes are either inadequate or not available. We hope that the results presented in this thesis will serve as grounds to encourage the TSOs to store and make available these data in the sampling rate and length suitable for power system dynamic analysis. This will enable the researchers to establish more accurate models, and the TSOs to ensure system security and stability.

The autocorrelation and correlation coefficients of the stochastic processes cause the standard deviations of power system's relevant quantities such as power injections of synchronous generators to increase. This increase in the standard deviations of the power injections of synchronous generators might cause the generators to reach their limits, which will affect the generators' capabilities to provide adequate reserves for frequency control. Thus, future work will involve studying the impact of autocorrelation and correlation coefficients of the stochastic processes on the provision of the ancillary services. Furthermore, the impact of these coefficients on the existing control strategies needs to be evaluated as well.

One of the main advantages of measurement data is that it can be used to evaluate the right modelling PDF type for the power system dynamic analyses. Note, however, that not only data but the dynamic simulations are also required to identify the worst

performing PDF type. In this thesis the time consuming MC has been utilised to account for the impact of a particular PDF type. The future work will focus on developing techniques, e.g., based on frequency analysis, that allow identifying the worst performing PDF type without resorting to TDSs.

Another important aspect that can be deduced from data is whether the correlation among processes is constant or variable with time. This can lead to various scenarios. Finally, we anticipate that the correlation of stochastic processes depends on the time-scale considered, e.g., short- or long-term dynamics. This appears to be another relevant topic to further investigate.

Appendices

Appendix A

Data

A.1 Frequency Data

Transmission System Operators (TSOs) generally keep a record of the power generation along the years but very rarely frequency measurements obtained with Phasor Measurement Units or other instrumentation are stored for a long time. Typically, only major events that lead to high frequency deviations are recorded. For this reason, the Advanced Modelling for Power System Analysis and Simulation (AMPSAS) project, carried out at University College Dublin has recorded the frequency within the university campus in Belfield for a period of four years, from 2014 to 2017. The measurements were obtained with a Frequency Disturbance Recorder (FDR) that has been lent to the last author by the Power system Group led by Prof. Yilu Liu, University of Tennessee, Knoxville [74].

The FDR is a FNET/GridEye device, developed at Virginia Tech, that measures the frequency, phase angle and voltage of the power signal found at ordinary electrical outlets. The main goal of the FNET project is to register and analyze frequency variations following large disturbances [37, 84]. One of the goals of the AMPSAS project, on the contrary, is to explore the statistical properties of the frequency over a long period. Preliminary results of these studies have been presented in [52] and [47].

The data for frequency have been collected at the AMPSAS project Laboratory using a FDR. The measured frequency data has been stored as time series records. Each measured value represents grid frequency every 0.1 second. The data are available starting from July 2014 to November 2017.

A.2 Wind Generation Data

The data utilized for penetration of wind in the AIITS, in this thesis, were provided to the authors by EirGrid Group, the Irish TSO, for the period of four years (2014-2017). The dataset acquired consists of instantaneous power in MW for wind production, system demand and total generation in 15-minute time series records. These values have been averaged using minutely measurements over a period of 15 minutes from the Supervisory Control And Data Acquisition system of the AIITS.

A.3 Wind Speed Measurement Data

The wind speed measurement data for power system dynamic simulations, utilized in this thesis, has been acquired from various open-source platforms. The data used in Chapters 4 and 6, are provided in Table A.1. Table A.1 shows wind speed measurement data obtained for various time-scales and locations. The references for data in Table A.1 can be found in [28].

Table A.1: Sampling rates and PDF types of measurement data

Data Set	Sampling Rate	PDF Type
1	1 hour	1-parameter Rayleig
2	10 minutes	3-parameter Gamma
3	1 minute	3-parameter Gamma
4	1 second	3-parameter Beta

The wind speed measurement data utilized in Chapters 4 and 6 are obtained from an open-source platform the Sustainable Energy Authority of Ireland (SEAI) [67]. Note that the wind data can be easily acquired from the website of SEAI. These data are obtained for ten wind sites in the AIITS. These wind sites are modeled in the wind distribution network presented in Chapter 3.

The wind correlation matrix utilised in the thesis is given in Table A.2.

Table A.2: Wind correlation matrix.

Wind Sites	Tralee A	Tralee B	Tralee C	Garrow A	Garrow B	Garrow C	Trien A	Trien B	Clahane	Cloghboola
Tralee A	1.00	0.97	0.49	0.39	0.37	0.35	0.51	0.47	0.85	0.68
Tralee B	0.97	1.00	0.51	0.40	0.39	0.37	0.50	0.46	0.77	0.67
Tralee C	0.49	0.51	1.00	0.47	0.48	0.45	0.61	0.53	0.46	0.56
Garrow A	0.39	0.40	0.47	1.00	0.90	0.90	0.46	0.43	0.37	0.41
Garrow B	0.37	0.39	0.48	0.90	1.00	0.91	0.42	0.39	0.34	0.37
Garrow C	0.35	0.37	0.45	0.90	0.91	1.00	0.40	0.38	0.32	0.37
Trien A	0.51	0.50	0.61	0.46	0.42	0.40	1.00	0.87	0.50	0.62
Trien B	0.47	0.46	0.53	0.43	0.39	0.38	0.87	1.00	0.48	0.60
Clahane	0.85	0.77	0.46	0.37	0.34	0.32	0.50	0.48	1.00	0.70
Cloghboola	0.68	0.67	0.56	0.41	0.37	0.37	0.62	0.60	0.70	1.00

Appendix B

Correlation between Variance of Frequency and Wind Penetration

This chapter studies the impact of wind penetration on the system frequency stability within the All-Island Irish Transmission System (AIITS). With this regard, a statistical analysis of frequency measurements as well as wind generation data for four years, namely from 2014 to 2017 is carried out.

Specific contributions are as follows:

- Quantify with proper statistical indices the correlation between the wind penetration and frequency fluctuations. These are Pearson's correlation coefficient and the p-value.
- Understand whether the increasing penetration of wind generation in the Irish system in the past four years has led to increase the volatility of the frequency.

B.1 Background on Wind Generation in the AIITS

This section presents a detailed discussion on the wind penetration in the AIITS system. An important aspect related to the wind penetration in the AIITS is the fact that, in the AIITS system, wind generation is often not fully dispatched (this operation is called *wind dispatch down*) P_{WD}:

$$P_{\text{WD}} = P_{\text{wind\_avail}} - P_{\text{wind\_gen}} \ , \tag{B.1}$$

where $P_{\text{wind\_gen}}$ is the actual wind power injected and $P_{\text{wind\_avail}}$ is the actual available wind power. If $P_{\text{WD}} > 0$, there is a wind power reserve and thus the stochastic variations of the wind do not affect the power unbalance of the network and are consequently not responsible for the frequency variations.

Finally, to properly decide the correlation between wind generation forecast and frequency deviations, some precautions have to be taken into account. In particular, the periods during which the load demand varies significantly (known as *demand ramping*) must be excluded from the analysis. The variation of the load, in fact, leads to generator rescheduling that causes fast variations of the frequency. These variations are clearly independent from wind generation.

The remainder of this section outlines the wind dispatch-down procedure and demand ramping up and down as defined in the network codes of the AIITS.

B.1.1 Wind Dispatch-Down

Wind dispatch-down refers to the available wind energy that is not allowed in the grid. This dispatch-down of wind is affected by both local network constraints and system-wide security issues and is necessary to ensure the safe and secure operation of the grid. Wind farms receive dispatch-down instructions from EirGrid [21]. This instructed dispatch is subject to curtailments and constraints [21]. To determine the dispatch-down volume required by the wind farms, EirGrid solves the power flow problem with all required constraints in place one hour before the dispatch instructions with the updated forecast of the available wind energy. Table B.1 shows the volume of monthly wind dispatch-down as percentage of the total available wind energy per year under study [19]. The technical procedures and constraints implemented by EirGrid are outlined below.

B.1.1.1 Curtailments

Curtailments refers to the dispatch-down of wind due to the limits imposed by the power system [19].

Table B.1: Wind dispatch-down as percentage of total available wind energy per year for the AIITS system in the period from 2014 to 2017.

Year	**2014**	**2015**	**2016**	**2017**
Jan	–	4.3	3.5	–
Feb	–	4.2	3.1	1.7
Mar	–	8.8	–	3.3
Apr	–	2.0	1.3	3.6
May	–	4.3	1.2	3.5
Jun	–	4.8	–	4.1
Jul	3.4	3.7	–	3.2
Aug	3.6	5.6	–	2.9
Sep	1.8	2.5	–	5.1
Oct	–	3.9	1.8	10.6
Nov	–	–	1.3	2.6
Dec	4.9	6.3	3.3	–

(a) *System Non-Synchronous Penetration Limit.* The system non-synchronous penetration limit (SNSP) is defined as:

$$\text{SNSP} = \frac{\text{Wind Gen} + \text{HVDC Imports}}{\text{System Demand} + \text{HVDC Exports}} \cdot 100 \ , \tag{B.2}$$

and is used by EirGrid for ensuring a secure and sustainable operation of the grid i.e., the grid frequency does not deviate much due to SNSP penetration [22]. The SNSP is calculated for each trading period using (B.2) [22]. The HVDC imports and exports of electricity in (B.2) come from Moyle and East-West HVDC interconnector with the Great British grid. There has been an increment of 5% per year in the SNSP limit starting from 50% in 2014 to 65% by the end of 2017 [20]. SNSP limit is imposed by system demand. This means the AIITS can accommodate more wind if demand levels are high as it happens during the day from 10:00 to 20:00 when demand is generally high. Wind curtailment will be higher in the case of low demand with high wind production.

(b) *Rate of Change of Frequency (RoCoF)/Inertia.* The system frequency is an indirect measurement of the balance between supply and demand. If a contingency involving the outage of a generator or the loss of load occurs, the frequency deviates from

the reference frequency under balanced operation, e.g., 50 Hz in Europe. The rate with which the frequency deviates away from the mean is known as the rate of change of frequency (RoCoF) [19]. An event causing high RoCoF rates can drive the system towards instability. EirGrid must ensure a minimum number of synchronous generators to be online in different locations of the power system to provide inertia to avoid higher RoCoF and hence, maintain system stability. For this reason, EirGrid may ask the wind farms to dispatch down in order to maintain the power system balanced and provide inertia to avoid high RoCoF rates. Note, however, that only a negligible volume of available wind energy was curtailed, during the period under study in this thesis, due to RoCoF/inertia [19].

(c) *Operating Reserve Requirements.* TSOs must ensure a certain amount of operating reserve to be available in the power system to provide for the imbalance occurred due to the greater variations of system demand. This reserve cannot be provided from non-synchronous wind penetration. Hence wind production has to be dispatched down to provide room for operating reserve. In the AIITS, wind curtailments are generally higher overnight, i.e., from 23:00 to 09:00 [19].

B.1.1.2 Constraints

The dispatch-down of wind due to technical constraints imposed by the network are known as constraints. Firstly, constraints can be understood as localized power carrying capacity of the network at the region of wind production. Secondly, outages in the network that may occur due to maintenance, upgrade works or faults. The dispatch-down of wind in the AIITS remains almost the same throughout the day irrespective of demand levels [19].

B.1.2 Demand Ramps

Figure B.1 shows the load profile of the AIITS during a typical day, for different months. Conventionally, the period from 10:00 to 16:00 is called *day hours* and the period from 16:00 to 10:00 *night hours*. The system demand generally ramps down between 18:00 and 04:00. Then system demand ramps up from 04:00 to 10:00 and from 16:00 to 18:00 hours. Load ramping leads to greater variations of the grid frequency during night hours. As discussed above, to be able to identify the impact of wind generation on the system,

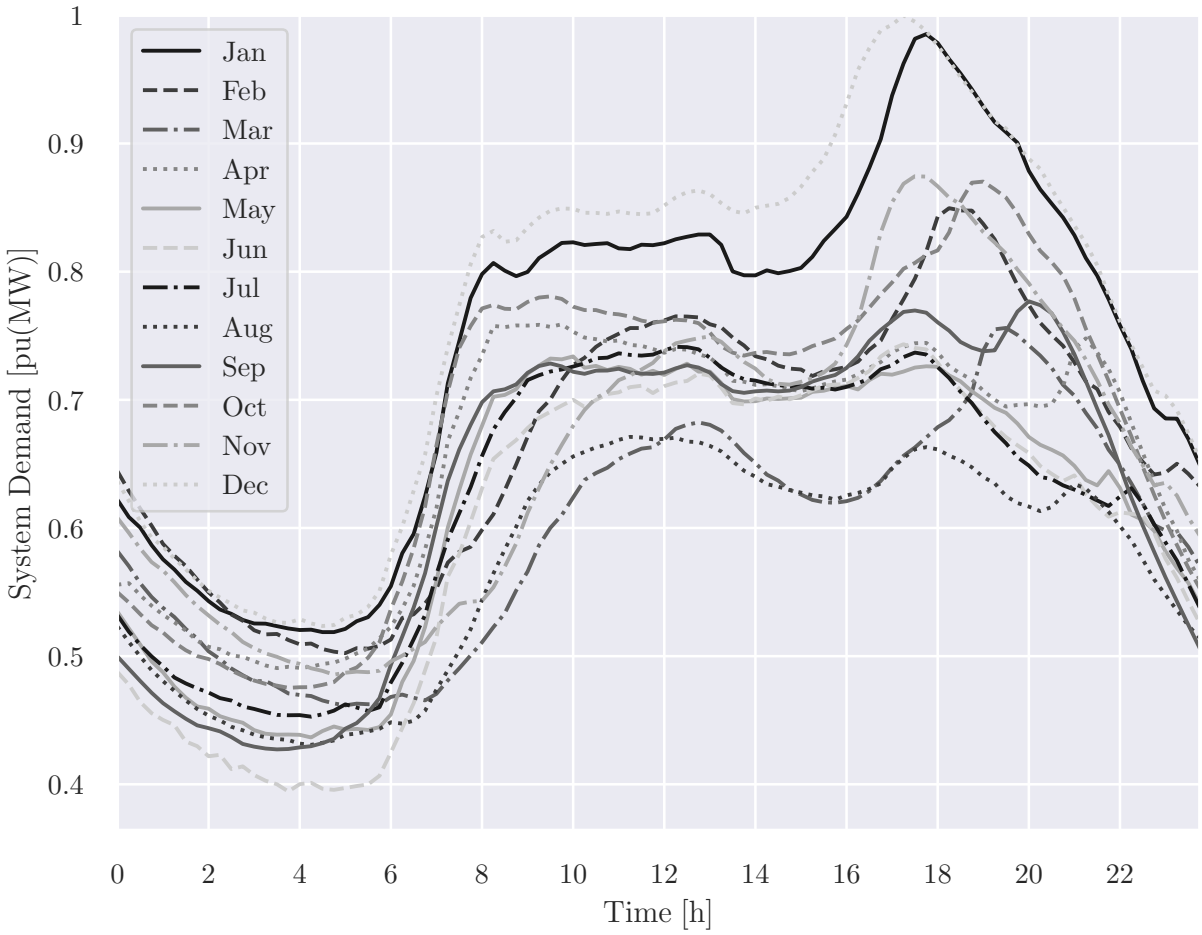

Figure B.1: System Demand for a particular day for all the months in 2016, with maximum demand at 6249.36 MW.

the effect of load ramping has to be separated as much as possible from the frequency deviations. In the case study, thus, only day hours are considered.

B.2 Correlation Indices

Two statistical indices to evaluate the correlation between wind generation and frequency deviations, namely, the Pearson's correlation coefficient and the p-value are considered.

B.2.1 Pearson's correlation coefficient

The Pearson's correlation coefficient is a measurement of the linear correlation between two variables [33], as follows:

$$r = \frac{\sum_i^N (X_i - \overline{X})(Y_i - \overline{Y})}{(N-1)\sigma_X \sigma_Y} \ , \tag{B.3}$$

where N is the number of observations; X_i and Y_i are the values of the two time series, with length N, whose correlation is to be calculated; $\overline{X}$ and $\overline{Y}$ are the mean values of the time series X_i and Y_i, respectively; and σ_X and σ_Y are the standard deviations of the time series X_i and Y_i, respectively.

The Pearson's correlation coefficient can take any value between -1 and 1. $r = 1$ and $r = -1$ indicate perfect linear relation between the variables, whereas $r = 0$ indicates a non-linear relation. In particular, $r > 0$ indicates that if X increases also Y increases. Only positive correlation coefficients are observed in the case study discussed in this thesis.

B.2.2 *p*-value

The Pearson's correlation coefficient reflects the degree of correlation between two variables but does not provide any information weather such a correlation is significant or not. The index used to express the statistical significance of a correlation is known as p-value [23].

Given the t-distribution:

$$t = \frac{r\sqrt{N-2}}{\sqrt{1-r^2}} \ , \tag{B.4}$$

the p-value is defined as:

$$p\text{-value} = 2\Pr(T > t) \ , \tag{B.5}$$

where T follows a t distribution with $N-2$ degrees of freedom. Hence the p-value is twice the probability (for double tail events) to obtain the current value of r if the correlation were actually zero (*null hypothesis*). The null hypothesis for this study is defined as the lack of correlation between wind generation and the hourly standard deviation of the frequency.

Being a probability, the p-value range is $[0, 1]$. A small p-value implies the rejection of the null hypothesis and imposes that the correlation r is significant. The conventional threshold $p = 0.05$ is chosen in the case study to validate statistical significance of a correlation between the variables [23]. So, if $p < 0.05$, the frequency fluctuations are assumed to be statistically correlated with the penetration of wind generation in the system.

B.3 Case Study

Two sets of data are considered in this case study. The Pearson's correlation coefficients and p-values are calculated taking $X = P_{\text{wind\%}}$, i.e., the instantaneous value (15-minute values averaged over 1 hour) of wind energy produced in an hour as percentage share of system demand:

$$P_{\text{wind\%}} = \frac{\text{Hourly Averaged Wind Production}}{\text{Hourly Averaged System Demand}} \cdot 100 \ , \tag{B.6}$$

and $Y = \sigma_{\text{f}}$, i.e., the standard deviation of the system frequency over the same period for which $P_{\text{wind\%}}$ is calculated.

Table B.2 shows the correlation of $P_{\text{wind\%}}$ with σ_{f} per month in the period from 2014 to 2017. Note that frequency data were not available for some months. The wind penetration and frequency fluctuation show a relatively large correlation ($r > 0.4$) in most of the months.

Table B.3 shows the p-values for the same months considered in Table B.2. All the values are well below 0.01 except for three months (January 2015, April 2016 and June 2017), which, consistently, are the same months that show the lowest values of the Pearson's correlation coefficients. Interestingly, these three months are all in different

Table B.2: Pearson's coefficients for $P_{\text{wind\%}}$ and σ_{f} for the AIITS system in the period from 2014 to 2017.

Year	**2014**	**2015**	**2016**	**2017**
Jan	–	0.2400	0.4939	–
Feb	–	0.5919	0.4233	0.4595
Mar	–	0.3923	–	0.3599
Apr	–	0.4756	0.2075	0.4971
May	–	0.5009	0.4127	0.5374
Jun	–	0.4198	–	0.1424
Jul	0.3692	0.5791	–	0.3987
Aug	0.5033	0.5514	–	0.4029
Sep	0.4513	0.3615	–	0.3063
Oct	–	0.5759	0.5793	0.3580
Nov	–	–	0.5997	0.4053
Dec	0.4619	0.3660	0.3374	–

Table B.3: p-values for $P_{\text{wind\%}}$ and σ_{f} for the AIITS system in the period from 2014 to 2017.

Year	**2014**	**2015**	**2016**	**2017**
Jan	–	$1.51 \cdot 10^{-2}$	$< 10^{-6}$	–
Feb	–	$< 10^{-6}$	$6.80 \cdot 10^{-6}$	$< 10^{-6}$
Mar	–	$1.21 \cdot 10^{-7}$	–	$5.84 \cdot 10^{-5}$
Apr	–	$< 10^{-6}$	$1.92 \cdot 10^{-2}$	$< 10^{-6}$
May	–	$< 10^{-6}$	$5.84 \cdot 10^{-5}$	$< 10^{-6}$
Jun	–	$< 10^{-6}$	–	$9.55 \cdot 10^{-2}$
Jul	$9.82 \cdot 10^{-5}$	$< 10^{-6}$	–	$3.44 \cdot 10^{-6}$
Aug	$< 10^{-6}$	$< 10^{-6}$	–	$< 10^{-6}$
Sep	$4.15 \cdot 10^{-7}$	$1.33 \cdot 10^{-5}$	–	$1.31 \cdot 10^{-4}$
Oct	–	$< 10^{-6}$	$< 10^{-6}$	$3.36 \cdot 10^{-6}$
Nov	–	–	$< 10^{-6}$	$7.71 \cdot 10^{-6}$
Dec	$< 10^{-6}$	$6.97 \cdot 10^{-6}$	$4.65 \cdot 10^{-5}$	–

years. The least correlated month is June 2017, while the maximum correlated month is November 2016. Figures B.2 and B.3 present the scatter plot where x-axis represents $P_{\text{wind\%}}$ and y-axis is σ_{f} for the months of June 2017 and November 2016, respectively. In June 2017, the wind penetration has been greater than 50% for a significant number of hours, whereas, in November 2016, the wind penetration remained below 50% all time. Still wind penetration and frequency fluctuations are more correlated in November 2016 than in June 2017. Moreover, in June 2017, there are several hours with a high standard deviation of the frequency but these hours are mostly characterized by low value of $P_{\text{wind\%}}$. In November 2016, the hours with higher σ_{f} are mostly characterized by high $P_{\text{wind\%}}$.

These apparently mixed results can be explained by comparing the values of wind dispatch down, i.e., P_{WD} in different periods. Figure B.4 shows the histogram of P_{WD} for four relevant months, where x-axis represents P_{WD} and y-axis shows the number of hours for which the wind dispatch-down happened. Comparing the histograms and looking at the values in Table B.2, it is evident that the month with greater number of hours during which P_{WD} is high shows a relatively low correlation between wind generation and frequency variations. This supports the argument made in Section B.1 that the higher the amount of wind rejected, the lower the correlation in a given month.

April 2016 is an exception to this rule. This month shows a low correlation between wind and frequency variations despite having a lower P_{WD} and fewer hours of wind curtailment,

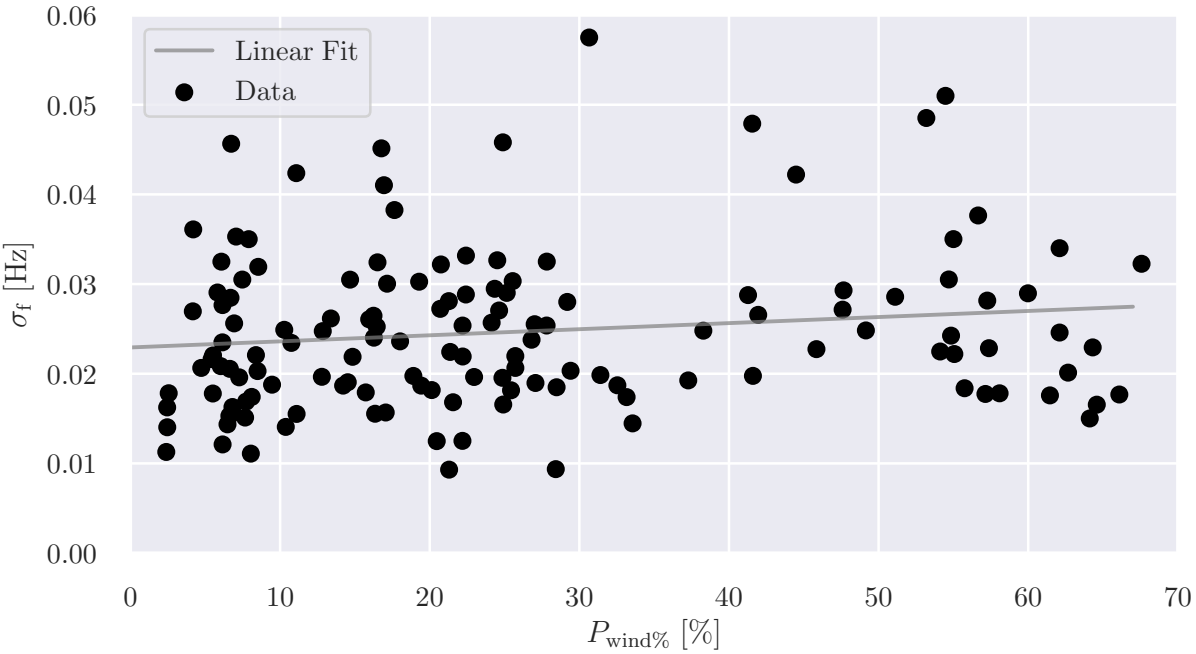

Figure B.2: Scatter plot of σ_f vs $P_{wind\%}$ for the month of June 2017.

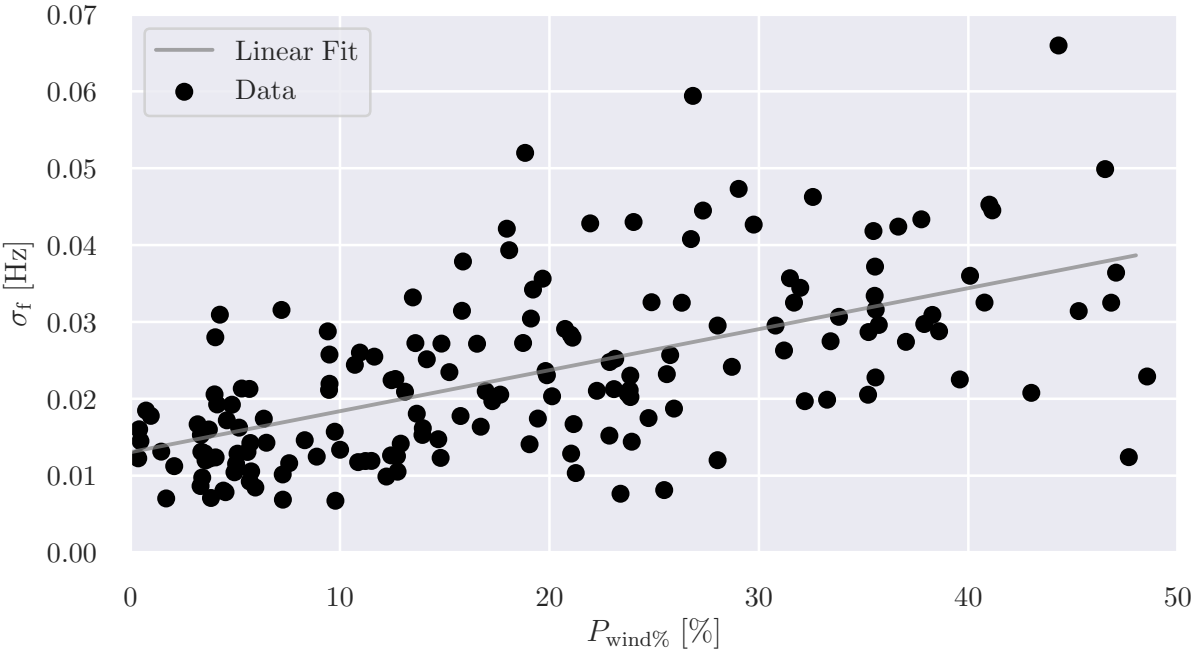

Figure B.3: Scatter plot of σ_f vs $P_{wind\%}$ for the month of November 2016.

compared to January 2015. However, note that, in 2016, the AIITS faced a significant number of the transmission outages, mainly due to maintenance and refurbishment of the transmission system [19]. These outages led to significant changes in the transmission network topology, which could be the cause for such a low correlation in the month of April 2016.

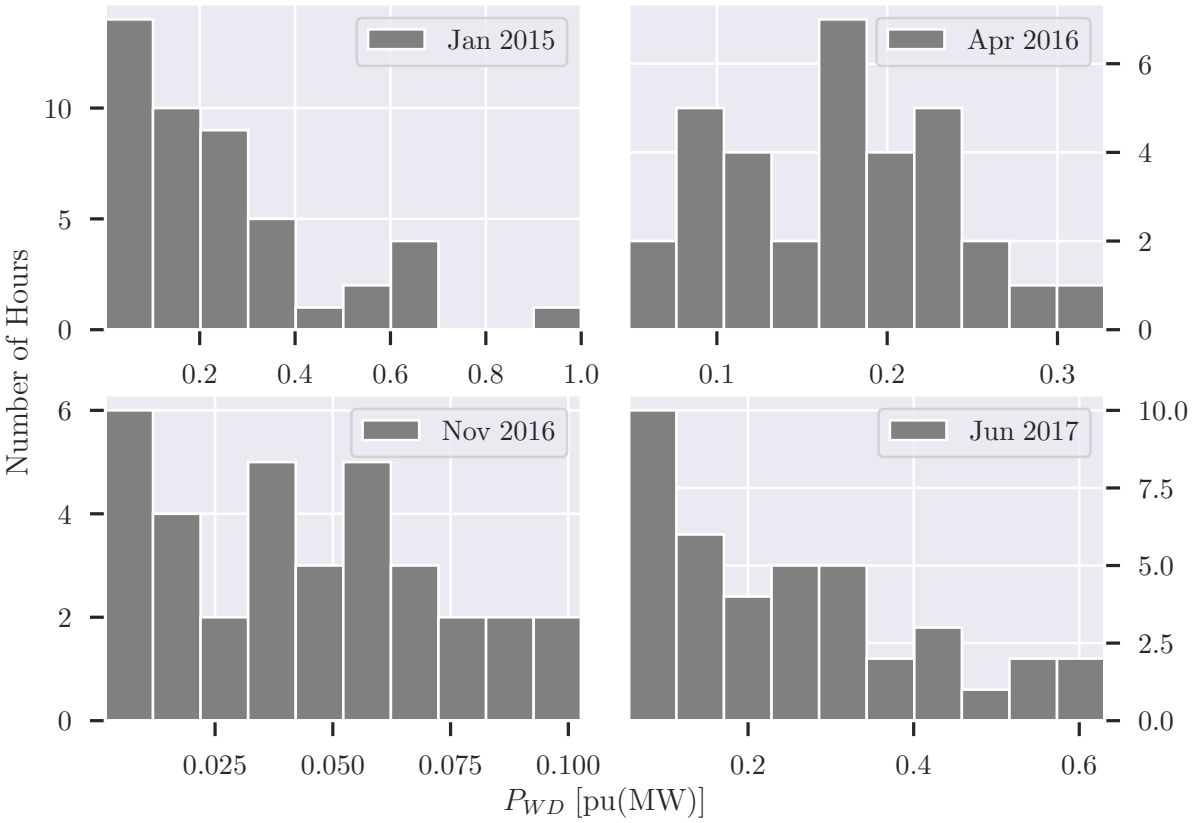

Figure B.4: Histogram of P_{WD} for the months of January 2015, April 2016, November 2016 and June 2017.

Bibliography

[1] S. Aboreshaid, R. Billinton, and M. Fotuhi-Firuzabad, "Probabilistic transient stability studies using the method of bisection [power systems]," *IEEE Transactions on Power Systems*, vol. 11, no. 4, pp. 1990–1995, Nov. 1996. 3

[2] M. Adeen, G. M. Jónsdóttir, and F. Milano, "Statistical correlation between wind penetration and grid frequency variations in the Irish network," in *2019 IEEE International Conference on Environment and Electrical Engineering and 2019 IEEE Industrial and Commercial Power Systems Europe (EEEIC / I CPS Europe)*, 2019, pp. 1–6. 1

[3] M. Adeen and F. Milano, "Modeling of correlated stochastic processes for the transient stability analysis of power systems," *IEEE Transactions on Power Systems*, vol. 36, no. 5, pp. 4445–4456, 2021. xiii, 11, 19, 21, 36, 38, 110, 120

[4] M. Adeen and F. Milano, "On the dynamic coupling of the autocorrelation of stochastic processes and the standard deviation of the trajectories of power system variables," in *IEEE PES General Meeting*, 2021, pp. 1–5. 69

[5] M. Adeen and F. Milano, "On the impact of auto-correlation of stochastic processes on the transient behavior of power systems," *IEEE Transactions on Power Systems*, vol. 36, no. 5, pp. 4832–4835, 2021. 84

[6] M. Adeen and F. Milano, "Stochastic aggregated dynamic model of wind generation with correlated wind speeds," in *Power Systems Computation Conference (PSCC)*, 2022, Online Available, http://faraday1.ucd.ie/archive/papers/windagg.pdf. 22, 26, 117

[7] A. M. S. Al-bayati, F. Mancilla-David, and J. L. Domínguez-García, "Aggregated models of wind farms: Current methods and future trends," in *2016 North American Power Symposium (NAPS)*, 2016, pp. 1–6. 43

[8] R. N. Allan, R. Billinton, A. M. Breipohl, and C. H. Grigg, "Bibliography on the application of probability methods in power system reliability evaluation: 1987-1991," *IEEE Transactions on Power Systems*, vol. 9, no. 1, pp. 41–49, Feb. 1994. 3

[9] J. P. Arenas-López and M. Badaoui, "The Ornstein-Uhlenbeck process for estimating wind power under a memoryless transformation," *Energy*, vol. 213, p. 118842, 2020. 18, 19, 26

[10] P. Benner, V. Mehrmann, V. Sima, S. Van Huffel, and A. Varga, "SLICOT – A subroutine library in systems and control theory," in *Applied and Computational Control, Signal and Circuits*, B. N. Datta, Ed. Birkauser, 1999, vol. 1, ch. 10, pp. 499–539. 60

[11] F. E. Benth, L. Di Persio, and S. Lavagnini, "Stochastic modeling of wind derivatives in energy markets," *Risks*, vol. 6, no. 2, 2018. 18, 26

[12] R. Billinton, M. Fotuhi-Firuzabad, and L. Bertling, "Bibliography on the application of probability methods in power system reliability evaluation 1996-1999," *IEEE Transactions on Power Systems*, vol. 16, no. 4, pp. 595–602, Nov. 2001. 3

[13] R. Calif, "PDF models and synthetic model for the wind speed fluctuations based on the resolution of langevin equation," *Applied Energy*, vol. 99, pp. 173–182, 2012. 19

[14] E. P. T. Cari, J. N. Neto, I. Erlich, and J. L. Rueda, "A methodology for parameter estimation of equivalent wind power plant," in *IECON 2013 - 39th Annual Conference of the IEEE Industrial Electronics Society*, 2013, pp. 1804–1808. 43

[15] A. J. Conejo, M. Carrión, and J. M. Morales, *Decision Making Under Uncertainty in Electricity Markets*. New York, NY: Springer, 2010. 4

[16] S. Dipple, A. Choudhary, J. Flamino, B. K., Szymanski, and G. Korniss, "Using correlated stochastic differential equations to forecast cryptocurrency rates and social media activities," *Applied Network Science*, vol. 5, no. 17, 2020. 21

[17] Z. Y. Dong, J. H. Zhao, and D. J. Hill, "Numerical Simulation for Stochastic Transient Stability Assessment," *IEEE Transactions on Power Systems*, vol. 27, no. 4, pp. 1741–1749, Nov. 2012. 2, 4, 11, 33

[18] EirGrid Group, "All-island generation capacity statement 2018-2027," 2018. [Online]. Available: http://www.eirgridgroup.com/site-files/library/EirGrid/Generation_Capacity_Statement_2018.pdf x, 65

[19] EirGrid, SONI, "Annual renewable energy constraint and curtailment reports." [Online]. Available: http://www.eirgridgroup.com 138, 140, 145

[20] EirGrid, SONI, "Delivering a secure sustainable electricity system (DS3 programme)." [Online]. Available: http://www.eirgridgroup.com 139

[21] EirGrid, SONI, "Quarterly wind dispatch down report user guide." [Online]. Available: http://www.eirgridgroup.com 138

[22] EirGrid, SONI, "System non-synchronous penetration definition and formulation." [Online]. Available: http://www.eirgridgroup.com 139

[23] R. A. Fisher, *Statistical Methods, Experimental Design, and Scientific Inference*. Oxford, UK: Oxford Science Publications, 1990. 142

[24] L. Freris and D. Infield, *Renewable Energy and Power Systems*. Wiley and Sons, 2008. 4, 103

[25] T. C. Gard, *Introduction to Stochastic Differential Equations*. New York, NY: Marcel Dekkler, 1987. 2

[26] C. Gardiner, *Stochastic Methods: A Handbook for the Natural and Social Sciences*. New York, NY, 4th edition: Springer-Verlag, 2009. 23

[27] J. Jacod and P. Protter, *Gaussian Random Variables (The Normal and the Multivariate Normal Distributions)*. Berlin, Heidelberg: Springer Berlin Heidelberg, 2000, pp. 121–135. 60

[28] G. M. Jónsdóttir and F. Milano, "Data-based continuous wind speed models with arbitrary probability distribution and autocorrelation," *Renewable Energy*, vol. 143, pp. 368 – 376, 2019. 2, 3, 18, 19, 25, 26, 28, 135

[29] G. M. Jónsdóttir and F. Milano, "Modeling correlation of active and reactive power of loads for short-term analysis of power systems," in *IEEE Int. Conf. on Environment and Electrical Eng.*, 2020, pp. 1–6. 11

[30] G. M. Jónsdóttir, M. A. A. Murad, and F. Milano, "On the initialization of transient stability models of power systems with the inclusion of stochastic processes," *IEEE Transactions on Power Systems*, vol. 35, no. 5, pp. 4112–4115, 2020. 4, 5, 59

[31] G. M. Jónsdóttir and F. Milano, "Modeling correlation of active and reactive power of loads for short-term analysis of power systems," in *20th International Conference on Environmental and Electrical Engineering (EEEIC)*, Madrid, Spain, 2020, pp. 1 – 5. 2, 4

[32] P. Ju, H. Li, C. Gan, Y. Liu, Y. Yu, and Y. Liu, "Analytical assessment for transient stability under stochastic continuous disturbances," *IEEE Transactions on Power Systems*, vol. 33, no. 2, pp. 2004–2014, March 2018. 3, 5, 11

[33] M. Kendall and A. Stuart, *The Advanced Theory of Statistics. Vol.2: Inference and Relationship*, 4th ed. London, UK: Griffin, 1979. 141

[34] E. Kloeden and E. Platen, *Numerical Solution of Stochastic Differential Equations.* New York, NY, third edition: Springer, 1999. 16

[35] E. Kloeden, E. Platen, and H. Schurz, *Numerical Solution of SDE Through Computer Experiments.* New York, NY, third edition: Springer, 2003. 18

[36] P. Kundur, *Power System Stability and Control.* Mc Graw-Hill, 1994. 53

[37] Y. Lei and Y. Liu, "The impact of synchronized human activities on power system frequency," in *IEEE PES General Meeting*, Jul. 2014. 134

[38] L. Li, X. Wang, Q. Chen, and Y. Teng, "Dynamic equivalence method of wind farm considering the wind power forecast uncertainty," in *2019 IEEE Innovative Smart Grid Technologies - Asia (ISGT-Asia)*, 2019, pp. 1677–1682. 43

[39] X. Li, X. Zhang, L. Wu, P. Lu, and S. Zhang, "Transmission line overload risk assessment for power systems with wind and load-power generation correlation," *IEEE Transactions on Smart Grid*, vol. 6, no. 3, pp. 1233–1242, 2015. 4

[40] H. Liu and Z. Chen, "Aggregated modelling for wind farms for power system transient stability studies," in *2012 Asia-Pacific Power and Energy Engineering Conference*, 2012, pp. 1–6. 43

[41] J. Liu, J. Liu, J. Zhang, W. Fang, and L. Qu, "Power system stochastic transient stability assessment based on Monte Carlo simulation," *The Journal of Engineering*, vol. 2019, no. 16, pp. 1051–1055, 2019. 18, 68

[42] X. Liu, Z. Zhang, W. Wang, H. Zheng, J. Hao, and Y. Chen, "Two-stage robust optimal dispatch method considering wind power and load correlation," in *2018 2nd IEEE Conference on Energy Internet and Energy System Integration (EI2)*, 2018, pp. 1–6. 4

[43] A. Loukatou, S. Howell, P. Johnson, and P. Duck, "Stochastic wind speed modelling for estimation of expected wind power output," *Applied Energy*, vol. 228, pp. 1328 – 1340, 2018. 3

[44] A. Loukatou, S. Howell, P. Johnson, and P. Duck, "Stochastic wind speed modelling for estimation of expected wind power output," *Applied Energy*, vol. 228, pp. 1328 – 1340, 2018. 18, 26

[45] A. Malvaldi, S. Weiss, D. Infield, J. Browell, P. Leahy, and A. M. Foley, "A spatial and temporal correlation analysis of aggregate wind power in an ideally interconnected europe," *Wind Energy*, vol. 20, no. 8, pp. 1315–1329, 2017. 103

[46] G. Margret Jónsdóttir, B. Hayes, and F. Milano, "Continuous-time arma models for data-based wind speed models," in *2018 Power Systems Computation Conference (PSCC)*, 2018, pp. 1–7. 18, 19

[47] F. M. Mele, Á. Ortega, R. Zárate-Miñano, and F. Milano, "Impact of variability, uncertainty and frequency regulation on power system frequency distribution," in *2016 Power Systems Computation Conference (PSCC)*, June 2016, pp. 1–8. 134

[48] X. Mi, J. Wang, and R. Wang, "Stochastic small disturbance stability analysis of nonlinear multi-machine system with Itô differential equation," *International Journal of Electrical Power and Energy Systems*, vol. 101, pp. 439 – 457, 2018. 3, 5, 11

[49] F. Milano, *Power System Modelling and Scripting*. London: Springer, 2010. 17, 61

[50] F. Milano, "A Python-based software tool for power system analysis," in *IEEE PES General Meeting*, Jul. 2013. 6

[51] F. Milano and R. Zárate-Miñano, "A systematic method to model power systems as stochastic differential algebraic equations," *IEEE Transactions on Power Systems*, vol. 28, no. 4, pp. 4537–4544, Nov 2013. 2, 4, 11, 33, 35, 38, 41, 68

[52] F. Milano, R. Zárate-Miñano, and F. M. Mele, "Characterization of Wind Power Fluctuations from Frequency Measurement Data," in *13th Wind Integration Workshop*, 2014. 134

[53] C. O. Nwankpa and S. M. Shahidehpour, "Stochastic model for power system planning studies," *IEE Proceedings-C*, vol. 138, no. 4, pp. 307–320, Jul. 1991. 38

[54] B. Øksendal, *Stochastic Differential Equations: An Introduction with Applications*. New York, NY, 6th edition: Springer, 2003. 23

[55] M. Olsson, M. Perninge, and L. Söder, "Modeling real-time balancing power demands in wind power systems using stochastic differential equations," *Electric Power System Research*, vol. 80, no. 8, pp. 966–974, Aug. 2010. 26

[56] S. Peng, J. Tang, and W. Li, "Probabilistic power flow for AC/VSC-MTDC hybrid grids considering rank correlation among diverse uncertainty sources," *IEEE Transactions on Power Systems*, vol. 32, no. 5, pp. 4035–4044, 2017. 4

[57] M. Perninge, M. Amelin, and V. Knazkins, "Load modeling using the ornstein-uhlenbeck process," in *2008 IEEE 2nd International Power and Energy Conference*, 2008, pp. 819–821. 3, 26

[58] M. Perninge, M. Amelin, and V. Knazkins, "Load modeling using the Ornstein-Uhlenbeck process," in *IEEE 2nd Int. Power and Energy Conference*, 2008, pp. 819–821. 26

[59] M. Perninge, F. Lindskog, and L. Söder, "Importance sampling of injected powers for electric power system security analysis," *IEEE Transactions on Power Systems*, vol. 27, no. 1, pp. 3–11, 2012. 2, 4

[60] P. E. Protter, *Stochastic Integration and Differential Equations*. New York, NY, second edition: Springer, 2004. 18

[61] S. Provost and A. Mathai, *Quadratic Forms in Random Variables: Theory and Applications/ A.M. Mathai, Serge B. Provost*, ser. Statistics: textbooks and monographs. Marcel Dekker, 1992. 60

[62] D. Rimorov, C. M. Rergis, I. Kamwa, A. Moeini, J. Huang, A. Darvishi, and B. Fardanesh, "Calculating impulse and frequency response of large power system models for realization identification," *IEEE Transactions Power Systems*, vol. 35, no. 5, pp. 3825–3834, 2020. 84

[63] C. M. Roberts, E. M. Stewart, and F. Milano, "Validation of the ornstein-uhlenbeck process for load modeling based on μPMU measurements," in *2016 Power System Computation Conference (PSCC)*, Genova, Italy, 2016. 2, 3, 11, 18, 28

[64] N. Shabanikia, A. A. Nia, A. Tabesh, and S. A. Khajehoddin, "Weighted dynamic aggregation modeling of induction machine-based wind farms," *IEEE Transactions Sustainable Energy*, vol. 12, no. 3, pp. 1604–1614, 2021. 43

[65] X. Shen, C. Zhou, and X. Fu, "Study of time and meteorological characteristics of wind speed correlation in flat terrains based on operation data," *Energies*, vol. 11, no. 1, 2018. [Online]. Available: https://www.mdpi.com/1996-1073/11/1/219 4, 103

[66] R. Sobolewski and A. Feijóo, "Estimation of wind farms aggregated power output distributions," *International Journal of Electrical Power & Energy Systems*, vol. 46, pp. 241–249, 2013. 4

[67] Sustainable Energy Authority of Ireland, https://gis.seai.ie/wind/. 135

[68] S. Tao, Y. Li, X. Xiao, and L. Yao, "Load forecasting based on short-term correlation clustering," in *2017 IEEE Innovative Smart Grid Technologies - Asia (ISGT-Asia)*, 2017, pp. 1–7. 4

[69] M. V. Tejeswini and I. J. Raglend, "Modelling and sizing techniques to mitigate the impacts of wind fluctuations on power networks: A review," *International Journal of Ambient Energy*, pp. 1–17, 2020. 43

[70] H. Verdejo, A. Awerkin, W. Kliemann, and C. Becker, "Modelling uncertainties in electrical power systems with stochastic differential equations," *International Journal of Electrical Power and Energy Systems*, vol. 113, pp. 322 – 332, 2019. 26

[71] W. C. B. Vicente, R. Caire, and N. Hadjsaid, "Stochastic simulations and stability to determine maximum wind power penetration of an island network," in *IEEE PES General Meeting*, 2017, pp. 1–5. 2, 4

[72] P. Vorobev, D. M. Greenwood, J. H. Bell, J. W. Bialek, P. C. Taylor, and K. Turitsyn, "Deadbands, droop, and inertia impact on power system frequency distribution," *IEEE Transactions on Power Systems*, vol. 34, no. 4, pp. 3098–3108, 2019. 3, 5, 59

[73] K. Wang and M. L. Crow, "Numerical simulation of stochastic differential algebraic equations for power system transient stability with random loads," in *IEEE PES General Meeting*, Jul. 2011. 2, 4, 11, 33, 68

[74] L. Wang, J. Burgett, J. Zuo, C. C. Xu, B. J. Billian, R. W. Conners, and Y. Liu, "Frequency disturbance recorder design and developments," in *IEEE PES General Meeting*, 2007, pp. 1–7. 134

[75] W. Wu, K. Wang, G. Li, and Y. Hu, "A stochastic model for power system transient stability with wind power," in *IEEE PES General Meeting*, 2014, pp. 1–5. 2, 4

[76] H. Xiaoying and P. Kloeden, *Random Ordinary Differential Equations and Their Numerical Solution*, ser. Probability Theory and Stochastic Modelling. Springer Singapore, 2017, no. 85. 5

[77] F. Xue, X.-F. Song, K. Chang, T.-C. Xu, F. Wu, and Y.-Q. Jin, "Equivalent modeling of DFIG based wind farm using equivalent maximum power curve," in *IEEE PES General Meeting*, 2013, pp. 1–5. 43, 44

[78] X. Yan, W. Fushuan, Z. Hongwei, C. Minghui, Y. Zeng, and S. Huiyu, "Stochastic small signal stability of a power system with uncertainties," *Energies*, vol. 11, no. 11, p. 2980, Nov 2018. 3, 5, 11

[79] Y. Yang and X. Zha, "Aggregating wind farm with DFIG in power system online analysis," in *2009 IEEE 6th International Power Electronics and Motion Control Conference*, 2009, pp. 2233–2237. 43, 44

[80] W. Yu, J. Zhang, and L. Guan, "Agent-based power system time-domain simulation considering uncertainty," in *2018 International Conference on Power System Technology (POWERCON)*, 2018, pp. 317–324. 2, 4

[81] R. Zárate-Miñano, F. M. Mele, and F. Milano, "SDE-based wind speed models with weibull distribution and exponential autocorrelation," in *IEEE PES General Meeting*, 2016, pp. 1–5. 19

[82] R. Zárate-Miñano and F. Milano, "Construction of SDE-based wind speed models with exponentially decaying autocorrelation," *Renewable Energy*, vol. 94, pp. 186 – 196, 2016. 2, 19, 28, 30

[83] R. Zárate-Miñano, M. Anghel, and F. Milano, "Continuous wind speed models based on stochastic differential equations," *Applied Energy*, vol. 104, pp. 42–49, Apr. 2013. 19, 25

[84] L. Zhan and et al., "Improvement of timing reliability and data transfer security of synchrophasor measurements," *IEEE PES T&D Conference and Exposition*, pp. 1–5, 2014. 134

[85] N. Zhou, J. W. Pierre, and D. Trudnowski, "A stepwise regression method for estimating dominant electromechanical modes," *IEEE Transactions Power Systems*, vol. 27, no. 2, pp. 1051–1059, 2012. 84

[86] N. Zhou, D. J. Trudnowski, J. W. Pierre, and W. A. Mittelstadt, "Electromechanical mode online estimation using regularized robust RLS methods," *IEEE Transactions on Power Systems*, vol. 23, no. 4, pp. 1670–1680, 2008. 84